

UNIVERSITI TEKNOLOGI PETRONAS

STRUCTURAL BEHAVIORE OF REINFORCED CONCRETE BEAMS  
STRENGTHED FOR SHEAR USING CFRP LAMINATES SUBJECTED TO  
CYCLIC LOADING

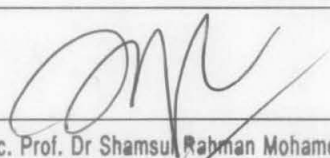
by

LOUAY MAHMOUD ABDEL WAHAB

The undersigned certify that they have read, and recommend to the Postgraduate Studies Programme for acceptance, for the fulfillment of the requirements for the DEGREE OF DOCTOR OF PHILOSOPHY IN CIVIL ENGINEERING.

Signature:   
Main Supervisor \_\_\_\_\_  
Dr Nasir Shafiq  
Associate Professor  
Civil Engineering Department  
Universiti Teknologi PETRONAS

Signature: \_\_\_\_\_  
Co-Supervisor \_\_\_\_\_

Signature:   
Head of Department: \_\_\_\_\_  
Assoc. Prof. Dr Shamsul Rahman Mohamed Kutty  
Head  
Civil Engineering Department  
Universiti Teknologi PETRONAS  
Bandar Seri Iskandar 31750 Tronoh  
Perak Darul Ridzuan, MALAYSIA

Date: \_\_\_\_\_

## STATUS OF THESIS

Title of thesis

STRUCTURAL BEHAVIORE OF REINFORCED CONCRETE  
BEAMS STRENGTHED FOR SHEAR USING CFRP  
LAMINATES SUBJECTED TO CYCLIC LOADING

I, LOUAY MAHMOUD ABDEL WAHAB,

hereby allow my thesis to be placed at the Information Resource Center (IRC) of  
University Teknologi PETRONAS (UTP) with the following conditions:

1. The thesis becomes the property of UTP
2. The IRC of UTP may make copies of the thesis for academic purposes only.
3. This thesis is classified as

Confidential

Non-confidential

If this thesis is confidential, please state the reason:

\_\_\_\_\_

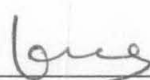
\_\_\_\_\_

The content of the thesis will remain confidential for \_\_\_\_\_ years.

Remarks on disclosure:

\_\_\_\_\_

\_\_\_\_\_

  
\_\_\_\_\_

Signature of Author *L. Mahmoud*

Endorsed by  
  
\_\_\_\_\_

Signature of Supervisor

Dr Nasir Shafiq  
Associate Professor  
Civil Engineering Department  
Universiti Teknologi PETRONAS

Permanent address: Juba University

Khartoum, Sudan

\_\_\_\_\_

\_\_\_\_\_

Date: 26-August-2010

Date: \_\_\_\_\_

STRUCTURAL BEHAVIORE OF REINFORCED CONCRETE BEAMS  
STRENGTHED FOR SHEAR USING CFRP LAMINATES SUBJECTED TO  
CYCLIC LOADING

by

LOUAY MAHMOUD ABDEL WAHAB

A Thesis

Submitted to the Postgraduate Studies Programme

as a Requirement for the Degree of

DOCTOR OF PHILOSOPHY

CIVIL ENGINEERING PROGRAMME

UNIVERSITI TEKNOLOGI PETRONAS

BANDAR SERI ISKANDAR

PERAK

AUGUST 2010

## DECLARATION OF THESIS

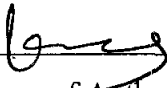
Title of thesis:

STRUCTURAL BEHAVIORE OF REINFORCED CONCRETE  
BEAMS STRENGTHED FOR SHEAR USING CFRP LAMINATES  
SUBJECTED TO CYCLIC LOADING

I, LOUAY MAHMOUD ABDEL WAHAB

I hereby declare that the thesis is based on my original work except for quotations and citations which have been duly acknowledged. I also declare that it has not been previously or concurrently submitted for any other degree at UTP or other institutions.

Witnessed by

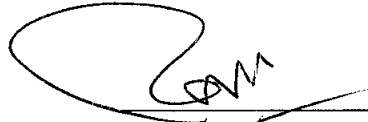


Signature of Author *L. Mahmoud*

Permanent address: Juba University,

Khartoum , Sudan

Date: 26-August-2010



Signature of Supervisor

Name of Supervisor  
Dr Nasir Shafiq  
Associate Professor  
Civil Engineering Department  
Universiti Teknologi PETRONAS

Date: \_\_\_\_\_

## **ACKNOWLEDGMENT**

First I would like to thank God the Almighty, for without his consent, it would be impossible to achieve what had been done in this work. And also I would like to thank my supervisors AP. Dr. Nasir Shafiq and AP. Ir. Dr. Muhd Fadhil Nuruddin who push me hard to overcome the complications of this investigation with all of their knowledge.

Also the author would like to thank the management and authorities of Universiti Teknologi Petronas for their constant support and encouragement for the accomplishment of this research study. Special thanks for laboratory technologist in concrete lab for their assistance during my experimental program.

## ABSTRACT

The application of an external strengthening technique such as bonded fibre-reinforced polymer (FRP) laminates seems to be an attractive technique to improve the structural behaviour of R.C elements under cyclic loading. FRP composite materials are widely employed because of their high strength to weight ratio, environmental resistance and ease of application over materials such as steel. In this research, an analytical model based on non-linear finite element algorithms coded in FORTRAN language was developed to enable the analysis of R.C beams externally strengthened for shear using CFRP laminates subjected to cyclic loads.

20-noded isoparametric quadrilateral elements with three degrees of freedom per each node were used to represent concrete. Material response is assumed to be orthotropic with tangent stiffness derived from stress-strain relationship for concrete under general biaxial state of stress. The reinforcement bars were represented in discrete manner. Three-dimensional space frame elements and space truss elements were used for this purpose. Material response is assumed to be elastic-perfectly plastic. 20-noded elements similar to those used to model concrete elements were used to represent CFRP side plates. Material response is assumed to be elastic-brittle. Discrete cracking approach was used to represent cracking.

Primary consideration has been given to the representation of shear transfer mechanisms due to aggregate interlock in cracked concrete and dowel action in reinforcement. Expressions were derived from an analytical model in conjunction with experimental data to provide shear stress and stiffness values for special elements used to model aggregate interlock mechanism. A comparable approach was used to derive expression for dowel action mechanism. The bond-slip phenomenon between concrete and reinforcement was accounted for by using non-dimensional

spring elements. Shear stiffness values for such elements are obtained from expression based on experimental data.

A new experimental methodology that enables to study the interfacial behaviour of CFRP-to-concrete joints under cyclic shear loading was developed. An experimental program consisted of testing specified number of push off specimens has been conducted. Mathematical formulation that govern the behaviour of the interface element was obtained, which are found in good agreement with the experimental results. This included the bond-slip behaviour, shear stiffness of interface and its degradation as number of cycle increased as well as the S-N curve. 3-d interface element is used to simulate this phenomenon. The element has sixteen nodes, eight nodes connect to concrete element and the other eight nodes connected to CFRP sheet. The interface was modelled by three linear springs connecting the joint nodes with the same coordinates.

A computer program with combined-iterative method was used to solve the non-linear cyclic problem. A parametric analysis has been carried out to study the effect of controlling factors such as shear span-depth ratio, CFRP thickness on structural behaviour of R.C beams strengthened for shear with CFRP laminates subjected to monotonic or cyclic loading. The results from the analytical model were compared with corresponding experimental ones in order to confirm the validity of the analytical algorithm. The comparison between the analytical results and the published results gave a good agreement which indicates that experimental methodology proved to be appropriate and valid and that the analytical algorithm is quite efficient tool to study the structural behaviour of such element under cyclic loading as well as monotonic loading.

## ABSTRAK

Penggunaan teknik pengukuhan luar seperti lapisan gentian tetulang polimer terikat (FRP) adalah satu teknik yang menarik bagi meningkatkan ciri-ciri struktur bagi unsur-unsur konkrit tetulang di bawah kesan bebanan berulang. Bahan komposit FRP digunakan dengan meluas kerana mempunyai nisbah kekuatan terhadap berat yang tinggi, ketahanan terhadap rintangan persekitaran yang baik dan penggunaan yang mudah berbanding bahan-bahan lain seperti keluli. Dalam penyelidikan ini, suatu model analisis berdasarkan kepada algoritma elemen terhad tidak linear dikodkan dalam bahasa FORTRAN telah disediakan bagi membolehkan analisis pada rusuk konkrit tetulang dikuatkan secara luaran untuk menguji sisihan menggunakan lamina CFRP di bawah kesan beban berulang.

Elemen-elemen 20 nod isoparametrik sisi empat dengan tiga darjah kebebasan setiap nod digunakan bagi mewakili konkrit. Respon bahan dianggap bersifat ortotropik dengan ketegaran tangen, hasil daripada hubungan antara tekanan dan terikan untuk konkrit di bawah dwipaksi tegasan umum. Bar-bar tetulang pula diperlihatkan dalam cara yang diskret. Selain itu, ciri-ciri rangka dan kekuda tiga dimensi telah digunakan untuk tujuan ini. Dalam kajian ini, respon bahan dianggap bersifat plastik anjal dengan sempurna. Elemen 20 nod yang menyerupai ciri-ciri model konkrit telah digunakan bagi mewakili plat sisi CFRP. Respon bahan dianggap bersifat anjal-rapuh. Pendekatan pemecahan diskret digunakan bagi mewakili pemecahan.

Pertimbangan utama telah diberikan kepada mekanisme pemindahan ricih kerana kesan saling kunci agregat dalam konkrit retak dan tindakan cemat dalam tetulang itu sendiri. Dengan itu, beberapa formula telah diterbitkan daripada suatu model analisis berdasarkan data percubaan untuk menyediakan tegasan ricih dan nilai kekukuhan untuk unsur-unsur khas dalam model mekanisme agregat saling kunci. Dalam kajian ini juga, satu pendekatan yang setara telah digunakan bagi menghasilkan formula

untuk tindakan mekanisma cemat. Fenomena ikatan-gelincir antara konkrit dan tetulang telah diambil kira dengan menggunakan elemen-elemen pegas tanpa dimensi. Nilai-nilai kekuatan ricih bagi unsur-unsur tersebut diperolehi daripada formula berdasarkan data eksperimen.

Satu kaedah percubaan baru yang membolehkan kajian hubungan antara muka CFRP-sendi konkrit di bawah kesan ricih beban berulang dilaksanakan. Dengan itu, sebuah program percubaan yang mengandungi bilangan ujian tertentu untuk spesimen tolakan telah dijalankan. Terdapat dua jenis persediaan yang digunakan bagi mencapai objektif ini. Formula matematik yang menghubungkan ciri-ciri antara muka telah dikenalpasti, dimana ia positif kepada keputusan percubaan eksperimen. Ini merangkumi ciri-ciri ikatan-gelincir, kekuatan ricih kepada elemen antara muka dan penurunan apabila bilangan kitaran serta lengkung S-N bertambah. Unsur antara muka 3-dimensi telah digunakan untuk mensimulasikan fenomena ini. Elemen ini mempunyai 16 nod, lapan nod telah disambungkan kepada elemen konkrit dan selebihnya disambungkan kepada lapisan CFRP. Bahagian antara muka CFRP telah dimodelkan oleh tiga pegas linear yang menghubungkan sendi-sendi nod dengan koordinat yang sama.

Satu program komputer dengan kaedah gabungan-berulang telah digunakan bagi menyelesaikan masalah kitaran tidak linear. Satu analisis parametrik telah dilaksanakan untuk mengkaji kesan pengawalan faktor-faktor seperti nisbah ricih rentang-kedalaman, ketebalan CFRP pada struktur rusuk konkrit tetulang yang mengukuhkan ricih beserta lapisan lamina CFRP di bawah monotonik atau pembebanan berulang. Keputusan model analisis dibandingkan dengan percubaan eksperimen yang bersesuaian bagi mengesahkan kesahihan analisis algoritma tersebut. Perbandingan antara analisa keputusan dan keputusan yang telah diterbitkan menunjukkan keputusan yang positif dimana ia memberikan indikasi bahawa kaedah penyelidikan yang telah dijalankan dalam kajian ini adalah terbukti berkesan dan sah. Selain itu, analisa algoritma juga terbukti menjadi salah satu kaedah yang efisien dalam kajian perlakuan struktur di bawah kesan bebanan berulang mahupun bebanan monotonik.

## **COPYRIGHT PAGE**

In compliance with the terms of the Copyright Act 1987 and the IP Policy of the university, the copyright of this thesis has been reassigned by the author to the legal entity of the university,

Institute of Technology PETRONAS Sdn Bhd.

Due acknowledgement shall always be made of the use of any material contained in, or derived from, this thesis.

© Louay Mahmoud Abdel Wahab, 2010  
Institute of Technology PETRONAS Sdn Bhd  
All rights reserved.

## TABLE OF CONTENTS

STATUS OF THESIS.....	i
APPROVAL PAGE.....	ii
TITLE PAGE.....	iii
DECLARATION OF THESIS.....	iv
ACKNOWLEDGMENT.....	v
ABSTRACT.....	vi
ABSTRAK.....	viii
COPYRIGHT PAGE.....	x
TABLE OF CONTENTS.....	xi
LIST OF TABLES.....	xiv
LIST OF FIGURES.....	xv
CHAPTER 1 INTRODUCTION.....	1
1.1 General.....	1
1.2 Problem Statement.....	3
1.3 Objectives and Scope of this Investigation.....	5
1.4 Scope and Methodology.....	5
1.4.1 Experimental study.....	6
1.4.2 Analytical Study.....	6
1.5 Thesis Outlines.....	6
CHAPTER 2 LITERATURE REVIEW.....	9
2.1 Introduction.....	9
2.1.1 Historical Back Ground.....	9
2.1.2 Definition of FRP.....	11
2.1.3 Advantages of FRP Materials.....	12
2.1.4 Feature and Benefit.....	13
2.1.5 Types of Fibres.....	13
2.1.6 Types of Resin.....	17
2.1.7 Bonding of FRP Composites.....	18
2.2 Strengthening of Concrete Structures.....	19
2.2.1 Flexural Strengthening.....	19
2.2.2 Shear Strengthening of RC Beams using FRP.....	27
2.2.3 Bond between FRP Sheet and Concrete Interfaces under Shear.....	35
2.3 Material Cyclic Models.....	41
2.3.1 Introduction.....	41
2.3.2 Concrete Cyclic Models.....	41
2.3.3 Steel Constitutive Models.....	48
2.3.4 Summary of Review on Cyclic Models.....	53
2.4 Finite Element Analytical Models.....	53
2.5 Concluding Remarks.....	61
CHAPTER 3 RESEARCH METHODOLOGY.....	62

3.1	Introduction .....	62
3.2	Experimental Investigation .....	62
	3.2.1 Background .....	62
	3.2.2 Objectives of Experimental Study .....	64
	3.2.3 Specimen Descriptions.....	64
	3.2.4 Materials Properties .....	65
	3.2.5 Mixing, Casting and Curing of Concrete.....	67
	3.2.6 Specimens Preparation.....	69
	3.2.7 Testing Procedure .....	70
	3.2.8 Loading Conditions.....	73
3.3	Analytical investigation.....	73
	3.3.1 Background.....	73
	3.3.2 Objectives of analytical investigation.....	75
	3.3.3 Analytical Algorithm Outlines.....	76
<b>CHAPTER 4 MATERIALS CYCLIC MODELS.....</b>		<b>78</b>
4.1	Introduction .....	78
4.2	Concrete Cyclic Model.....	79
	4.2.1 Introduction.....	79
	4.2.2 Proposed Cyclic Model for Concrete.....	80
4.3	Steel Cyclic Model .....	92
	4.3.1 Introduction.....	92
	4.3.2 Proposed Cyclic Model for Steel.....	93
4.4	FRP Cyclic Model.....	94
	4.4.1 Proposed cyclic model for FRP laminates .....	94
<b>CHAPTER 5 CHAPTER 5 MODELING OF SHEAR TRANSFER MECHANISMS AFTER CRACKING .....</b>		<b>96</b>
5.1	Background .....	96
5.2	Modelling of Aggregate interlock.....	97
	5.2.1 Proposed cyclic model for aggregate interlock.....	98
5.3	Modelling of Dowel action mechanism .....	99
	5.3.1 Proposed cyclic model for dowel action.....	101
5.4	Bond-slip cyclic models.....	104
	5.4.1 Background.....	104
	5.4.2 Proposed cyclic model for bond slip mechanism .....	106
<b>CHAPTER 6 INTERFACE MODEL BETWEEN CFRP SIDES PLATES AND CONCRETE.....</b>		<b>109</b>
6.1	Introduction .....	109
6.2	Interfacial Behaviour of CFRP-to-Concrete Joints under Monotonic Loading.....	110
	6.2.1 Shear Capacity .....	110
	6.2.2 Monotonic Bond Stress– Slip behaviour .....	111
	6.2.3 Shear stiffness of interface element .....	114
	6.2.4 Failure criteria of interface element.....	115
6.3	Interfacial Behaviour of CFRP-to-Concrete Joints under Cyclic Loading.....	116
	6.3.1 Fatigue Behaviour of Specimens .....	116

6.3.2	Cyclic Bond Stress– Slip Behaviour.....	119
6.3.3	Shear Stiffness of Interface Element under cyclic loading.....	127
6.3.4	Degradation of the Shear Stiffness under Cyclic Loading.....	128
6.3.5	Stress Level– fatigue Life Relationship.....	132
6.3.6	Failure criteria of interface.....	134
CHAPTER 7 ANALYTICAL MODELLING USING FINITE ELEMENT		
	METHOD (FEM).....	139
7.1	(FEM) Basic Concepts .....	139
7.2	Advantages of using Finite Element Analysis .....	141
7.3	Basic Steps in Finite Element Procedure .....	141
7.4	Non-linear Finite Element Analysis [NLFEA] .....	145
	7.4.1 Non-linear Numerical Techniques using Finite Element Method .....	146
7.5	Selection of Element and Representation of Cracking.....	151
7.6	Representations of Elements .....	151
	7.6.1 Representations of Concrete and CFRP.....	152
	7.6.2 Representation of Reinforcement .....	157
	7.6.3 Representation of Shear Resisting Mechanism.....	169
	7.6.4 Representation of Interaction between CFRP Side Plates and	
	Concrete Surface.....	172
	7.6.5 Representation of Cracking.....	179
7.7	Solution strategy using iterative method.....	184
CHAPTER 8 APPLICATIONS AND RESULTS .....		186
8.1	Introduction .....	186
8.2	Material and Specimen Descriptions .....	187
8.3	Instrumentation.....	188
8.4	Loading conditions.....	189
8.5	Experimental response .....	191
	8.5.1 Mode of failure .....	192
	8.5.2 load-displacement curve .....	194
	8.5.3 Strains measurement .....	194
8.6	Analytical response .....	195
8.7	Comparison between experimental and analytical results .....	199
	8.7.1 Cyclic behaviour .....	199
	8.7.2 Static behaviour .....	203
8.8	Parametric analysis.....	204
	8.8.1 Introduction.....	204
	8.8.2 Effect of Shear span/depth ratio.....	205
	8.8.3 Effect of CFRP thickness.....	207
CHAPTER 9 CONCLUSIONS AND RECOMMONDATIONS.....		212
9.1	Conclusions .....	212
9.2	Recommendation for Future Work .....	213
REFERENCES .....		215
LIST OF PUBLICATIONS .....		224

## LIST OF TABLES

Table 2.1 MAJOR CHARACTERISTIC AND APPLICATIONS OF FRP COMPOSITES .....	17
Table 2.2 INFLUENCING FACTOR IN BOND OF FRP SHEET-CONCRETE INTERFACE CHEN ET AL (2001) .....	35
Table 3.1 Properties of concrete and reinforcement .....	66
Table 3.2 Epoxy-resin and CFRP composite laminate properties .....	67
Table 3.3 TRIAL TESTS .....	67
Table 6.1 SHEAR CAPACITY (AXIALLY LOADED CASE) .....	110
Table 6.2 SHEAR CAPACITY (ECCENTRICALLY LOADED CASE) .....	111
Table 6.3 RESULTS OF FATIGUE LIFE FOR SPECIMEN IN GROUP A .....	116
Table 6.4 RESULTS OF FATIGUE LIFE FOR SPECIMEN IN GROUP B .....	117
Table 6.5 VALUES $C_1$ AND $C_2$ .....	120
Table 6.6 VALUES OF $C_3$ AND $C_4$ .....	122
Table 6.7 VALUES OF $C_5$ AND $C_6$ .....	124
Table 6.8 VALUES OF $C_7$ AND $C_8$ .....	126
Table 6.9 VALUES OF $C$ AND $\tan\phi$ (AXIALLY LOADED CASE) .....	135
Table 6.10 VALUES OF $C$ AND $\tan\phi$ [ECCENTRICALLY LOADED CASE] .....	137
Table 7.1 SUMMARY OF NON-LINEAR ANALYSIS TECHNIQUES .....	150
Table 7.2 SHAPE FUNCTION FOR 20-NODED ISOPARAMETRIC ELEMENT .....	153
Table 7.3 GENERALIZED FORM FOR SHAPE FUNCTION INTERFACE ELEMENT .....	175
Table 8.1 PROPERTIES OF CONCRETE MIX .....	188
Table 8.2 MECHANICAL PROPERTIES OF STEEL REINFORCEMENT BARS .....	188
Table 8.3 PROPERTIES OF CFRP .....	188
Table 8.4 DEFLECTION MEASUREMENT .....	194
Table 8.5 STRAIN MEASUREMENT .....	195
Table 8.6 EFFECT OF SHEAR SPAN-DEPTH RATIO .....	207
Table 8.7 EFFECT OF CFRP THICKNESS .....	211

## LIST OF FIGURES

Fig. 2.1 TYPICAL APPLICATIONS OF FRP IN STRENGTHENING OF RC STRUCTURES .....	10
Fig. 2.2 REPRESENTATION OF FRP MATERIAL .....	11
Fig. 2.3 COMPARISON AMONG CFRP, AFRP, GFRP SHEETS AND STEEL.....	15
Fig. 2.4 TRAINTAFILLOU'S MODEL (1998).....	30
Fig. 2.5 VARIOUS SCHEMES FOR WRAPPING TRANSVERSE FRP REINFORCEMENT .....	32
Fig. 2.6 (a) U-wrap without end anchor. (b) U-wrap with end anchor. ....	32
Fig. 2.7 SHEAR REINFORCEMENT DISTRIBUTION (a) Continuous. (b) Strips. ....	33
Fig. 2.8 FIBER OREINTATION. (a) 90 <sup>0</sup> wrap. (b) 45 <sup>0</sup> wrap. ....	33
Fig. 2.9 BI-AXIAL FRP ORIENTATION. (a) 90 <sup>0</sup> /0 <sup>0</sup> . (b) ± 45 <sup>0</sup> .....	33
Fig. 2.10 CLASSIFICATION OF BOND TESTS (Chen 2001) .....	39
Fig. 2.11 GENERLIZED STRESS-STRAIN CURVE FOR CONCRETE.....	42
Fig. 2.12 LOADING AND UNLOADING CURVES.....	44
Fig. 2.13 STRESS-STRAIN CURVES .....	45
Fig. 2.14 Model for Concrete under Cyclic Loading, taken from Darwin and Pecknold(1976) .....	46
Fig. 2.15 SCHEMATIC OF LOADING AND UNLOADING RESPONSE .....	48
Fig. 2.16 STEEL STRESS-STRAIN HISTORY AS PREDICTED BY PLASTIC THEORY .....	49
Fig. 2.17 ENGINEERING VERSUS NATURAL STRESS-STRAIN HISTORY FOR REINFORCEMENT STEEL SUBJECTED TO MONOTONIC TENSION AND COMPRESSION LOADING (Dodd and Restrepo-Posada (1995)) .....	53
Fig. 2.18 COMPARISSON BETWEEN EXPERIMENTAL AND FE RESULTS ....	55
Fig. 2.19 ANALYSIS OF FRP REPAIRED BEAM.....	56
Fig. 2.20 FINIOTE ELEMENT RESULTS (Zarnic et al. (1999)). ....	57
Fig. 2.21 BOND LINK ELEMENT.....	58
Fig. 2.22 BOND LINK ELEMENT.....	58
Fig. 2.23 Finite element mesh of Limam and Hamelin (1998). ....	59
Fig. 3.1 CFRP SHEAR DEBONDING.....	63

Fig. 3.2 SPECIMEN DESCRIPTION .....	65
Fig. 3.3 STANDARD CUBES BEFORE CASTING.....	68
Fig. 3.4 MIXING MACHINE.....	68
Fig. 3.5 CONCRETE CUBES UNDER TESTING.....	68
Fig. 3.6 SPECIMEN UNDDER TESTING .....	71
Fig. 3.7 SPECIMEN SCHEMATIC DESIGN.....	71
Fig. 3.8 SPECIMEN UNDDER TESTING .....	72
Fig. 3.9 SPECIMEN SCHEMATIC DESIGN.....	72
Fig. 4.1 MONOTONIC UNIAXIAL STRESS-STRAIN CURVE.....	83
Fig. 4.2 PROPOSED UNIFIED FAILURE SURFACE.....	87
Fig. 4.3 METHOD OF DETERMINING STATE OF STRESSES AT FAILURE.....	89
Fig. 4.4 STEEL CYCLIC MODEL .....	93
Fig. 4.5 STRESS-STRAIN RELATION OF CFRP UNDER CYCLIC LOADING..	94
Fig. 5.1 shear resisting mechanism .....	96
Fig. 5.2 PROPOSED MODEL FOR AGGREGATE INTERLOCK.....	98
Fig. 5.3 LOAD-DISPLACEMENT RESPONSE FOR DOWEL BAR.....	101
Fig. 5.4 LOAD-DISPLACEMENT RESPONSE FOR DOWEL BARS.....	102
Fig. 5.5 PROPOSED CYCLIC MODEL FOR BOND-SLIP MECHANISM.....	107
Fig. 6.1 FAILURE MODE OA AXIALLY LOADED SPECOIMEN .....	110
Fig. 6.2 MONOTONIC BOND-SLIP CURVE (AXIALLY LOADED CASE).....	112
Fig. 6.3 MONOTONIC BOND-SLIP CURVE (ECCENTRICALLY LOADED CASE) .....	113
Fig. 6.4 RELATION BETWEEN $\tau_b$ AND $\sigma$ (AXIALLY LOADED CASE).....	115
Fig. 6.5 RELATION BETWEEN $\tau_b$ AND $\sigma$ (AECCENTRICALLY LOADED CASE) .....	116
Fig. 6.6 SPECIMEN $B_6$ AFTER TESTING .....	118
Fig. 6.7 STRESS ACTING IN SHEAR PLANE.....	118
Fig. 6.8 CYCLIC BOND-SLIP CURVE (AXIALLY LOADED CASE).....	119
Fig. 6.9 CYCLIC BOND-SLIP CURVE (ECCENTRICALLY LOADED CASE)..	119
Fig. 6.10 $C_1$ - $N$ RELATIONSHIP.....	121
Fig. 6.11 $C_2$ - $N$ RELATIONSHIP.....	121
Fig. 6.12 $C_3$ - $N$ RELATIONSHIP.....	123
Fig. 6.13 $C_4$ - $N$ RELATIONSHIP.....	123
Fig. 6.14 $C_5$ - $N$ RELATIONSHIP.....	124
Fig. 6.15 $C_6$ - $N$ RELATIONSHIP.....	125

Fig. 6.16 $C_7$ - $N$ RELATIONSHIP.....	126
Fig. 6.17 $C_8$ - $N$ RELATIONSHIP.....	126
Fig. 6.18 $E_b - \text{Log}N$ (AXIALLY LOADED CASE).....	129
Fig. 6.19 $(E_w)_b - N$ (AXIALLY LOADED).....	130
Fig. 6.20 $E_b - \text{Log} N$ (ECCENTRICALLY LOADED).....	131
Fig. 6.21 $(E_w)_b - N$ (ECCENTRICALLY LOADED).....	131
Fig. 6.22 $\tau_b - \text{Log}N$ (AXIALLY LOADED).....	133
Fig. 6.23 $\tau_b - \text{Log}N$ (ECCENTRICALLY LOADED).....	133
Fig. 6.24 RELATION BETWEEN $\tau_b$ AND $\sigma$ (AXIALLY LOADED CASE).....	134
Fig. 6.25 RELATIONBETWEEN $\tau_b$ AND $\sigma$ (ECCENTRICASLLY LOADED CASE).....	135
Fig. 6.26 $C$ - $N$ (AXIALLY LOADED CASE).....	136
Fig. 6.27 $\tan\phi$ - $N$ (AXIALLY LOADED CASE).....	136
Fig. 6.28 $C$ - $N$ [(ECCENTRICALLY LODED CASE)].....	137
Fig. 6.29 $\tan\phi$ - $N$ [ECCENTRICALLY LODED CASE].....	138
Fig. 7.1 Incremental Method.....	148
Fig. 7.2 ELEMENT LOCAL COORDINATES SYSTEM.....	152
Fig. 7.3 DISTRIBUTED REPRESENTATION OF REINFORCEMENT.....	157
Fig. 7.4 EMBEDDED REPRESENTATION OF REINFORCEMENT.....	158
Fig. 7.5 DISCRETE REPRESENTATION OF REINFORCEMENT.....	159
Fig. 7.6 SPACE FRAME ELEMENT.....	160
Fig. 7.7 DEGREES OF FREEDOM CORRESPOND TO EACH TYPE OF DEFORMATION.....	161
Fig. 7.8 LOCAL AND GLOBAL COORDINATES SYSTEM.....	164
Fig. 7.9 Transformation for Vertical Element.....	165
Fig. 7.10 SPACE TRUSS ELEMENT.....	167
Fig. 7.11 3-D LINKAGE EWLEMENT.....	169
Fig. 7.12 16-NODE JOINT/INTERFACE ELEMENT.....	174
Fig. 7.13 DISCRETE CRACKING.....	182
Fig. 7.14 DISTRIBUTED CRACKING.....	184
Fig. 8.1 specimen descriptions:.....	187
Fig. 8.2 INSTURMENTATION.....	189
Fig. 8.3 BEAM SET UP.....	190
Fig. 8.4 FAILURE OF CONTROL BEAM (S0-1L).....	192

Fig. 8.5 (a) STRENGTHENED BEAM (S1-1L) BEFORE TESTING, (b) STRENGTHENED BEAM (S1-1L) AFTER TESTING.....	193
Fig. 8.6 (a) CONCRETE ELEMENT LAYOUT, (b) STEEL ELEMENT LAYOUT, (c) CFRP LAMINATES LAYOUT, (d) LINK ELEMENT LAYOUT and (e) 16-NODE INTERFACE ELEMENT .....	198
Fig. 8.7 CONCRETE STRAIN- <i>N</i> .....	199
Fig. 8.8 LONGITUDINAL STEEL STRAIN- <i>N</i> .....	200
Fig. 8.9 TRANSVERSE STEEL STRAIN- <i>N</i> .....	201
Fig. 8.10 CFRP STRAIN- <i>N</i> .....	202
Fig. 8.11 DEFLECTION- <i>N</i> .....	203
Fig. 8.12 LOAD-DEFLECTION RESPONSE .....	204
Fig. 8.13 LOAD DEFLECTION CURVES FOR DIFFERENT SHEAR SPAN- DEPTH RATIOS .....	205
Fig. 8.14 DEFLECTION- <i>N</i> .....	206
Fig. 8.15 DEFLECTION- <i>N</i> .....	208
Fig. 8.16 LOAD-DEFLECTION CURVES FOR DIFFERENT CFRP THICKNESSES .....	209
Fig. 8.17 FAILURE OF BEAM STRENGTHENED WITH TWO LAYERS OF CFRP LAMINATES.....	210

# CHAPTER 1

## INTRODUCTION

### 1.1 General

Rehabilitation of civil engineering infrastructure such as bridge deck slab, building, beams, girders, parking structures, marine structures, road etc is one of the major issues since last few years. The deterioration of such structures might be due to ageing, poor maintenance, poor environmental conditions, poor initial design, construction, and accidental situation like earthquake. The need to upgrade the deteriorated civil engineering infrastructures greatly enhances with ever-increasing demand. For example, continuous increase in traffic loading conditions should match with the initial design load assumption. Therefore, rehabilitation of existing civil engineering infrastructure has been identified as important issue to be addressed.

The aging infrastructure urged the engineers, researchers and organizations to seek alternative materials and techniques to regain the original capacity of the deteriorating and deficient structures. Advanced composite materials, known as fiber reinforced polymer (FRP) composites, have received significant attention as one of the most promising materials for use as external reinforcement for repair and strengthening of deficient reinforced concrete (RC) structures. FRP is a composite material generally consists of high strength carbon, aramid, or glass fibers in a polymeric matrix (e.g., thermosetting resin) where the fibers are the main load-carrying element. Among many options, this type of reinforcement may be in the form of preformed laminates or flexible sheets. The laminates are stiff plates or shells that are pre-cured and are installed by bonding them to the concrete surface with a thermosetting resin. The sheets are either dry or pre-impregnated with resin (known as pre-preg) and cured after installation onto the concrete surface. This installation technique is known as wet lay-up.

FRP materials offer to the engineers and practitioners an outstanding combination of physical and mechanical properties, such as high tensile strength, lightweight, high stiffness, high fatigue strength, and excellent durability characteristics. The lightweight and formability of FRP reinforcement make FRP systems easy to install. Since these systems are non-corrosive, non-magnetic, and generally resistant to chemicals, they are an excellent option for external reinforcement. The properties of FRP composites and their versatility have resulted in significant saving in construction costs and reduction in shut down time of facilities as compared to the conventional strengthening methods (e.g., section enlargement, external post-tensioning, and bonded steel plates).

Strengthening with externally bonded FRP, sheets are capable for variety of applications in different types of structural members. FRP sheets may be adhered to the tension side of structural members (e.g., slabs or beams) to provide additional flexural strength (Arduini et al (1996)). FRP may be adhered to web sides of joists and beams or wrapped around columns to provide additional shear strength (Berset et al (1992), Chajes et al (1995) and Sato et al (1996)). FRP may be wrapped around columns to increase concrete confinement and thus strength and ductility of columns (Nanni et al (1993)). Among many other applications, FRP sheets may be used to strengthen concrete and masonry walls for improvement their resistance against lateral loads (Hartley et al (1996) and Triantafillou et al (1996)) as well as circular structures (e.g., tanks and pipelines) to resist internal pressure and reduce corrosion (Arizona Public Service Corporation (1997)).

In recent years, several studies have been conducted to investigate the flexural strengthening of RC members with FRP; however, few studies have specifically addressed shear strengthening. Shear failure of RC members is catastrophic and occurs with no advanced warning or distress. In order to utilize the maximum ductility of RC members, it is recommended that its ultimate strength should be governed by flexure rather than shear. In several instances, existing RC beams have been found deficient in shear and required strengthening. Deficiencies are caused by many reasons such as insufficient shear reinforcement resulting from design errors or use of outdated codes, reduction in steel area due to corrosion, increase in demand of service load, and construction defects. Research on shear strengthening using externally bonded FRP reinforcement was first started by Berset et al (1992); most of the studies

in shear strengthening were focused on static loading condition. Shear strengthening techniques under cyclic loading conditions is one of the gaps in this area of research.

It required that the future research should be focused to study structural behaviour of RC beams externally strengthened for shear using CFRP laminates subjected to cyclic loading and further works also needed to develop a new interfacial model that enables to simulate the bond between FRP and concrete surface under cyclic loading.

## **1.2 Problem Statement**

To insure safety and adequate warning before failure happens; structures should be designed to fail in ductile mode. It is well known that the deficiency RC beams for cyclic performance is mainly induced by the lack of shear strength and ductility. The shear strength should be high enough in order to avoid the brittle shear failure that may occur before flexure failure. This is so-called strong-shear—weak-flexure philosophy. Thus, the shear strength should be evaluated for RC beams subjected to cyclic loads. It is evident that in members with shear-dominated behaviour the hysteretic loops are narrower than in the flexure-dominated slender members and attain a pronounced inverted *S*-shape, i.e. pronounced pinching. This indicates a very poor hysteretic energy dissipation capacity. Loops are narrow because the behaviour is controlled by the concrete along the compression diagonal, which leads to a rather limited capacity of deformation compared to flexure-dominated members in which the longitudinal reinforcement has a larger contribution to the overall deformation. Therefore the sources of potential structural brittle failure must be eliminated and degradation of stiffness and strength under cyclic loading must be minimized or delayed enough to allow sufficient energy to be dissipated through stable hysteretic behaviour. Under cyclic loading, opening and closing of diagonal cracks in two opposite directions tend to reduce the compressive strength and concrete stiffness; results in decreasing the effectiveness of aggregate interlock mechanism, which takes a major part of the shear stress after cracking. Limited spacing between internal transverse reinforcement necessitated the use of an external transverse reinforcement such as bonded CFRP laminates to improve the shear behaviour of RC beams subjected to cyclic loading.

The success of most of the strengthening or retrofitting technologies for concrete structures by using external bonded FRP sheets highly depends on the interface bond between FRP sheets and concrete substrates because the bonding interface is relatively weak in comparison with the neighbouring materials in the whole upgraded system. In most of strengthening cases, the interface bond is critical in transferring stresses from the existing concrete structures to the externally bonded FRP composites. Therefore, a good understanding on the interface bond is a prerequisite for achieving more reliable but rational design for concrete structures externally bonded with FRP composites. Interface must be included in any numerical model if the response is to be accurately predicted by such model. Various experimental and analytical investigations of the behavior of bonded FRP-to- concrete joints have been carried out. Researchers have proposed bond stress–slip relationship models including the linear cut off model, bilinear model, tri-linear model, and Popovics formula (Brosens et al (1999); Nakaba et al (2001) and Ueda et al (1999)) However, these models have generally been limited to monotonic loading conditions behaviors; cyclic bond behavior has not yet studied. This requires an improved mathematical modeling of hysteretic behavior of interface element, necessitating more experimental and analytical research on the interfacial behavior of bonded FRP-to- concrete joints under cyclic loading.

It is very clear that the experimental approach is costly and time consuming; also, it is limited to very little parameters. An advantages associated with the use of analytical approach like reduction in cost , ability to study overall response of structures by considering large number of parameters and acceptability to any new modifications due changes in standard codes make this approach more attractive than experimental one which has very limited scope. In addition, the use of the analytical approach in parallel with computer tools makes this approach faster with acceptable level of accuracy.

The analytical solution of a typical structural cyclic problem is considerably more complicated as compared to its static counterpart. For most practical situation, the solution is possible only using high-speed digital computer, which has become standard tools for structural analysis to this type of problems. An approach based on

finite element method provides a convenient and reliable idealization of the system and is particularly effective in digital computer analysis.

### **1.3 Objectives and Scope of this Investigation**

The principal objective of this research study was to investigate the fatigue performance of RC beams strengthened for shear with externally carbon fiber reinforced plastic, CFRP sheet.

The following are the specific objectives that serve the principal objective:

1. To develop an experimental methodology that enables to study the interfacial behaviour of CFRP-to concrete joints under cyclic shear loading that incorporate the following aspect:
  - To determine the effectiveness of using CFRP for extension of fatigue life of CFRP-to-concrete joints as well as cyclic bond stress– slip behaviour.
  - To derive mathematical formulas that calculate shear stiffness of interface element between CFRP side plats and concrete under cyclic shear loading and to investigate its degradation with respect to number of cycles.
  - To obtain the  $S-N$  curve for CFRP-to-concrete joints under pure shear as well as shear- moment interaction condition.
2. To propose a new experimental setup that enables to obtain failure criteria and constitutive relations for interface element under cyclic shear loading.
3. To develop a new analytical algorithm based on non-linear finite element method coded in FORTRAN language to investigate the efficiency of using CFRP as external shear strengthening reinforcement for RC beams subjected to cyclic loads.

### **1.4 Scope and Methodology**

The overall scope of this research study was divided into two major methodologies that describe as follows:

- Experimental method was designed to simulate the interfacial behaviour of side plated CFRP-to-concrete joints under cyclic shear loading.
- Analytical method was aimed to study the overall shear performance of reinforced concrete beams strengthened with CFRP laminates subjected to cyclic loading.

#### **1.4.1 Experimental study**

A new interfacial model was developed to simulate interfacial behaviour of side plated CFRP-to-concrete joints under cyclic shear loading. An experimental methodology consisted of testing of specified number of push off specimens was conducted. The CFRP composite strips were used herein to strengthen these specimens externally at a known failure plane to resist shear stresses in shear friction. The test setup and supports were designed such that there is a direct shear at the CFRP-to-concrete interface. Experimental results for cyclic bond stress-slip behaviour, *S-N* curve, failure criteria of interface and the mathematical formulations for stiffness of interface element and its degradation as number of cycles increased have been obtained and discussed. The results included the behaviours of interface under pure shear as well as shear-moment interaction conditions.

#### **1.4.2 Analytical Study**

An analytical model based on non-linear finite element algorithms coded in FORTRAN language has been developed to enable the analysis of RC beams externally strengthened for shear with CFRP laminates under cyclic loads. Selection of elements type for better idealization of structures in three-dimensional space, suitable cyclic models to predict the actual behaviour of the structures the non-linear analysis technique to solve the cyclic problem were discussed.

### **1.5 Thesis Outlines**

**Chapter 2** of this dissertation contains a brief review of CFRP materials and their applications in the structural engineering field. This included current experimental and analytical previous work in reinforced concrete beams strengthened with CFRP

laminates as well as previous models used in finite element method to simulate their behaviour under cyclic loading.

**Chapter 3** gives general out-lines about the methodology that was used in this research.

**Chapter 4** presents the material cyclic models that were used in this research to simulate the behaviour of concrete, steel and CFRP under cyclic loading. 3-D constitutive law uses an orthotropic model with the axes of orthotropic parallel to the principal stress directions was used to model the concrete. Principal strain and principal stress directions are not coaxial. Reinforcement bars were assumed to be elastic perfectly plastic. The behaviour of CFRP materials is assumed linear elastic until failure.

**Chapter 5** gives special consideration to simulate shear transfer mechanisms due to aggregate interlock in cracked concrete and dowel action in reinforcement. Expressions were derived from an analytical model in conjunction with experimental data to provide shear stress and stiffness values for special elements used to model aggregate interlock mechanism. A comparable approach was used to derive expression for dowel action mechanism. The bond-slip phenomenon between concrete and reinforcement was accounted for by using non-dimensional spring element.

**Chapter 6** provides complete information about the constructing of a new interaction model between sides plated CFRP and concrete under cyclic shear loading. The mathematical formulations govern the fatigue behaviour of interface element were approved.

**Chapter 7** gives a brief description of the finite element method. Element representation and mathematical formulation for stiffness matrix for each element are discussed. In this research, 20-noded brick element with three degrees of freedom per each node will be used to represent concrete and CFRP elements. The reinforcement bars were represented in discrete manner 2-noded space frame elements and space truss elements were used for this purpose. Three dimensional link elements were used

to represent shear transfer mechanisms due to aggregate interlock, dowel action and bond slip. 16-noded interface elements were used to model the interaction between CFRP and concrete. Discrete cracking approach was used to represent cracking. A computer program with combined-iterative method was used to solve the non-linear cyclic problem.

**Chapter 8** describes some applications for RC beams strengthened for shear using CFRP laminates. An experimental investigation carried out by Omar Chaallal et al (2009) has been chosen to test the efficiency of the analytical algorithm. The analytical results obtained from the finite element algorithm were compared with corresponding results that obtained from the experimental investigation. A parametric analysis has been carried out to study the effect of controlling factor such as shear – span depth ratio, thickness of CFRP laminates and compressive strength.

**Chapter 9** shows the main output from this investigation and gives general recommendations for further work. The new experimental methodology studied in this investigation proved appropriate and valid. The comparison between the analytical results and the published results proved that the non-linear finite element algorithm is powerful tool to study the structural behaviour of RC beams strengthened for shear using CFRP laminates for cyclic loading as well as monotonic conditions with acceptable level of accuracy. A parametric analysis showed that the shear span-depth ratio and CFRP thickness are main factors controlling the behaviour of such element.

## **CHAPTER 2**

### **LITERATURE REVIEW**

#### **2.1 Introduction**

The principal aim of this literature review was to understand the concept of CFRP application for strengthening and upgrading of concrete structures, to study the issues and problems reported by researchers and to find out the possible gaps that needed to be further investigated. Following were the focus areas, where a number of research material were reviewed:

- Historical back ground, definition of FRP , their advantages, types and method of bonding
- Flexural strengthening
- Shear strengthening
- Bond of FRP Sheet-concrete interfaces
- Materials cyclic models
- Finite element (FE) modelling: techniques and algorithms

##### **2.1.1 Historical Back Ground**

FRP products were first used in reinforced concrete structures in the 1950s. At that time material properties, construction and fabrication techniques were not very advanced. The significant use of such materials for external reinforcement of concrete bridge structure's was initially started in the 1980s, as a substitute to steel plate bonding and later on substituted the steel confinement shells of bridge columns. The external retrofiting techniques were primary developed in Japan (sheet wrapping) and Europe (laminare bonding). Currently more than a thousand concrete girder bridges in Japan have been strengthened with sheet bonding to the slabs. In

addition, many thousands of bridge columns have been seismically upgraded with the same materials. Ongoing development of cost-effective production of FRP composites has progressed to the level that they are ready for the construction industry. Reduced material cost, coupled with labour savings inherent with its low weight and comparably simpler installation, relatively unlimited material length availability, and immunity to corrosion, make FRP materials an attractive solution for post strengthening, repair and seismic retrofit. Concrete structures can be turned into an unacceptable structural condition due to decrease in material behaviour or the increase in loading conditions of the structure. Now as result of strengthening the concrete structure using external FRP reinforcements, the structural lifetime could be extended to an acceptable level. The principles behind externally bonding FRP plates or wraps to concrete structures are very similar to the principles used in application of bonded steel plates. In general, the member's flexural, shear, or axial strength is increased or better mobilized by the external application of high tensile strength material. FRP composite systems have been applied to many structural elements including beams, columns, slabs and walls as well as many special applications such as chimneys, pipes and tanks. More recently, such techniques have been applied to infrastructure security applications relating to hardening and blast mitigation of structures.

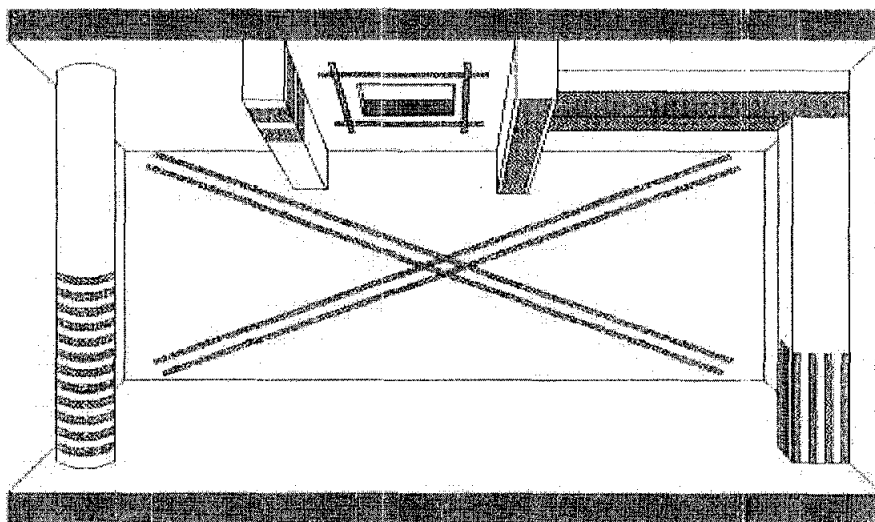


Fig. 2.1 TYPICAL APPLICATIONS OF FRP IN STRENGTHENING OF RC STRUCTURES

### 2.1.2 Definition of FRP

Fiber Reinforced Polymer (FRP) composites is defined as a polymer (plastic) matrix, either thermo set or thermoplastic, that is reinforced (combined) with a fiber or other reinforcing material with a sufficient aspect ratio (length to thickness) to provide a discernable reinforcing function in one or more directions.

FRP composites consist of high strength fibbers embedded in a polymer resin. The fibbers are the main load-carrying element and have a wide range of strengths and stiffness that exhibit a linear stress-strain relationship until failure. Typically, types of Fibres used in the fabrication of FRP composites for construction are carbon, glass, and aramid, which are commercially available as continuous filaments.

The polymer resin surrounds and encapsulates the fibbers to bind them together, protect them from damage, maintain their alignment, and allow distribution of load among them (see Fig.2.1). Polymers are available as two categories, thermosetting polymers (e.g. epoxy and polyester) and thermoplastic polymers (e.g. nylon). The chemical compositions and mechanical properties of the various types of fibbers and polymers are currently given in many textbooks.

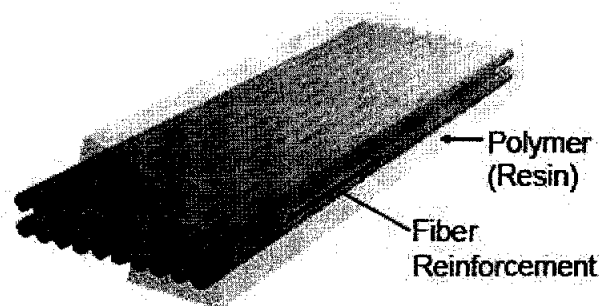


Fig. 2.2 REPRESENTATION OF FRP MATERIAL

The corrosion of steel plates, deterioration of bond between steel and concrete, installation difficulties because of employment heavy equipments have been identified as major drawback of bonding steel plate technique. FRP composites have become more popular and accepted by designers, contractors, and owners due to combinations of their unique characteristics.

### 2.1.3 Advantages of FRP Materials

There are many of advantages of using FRP system such as:

1. **High strength and stiffness retention:** The ultimate strength is 8 to 10 times higher than that of steel plate.
2. **Resistance to environmental factor:** FRP systems are non-corrosive, non-magnetic, and generally have excellent resistant to chemical attack, so there is no harm of corrosion that is usually associated with the use of steel plates, particularly if the concrete to which they are fixed is cracked or chloride contaminated.
3. **Low weight:** Density of FRP materials is about one fifth of the density of steel, so it can be easy transported without need of subsequent crane age facilities.
4. **Simple installation:** Man-access platforms are enough for handling and installing in FRP system rather than full scaffolding platforms used in steel plate technique. Installing of FRP system does not require extensive jacking and support system to move and hold in place.
5. **Unlimited material length availability:** FRP are available in very long lengths while steel plates are generally limited to 6 m lengths.
6. **Reduction in construction period:** It can be installed within a very short time periods compare with time taken for installing of steel plates
7. **Labour saving:** low weight, simple installation and limited construction period result in decreasing the cost of labour of FRP system
8. **Durability factor:** FRP system does not require maintenance that may cause traffic disruption and access cost associated with use of steel plate system.
9. **Flexibility:** FRP come in very thin layers with negligible flexural stiffness and can easily follow a curved profile without any pre-shaping. In addition, irregularities of the concrete surface can easily be taken up. This is solved the shortcoming of using Steel plates which have their own shape and non-negligible flexural stiffness. Therefore when applied to a structural element of a slightly different shape, due to construction tolerances, initial stresses are induced in the plates and in the bonding system (resin/bolts). Also for a curved surfaces the material need to be bent in advance.

The main disadvantages of FRP materials are the risks of fire and accidental damage. A particular concern for bridges over roads is the risk of soffit reinforcement being

ripped off by over height vehicles. The materials are relatively expensive but generally, the extra cost of the material is balanced by the reduction in labour cost. In addition, it is still difficult to find contractor with the appropriate expertise for the application FRP.

#### **2.1.4 Feature and Benefit**

The main feature and benefit of FRP system technique are:

1. **Repair damaged concrete structures:** FRP composite systems can be used to repair damaged concrete structures. It restores the structure to pre-damaged load rating.
2. **Strengthening:** It can be used to strengthening undamaged concrete structures that require greater load capacity due to functional change, additional load, code change or other reasons
3. **Seismic retrofit:** Because FRP is heterogeneous material, the FRP have possibility to produce both excellent static and dynamic properties. It can be used to strengthening structures in seismically active regions to satisfy seismic requirements, which are not included in their initial design.

The use of FRP composites system is accomplished by utilizing the tensile strength and stiffness of the composite and the strain compatibility of the composite to the existing member. The design must include proper selection of the adhesive used to bond the FRP reinforcement to the surface of the concrete to be strengthened. The type of composite, the number of layers, the orientation of fibbers, and the preliminary work and surface preparation, all depend on the design goals and type of structural element as determined by the project.

#### **2.1.5 Types of Fibres**

The selection of the type of fiber to be used for a particular application is depended on the factors such as the type of structure, the expected loading, and the environmental conditions.

Following fibbers are commonly used for strengthening and upgrading

- Carbon fiber
- Glass fiber
- Aramid fiber.

#### **2.1.5.1 Carbon Fibres (CFRP)**

Carbon fibbers are used for the fabrication of high performance composites and are characterized by their high value of strength and stiffness. The failure is usually brittle with low energy absorption. They are not very sensitive to creep and fatigue and exhibit negligible loss of strength in the long term. Fibres have a crystalline structure similar to graphite's one which is hexagonal, with carbon atoms arranged in planes held together by Van Der Waals forces. Atoms in each plane are held together by covalent bonds, much stronger than Van Der Waals forces, resulting in high strength and stiffness in any direction within the plane. The modern technology of production of carbon fibbers is based on the thermal decomposition in the absence of oxygen of organic substances, called precursors. The most popular precursors are polyacrylonitrile and rayon fibbers. Fibres are first stabilized, through a thermal treatment inducing a preferential orientation of their molecular structure, and then they undergo a carbonization process in which all components other than carbon are eliminated. The process is completed by a graphitization during that, the fibbers are crystallized in the form similar to graphite. Fibres with carbon content higher than 99% are sometime called graphite fibbers.

#### **2.1.5.2 Aramid Fibres (AFRP)**

Aramid fibbers are organic fibbers, made of aromatic polyamides in an extremely orientated form. Introduced for the first time in 1971 as "Kevlar", these fibbers are distinguished for their high tenacity and resistance to manipulation. Their strength and stiffness is usually in the middle of that of glass and carbon fibbers. The compressive strength is usually about 1/8 of the tensile strength; that is due to the anisotropy of the structure of the fiber that made the compression loads to trigger the localized yielding and buckling, which resulted in the formation of kinks. This kind of fibbers can

decompose under sunlight that can cause a loss of strength of up to 50%. They can also be sensitive to moisture, exhibit creep and sensitive to fatigue. The technology of fabrication is based on the extrusion of the polymer at high temperature in a solution and subsequent rapid cooling and drying. The synthesis of polymer is done before the extruding equipment by using Awdic solutions. It is finally possible to apply a thermal orientation treatment to improve the mechanical characteristics.

### 2.1.5.3 Glass Fibres (GFRP)

Glass fibers are widely used in the naval industry for the fabrication of composites with medium to high performance. They are characterized by high strength. Glass is mainly made of silica ( $\text{SiO}_2$ ) in the tetrahedral structure. Aluminium and other metal oxides are added in different proportions to simplify processing or modify some properties. The technology of production is based on the spinning of a batch that is essentially made of sand, alumina and limestone. The components are dry mixed and melted at  $1260^\circ\text{C}$ . Fibres are originated from the melted glass. Glass fibers are less stiff than carbon and aramid fibers are sensitive to abrasion effect. Due to the latter care must be used when manipulating fibers before impregnation. This kind of fibers exhibit non-negligible creep and are fatigue sensitive.

A comparison among carbon FRP, aramid FRP (AFRP), and glass FRP (GFRP) sheets (Nanni et al 1993) and reinforcing steel in terms of stress strain relationship is illustrated in Fig. 2.3.

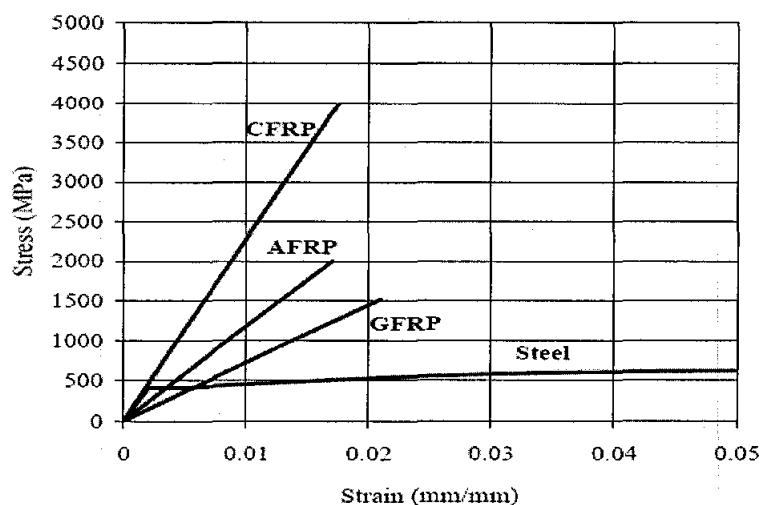


Fig. 2.3 COMPARISON AMONG CFRP, AFRP, GFRP SHEETS AND STEEL

Forms of FRP system are categorized based on the method of delivery and installation at site as follows:

- Wet lay-up
- Pre-cured
- Near Surface Mounted (NSM)

*Wet lay-up* systems consist of dry unidirectional or multidirectional fiber sheets or fabrics that are impregnated on-site with a saturated resin, which is used to provide a binding matrix for the fiber and bond the sheets to the concrete surface. Wet lay-up systems are saturated with resin and cured in place and in this sense are analogous to cast-in-place concrete. This system is flexible and suitable for irregular structures because it can be easily shaped on site to cope with complex shapes.

*Pre-cured* systems consist of a wide variety of composite shapes manufactured in the system supplier's facility and shipped to the job site. Typically, an adhesive is used to bond the pre-cured flat sheets, rods or shapes to the concrete surface or inserted into slots cut into the wall. In a technique the adhesive does not become the matrix for the FRP, so a well-defined bond-line is created. This technique does not offer the flexibility as exhibits by the wet lay-up procedure.

*Pre-cured (NSM)* systems are generally applied as an alternative for reinforcing concrete and masonry structures similar to surface laminates. *NSM* Rods/shapes provide a discrete solution to strengthen the structures; the rods are generally inserted into the masonry or concrete structure through slots or saw cuts. Generally, shapes can vary in size depending on application but typically are provided in round and rectangular cross-sections. An epoxy adhesive or cementitious grout is used to bond the pre-cured rods in the groove cut into the surface. Adhesive are applied for the proper transfer of load between the wall and the cured reinforcement. Table 2.1 gives general descriptions about the main characteristic and typical applications aspect for each type.

Table 2.1 MAJOR CHARACTERISTIC AND APPLICATIONS OF FRP COMPOSITES

Descriptions	Pre-cured (Pre-fabric)	Cured in situ (Wet lay-up)
Shape	Strip or laminates	Sheet or fabric
Thickness	About 1-1.5mm	About 0.1-0.5mm
Use	Simple bonding of factory made element with adhesive	Bonding and impregnation of sheet or fabric with resin(shaped and cured in situ)
Typical applications aspect	<ul style="list-style-type: none"> <li>- If not pre-shaped only for flat surfaces</li> <li>- Thixotropic adhesive or bonding</li> <li>-Normally one layer, multiple layer possible</li> <li>- Stiffness of strip and use of thixotropic adhesive allow for certain surface unevenness</li> <li>- Simple in use high quality guarantee (pre-fabric system)</li> </ul>	<ul style="list-style-type: none"> <li>- regardless of the shape, sharp corners should rounded</li> <li>- low viscosity resin for bonding and impregnation</li> <li>- often multiple layers</li> <li>- often a putty is needed to prevent debonding due to unevenness</li> <li>- very flexible in use, need rigorous quality control</li> </ul>
	Quality control(wrong application and bad work man ship loss composites action between FRP and substrate structure	lack of long term integrity of the system

### 2.1.6 Types of Resin

There are many types of resins used with FRP system; the most commonly used resin can normally be used in different environmental conditions. According to ACI committee 440 (2002), FRP systems require the following characteristic of resin:

- Compatibility with and adhesion to the concrete substrate and FRP system
- Resistance to environmental effect
- Filling ability and workability
- Pot life consistent with the applications
- Development of appropriate mechanical properties of FRP system

The most common resins used in the field of civil engineering are epoxy resins. In some cases polyester or vinyl, resins can also be used.

#### ***2.1.6.1 Epoxy Resins***

Epoxy resins are better moisture repellent and offer good resistance to chemical attacks; their maximum working temperature depends on the type of epoxy but is typically below 60° C. Now a days epoxy resins with higher working temperatures are available, usually there are no limits on the minimum temperature. The main reagent is composed by organic liquids with low molecular weight containing epoxy groups, rings composed of two atoms of carbon and one atom of oxygen. The pre-polymer of the epoxy is a viscous fluid, with a viscosity depending on the degree of polymerization. A polymerizing agent is added to the above mix to solidify the resin.

#### ***2.1.6.2 Polyester Resins***

Polyester resins are characterized by a lower viscosity when compared to the epoxy resins. However, their chemical resistance and mechanical properties are not as good as that of epoxy resins. Polyesters are polymers with high molecular weight and double bonds between carbon atoms, capable of chemical reaction. At ambient temperature, the resin is usually solid; a solvent is added before use. The latter also reduces the viscosity of the resin and facilitates the impregnation of the fibbers.

### **2.1.7 Bonding of FRP Composites**

FRP are chemically bonded to the structural elements through adhesives. Chemical bonding is the most practical method because it does not induce stress concentrations, is easier than the mechanical devices to be installed and does not damage the base material and/or the composite. The most suitable adhesives for composite materials are epoxy resin based adhesives. An adhesive is made of a two-component mix; the principal component is consisted of organic liquids containing epoxy groups, rings composed of an oxygen atom and two carbon atoms. A reagent is added to the above mix to obtain the final compound.

The adhesive adhere to the materials to be bonded through interlocking and the formation of chemical bonds. The preparation of the surfaces to be bonded plays a key role for the effectiveness of the adhesive. Treatments of the surfaces can be done as:

1. Construction defects, remarkable deterioration and cracking in the surface of concrete shall be repaired appropriately, embrittled sections , projections, level differences and other unevenness in the surface of concrete shall be removed through chipping or polishing to make the surface smooth
2. Treatments of the surfaces are aimed to have a clean surface, free of any contaminant such as oxides, powders, oils, fat and moisture. Cleaning is performed using solvents and same tunes sand blast is done for preparation of a rough surface to obtain good interlocking. The surface of pre-impregnated laminates is often ready for the application of the adhesive and protected by a tape to be removed right before the application. For porous surfaces, a priming coat may be required, which must be compatible with the adhesive.
3. When continuous fiber sheets and continuous fiber strands are placed perpendicular to corner angles, the corner angles shall be rounded through chipping or polishing, or using a smoothing agent.

When the material is placed on the prepared concrete, sufficient pressure is applied with rollers to ensure a uniform adhesive layer and to expel any entrapped air, remove surplus adhesive epoxy from sides of plates while adhesive is uncured. Finally, the impregnation resin is cured thoroughly.

## **2.2 Strengthening of Concrete Structures**

### **2.2.1 Flexural Strengthening**

There is a wide range of research pertaining to the use of FRP in bridge repair. Rebar, grating into concrete, and wrapping around columns and piers are just a few examples of the broad applications of these composites (Norris & Saadatmanesh, 1994).

The following section was limited to research of FRP material externally bonded to the tensile face of concrete beams. In particular, research studying the effect of externally applied FRP materials on the flexural performance of reinforced concrete beams was reported.

### ***2.2.1.1 Analytical Studies***

An et al. (1991) developed a model to predict the stresses and forces of a reinforced concrete beam with externally applied glass fiber reinforced plastics (GFRP). Their study was based on five assumptions: 1) linear strain distribution throughout the beam; 2) small deformations; 3) tensile strength of concrete was ignored; 4) shear deformation was ignored; 5) perfect bond between concrete and GFRP. They used classical flexural theory and strain compatibility effects, variables such as material strength, modulus of elasticity, and reinforcement ratios of the steel and GFRP were considered. Analytical results were compared with experimental results of an earlier research done by (Saadatmanesh & Ehsani (1991)). Predicted results based on model were found in well agreement with experimental.

Triantifillou & Plevris (1991) used strain compatibility and fracture mechanics to analyze reinforced concrete beams strengthen with externally bonded carbon fiber reinforced plastics (CFRP). They use the same assumptions as An et al. (1991) used that included rectangular compression stress distribution in the concrete at failure. The applied moments that would cause each of the three failure modes were predicted. The three failure modes were yielding of the steel reinforcement followed by CFRP rupture; yielding of the steel reinforcement followed by the crushing of the concrete compression zone; and concrete crushing before the failure of tensile component fails. These models were compared with experimental studies and seemed creditable.

Moment, stiffness, and deflection models of reinforced concrete beams with applied FRP were developed by Bhutta (1993). Glass, carbon, and kelvar fiber reinforced plastics were utilized. Beams reinforced with kelvar showed the highest increase in moment capacity and stiffness, while the smallest was the beams

reinforced with glass. The moment capacity of beams reinforced with carbon was found in between these two composites.

Naaman and Jeong (1995) developed a new definition for the measurement of the ductility index. According to Naaman and Jeong, the conventional definition, which is based on yielding of the reinforcement, is inappropriate for evaluating concrete beams that are reinforced with FRP. This is due to the inability of most FRP materials to yield.

The new definition is defined as the ratio of the total energy of beam and the elastic energy released at failure. This index is applicable to concrete beams reinforced with steel tendons, FRP tendons, or a combination of both. To determine the proposed ductility index, a series of 24 pre-stressed concrete beams, which were previously tested by Naaman and Jeong and other researchers, were studied. The results showed the FRP pre-stressed concrete beams have less ductility than pre-stressed concrete beams with steel strands. In addition, the proposed ductility index accurately predicted the ductility of the beams.

### ***2.2.1.2 Experimental Studies***

Experimental studies involved bonded CFRP to reinforced concrete beams is being performed by Meier et al. since 1985 at the Swiss Laboratories for Materials Testing and Research. This program envisions the replacement of steel plates with FRP laminates for repairing and strengthening of reinforced concrete beams by examining the strength and stiffness of beams with unidirectional CFRP plates was the primary focus of their past research. An earlier study by Meier et al., (1991) encompassed externally bonding CFRP sheets to twenty-six concrete beams. Each beam dimension was (6"x10"x79") and minimally reinforced with 2 5/16" diameter bars on top and bottom and shear reinforcement 1/4" link at every 8 1/2". The test set-up consisted of a four point loading on simple supports. By applying a unidirectional CFRP laminate sheet (0.012"x8"x79") to the tensile side of the specimens the deflection of the strengthened beam was found to be 50% lower than that of the control beam. The cracks in the repaired beams were small and closely spaced along the length of the member. That contradicted the crack pattern of control beam, which was like a classic

reinforced concrete crack pattern of fewer and larger cracks. This study was the first evidence that FRP laminates could help in the repair of deteriorated concrete beams. Meier et al. (1991) also studied the failure modes related to FRP repaired beams. A preliminary study dealt with three different failures:

1. Tensile failure of the CFRP sheets.
2. Classical concrete failure in the compressive zone.
3. Continuous peeling-off of the CFRP sheets due to an uneven concrete surface

Tensile failure of the CFRP is described as very sudden and explosive, but is easily predicted due to cracking sounds. Peeling-off of the laminate is caused by vertical displacement across shear cracks in the concrete. In the following year, Meier et al. (1992) expanded the possible failure modes to nine. The additional six failures are as follows:

1. Shearing of the concrete in the tensile zone.
2. Interlaminar shear within the CFRP sheet.
3. Failure of the reinforcing steel in the tensile zone.
4. Cohesive failure within the adhesive.
5. Adhesive failure at the interface CFRP sheet/adhesive.
6. Adhesive failure at the interface CFRP concrete/adhesive.

The latter three were not observed but described as “theoretically possible”.

The first full-scale FRP strengthened beam tests conducted in the United States were reported by Saadatmanesh & Ehsani (1991). The tests consisted of six large concrete beams, five rectangle cross-sections (8”x18”) and one T-beam (3”x24” flange, 8”x18” web). All the specimens were 192” long and tested as a simple span at four points loading. Steel reinforcement ratios, shear reinforcement, and cambering were varied in all the six beams. However, the externally applied GFRP was identical for each beam (1/4”x10”x168”). The research concluded that adding of GFRP plates improved the strength and stiffness of the specimens. The tests showed the GFRP sheets carried a portion of the tensile force, which cause decrease in the stress in the steel reinforcement. This was particularly observed in the smaller steel reinforcement ratios.

Unidirectional and bi-directional GFRP sheets bonded to concrete beams using epoxy adhesive and a combination of epoxy and bolts were investigated by Deblois et al. (1992). A series of specimens (5"x5"x40") reinforced with steel (2- 7/16" diameter bars) in the tension region and shear reinforcement consisted of one of the following lay-ups for the GFRP:

1. Bi-directional sheets with epoxy bonding.
2. Bi-directional sheets with combination epoxy and bolt bonding.
3. Unidirectional sheets with epoxy bonding.
4. Combination of unidirectional and bi-directional sheets with epoxy and bolt bonding.

The unidirectional sheets increased the ultimate load by 58% over the control beam, while the bi-directional laminate caused a 32% increase in the load. However, the maximum load was observed with a combination of the two sheets. The maximum load of this specimen was 77% larger than that of the control beam. The two bonds capacity used with the bi-directional sheets caused very little difference in the ultimate load. The beam bonded with the addition of bolts increased the ultimate load to 2% as compared to the epoxy-bonded beam.

Additionally, a larger specimen (8"x12"x160"), strengthened using the combination of the two GFRP sheets, was tested. Similar to the previous results, the maximum load capacity increased 66% with respect to the control beam. Due to the GFRP sheet, the ductility of all the beams decreased along with the deflection due to maximum load.

Ritchie et al. (1992) tested sixteen concrete beams (6"x12"x108") with minimum steel reinforcement (2- 1/2" diameter bars) to study the effects of external strengthening using three different types of FRP; glass, carbon, and aramid fibers. The beams were tested in flexure under four-point loading. An analytical model was also developed to predict the strength and stiffness of the FRP strengthened beams. The results showed an increase in stiffness from 17% to 99% and an increase in strength of 40% to 97% based on the type, amount, and orientation of FRP that was applied to the beam. In addition, the predicted and actual behaviour showed good agreement, except that the analytical model predicted a slightly stiffer response than that observed during the tests. Ritchie et al. also investigated the anchorage methods

for the FRP, because the beams during initial tests were failed at the ends of the FRP plate instead of at the constant moment region, a series of anchorage types were developed for the reason to shift the failure in the constant moment region. The first consisted of anchoring the ends of the plate with fibreglass angles. This led to a larger load capacity, but the failure was still located at the ends of the plate. The second method consisted of wrapping FRP plates around the beam at the ends. This type also increased the load capacity, but was unsuccessful in transferring the failure to the constant moment region. The final method consisted of extending the plates up to the supports. This method was very successful in both increasing the load capacity and shifting the failure to the constant moment region.

Norris and Saadatmanesh (1994) cast thirteen concrete beams for flexural tests to compare three different fiber/epoxy systems and several orientations of fiber. The beams

(5"x8"x96") contained close to the minimal amount of steel reinforcement (two 3/8" diameter bars) and were over-designed against shear. Some beams were pre-cracked before the application of the CFRP to see if pre-cracking caused any substantial differences in behaviour. Two types of fiber were tested with 0°, 90°, and ±45° orientations, and the third fiber was used with orientations of 0°/90° and ±45° with respect to the longitudinal axis. The same fiber weight was applied to every beam. The research showed little difference in the results between the fiber types or the behaviour between pre-cracked and uncracked beams, but the different fiber orientations provided amiable results. The unidirectional fibbers (0°) yielded the largest strength and stiffness increase and deflection decrease with respect to the control beam. These beams failed very abruptly due to the peeling-off of the CFRP. The 0°/90° fibbers had a maximum strength, which was 20% less than the unidirectional, but showed much more ductility and deflection (40% greater than 0°). They also failed less explosively than the unidirectional fibbers. A 45% decrease in strength and stiffness occurred with the ±45° laminate compared to the 0° orientation. However, the ±45° laminate experienced much more ductility than the other lay-ups. Failure of the beam applied with ±45° laminate acted in such a slow, ductile manner that loading had to be stopped. Norris et al. concluded that off-axis CFRP laminates need to be studied at length. Use of different orientations could increase the strength

and stiffness of concrete beams without causing catastrophic, brittle failures associated with unidirectional laminates. In addition, they may provide ductile yielding properties that are very important in the civil engineering field.

Shahawy et al. (1995) assessed the effectiveness of external reinforcement in terms of the cracking moment, maximum moment, deflection, and crack patterns. Four beams (8"x12"x108") were tested using minimum steel reinforcement (two ½" diameter bars) and varying the layers of unidirectional CFRP. In addition, non-linear finite element computer model was used to compare to the results of the experiment. The cracking moment of the CFRP repaired beams was much larger than that of the control beam. For one, two, and three layers of GFRP, the cracking moment increased 12%, 61%, and 105%, respectively. The maximum moment also became larger and corresponded well to the theoretical data. A 13%, 66%, and 105% increase was observed for the three different layers. This showed the CFRP behaved similarly before and after cracking of the beam. The deflection and cracking patterns showed results similar to experiments previously discussed. The deflection decreased inversely with the number of CFRP layers on each beam. This, alternatively, caused the stiffness to increase. The cracking patterns between the control and the CFRP repaired beams exhibited different patterns. The control had wider cracks while the repaired beams showed smaller cracks at relatively close spacing. This shows an enhanced concrete refinement due to the CFRP sheets.

The research by Bazaa et al. (1996) was based on optimizing the length and orientation of the CFRP to increase beam strength and ductility. Eight beams (8"x12"x120') were minimally reinforced with steel (two 7/16" diameter bars) and over designed for shear to cause a flexural failure. One beam was used as a control while the others were bonded with three layers of CFRP (0.012"x6.6"). The sheets varied in length and orientation of the fibers. Four had unidirectional fibers with different lengths, and the other three had various fiber directions with regard to the longitudinal direction ( $\pm 6^\circ$ ,  $\pm 9^\circ$ ,  $\pm 12^\circ$ ). The results of the experiment showed an increase in strength and stiffness and a decrease in deflection as compared to the control beam. All failures occurred at a load at least 57% higher than the control beam. The stiffness was similar until the cracking moment. At this point, less

deflection was observed in the repaired beams. The load versus deflection plots exhibit three different section modulus; the start of the experiment to first crack, first crack to yielding of the steel began, and yielding of the steel to failure of the member. The use of small angle, off-axis laminates and different CFRP sheet lengths had no effect on strength or stiffness of the repaired beams. However, the off-axis CFRP provided improved warning of failure due to a cracking sound.

### ***2.2.1.3 Summary of Flexural Strengthening:***

The following remarks are drawn from the previous studies related to flexural strengthening of RC beams using FRP laminates that may lead to determine gaps:

1. Past research concluded applying FRP to the tensile face of a reinforced concrete beams increases the stiffness and load capacity and decreases the deflection of reinforced concrete beams.
2. failure modes of strengthened beams can be divided into two categories
  - Full composites action of concrete and FRP is maintained until concrete reaches crushing in compression or FRP fails in tension (classical failure).
  - Composites action of concrete and FRP is lost prior to failure due to debonding or peeling-off of FRP. Premature failure may occur before ultimate flexural capacity of the beam is reached owing to debonding, therefore bond failure mode need careful consideration.
3. Using of end anchorage system improve the load carrying capacity of strengthened beams. Mechanical anchorage accomplished with anchor bolts and anchor plates can verify by confirming that the anchorage has sufficient strength to prevent anchorage failure.
4. The strength gain and reduction in ductility are the two main sub sequences for flexural strengthening of RC beams with FRP plates. Beams, which fail by crushing of concrete when a large mount of FRP used, shows much reduced ductility. This mode is brittle and certainly undesirable.

## **2.2.2 Shear Strengthening of RC Beams using FRP**

### **2.2.2.1 Background**

Shear collapse of RC members is catastrophic and occurs with no advance warning distress. Existing RC beams with shear deficiencies ultimately need strengthening. Deficiencies may occur due to factors such as insufficient shear reinforcement, reduction in steel area due to corrosion, increased service load, and design/construction defects. In such situations, it has been shown that externally bonded FRP sheets increase the shear capacity significantly.

This section contains some of the published research studies regarding the shear strengthening of RC members with externally bonded FRP reinforcement. The first research focusing on shear strengthening of RC beams with composite materials was performed by Berset et al (1992) by testing RC beams with externally bonded (GFRP) laminates. Berset proposed a simple analytical model to compute the contribution of the external reinforcement to the shear capacity similarly to stirrups contribution and based on a maximum allowable strain, which is determined from experiments. Uji et al (1992) carried out the tests of eight simply supported RC beams strengthened for shear with CFRP sheets using two different wrapping schemes, total wrap or two sides of the beam. He concluded that the application of CFRP substantially improves the shear capacity of RC members. He also found that the strains in the stirrups and the CFRP were different even at the same location. This is because a stirrup stretches evenly over its length, while only a limited area of CFRP stretches at the crack. Thus, the strain in CFRP is greater than in stirrups at the crack location. In his study, the maximum shear force carried by CFRP was assumed the product of the bond area assumed as the triangle above the middle point of the diagonal crack and the bond stress of 1.27 MPa, which was determined based on his test results.

Chajes et al (1995) tested T-beams to study the effectiveness of externally bonded composites for shear capacity. Woven composites fabrics made of aramid, E-glass, and carbon fibers were used in their study. For beams with external reinforcement, the average increase in ultimate strength of 83 to 125 percent was observed. In their study, the FRP contribution to shear capacity was modelled similar to stirrups

contribution. It was assumed that an average FRP strain of 0.005 mm/mm that was determined from the tests, governed the design. However, the specimens used in this study were very small and only one wrapping scheme was used (i.e. U-wrap).

Umezu et al (1997) carried out an extensive experimental program in order to determine the effects of aramid and carbon FRP sheets on the shear capacity of simply supported RC beams. They used total wrap as strengthening scheme for all of their test beams. The application of FRP sheets was found to enhance shear capacity and deformation characteristics. Based on analysis, they stated that the contribution of AFRP to shear capacity could be evaluated by the truss theory, based on an average stress of AFRP equal to the tensile strength of the sheet multiplied by a reduction coefficient that was determined from the test results as 0.4.

Araki et al (1997) tested RC beams strengthened with various types and amount of much wrapped FRP sheets under anti-symmetrical moment condition. The conclusion was that the shear capacity of RC members increased in proportion to the amount of FRP sheets. The contribution of FRP to the shear capacity was evaluated similar to calculation of stirrups contribution. A reduction factor to the tensile strength of the sheets was proposed. In this study, the values of 0.6 and 0.45 were adopted for CFRP and AFRP sheets, respectively.

Malek and Saadatmanesh (1998) presented a method for calculating the inclination angle of the shear cracks as well as the ultimate shear capacity of RC beams strengthened for shear with bonded FRP plates. The compression field theory was used in their analysis. The model included simplified assumptions such as no stress concentration effect and complete composite action between the FRP plate and the beam. It was, however, shown that shear failure of the strengthened beams was controlled by either FRP fracture at a stress level below its ultimate strength due to stress concentration or by debonding of FRP from the concrete surface.

A design model for computing the shear capacity of RC beams strengthened with FRP composites was presented by Ttraintafillou et al (1998), in his model, the external FRP shear reinforcement was treated similar to the internal reinforcement. It was assumed that at the ultimate shear limit state the FRP develops an effective strain,  $\epsilon_{fe}$ , which is

less than the ultimate tensile strain,  $\epsilon_{fu}$ , of FRP. The expression for computing the FRP contribution to the shear capacity of an RC beam,  $V_f$ , was determined as:

$$V_f = \frac{0.9}{\gamma_f} \rho_f E_f \epsilon_{fe} b_w d (1 + \cot\beta) \sin\beta \dots\dots\dots 2.1$$

Where

$V_f$  = The partial safety factor for FRP in tension, which is recommended as 1.15

$\rho_f$  = The FRP area fraction that is equal to  $(2 t_f / b_w)(w_f / S_f)$

$t_f$  = The FRP reinforcement thickness

$w_f$  = The width of FRP strip

$s_f$  = The spacing of strips

$b_w$  = The beam width

$E_f$  = The elastic modulus of FRP

$d$  = the effective depth of the beam

$\beta$  = Angle between principal fiber orientation and longitudinal axis of the beam.

The application of Equation (2.1) requires the quantification of the effective strain,  $\epsilon_{fe}$ . Triantafillou suggested that the effective strain is the function of the axial rigidity of FRP sheet and expressed as  $\rho_f E_f$ . The effective strain was, therefore, determined from experimental analysis for  $V_f$  using variable rigidities of FRP sheet. Based on the experimental results, the effective strain was back calculated and plotted against the axial rigidity. A relationship between effective strain and axial rigidity was derived experimentally through curve fitting of about 38 test results and following equation was proposed:

$$\epsilon_{fe} = 0.0119 - 0.0205 (\rho_f E_f) + 0.0104 (\rho_f E_f) > 2 \text{ for } 0 \leq \rho_f E_f \leq 1 \text{ GPa} \dots\dots\dots 2.2a$$

$$\epsilon_{fe} = 0.00245 - 0.00065 (\rho_f E_f) \text{ for } \rho_f E_f > 1 \text{ GPa} \dots\dots\dots 2.2b$$

The modelling approach of Triantafillou had the following shortcomings:

- a. The data used to produce Equations (2.2a and 2.2b), 38 test results, included three types of FRP (CFRP, AFRP, and GFRP), where the fracture capacity of each type is different.
- b. The wrapping schemes (totally wrapped, U-wrap, and FRP on both sides of the beam) have a significant effect on FRP contribution and mode of failure was not considered as the design variable.



## ***2.2.2.2 Shear Strengthening Options***

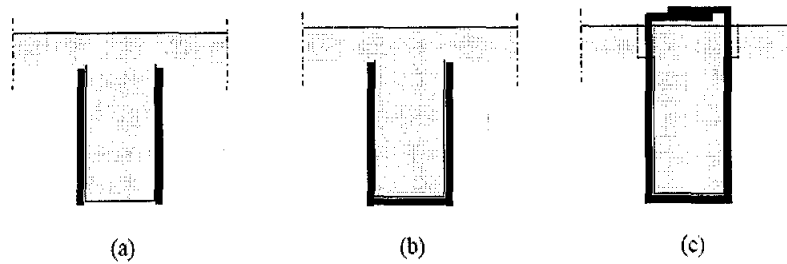
### ***2.2.2.2.1 General***

For shear strengthening of RC beam, externally bonded FRP reinforcement is used to wrap the beam cross section with the fibers in the transverse direction in order to reinforce diagonal tension cracks in much the same way as steel stirrups. From this general approach, several configurations of FRP shear reinforcement have been devised and investigated by Master Builders Technologies (1998). The main purpose of this section is to describe several alternatives for shear strengthening options that are available to the designers.

### ***2.2.2.2.2 Bonded Surface Configurations***

In shear strengthening situations of RC beams, three options of FRP bonded surface configurations as shown in Fig .2.5, and Fig .2.6, have been investigated by Beret et al (1992), Sato et al (1996) and Taerwe et al (1997). The first option is to apply the FRP reinforcement on both sides of the beam. The effectiveness of this configuration is limited due to possible debonding failure of the FRP reinforcement (Master Builders Technologies (1998)). The second option is to wrap the sides and bottom of the beam by U-wrap. The U-wrap is practical and is relatively effective in increasing the shear capacity of the beam. Sato et al (1996). However, when the shear cracks develop at approximately 45 degree, the FRP reinforcement (U-wrap) may have minimum bonded length near the compression flange of a T-section, usually leading to a premature failure due to debonding. This situation is even more critical in negative moment regions as cracks develop from the topside of the member. It has been found that total wrap or U-wrap with end anchor are the alternative solution for U-wrap if debonding is to be avoided, Araki et al (1997) and Sato et al (1997b). However, total wrap is not practical from constructability standpoint of view in presence of monolithic slabs that prevent wrapping the sheet around the top of the section. One option might be to drill holes through the slab and wrap strips of FRP around the section. However, this method is rather complicated. On the other hand, it has been

shown that the anchorage of the ends of U-wrap is practical and effective, (Sato et al (1997a) and (1997b))



(a) FRP bonded to the two beam sides. (b) FRP “U” wraps. (c) FRP wrapped entirely around the beam.

Fig. 2.5 VARIOUS SCHEMES FOR WRAPPING TRANSVERSE FRP REINFORCEMENT

### 2.2.2.2.3 End Anchor

It has been shown that the anchorage of the ends of the sheets with steel plates and bolts is effective and can increase the shear capacity of RC members (Fig. 2.6). In the case of U-wraps, it was observed that anchorage increased the shear capacity by about 20% with respect to the specimens without end anchorage Sato et al (1997a). By using this technique and testing specimens under a cyclic load, Sato et al. (1997b) showed that the seismic retrofitting of RC beams using FRP sheets becomes practical and efficient. Although the mechanical anchors made of steel proved to be effective in the laboratory studies, in reality are not very practical for field application due to drawbacks such as stress concentration and in the case of bolting, discontinuity of the FRP at drilling locations. In the case of carbon FRP, the likelihood of galvanic corrosion due to steel-carbon fiber contact is also a concern.

In order to eliminate the problems associated with traditional anchors, an innovative anchoring system was proposed by Khalifa et al (1999) using FRP materials only. The system has been called U anchor.

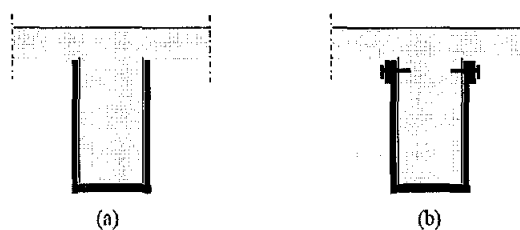


Fig. 2.6 (a) U-wrap without end anchor. (b) U-wrap with end anchor.

#### 2.2.2.2.4 Shear Reinforcement Spacing

The transverse FRP reinforcement may be in the form of a continuous wrap or as spaced strips as illustrated in Figure 2.7. The use of strips may be effective in optimizing the amount of material used.

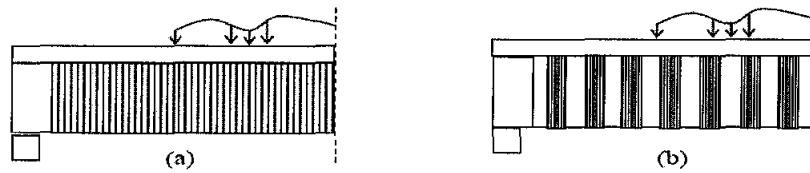


Fig. 2.7 SHEAR REINFORCEMENT DISTRIBUTION (a) Continuous. (b) Strips.

#### 2.2.2.2.5 Fiber Orientation

Because FRP is an anisotropic material with high strength in the direction of the fibers, the fibers may be oriented in such a way to best reinforce diagonal tension cracks. This is achieved by the use of inclined strips (Fig. 2.8). However, vertical plies are easier to install just as in the case of vertical and inclined stirrups.

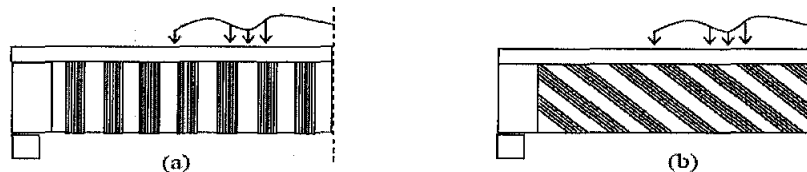


Fig. 2.8 FIBER ORIENTATION. (a)  $90^{\circ}$  wrap. (b)  $45^{\circ}$  wrap.

#### 2.2.2.2.6 Bi-axial Reinforcement

It has been found that the use of bi-axial FRP reinforcement may enhance the overall performance of the strengthening system (Hutchinson et al 1997). Bi-axial FRP reinforcement is achieved by applying two unidirectional FRP plies in perpendicular directions (Fig. 2.9).



Fig. 2.9 BI-AXIAL FRP ORIENTATION. (a)  $90^{\circ}/0^{\circ}$ . (b)  $\pm 45^{\circ}$

### ***2.2.2.3 Summary of Shear Strengthening***

The following remarks are drawn from the previous studies related to shear strengthening of RC beams using FRP laminates:

- Literature review showed that most of the experimental studies were focused on the capability of the externally bonded FRP composites to enhance the shear capacity of RC beams, and the investigation of the possible failure modes. However, the factors that influence shear strength of the strengthened beams were not systematically addressed. Most of the studies deal with simply supported rectangular beams and the effectiveness of the strengthening system to increase the shear capacity in negative moment regions and T cross-section beams not clearly investigated. In addition, some of the available tests were conducted on specimens with impractical dimensions Chajes et al (1995) and Traintafillou et al (1998); that might have affected the failure mode.
- From the analytical standpoint, it is clear from the above review that although some studies on shear strengthening of RC beams exist, the design of such members is not very straightforward and some times contradictory. Moreover, the relatively good agreement between models and experimental results is attributed to the fact that, the same set of data has been used for calibration and comparison, (Berset et al (1992), Uji et al (1992) , Chajes et al (1995), Umezu et al (1997) and Araki et al (1997)).
- Based on the current level of knowledge that was based on available research, it can be concluded that there are many gaps to be filled that require more experimental and analytical work.

## 2.2.3 Bond between FRP Sheet and Concrete Interfaces under Shear

### 2.2.3.1 Background

The most important role of the bond interface between FRP sheets and concrete is to transfer shear stresses from existing concrete structures to externally bonded FRP sheets for both shear strengthening and flexural strengthening cases. Therefore, the shear bond properties of FRP sheet-concrete interfaces have been extensively studied. Various test methods have been developed to characterize the local interfacial shear bond behaviors by studying the strain distribution in the FRP sheets or to evaluate the average interfacial bond strength. The evaluated interface characteristic parameters include average shear bond strength, effective bond length, maximum shear bond stress, interfacial fracture energy, as well as the local bond stress-slip relationship. All studied experimental parameters can be summarized as shown in Table 2.2.

Table 2.2 INFLUNCING FACTOR IN BOND OF FRP SHEET-CONCRETE INTERFACE  
CHEN ET AL (2001)

		Influencing factor	
Mechanical	Concrete	Modulus of elasticity, Thickness, Surface treatment, Strength, Drying shrinkage, Water content	
	FRP sheet	Continuous fiber sheet	Modulus of elasticity, Strength, Thickness, Stiffness, Length/width of sheet, Weave
		Bonding resin	Modulus of elasticity, Strength, Glass transition temperature, Spread
		Primer Putty	
Environmental		Loading condition (bending, shearing, punching, cyclic), Environmental actions (ambient temperature, moisture, sun light radiation, etc.)	

### 2.2.3.2 Factors affecting bond of FRP sheet-concrete interfaces

#### 2.2.3.2.1 Bond Length of FRP Sheet

Many researchers have studied the effects of sheet bond length. Generally, bond strength increases as the sheet bond length is increased. When the sheet bond length is increases beyond a certain extent, the bond length does not increase any further. Therefore, the average bond length decreases with the increase of sheet bond length. In other words, there exists an effective bond length. Besides the premature

debonding phenomenon caused by shear stress concentration, the existence of effective bond length is another factor that causes the tensile strength of FRP materials not to be fully utilized. Nevertheless, giving the different definitions by different researchers and the dissimilar materials used in their tests, the effective bond lengths can vary significantly such as 45 mm [Sato et al (1997)], 75 mm [Bizindavyi et al (1999)], 100 mm [Ueda et al (1999)], 93 mm [Lorenzis et al (2001)] and 275 mm [Brosens et al (1997)].

#### **2.2.3.2.2 Bond Width of FRP Sheets**

The investigations done by Brosens et al (1999) and Sato et al (2001) have been showed that the sheet width does not influence the average bond strength of interfaces when the width of sheets ranges from 50 mm to 200 mm. However, when the sheet bond width is less than 50 mm, the smaller the sheet width, the higher average shears bond strength that the interface can achieve.

#### **2.2.3.2.3 Stiffness of FRP Sheets**

Much of the literature has reported the effects of the stiffness of FRP sheets (elastic modulus  $\times$  thickness). The bond strength increases with the stiffness of FRP sheets. Meanwhile, a higher FRP stiffness will result in longer anchorage length.

#### **2.2.3.2.4 Strength of Concrete**

Concrete strength is thought to be a factor that significantly affects the interface bond. In fact, it is rather difficult to verify its effects by experimental study. When the concrete strength is high then its effects become visible. Yoshizawa et al (2000) and Lorenzis et al (2001) indicated that the dependence of the interfacial fracture energy on the concrete compressive strength is negligible. However, Chajes et al (1996) and Horiguchi (1997) reported that the bond strength is proportional to concrete strength. Brosens et al (1997) reported that the bond strength is proportional to the square root of concrete tensile strength. Nakaba et al (2001) and Sato et al (2000) reported that the maximum interfacial bond stresses are proportional to  $f_c^{0.19}$  and  $f_c^{0.2}$  respectively.

#### ***2.2.3.2.5 Surface Treatment of Concrete***

The test results presented by Chajes et al (1996) showed that the surface preparation of the concrete influences the bond strength. They found that the use of mechanical abrasion achieved the higher average interfacial bond strength. Mitsui et al (2000) conducted a further quantitative study on the effects of surface condition. They evaluated the surface roughness index of concrete by changing the treatment methods, which were sandpaper polishing, disk sander grinding, sandblasting and chipping. They observed the three-dimensional profile of the concrete surface, using an optical displacement meter and obtained measurements of the maximum depth, superficial area and so on. They concluded that the methods of sandblasting and chipping could lead to higher bond strength. It was observed that the greasy surface of concrete remarkably reduced the bond strength.

#### ***2.2.3.2.6 Properties of layer***

Dai et al (2001) and Nishida et al (1999) mentioned that the bond layers with lower elastic modulus, but good ductility, could lead to higher interface bond strengths. The mechanical properties of bond layers can be adjusted through changing the elastic modulus of either bonding resin or putty. However, the effective bond length increases when the elastic modulus of bond layers decreases. It was also reported that using ordinary primer with a viscosity of 20 MPa is better than using high permeability primer with a viscosity of 90 MPa. The latter primer leads to lower bond strength.

#### ***2.2.3.2.7 Interface Defects***

The lifting of bonded sheet represents the interface defects that can be induced during bonding. JCI technical committee(2003) reported that a 12×12 mm lifting area of FRP sheets in specimens prepared for pull-out shear bond tests, which was equivalent to 6 % to 13% of the whole sheet bonding area, has no significant effects on the overall pull-out bond strength.

#### 2.2.3.2.8 Bond stress-slip ( $\tau$ - $s$ ) relationship

The bond stress-slip ( $\tau$ - $s$ ) relationship is one of the most important correlations that describe the interface performance of the two bonding materials. A number of  $\tau$ - $s$  relationships have been developed by different researchers, which differ to each other because different variables used in each of the study. For example, many configurations for the  $\tau$ - $s$  relationships, including cut-off type, bilinear type, elasto-plastic type, and Popovics type have been reported [Sato et al (1997), Lorenzis et al (2001), [Nakaba et al (2001)], Sato et al (2001) and Yoshizawa et al (2000)]. Those differences indicate the difficulty in defining a reliable local  $\tau$ - $s$  model for an FRP sheet-concrete interface from conventional pullout bond test results. This is due to various reasons. First, the effective bond length of FRP sheet-concrete interfaces is rather short, and it is difficult to arrange many strain gages in an active, but short, load transfer length. Second, the FRP sheets have rather small bending stiffness, so that the strains observed on the surface of FRP sheets have a larger scatter due to local bending deformations. Third, the interface between FRP composites and concrete easily exceeds the peak shear bond stress, even if there is a low tensile stress level in FRP sheets, so the interfacial  $\tau$ - $s$  relationship is highly non-linear (Santos et al 2003).

The current experimental studies conducted using single shear tests (Bizindavyi et al 1999; Chajes et al 1995 and 1996 ; Tajestin et al 1997), double shear tests (Brosens 1997; Fukuzawa et al 1997 ; Hiroyuki et al 1997 ; Kobatake et al 1993; Maeda et al 1997 ; Neubauer et al 1997; Swamy et al 1986 ;van Gemert et al 1980 ; De Lorenzis et al 2001) and modified beam tests (Brosens et al 1998; van Gemert et al 1980 ; Ziraba et al 1995). Few theoretical studies have been conducted using fracture mechanics analysis (Brosens et al 1998; Holzenka et al 1994; tajestin et al 1994 and 1996; Triantafillou et al 1992; Wu ZS et al 2002; Yuan et al 2001 and 2004), finite element analysis (Niu et al 2001; chen et al 2001) and the development of empirical models (Bizindavyi et al 1999; van Gemert et al 1980; Challal et al 1998; Khalifa et al 1998). A review of these studies is given by Chen et al 2001. He classified the existing test set-ups into the following six types:

- (a) Double-shear pull tests
- (b) Double-shear push tests

- (c) Single-shear pull tests
- (d) Single-shear push tests
- (e) Beam (or bending) tests
- (f) Modified beam test

For better clarity, the first four test methods are renamed here as: (a) far end supported (FES) double-shear tests; (b) near end supported (NES) double-shear tests; (c) far end supported (FES) single-shear tests; and (d) near end supported (NES) single-shear tests (Fig .2.10). Collectively, all these four tests may also be referred to as pull tests, as the plate is always directly pulled by a tensile force.

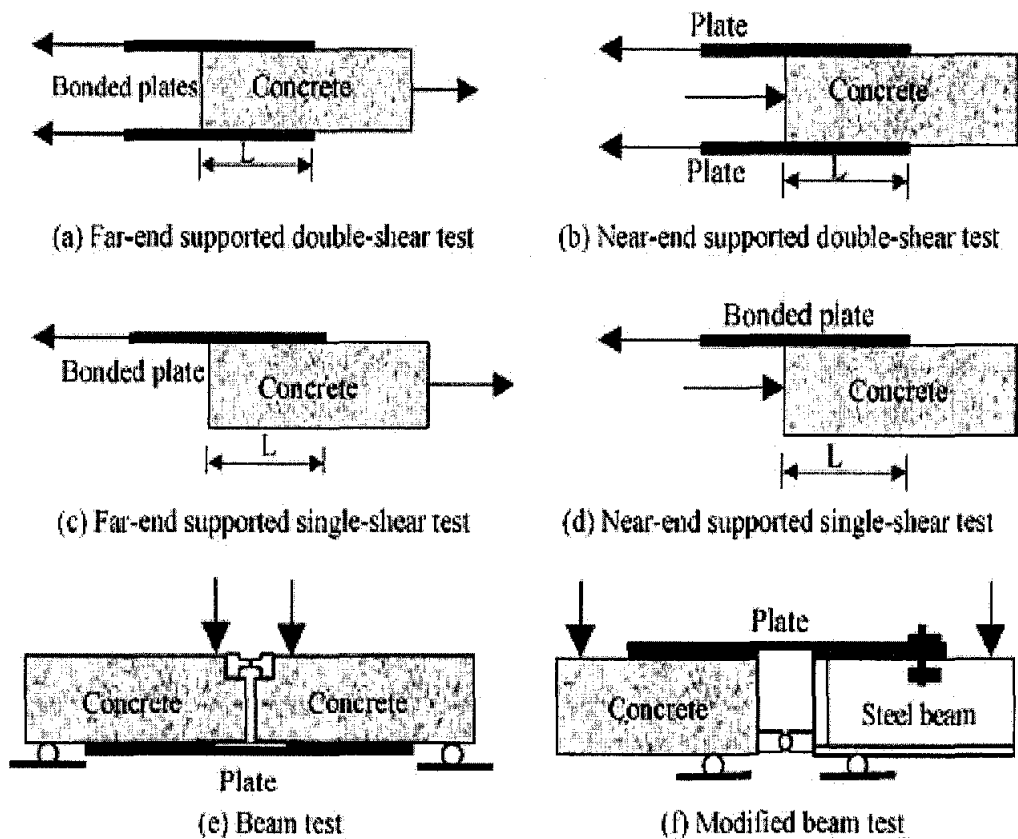


Fig. 2.10 CLASSIFICATION OF BOND TESTS (Chen 2001)

### 2.2.3.3 Summary of Bond studies

The following remarks are drawn from the previous studies related to Bond between FRP Sheet and Concrete Interfaces under Shear:

1. Major failure mode of FRP-to-concrete joints in shear tests is cracking of concrete under shear that commonly occurs at a few millimetres from the adhesive-concrete interface (Bizindavyi et al 1999)
2. FRP-to-concrete bond strength model is important for accurate prediction of debonding failures in FRP-strengthened RC beams, including shear crack-induced debonding failures (Mohamed Ali et al 2001 ; Teng et al 2003) as well as intermediate flexural or flexural shear crack-induced debonding failures (Chen et al 2003).
3. Effectiveness of the repair scheme usually depends upon the bond–slip response between the concrete and the FRP composite was not properly modelled. Recently, an improved analytical procedure, which considered a linear bond–slip relationship for the interface has been developed. Implementation of this analytical model to predict the load response of beams undergoing debonding requires accurate material model for the interface bond, which account for the gradual degradation of the stress transfer with increasing slip.
4. Various experimental and analytical investigations of the behaviour of bonded FRP-to-concrete joints have been carried out. Researchers have proposed bond stress–slip relationship models including the linear cut-off model, bilinear model, tri-linear model, and Popovics formula(Brosens et al 1999; Nakaba et al 2001; Ueda et al 1999) However, these models have generally been limited to monotonic “static” loading conditions; cyclic bond behaviour has not yet studied.

## **2.3 Material Cyclic Models**

### **2.3.1 Introduction**

For the analysis of reinforced concrete structures subjected to general loading conditions, realistic constitutive models and analytical procedures are required to produce reasonably accurate simulations of structural behaviour. Models that provide accurate simulations under reversed cyclic loading are less common than models applicable to monotonic loading. In addition to utilize a realistic procedure, the constitutive models for cyclic loading of concrete should capture the actual behaviour of the structure. The shape of the unloading and reloading curves of structural components should accurately predict the energy dissipation of the structure and the damage of the material due to load cycles. The models should not be limited to the compressive behaviour only but also include the tensile behaviour. The latter also plays a key role in the overall behaviour of reinforced concrete structures.

### **2.3.2 Concrete Cyclic Models**

For the analysis of reinforced concrete structures, many diversified approaches have been used for material modelling. These include plasticity-based procedures, fracture mechanics, and various non-linear elastic models. In the last case, approaches range from discrete to smeared crack models, and from fixed to rotating crack models. Researchers working in each of these areas generally have been successful in producing models that yield results of acceptable accuracy for conditions of monotonic loading.

Models that provide accurate simulations of structural behaviour under general loading conditions, specifically under reversed cyclic loading, are less common. The smeared crack approach is most commonly employed. Many researchers have documented fixed crack directions in their models, correlated to the experimental results that are reasonably incorporating the rotating crack assumption are not much common, which is more realistic of observed structural behaviour.

Sinha, Gerstle, and Tulin (1964) were the first, whom to describe qualitatively and quantitatively the stress-strain response of concrete under cyclic loading. At the

time of their work, there was a complete lack of information on the behaviour of concrete subjected to cyclic loading.

Qualitatively their work was instrumental in providing the following contributions:

1. Concrete produces unloading and reloading curves with pronounced hysteresis. Straight-line representation for both unloading and reloading neglects the hysteresis effects.
2. The stress-strain paths under cyclic loading do not exceed an envelope curve. It may be considered unique and identical with the stress-strain response obtained under monotonic loading.
3. Unloading can be represented by a quadratic equation, and reloading with a straight line.
4. The point at which the reloading curve crosses the unloading curve forms a shakedown limit. Stresses above this limit lead to additional strains, while maximum stresses at or below this limit do not occur. Essentially, closed loops will be formed below this limit.

A flaw in their initial assumption is reflected in their modelling, is that the unloading and reloading curves remain independent of previous load history. Therefore, relations determined from one set of load histories can be utilized to predict the behaviour of the material for any general history of loading. Figure 2.11 is a representation of the modelling assumptions that was taken from Sinha et al (1964). Karsan and Jirsa (1967) later demonstrated that unloading and reloading are not unique and are dependent on the previous load history.

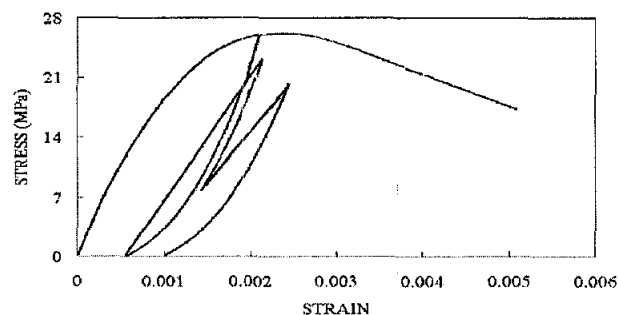


Fig. 2.11 GENERALIZED STRESS-STRAIN CURVE FOR CONCRETE  
Sinha et al (1964)

Karsan and Jirsa set out an experimental program that consisted of 46 short rectangular columns of plain concrete to investigate further the findings of Sinha, Gerstle, and Tulin. They concluded that there exists an envelope curve that can be

represented by the monotonic response of similar concrete properties, and that the envelope curve is reasonably approximated by the Smith-Young expression given by:

$$F_E = 0.85S_E^{(1-S_E)} \dots\dots\dots 2.3$$

Where  $F_E$  &  $S_E$ , are normalized stress parameters, normalized with respect to the cylinder compressive strength and the cylinder strain at peak stress, respectively. The researchers, based on the experimental results, provided a more rigorous definition of the stability limit (shakedown limit). They found that intersecting points of unloading and reloading to the envelope curve constitute an upper limit of the shakedown limit. This was termed as the common point limit. Introducing cycles with lower stress levels caused the point of intersection to be lowered, eventually leading to a stabilized point. This lower bound was referred to as the stability limit. Stresses below the stability limit did not cause additional strains. The common point limit and the stability limit were modelled exponentially in the form similar to the envelope curve, and represented as:

$$F_C = \beta \frac{S_C}{0.315 + 0.77\beta} e^{\left[ \frac{1-S_C}{0.315+0.77\beta} \right]} \dots\dots\dots 2.4$$

Where

$F_C$  &  $S_C$ , are the stress ratios at the common point, respectively. A value of 0.76 is used for the common point limit, and a value of 0.63 for the stability limit.

Karsan and Jirsa(1976) were the first to establish non-recoverable compressive strains in concrete, commonly referred to as plastic strains that arise during unloading to a zero stress level. Plastic strains influence the shape of the unloading and reloading curve, thus these curves are not unique and are dependent on the previous loading history. A model was formulated describing the relationship of the plastic strains with the strain at the onset of unloading (maximum strain in the history of loading) by the following expression:

$$S_p = 0.145S_E^2 + 0.13S_E \dots\dots\dots 2.5$$

Where  $S_p$  is the normalized plastic strain and  $S_E$  is the normalized unloading strain. Second-degree polynomials were used for unloading and reloading as illustrated in Fig. 2.12.

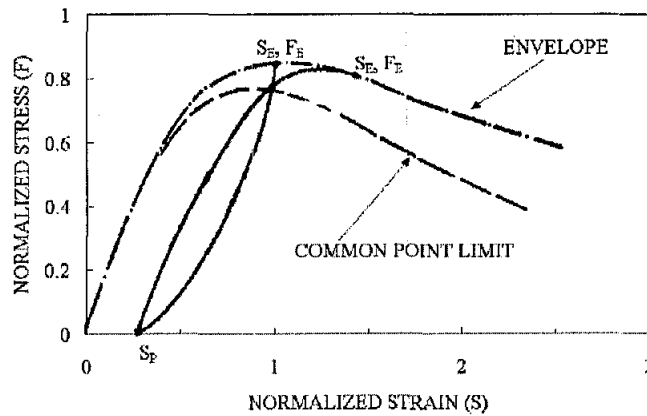


Fig. 2.12 LOADING AND UNLOADING CURVES  
Karsan and Jirsa (1969)

There is little gain in modelling the reloading curves as non-linear (e.g. parabolic) considering the increased complexity of the computations; data indicates that a linear approximation provides reasonable results. The assumed reloading curves address the damage in the concrete due to cyclic effect, as the reloading stress at the previous maximum strain is less than the previous unloading stress. The formulations were established and corroborated to uniaxially loaded cylinders and produced results that compared well.

Park, Kent (1972), and Simpson<sup>13</sup> conducted one of the first experimental investigations on reinforced concrete members subjected to cyclic loading. The experimental program consisted of applying cyclic loads to beam-column sub assemblies. Analytical models were proposed for concrete and reinforcement to reproduce moment-curvature responses.

Figure 2.13 is the schematic representation of the proposed concrete model. To model the concrete, a piecewise approach is used. The model does not accurately reproduce the unloading and reloading curves of actual behaviour.

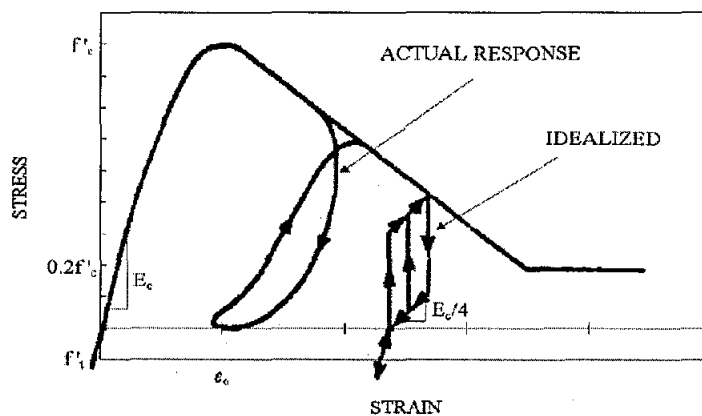


Fig. 2.13 STRESS-STRAIN CURVES  
Park et al (1972)

It was incorrectly assumed that, upon unloading, 75 % of the previous stress is lost without a decrease in strain. The unloading response is then incorrectly assumed to follow a linear slope of 25 % of the initial tangent modulus to a zero stress level. In this approach, the plastic strain is independent of the unloading strain as established by other researchers. Reloading begins with an increase in stress, identical to that of the unloading branch, without an increase in strain, followed by a linear slope to the backbone curve. It is also assumed that reloading terminates at the previous maximum unloading stress. Thus, the damage that concrete experiences due to cycling is neglected. Pre-cracking tensile stresses in the concrete is considered in the modelling; however, no consideration is given to tension stiffening.

The models were written into a computer program based on a layered approach. The theoretical responses compared reasonably well with the experimental responses, even though an unrealistic concrete model was used. The experimental responses seemed to be dominated by yielding of the reinforcement, and therefore, the concrete response was not as critical. The concrete modelling becomes more critical in cases where the reinforcement does not yield and the behaviour of the structure is controlled by shear or crushing of the concrete. In this case, the above models would prove unsatisfactory results.

The application of finite elements for reinforced concrete made it possible to analyze complex structures including structures subjected to seismic type forces. Darwin and Pecknold (1976) were the first to apply a finite element procedure to model cyclic loading. Fig. 2.14 shows Darwin and Pecknold proposed cyclic model of concrete

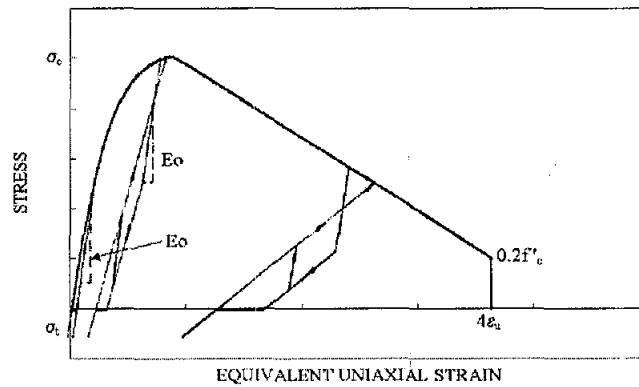


Fig. 2.14 Model for Concrete under Cyclic Loading, taken from Darwin and Pecknold(1976)

The effect of biaxial cyclic compression on concrete was ignored in the earlier works. Ukozturk and Tseng (1984) investigated this behaviour by subjecting 127 x 127 mm flat concrete plates of 25 mm thickness to cyclic loading in one direction, with a constant confining strain in the orthogonal direction. Analysis of the experimental data provided insight into the biaxial cyclic behaviour of concrete and was concluded to be consistent with the uniaxial cyclic loading behaviour. The similarities include:

1. Concrete exhibits typical hysteretic behaviour where the area within the hysteresis loops, represents the energy dissipated during a cycle, becomes larger as the unloading strain increases.
2. Reloading curves are nearly linear up to the intersection with the unloading curve, after which there is a softening in the response.
3. The unloading curves are non-linear with remarkable increase in curvature near the residual strain.
4. A continuous degradation of the concrete is reflected in the decrease of the slopes of the reloading curves.
5. The plastic strains are dependent on the strain at unloading and are not affected by the confining strains.

In their further work, the researchers proposed formulations for concrete under cyclic loading including the effects of confinement. The model was based on an incremental orthotropic formulation and used an equivalent one-dimensional approach to represent the multiaxial behaviour. It was essentially a tangent stiffness approach.

The Popovics curve was used to describe the envelope response of concrete in compression and is presented in the equivalent stress-strain form as:

$$\frac{\sigma}{\sigma_p} = \frac{n}{n-1 + \left(\frac{\epsilon_e}{\epsilon_p}\right)^n} \left(\frac{\epsilon_e}{\epsilon_p}\right) \dots\dots\dots 2.6$$

Where  $\sigma_p$  is the principal peak stress,  $\epsilon_p$  is the equivalent strain at peak stress,  $n$  is a shape factor,  $\sigma$  is the principal stress, and  $\epsilon_e$  is the equivalent strain. The unloading branch was assumed parabolic with a finite stiffness at the onset of unloading, and passing through the plastic strain at zero stress. A relation between the plastic strain and the strain at unloading was determined from the test data as follows:

$$\frac{\epsilon_r}{\epsilon_p} = 0.162 \left(\frac{\epsilon_u}{\epsilon_p}\right) + 0.334 \left(\frac{\epsilon_u}{\epsilon_p}\right)^2 \dots\dots\dots 2.7$$

Where  $\epsilon_r$  is the residual (plastic) strain and  $\epsilon_u$  is the strain at unloading condition. The above formulation produces slightly larger residual strains than that proposed by Karsan and Jirsa (1969). The latter seems to be a lower bound solution. For reloading, the Popovics curve was used with modifications to the initial slope of reloading. The model provided reasonable correlations to the test data and can be implemented into a non-linear finite element algorithm based on a tangent stiffness approach. The tests and formulations, however, did not consider confinement in the out-of-plane direction. Much of the pioneering work discussed above provides a benchmark for which current and future analytical modelling can be derived.

Bahn and Hsu (1998) in their experimental studies considered the effect of random cycles in compression. This research consisted of testing (76 x 152 mm) concrete cylinders that proposed models for the general loading conditions of concrete in compression (see Fig. 2.150. Four different loading regimes were introduced: monotonic loading; cycles to envelope curve; cycles to common point; and cycles with random loading.

Based on the tests, the following conclusions were made, confirming what previous researchers have stated:

1. The envelope curve for cyclic loading could be represented by the response of concrete to monotonic loading.

2. The residual strains are a function of the strain at unloading, and an increase in the unloading strain causes approximately the same increase in the accumulated residual strain.
3. The unloading and reloading lines do not coincide. The average slope of the unloading and reloading curves is inversely proportional to the plastic strain. This suggests that there is stiffness degradation for the entire stress-strain curve.

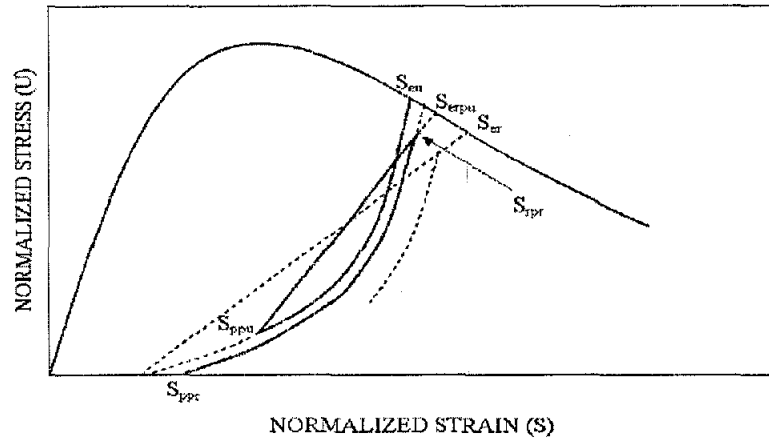


Fig. 2.15 SCHEMATIC OF LOADING AND UNLOADING RESPONSE  
Bahn and Hsu(1998)

### 2.3.3 Steel Constitutive Models

Many researchers have proposed models to characterize the response of reinforcing steel for use in the analysis of reinforced concrete structures. Some of these models are developed based on material constitutive laws; however, the majority of these are phenomenological models that characterize the macroscopic response based on experimental data. The fundamental characteristics of the one-dimensional steel response are relatively simple. Thus, the appropriate material model not only predicts this response with a reasonable level of accuracy but also calibrates to fit experimental data with relative ease and is computationally efficient.

### 2.3.3.1 Applications of Material Constitutive Theory for Modelling of Steel Behaviour

Various theories have been proposed to characterize the response of reinforcing steel subjected to reverse cyclic loading based on microscopic material response. A number of these models are identified and discussed by Cofie [1983]. The simplest and most computationally efficient model for predicting steel behaviour is that developed based on modern plasticity theory. The one-dimensional behaviour of reinforcing steel is representative of an elastic-plastic material. In particular, results of experimental testing show the accumulation of unrecoverable, plastic deformation and an unloading stiffness that is approximately equal to the initial elastic material stiffness. Additionally, steel exhibits isotropic strain hardening, characterized by increased strength under increased inelastic strain demand. Further, the premature yielding associated with the Bauschinger effect may be characterized by a plasticity model that incorporates kinematic strain hardening.

Figure 2.16 shows a typical stress-strain history of steel that predicted on basis of plastic theory. This model can be calibrated to predict steel strength near cyclic peak strain demands, the model does not represent well the observed steel response along the path between points of peak strain demand. However, for some applications, the inaccuracy of this model is acceptable given the simplicity of the formulation and the ease with which it may be calibrated to best fit observed response.

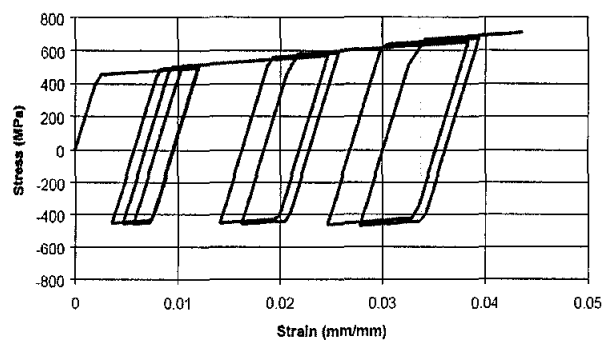


Fig. 2.16 STEEL STRESS-STRAIN HISTORY AS PREDICTED BY PLASTIC THEORY

The accuracy with which the plasticity model predicts the observed response may be improved through use of a more sophisticated hardening rule and additional hardening variables. However, this may not be the most efficient model for characterizing steel response.

### 2.3.3.2 Phenomenological Model

A more representative model for the response of reinforcing steel subjected to reverse cyclic loading can be achieved through the use of phenomenological models in which non-linear equations are calibrated based on experimental data. One of the first models of this type is that proposed by Ramberg and Osgood [1943]. Various other models have followed the same a number of models have been developed because of work done by Menegotto and Pinto [1973]. Recently, several models have been developed that characterize behaviour of the basis of the natural steel stress rather than the engineering stresses and strains.

### 2.3.3.3 Characterization of Steel Response Using the Ramberg-Osgood Equation

The model proposed by Ramberg and Osgood uses a single non-linear equation to characterize the observed curvilinear response of reinforcing steel subjected to monotonic loading. This model defines the normalized strain to be a function of the normalized stress (stress increments are normalized with respect to twice the yield value):

$$\epsilon_{norm} = \beta \sigma_{norm} (1 + \alpha |\sigma_{norm}|^{n-1}) \dots\dots\dots 2.8$$

Where  $\sigma_{norm}$  &  $\epsilon_{norm}$  are the normalized stress and normalized strain respectively. The model may be extended for the case of reversed-cyclic loading by introduction into Eq.(2.9) of the stress and strain at which load reversal occurs. The model predicts the one-dimensional steel response with acceptable accuracy, the explicit dependence on the stress reduces the ease with which this model is implemented in a typical strain-driven finite element analysis program. Additionally, using the model to represent monotonic response does not provide for description of the yield plateau, a characteristic of response that may control system behaviour. These issues are addressed in the recent models; in that the stress is defined as an explicit function of the strain and the monotonic response can be accurately characterized.

### 2.3.3.4 Characterization of Steel Response Using the Menegotto-Pinto Equation

Menegotto and Pinto [1973] proposed a model that characterized reinforcing steel in which the response is defined by the following equation:

$$\sigma^* = b\varepsilon^* + \frac{(1-b)\varepsilon^*}{(1 + \varepsilon^{*R})^{1/R}} \dots\dots\dots 2.9$$

Where the effective strain and stress ( $\sigma^*, \varepsilon^*$ ) are a function of the unload/reload interval,  $b$  is the ratio of the initial to final tangent stiffness and  $R$  is a parameter that defines the shape of the unloading curve. For this case, it is assumed that the reference curves (stress-strain curves that bound the cyclic response) as well as unloading and reloading response may be characterized by Eq.2.9 This implementation also neglects characterization of the yield plateau. In recent years, many of researchers have proposed material models that use the Menegotto-Pinto equation to characterize the unloading-reloading response of reinforcing steel. One such model is that proposed by Stanton and McNiven [1979]. This model uses an approximate version of the Menegotto-Pinto equation Eq.2.9 to improve computational efficiency and assumes that the reference curves for steel subjected to cyclic loading follows the monotonic envelope. A second model is that proposed by Filippou et al. [1983]. This model incorporates Eq.2.9 exactly to describe unloading response. The model followed assumption that the reference curve defining the cyclic stress-strain response is tri-linear. Isotropic, cyclic strain hardening is incorporated through shifting of the reference curve as a function of the plastic strain increment. Recently, Eq.2.9 has been incorporated into a sophisticated model proposed by Chang and Mander [1994]. This model assumes that the shape of the reference curve is defined by the monotonic stress-strain response. The model accounts for cyclic strain hardening through shifting of the reference curve as a function of strain history. Additionally, the model incorporates variability in initial unloading stiffness, cyclic strain softening and memory of multiple loads-unload cycles. Each of these four models predict with acceptable accuracy of the observed cyclic response of reinforcing steel subjected to strain histories typically of those observed in reinforced concrete structures subjected to simulated earthquake loading. Of these models, that proposed by Chang and Mander [1994] provides quite accurate prediction of steel response while that

proposed by Filippou et al. [1983] provides both reasonably accurate prediction of response and relatively simple implementation and calibration.

All of the previously discussed models assume a symmetric response for loading in compression and tension. However, data suggest that this may not be an appropriate assumption (Fig.2.17). It is also shown that the monotonic response in compression and tension are essentially the same if the response is characterized by the natural strains and stresses  $(\bar{\sigma}, \bar{\epsilon})$ , defined as follows:

$$\begin{aligned} \bar{\epsilon} &= \ln(1 + \epsilon) \\ \bar{\sigma} &= \ln(1 + \sigma) \dots\dots\dots 2.10 \end{aligned}$$

Two models proposed by [Dodd and Restrepo-Posada (1995); Balan et al., (1998)] define material response on the basis of the natural stress-strain history. These models assume a shape for the cyclic reference curve as defined by the monotonic natural stress-strain history. These models predict various aspects of cyclic response including the Bauschinger effect, reduced elastic modulus, isotropic strain hardening, and cyclic strain softening. The models differ in the non-linear equations used to model individual characteristics of material response. The symmetry of compression and tension response as characterized in the natural stress-strain system is conceptually satisfactory; however, it is not obvious that this is necessary for modelling the response of reinforcing steel in reinforced concrete structures subjected to earthquake loading. For this steel, typically the load history is not symmetric with load histories showing significant tensile strain demand and limited compressive strain demand. For these cases, characterization of the model on the basis of the tensile monotonic response is perhaps appropriate. Additionally, it is not clear that the enhanced accuracy of this model justifies the additional complexity and computational effort.

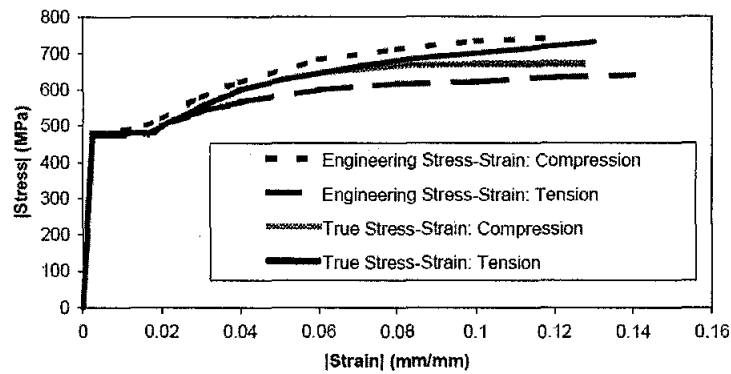


Fig. 2.17 ENGINEERING VERSUS NATURAL STRESS-STRAIN HISTORY FOR REINFORCEMENT STEEL SUBJECTED TO MONOTONIC TENSION AND COMPRESSION LOADING (Dodd and Restrepo-Posada (1995))

### 2.3.4 Summary of Review on Cyclic Models

The following remarks are drawn from this section:

1. Reversed loading cycles produced degradation of bond strength and bond stiffness that was found more server than the same number of load cycles with unidirectional loading. Primarily Degradation depends on the peak slip in either direction that reached earlier. Other significant parameters are rib pattern, concrete strength, confining effect, number of load cycles and peak value of slip between which the bar is cyclically loaded.
2. The models simplify the real structural behaviour, they intend to take into account the parameters which appear to control behaviour in experimental investigations, these being: deterioration of related slip, increase of slip under load controlled reversals, decrease of bond under slip-controlled reversal, deterioration of frictional bond stress and deterioration of residual bond stress.

### 2.4 Finite Element Analytical Models

Since its inception in 1960 by Clough finite element (FE), models are powerful tools for the analysis of concrete structures. Advancements in the modelling are continuously made as reported by Zeinkiewicz and Cheung (1967), Ngo and Scordelis (1967) and Červenka (1970). The method has been developed to an advanced level

with regards to the concrete state, steel state, concrete-steel interactions and other important elemental components such as the representation of bond behaviour between concrete and steel, aggregate interlock and dowel action.

The FE methodology for analysis of reinforced concrete structures can broadly be classified into two approaches. First is the “smeared crack approach” that represents cracking as a change of element characteristics and second is the “discrete crack approach” that introduces special elements such as bond link or bar elements. The smeared crack concept considers the element as a continuum that transforms from an initial isotropic material to an orthotropic material law upon cracking, crushing, or other non-linear effects. For the discrete crack approach, it is easy to analyze a structure with pre-defined cracks but more complicated when crack locations are unknown at the beginning of analysis. Therefore, the smeared crack approach is widely used because the topology of the original finite element mesh is maintained. Furthermore, the smeared crack approach does not impose restrictions to the orientation of the cracking planes.

There is some literature available on FE modelling of RC elements strengthened with CFRP laminates.

Arduini et al. (1997) modelled RC beams strengthened with CFRP plates and sheets using commercial software (ABAQUS) based on the smeared cracking approach. Beams strengthened with CFRP plates were analyzed using a two-dimensional mesh, while those bonded with CFRP sheets were modelled in three dimensions. The FRP reinforcement was applied directly over the concrete elements assuming perfect bond. The authors reported that the results of the FE analysis showed a good correlation with the experimental investigations. However, the FE analysis results were stiffer than the test results (Figure 2.18). It may be because of making assumption of perfect bond and the limited number of nodes that could be used. From FE analysis high stresses at the end of the FRP plate were sustained because of the delamination failure of the beam.

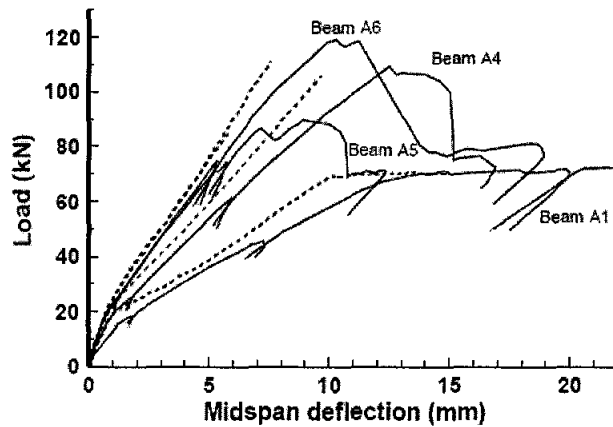
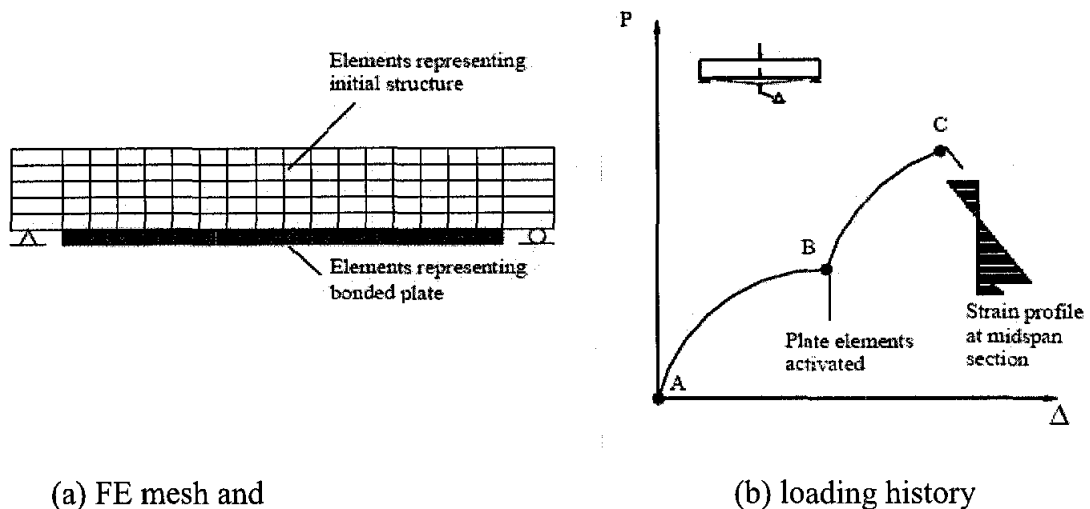


Fig. 2.18 COMPARISON BETWEEN EXPERIMENTAL AND FE RESULTS (Arduini et al. (1997)).

Ross et al. (1999) used ADINA to analyze test beams. The beams section was  $200 \times 200$  mm and they were 3050 mm long with a clear span of 2740 mm using four point bending. Two-dimensional, eight-node plane stress elements were used to represent the concrete, while the reinforcing steel and FRP plates were modelled by three-node truss elements. A hypo-elastic constitutive relationship was used for the concrete based on uniaxial stress-strain relationship that accounts for biaxial and triaxial conditions. An elastic-plastic response was assumed for the steel and the CFRP and modelled as linear elastic until failure. The results of the FE analyses were compared to the experimental results and good agreement for the global behaviour observed. However, the predicted failure mode was not achieved due to the delamination of the FRP plate. It was concluded that the single most important factor affecting the beam behaviour was the bond strength between the concrete and FRP. The use of an anchorage system was suggested to prevent debonding, hence the full capacity of the plate could be utilized.

Sheikh et al. (1998) and Vecchio and Bucci (1999) used non-linear finite element models that were developed for the analysis of repaired structures by taking into account the chronology of the loading, damage and repair (Figure 2.19). The experimental details consisted of a plate added to the soffit of a flexural member after it has been subjected to load and sustained damage (e.g., cracking or crushing of the concrete or yielding of the reinforcement). The finite element mesh was formulated to represent both the initial structure and with the repair components that was

subsequently added. A plastic strain offset was used for the FRP element to account for the pre-damaged concrete member. After the repair, the elements representing the bonded soffit plate were logged and become active. Analyses of both the control and repaired specimens were undertaken and a reasonably good correlation was observed between the simulated responses, with the experimental results. In particular, the influences of the FRP on the strength and failure mode of the specimens were observed well.



(a) FE mesh and (b) loading history  
**Fig. 2.19 ANALYSIS OF FRP REPAIRED BEAM**  
 (Sheikh et al (1998) and Vecchio and Bucci, (1999))

Zarnic et al (1999) used a non-linear 3D FEM program to model short span beams. Each component of the beam consisting of concrete, steel reinforcement, epoxy and the CFRP plate were modelled (Figure 2.20). The numerical results showed a fairly good agreement with the measured response of the test beams for the ultimate loads (Figure 2.20). Beyond the initial response, however, the post-cracking stiffness was found higher than the test data.

Rahimi and Huchinson (2001) utilized the LUSAS FE program to calculate the response of externally reinforced beams. They used a smeared crack model incorporating an isotropic damage model to simulate the non-linear behaviour of the concrete. Four-node or eight-node quadrilateral isoparametric elements were used to model the concrete, with the steel reinforcement smeared onto concrete as two- or three-node bar elements. For the strengthened beams, triangular elements were placed in the transition zone to reduce the element size toward the bond region. The adhesive

layer and FRP laminates were modelled with a row of four- or eight-node elements, the adhesive layer was assumed to be elastic. The FE calculations were found sensitive to concrete tensile strength, a value of 1.5 MPa found to give the best agreement with the experimental load-deflection response (for a concrete compressive strength between 54 and 69 MPa). The stiffness was slightly overestimated, but all calculated solutions for the beam strengths were within 20 percent of the test results.

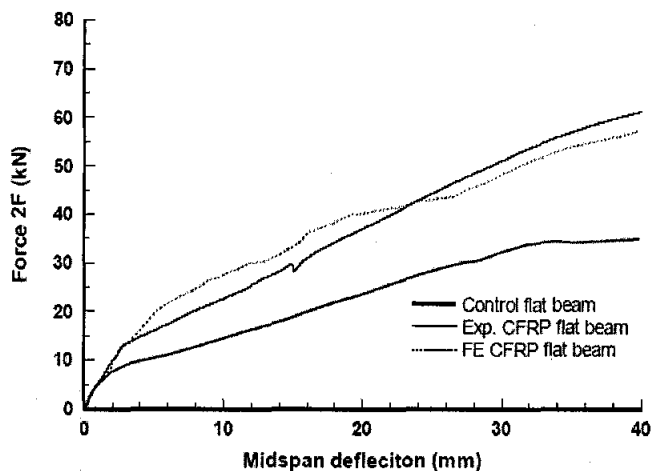


Fig. 2.20 FINIOTE ELEMENT RESULTS (Zarnic et al. (1999)).

The FE analysis for FRP strengthened or repaired reinforced concrete structures have proved to be a powerful tool to determine the local and global mechanisms when bond is included in the model. Acceptable agreement between the model results and the experimental data were obtained. To model bond between the concrete surface and the FRP, interface elements can be used. For the concept of using bond link elements to model slip at the interface of steel and concrete can be referred back to Ngo and Scordelis (1967). Ngo and Scordelis' link element (shown in Figure 2.21) has no physical dimension, that is, the connected nodes  $i$  and  $j$  have the same spatial coordinates. The limitation of this model, however, is that it provides a discreet connection. An alternative is the use of one-dimensional contact elements that provides for a continuous connection between the two adjacent elements.

Goodman et al. (1968) are recognized as the first to have developed interface elements for the modelling of slip in their work in the modelling of rock joints. Hoshino (1974) introduced the Goodman contact element for the modelling of bond in

reinforced concrete and the element was further developed and generalized by Schäfer (1975) as described in Figure 2.22. Interface elements are now commonly used in modelling of slip between concrete and reinforcement (Mehlhorn and Keuser (1985), Rots (1985), Rots (1988)) and for modelling of propagation of discrete cracks (Červenka (1994)).

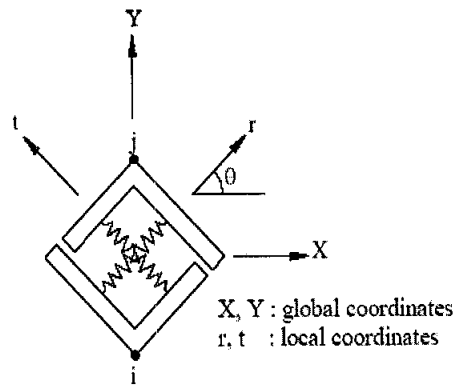


Fig. 2.21 BOND LINK ELEMENT  
 Ngo and Scordelis (1967)

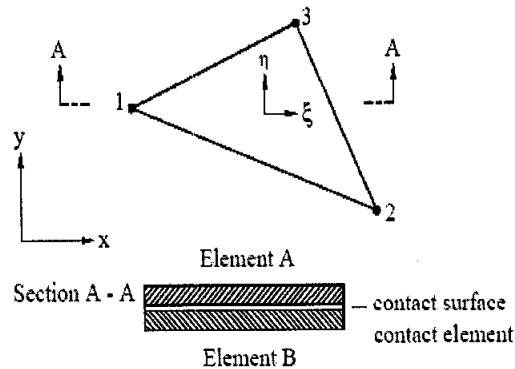


Fig. 2.22 BOND LINK ELEMENT  
 Schafer (1975)

Limam and Hamelin (1998) used a 2D non-linear FE analysis to calculate the response of reinforced concrete beams with CFRP sheets bonded to the tensile face. Eight-node membrane elements were used to represent the concrete and two-node truss elements were adopted for the steel and CFRP reinforcement. Perfect bond was assumed between the steel reinforcement and the concrete, bond slip was considered at the concrete-FRP interface through the use of two-node continuous contact elements (Figure 2.23). The concrete model was based on different yield surfaces in

the tensile and compressive regions using a smeared crack approach. The steel reinforcement was modelled using an elasto-plastic model with strain hardening. The results from experimental tests were used to define a constitutive law for the interface elements based on Mohr-Coulomb failure criteria.

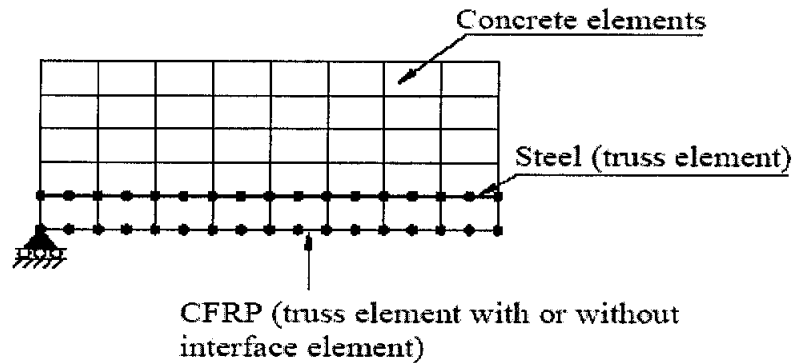


Fig. 2.23 Finite element mesh of Limam and Hamelin (1998).

Comparisons of numerical results with the experimental data showed that the ultimate load and deflections were found within 10 percent of the measured, they were dependent on the modelling of the interface layer (Figure 2.23). They concluded that a non-realistic model for the interface leads to large discrepancies between the analytical and the test results thus showing the importance of accurately modelling the concrete-CFRP interface.

Shin and Lee (2003) used a layered finite element method to analyze strengthened reinforced concrete beams. In this method, strain compatibility was assumed with each cross section of the member was divided into layers. Some of the layers represented the reinforcing bars or externally reinforced bonded plates or CFRP laminates with other layers represented the concrete. Based on beam theory, the model was modified to take into account the effect of strengthening on the flexural behaviour of reinforced concrete beams. The modification was made assuming perfect adhesion between the bottom fiber of the beam and the CFRP laminates. The constitutive models adopted used a strain softening relationship for the concrete and an elastic-plastic model for the steel reinforcement. The CFRP was taken as elastic brittle. The model predicted fairly agreed values with test results.

Sang (2003) studied the response of FRP strengthened beams using two-dimensional FE modelling using the software DIANA. The effects of beam size and FRP thickness on interfacial shear stress concentration were investigated. The

smear crack approach was used to simulate concrete cracking. Three-node plane stress triangle and four node plane stress quadrilateral elements were used to model the concrete and four-node plane stress quadrilateral elements were used to model the adhesive and CFRP layers. Two node bar elements were used to model the steel reinforcement. The FE model calculated the load deflections and CFRP strains of the strengthened beams those were reasonably comparable with the test data.

Wong and Vecchio (2003) used 2D non-linear FE analysis for CFRP slabs and beams strengthened in flexure and shear. The formulation developed by the authors was based on a smeared, rotating crack approach to model the concrete. The steel reinforcement was taken as an elastic-hardening material while the FRP reinforcement was assumed to be linear elastic & brittle. Wong and Vecchio used a one dimensional bond element to determine the bond-slip behaviour between the concrete and CFRP laminates. Two bond-slip relationships were considered, the first was based on elastic-brittle model and the second was elastic-plastic model. The first set of flexural specimens modelled was the slabs and beams of Zarnic et al. (1999). The slab specimens were 800 mm wide, 120 mm deep and 3250 mm long with one unstrengthened specimen tested as a control and three, identical, strengthened specimens. The beams were similar to the slabs in length but with a cross section of 200 mm wide by 300 mm deep. The CFRP plates were 50 mm wide and 1.2 mm thick and were bonded prior to the application of the four-point loading.

The second set of numerical examples analyzed by Wong and Vecchio were a series of five reinforced concrete continuous beams tested by El-Rafaie et al. (2001). The dimensions of the beams were 8500 mm long, 150 mm wide and 250 mm deep and spanned 3830 mm. Each beam was subjected to centre-point loading. The results showed that with the LE bond law the failure loads were 20 percent lower than the test data while the analyses with the EP bond model underestimated the ultimate loads by approximately 7 percent. The third set of examples was the slabs and beams tested by De Rose and Sheikh (1997). The analysis of the slabs using the EP bond stress versus slip model gave an ultimate load 7 to 9 percent lower than the test data. The results for beams using the EP model were within 2 percent of the experimental data.

The final set of specimens analyzed by Wong and Vecchio were their shear strengthened beams tests. The CFRP shear strips were modelled using bar elements and an EP bond-slip law was adopted for the CFRP-concrete interface. The calculated

load-deflection curves, along with the comparisons with the experimental results, are plotted in with a good correlation observed.

## **2.5 Concluding Remarks**

The Following remarks were drawn from the previous studies:

1. A lot of investigations have been conducted with regard to the flexural behaviour of reinforced concrete beams externally strengthened with FRP laminates. These investigations considered several factor like load capacity, failure mode, ductility and end anchorage system
2. More experimental and analytical work is needed to investigate the performance and the factors affecting the shear capacity of strengthened beams and to propose a better and more rational design approach for those members with the attention should be focused on cyclic behaviour.
3. A lot of cyclic models were available in the literature review that was capable of providing accurate simulations for reinforced concrete elements under reversed cyclic loading.
4. Various experimental and analytical investigations of the behaviour of bonded FRP-to- concrete joints have been carried out. Researchers have proposed bond stress–slip relationship models including the linear cut-off model, bilinear model, tri-linear model, and Popovics formula However, these models have generally been limited to monotonic “static” loading conditions behaviours; cyclic bond behaviour has not yet studied.
5. FE method have been demonstrated as powerful analytical technique to idealized reinforced concrete structures strengthened or repaired with FRP laminates.

## CHAPTER 3

### RESEARCH METHODOLOGY

#### 3.1 Introduction

This research study encompassed two major parts they are:

- Experimental investigation, and
- Analytical modeling using FEM method

*In the first* part, an experimental program has been conducted to study the interfacial behavior of CFRP-to-concrete joints under monotonic and cyclic loading conditions.

*In the second* part, a new analytical algorithm based on non-linear finite element method coded in FORTRAN language was developed to investigate the fatigue performance of RC beams strengthened for shear using externally bonded carbon CFRP sheets.

#### 3.2 Experimental Investigation

##### 3.2.1 Background

With the development of the technology of upgrading, the existing concrete structures by using externally bonded FRP composites, a number of anticipated issues related to the conventional structural behaviors after being upgraded have been studied in majority of previous studies. The emphasis was given to clarify the mechanisms of the interface bond between FRP composites and concrete substrates, because the interface is band supposed relatively weak in comparison with the neighbouring materials in the over all system. In most of the cases, the interface bond is critical in transferring stresses from the existing concrete structures to the externally bonded FRP

composites. When a structural element is encircled in FRP composites the mechanical role of interface bond becomes less important, but it still has the function of keeping the integrity and durability of the composite FRP-concrete systems. Therefore, a good understanding on the interface bond is a prerequisite for achieving more reliable but rational design for concrete structures externally bonded with FRP composites.

Interface must be included in any numerical model if the response is required to be accurately predicted using such model. In order to evaluate the interfacial bond mechanisms quantitatively and carry out numerical simulation for FRP sheets strengthened RC structures, defining an accurate bond stress–slip ( $\tau$ - $s$ ) relationship has become a main task among the bond issues studied in the past. Various experimental and analytical investigations of the behaviour of bonded FRP-to-concrete joints have been carried out. Researchers have proposed bond stress–slip relationship models including the linear cut-off model, bilinear model, tri-linear model, and Popovics formula. However, these models have generally been limited to monotonic “static” loading conditions. There are no such studies available on cyclic behaviour.

The analysis of structural components, those are externally strengthened to increase the flexural capacity, are analogous to that for conventionally reinforced concrete. Special attention must be paid to the formation of shear cracks in the concrete. Such shear cracks leads to an offset on the strengthened surface. This can cause a peeling-off or debonding of the strengthening strips. Thus, limiting shear crack formation is design criterion for slender member. Fig. 3.1 shows the formation of shear cracks following by debonding of CFRP laminates from the face of concrete.

A recent survey done by Chen et al 2001 showed that many different experimental set-ups have been used for determining the CFRP-to-concrete bond strength, but no consensus on a standard test procedure has been reached.

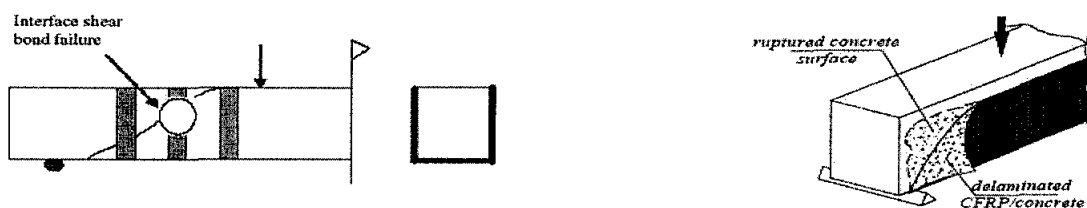


Fig. 3.1 CFRP SHEAR DEBONDING

### 3.2.2 Objectives of Experimental Study

The main objectives of this experimental research program were to:

1. Propose a new methodology that enables to study the interfacial behaviour of CFRP-to concrete joints under cyclic and monotonic shear loading.
2. Study the effectiveness of using CFRP for increasing the shear capacity, extending fatigue life of CFRP-to-concrete joints as well as bond stress– slip behaviour.
3. Propose new mathematical formulas to calculate the shear stiffness of interface element between CFRP side plates and concrete under cyclic shear loading and to study its degradation with respect to number of cycles.
4. Obtain the  $S-N$  curve for CFRP-to-concrete joints under pure shear as well as shear-moment interaction condition
5. Propose a new experimental setup that enables to obtain failure criteria and constitutive relations for interface element under cyclic shear loading.

To achieve these objectives; two different types of test setup were adopted. In the first type, axial load was applied to the specimen and the axial shear bond stress and the relative displacement between the concrete and CFRP sheet were computed. In the second type, lateral stress was added to previous setup in order to simulate the bond stress that becomes one of the major variables in failure criteria of interface element. Pre-stressed steel rod and two lateral steel plates were attached at the side face of the specimen were used for this purpose. The following section gives brief description about the specimen used in experimental program.

### 3.2.3 Specimen Descriptions

An experimental program consisted of testing specified number of push off specimens has been conducted. The CFRP composite strips were used herein to strengthen these specimens externally at a known failure plane to resist shear stresses under shear friction.

The uncracked push-off specimens for concrete externally reinforced with CFRP composites were designed to fail in shear at a known plane, as shown in Fig. 3.2. To ensure the failure of the push-off specimen to be happening in shear friction across the

given plane and prevent undesirable failure modes, reinforcing steel was placed apart from the shear plane so the other mode of failure such as flexural, compression, or bearing could be prevented.

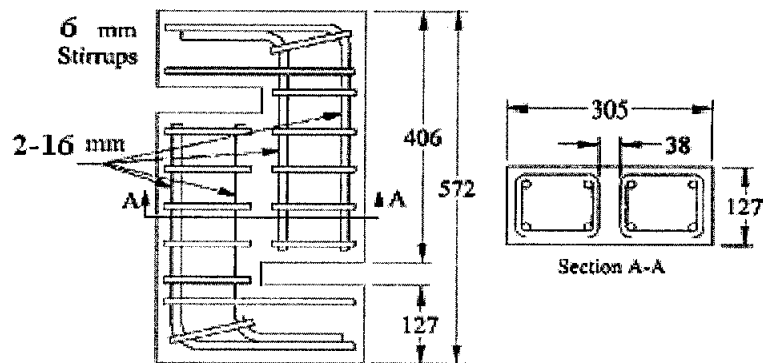


Fig. 3.2 SPECIMEN DESCRIPTION

### 3.2.4 Materials Properties

Concrete mix properties were made for 28 days cube strength of 50 Mpa, with cement content of 360Kg/m<sup>3</sup> and slump of 40mm. The mix proportions were based on mass ratio of: 1.0 (ordinary Portland cement), 2 (sand), 3.2 (coarse aggregate of 14 mm maximum size), a water-cement ratio 0.40, and superplasticizer 1.5%.

Twenty six specimens were cast as per details given in last section. The properties of the materials used are given as follow:

#### 3.2.4.1 Cement

Ordinary Portland cement (CEM-I) was supplied by YTL cement Berhad, Malaysia that was confirmed the requirements of BS EN 197-1 was used to fabricate the push-off specimens.

#### 3.2.4.2 Aggregate

Mining sand from Tronoh, Malaysia, was used as fine aggregate while granite gravel with maximum size of 14mm was obtained from Papan granite; Ipoh, Malaysia was employed as coarse gravel. Both fine and coarse aggregate conformed to BS 882:

1992. The particle size distribution curves for them are shown in Fig.A1 and Fig.A2 in appendix-I.

### 3.2.4.3 Superplasticizer

To obtain the required strength with acceptable level of workability a material such as water reducing admixture was added to the concrete mix. The superplasticizer in the form of aqueous solution commercially known as naphthalene formaldehyde sulphonate was used as water reducing admixture(WRA) that complied to BS 5075:PART 3:1985.

### 3.2.4.4 Reinforcement

16mm and 6mm steel reinforcement bars were used with yield strength of 460 MPa and 250 Mpa respectively table 3.1 shows the properties of concrete and steel bars that were used in this research.

### 3.2.4.5 Epoxy-resin and CFRP Composite Laminate

1.2 ×100×240mm CFRP strips were supplied by Sika, Malaysia and known as CarboDur S1012 were used in this research as an external strengthening materials.

An epoxy material known as SikaDUR-30 was used to glue the CFRP laminates at both sides of the specimen. The epoxy was consisted of two components; Part A was white coloured base; Part B was a dark grey coloured hardener. The mix ratio of the two parts is 3:1 by weight. The mixture of the two is light grey in colour.

The epoxy-resin and CFRP composite laminate properties are described in Table 3.2.

Table 3.1 Properties of concrete and reinforcement

Material type	Ultimate strength (Mpa)	Elastic modulus (Gpa)	Elongation at break (%)
Concrete	50.8	-	-
Steel D=16mm	460	230	-
Steel D=6mm	250	230	-

Table 3.2 Epoxy-resin and CFRP composite laminate properties

Material type	Ultimate strength (Mpa)	Elastic modulus (Gpa)	Elongation at break (%)	Adhesive strength on concrete (Mpa)	Adhesive strength on steel (Mpa)
CFRP 10cm width	2400	150	1.4	-	-
Epoxy-resin SikaDur – 30	100	12.8	-	>2	>25

### 3.2.5 Mixing, Casting and Curing of Concrete

All concrete ingredients were mixed according to BS 8110:1997. The mix proportions were made for 28 day target strength of 50 Mpa and the required slump range was 80-30 mm. Table 3.3 gives the summary of these trial tests. After achieving the required workability of concrete, the specimens were cast to determine the hardened concrete properties. After casting, plastic sheet were used to cover the specimens to prevent the water from evaporating. After 24 hours, the specimens were demoulded and placed for curing according to BS 1881: Part 108:1983.

All of the push-off specimens were cast in four batches; six 150 ×150 mm concrete cubes were cast from each batch for testing at the age of 7 and 28 days. The specimens were cured in water bath. All the compression tests were performed under a constant rate of 6.8 KN/s according to BS 1881: Part 116:1983. The average concrete compressive strength  $f_{cu}$  of 50.8 Mpa was obtained after 28 days from casting day.

Table 3.3 TRIAL TESTS

Mix proportion	w/c	Sp(% of cement)	Slump(mm)
1:2:3.2	0.36	1	0
1:2:3.2	0.36	1.5	0
1:2:3.2	0.36	2	12
1:2:3.2	0.4	1	20
1:2:3.2	0.4	1.5	40
1:2:3.2	0.4	2	95

Note: selected mix 1:2:3.2 with water cement ratio 0.4 and Superplasticizer content 1.5% from the weight of cement

Fig. 3.3, Fig. 3.4 and Fig. 3.5 Show part of test preparation

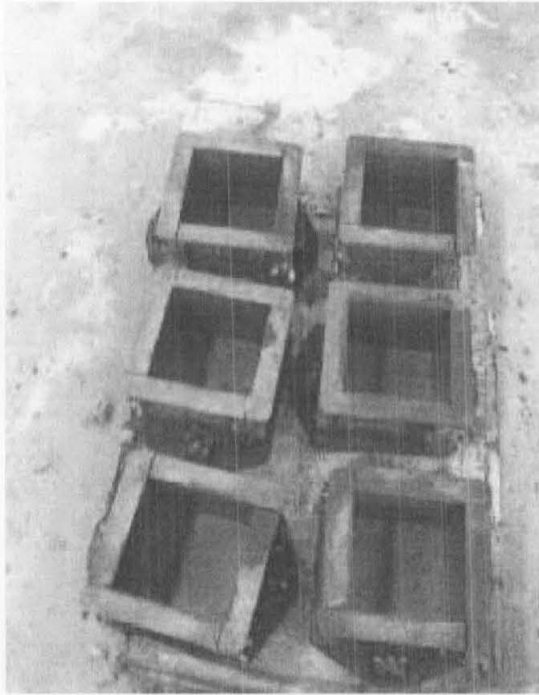


Fig. 3.3 STANDARD CUBES BEFORE CASTING

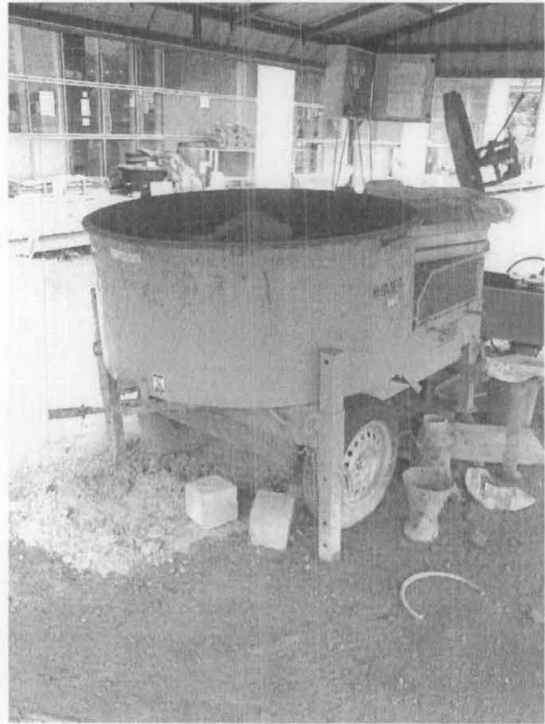


Fig. 3.4 MIXING MACHINE



Fig. 3.5 CONCRETE CUBES UNDER TESTING

### 3.2.6 Specimens Preparation

The following steps were made to prepare the push-off specimens for the purpose of testing:

- The concrete surface of the specimens was roughened using a mechanical grinder to remove the surface laitance and expose the coarse aggregates.
- The concrete surface was sandblasted and then cleaned by air blasting.
- The specimens were blown with compressed water to remove the dust or any loose particles.
- The CFRP plates were cut to the required length (240mm)
- The CFRP plates were cleaned with acetone, this process was repeated until the washcloth was no longer blackened.
- For the first part of experimental program, 1-dimensional embedded strain gauges were fixed at centre of shear plane to measure axial strains in concrete.
- Uniform thickness of 2.5–2.7 mm of adhesive layer was maintained by using aluminium guides.
- CFRP plates were then smoothly hand-laid to achieve wrinkle-free surface, and extra epoxy was squeezed out and removed keeping the thickness of epoxy between acceptable rang.
- The bonded joints were allowed to cure for a minimum of 7days before the push-off tests were performed.
- For the first part of experimental program, 1-dimensional external strain gauges with same position of that of embedded ones were fixed at the face of CFRP plates to measure the axial strains as expected to happen during the test. For the second part of experimental program, 2-dimensional external strain gauges were fixed at the face of CFRP plates to measure the axial and lateral strains in CFRP sheet.
- For the second part of experimental program two steel plates with 2 mm thickness were attached to the rough sides of the specimen using steel rod passed through the void and tied at its two ends by steel nudes. This was done to produce additional stress in the lateral direction.

### 3.2.7 Testing Procedure

The prepared specimen was placed at the testing rig as shown in Fig.3.6. The specimen was subjected to static and cyclic loading under compression mode. For group *A* specimens the load *P* was applied at the centre produce pure shear load. For group *B* the load *P* was applied at an eccentricity of 50 mm. This was done to study the interfacial behaviour at shear-moment interaction condition. The test setup and supports were designed to produce a direct shear at the CFRP-to-concrete interface.

For the first part of experimental program specimens were instrumented with linear variable differential transducers LVDTs and strain gauges for the purpose of monitoring the following parameters:

1. The slip of the joint (the displacement of the upper end along the joint relative to that for the lower end).
2. The axial strains in the CFRP laminate and concrete.

One-dimensional embedded strain gauges (30 mm in length) with a resistance of  $(119.8 \pm 0.2)$  were bonded on the central axis of the concrete surface to measure the concrete strains during the push-off tests. One-dimensional external strain gauges (10 mm in length) with a resistance of  $(119.6 \pm 0.4)$  were bonded on the central axis of the CFRP to measure strains produced in CFRP plates during the test. It was assumed that the composite strain will remain entire constant on the whole width of the CFRP. It was also assumed that the strains are equal on both sides of the specimen because of the symmetric geometry. This assumption was confirmed later after obtaining the strain gauges readings. Two displacement sensors (Linear Variable Displacement Transducers,) LVDTs, with a range of (50-100) mm and a resolution/accuracy of  $(10^{-4}$  mm/0.05%) were installed to measure the slip between the concrete and CFRP plates as shown in Fig.3.6. All strain gauges and LVDTs used in this research were supplied by MAKAWA Company.

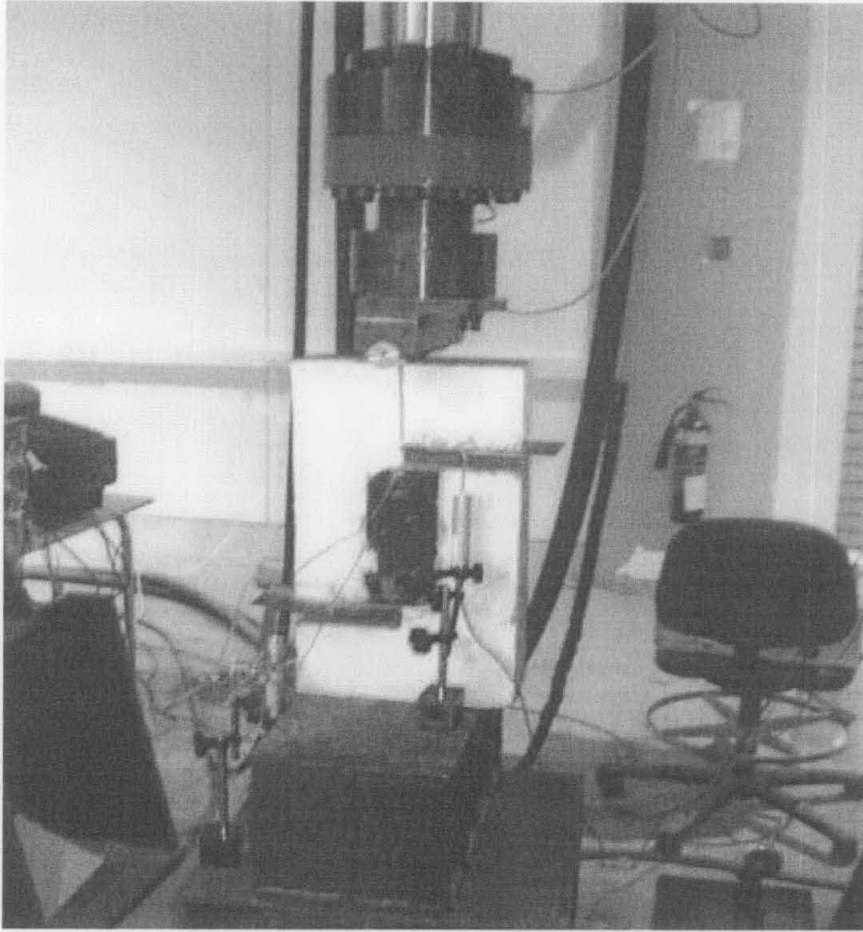
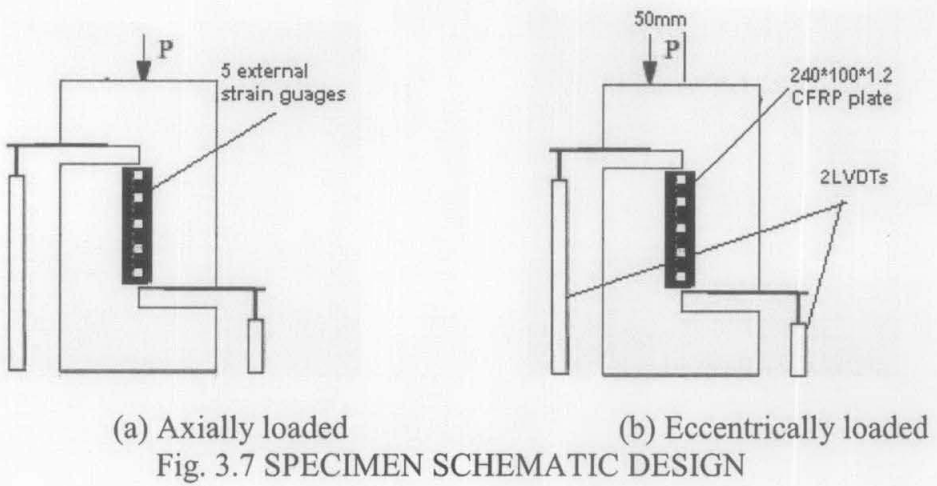


Fig. 3.6 SPECIMEN UNDER TESTING

Fig.3.7 shows the specimen schematic design for axially loaded case as well as eccentrically loaded condition



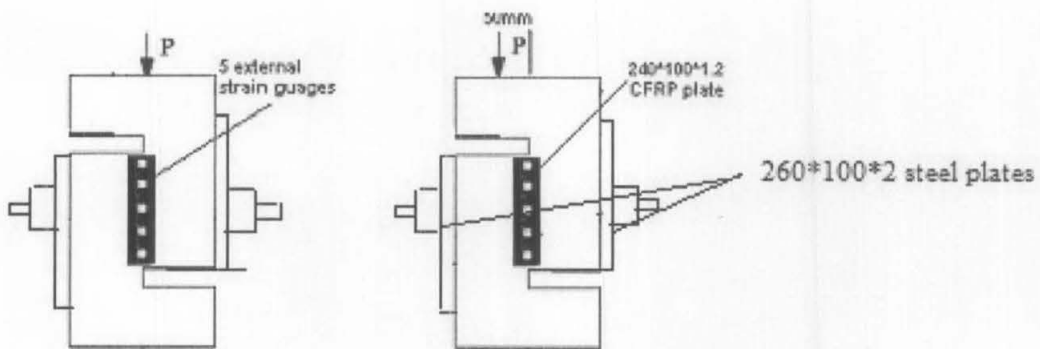
For the second part of experimental program, the specimens were instrumented with 2-dimensional external strain gauges which were fixed at the face of CFRP plates to collect the following data:

1. Shear stress in axial direction
2. Bond stress in lateral direction



Fig. 3.8 SPECIMEN UNDER TESTING

Fig.3.9 shows the specimen schematic design for second part of experimental program



(a) Axially loaded

(b) Eccentrically loaded

Fig. 3.9 SPECIMEN SCHEMATIC DESIGN

### 3.2.8 Loading Conditions

- *For static applied loading condition*, all the tests were performed under a control load rate of 0.25KN/s.
- *For static applied loading condition*, all specimens were tested under high cyclic load (10%-80%) of failure load that was obtained from static test results of the control specimen from each group. Each test was performed under a constant-amplitude sinusoidal loading at a frequency of 3 Hz. This frequency was selected because conventional civil engineering structures are typically subjected frequencies varying between 1 to 5 Hz (Chen et al 2001).
- *Specification of loading frame*: Zwick Roell HA500 testing supplied by RB CAPITOL SDN BHD was used for both static and cyclic tests.

The next section gives brief description about the analytical methodology used in this research to study the over all shear behaviour of R.C beams externally strengthened CFRP laminates.

## 3.3 Analytical investigation

### 3.3.1 Background

Appropriate Finite Element modelling approach is required for predicting structural behaviour of reinforced concrete structures. An overview of typical approaches, their objective and range of application is discussed to provide background for the adopted models. Within the framework of the finite element method; reinforced concrete can be represented either by superimposition of the material models for the constituent parts (i.e., for concrete and for reinforcing steel), or by a constitutive law for the composite concrete and embedded steel considered as a continuum at the macro level. Because of their wide range of application, earlier modelling approaches are more acceptable.

The finite element method is well suited for superposition of the material models for the constituent parts of a composite material. Material models of this type can be employed for virtually all kinds of reinforced concrete structures. Depending on the

type of problem to be solved, concrete can be represented by solid elements, shell or plate elements, or beam elements.

The reinforcement is modelled either by separate truss or beam elements (discrete representation) or by separate elements of the same type as the concrete elements, which are superimposed on the latter (embedded representation) or by distribution of reinforcement to thin layers of equivalent thickness (distributed representation). Superposition of concrete and reinforcement in the models requires constitutive relationship to account for bond and dowel action on the concrete-steel interface.

Discrete representation of reinforcement allows modelling of bond and dowel action by means of special elements that connected the adjacent nodes of concrete and steel elements. The distributed representation and the embedded representation of the reinforcement, however, do not permit the use of bond elements, because the displacements of concrete and steel at the interface are presumed to be the same. Consequently, the effect of bond slip can only be accounted for implicitly by modifying the constitutive relations for concrete or steel.

If reinforced concrete is modelled by a constitutive law for the composite concrete and embedded steel considered as a continuum, the material behaviour of reinforced concrete at the macro level is described as if the composite material was a single material. Constitutive models of this type are essentially based on the results of experimentation on reinforced concrete panels [Vecchio et al (1986), Vecchio et al(1996) and Maekawa (2003)] ; Since reinforced concrete is treated as a single material, neither the reinforcement nor the steel-concrete interaction needs to be modelled separately. Models of this type are only appropriate if reinforcement is distributed uniformly.

Solid elements are also convenient because the better representation of multi-axial stress states enables the effective use of refined constitutive laws for concrete. These elements can be attached to interface elements to model bond slip behaviour in an explicit manner. This theorem to be very useful for both a good prediction of the overall behaviour of the structural elements and for an accurate evaluation of the interface stresses and strains which are critical in the delamination failure modes of these systems. The solid elements used are:

- Linear and quadratic plane strain and plane stress two-dimensional elements
- Linear and quadratic three-dimensional elements

Solid elements have been used in the different models for concrete, for steel reinforcement and for FRP plates. Alternatively truss elements have been used in two-dimensional analyses for steel bars and FRP. Different constitutive laws have been tested for concrete. The material models used cover damage models [Lemaitre et al (1994) and LUSAS - User Manual. (1999)], elasto-plastic models [Wrankw (1974) and am et al (1994)], cracking models [Loo et al (1991) and Maekawa (2003)]. These models are described in the chapter on modelling of concrete.

In this research a non-linear FE algorithm was developed and it consisted of the following main parts:

- Selection of elements type
- Material cyclic models
- Modelling of shear resisting mechanisms
- Interfacial model between concrete and CFRP laminates
- Non-linear analysis technique

### **3.3.2 Objectives of analytical investigation**

The main objectives of the analytical investigation were to analyze the fatigue performance of RC beams strengthened for shear using externally bonded carbon CFRP sheets. This includes the following

1. Factors affecting shear capacity
2. Contribution of shear resisting mechanism
3. Efficiency of using CFRP sheets
4. Mode of failure

The following section demonstrates general outlines regarding the FE algorithm that was developed in this research to simulate the fatigue performance of RC beams strengthened for shear using externally bonded CFRP sheets.

### 3.3.3 Analytical Algorithm Outlines

An analytical model based on non-linear finite element algorithms coded in FORTRAN language has been developed to enable the analysis of RC beams externally strengthened for shear using CFRP laminates under cyclic loads.

20-noded isoparametric quadrilateral elements with three degrees of freedom per each node were used to represent concrete. Material response is assumed to be orthotropic with tangent stiffness that was derived from stress-strain relationship for concrete subjected to general biaxial state of stress.

The reinforcement bars were represented in discrete manner. 2-noded space frame and space truss elements were used for this purpose. Material response was assumed to be elastic-perfectly plastic.

20-noded elements similar to those used to model concrete elements were used to represent FRP side plates. Material response was assumed to be elastic-brittle. Discrete cracking approach was used to represent cracking.

Primary considerations have been given to the representation of shear transfer mechanisms due to aggregate interlock in cracked concrete and dowel action in reinforcement. Expressions were derived from an analytical model in conjunction with experimental data to provide shear stress and stiffness values for special elements used to model aggregate interlock mechanism. A comparable approach was used to derive expression for dowel action mechanism.

In the phenomenological modelling of bond the concrete and the reinforcing bars are discretized by three-dimensional finite elements. The link between the bar and the concrete can be realized, either by a continuous or discontinuous connection. In the continuous connection the macroscopic stress-strain constitutive relationship has to be employed whereas in the discontinuous approach, bond is defined by discrete. The bond-slip phenomenon between concrete and reinforcement has been accounted for by using non-dimensional zero-thickness elements (springs) whose behaviour is controlled by the stress-slip relationship. The bond element is a two-node finite element and it connects a truss/bar finite element (reinforcement) with a three-dimensional solid finite element (concrete). The element displacement field is a slip, which is defined as the relative displacement between the reinforcing bar and the concrete in the direction of the reinforcing bar. Shear stiffness values for such elements are obtained from expression based on experimental data.

A new interfacial model has been developed to simulate interfacial behaviour of CFRP-to-concrete bonded joints under cyclic loading. 3-D interface element is used to simulate this phenomenon. The element has sixteen nodes, eight nodes connect to concrete element and the other eight nodes connected to CFRP sheet. The interface was modelled by three linear springs connecting the joint nodes with the same coordinates. The element displacement field is a slip, which is defined as the relative displacement between concrete and CFRP sheet. Shear stiffness and failure criteria of the elements represented this phenomenon was adopted from expression based on test results obtained from the experimental part of this research.

Brief description about materials and shear resisting mechanism models can be found in chapter 4 and chapter 5. Selection of element types, derivation of stiffness matrix for each element, how the strains and stresses can be obtained, and the non-linear analysis technique used to solved the cyclic problem can be found in details in chapter 7.

## CHAPTER 4

### MATERIALS CYCLIC MODELS

#### 4.1 Introduction

The challenge in numerical modeling of structural concrete arises from the material's composite nature. Structural concrete's non-linear behavior includes; cracking, crushing, tension stiffening, compression softening, and bond-slip. Cyclic loading induces further complexities, such as stiffness degradation in concrete, the Bauschinger effect in reinforcement, and bond degradation between concrete and reinforcement. The accuracy and reliability of numerical modeling of reinforced concrete is due to the abilities of the underlying constitutive relations to capture different types of non-linear behavior.

A set of models for structural concrete was evaluated and used to simulate a variety of cyclically loaded component experiments that exhibit different hysteretic responses. The focus of these simulations is on finite-element analyses (FEA) to facilitate the evaluation of new and existing structural designs when only material and geometric properties are known. Since the first use of non-linear FEA to simulate reinforced concrete (Ngo and Scordelis 1967), significant developments have been followed for more realistic modeling of structural concrete behavior. A large number of sophisticated constitutive models that can be successfully use to capture behavior at the material have been developed, as summarized in state-of-the-art reports by ASCE-ACI (1982, 1993) and CEB (1996). Less has been reported on the successful application of these material models to predict the behavior of structural components under cyclic loading.

This chapter focuses on the selection of non-linear material models to predict the cyclic behavior of concrete, steel and CFRP laminates

## 4.2 Concrete Cyclic Model

### 4.2.1 Introduction

Concrete is a non-homogeneous and anisotropic material. Its response is non-linear even under small stress levels. Furthermore, concrete exhibits a different behavior under tension and compression stresses. In compression, the response hardens up to a peak stress value that depends on the level of lateral confinement. The post peak behavior depends in general on the level of lateral confinement [Kang et al (1998)]. Under low confinement; the post-peak response is brittle softening. For increasing confinement stresses, the response of concrete changes to ductile hardening [Kang et al (1998), Smith et al (1989)]. Under tensile stresses, concrete cracks and eventually loses strength entirely.

The response of concrete under triaxial states of stress greatly depends on the formation and expansion of microcracks [Willam et al (1986)]. Several tests have shown that the evolution of the microcracks governs the concrete brittleness, ductility, dilatancy and the failure modes. All these phenomena depend in general on the triaxial state of stress applied to the concrete. Under low lateral confinement, the failure mode observed in uniaxial compression tests is caused by vertical tension splitting. A sharp post peak loss of strength is observed. Under gradually larger confinement, cracking and damage become more distributed and concrete becomes ductile, with little or no post-peak degradation.

Under even small values of applied stress, concrete exhibits very complex structural response with the following material specific characteristics: non-linear stress strain behavior from the outset, tensile cracking, temperature-dependent creep deformation, and dilatation under high compressive stress (Berg(1961); Geniev (1974); Karpenko (1976) ; Cedolin et al (1977); Kotsovos and Newman (1977); bathe and Ramaswamy(1979); Bazant and kim(1979); Elwi and Murray(1979); Chen(1982); Chen and Buyukozturk(1985); Vicchio and Collin(1986). All these non-linear response characteristics depend strongly on the multi-axial state of stress.

The complex non-linear behavior of concrete makes it a difficult material to model. In spite of the widespread interest in modeling of concrete under three-

dimensional states of stresses, few models are available for immediate and simple numerical implementation in finite element codes. Current models range from very sophisticated laws based on plasticity theory that rely on the definition of a plastic flow rule and on the separation of the deformation increments into plastic and elastic components.

The application of the concrete constitutive law to the 3-D finite element analysis of reinforced concrete structural elements urged the availability of models that are both mechanically justified and computationally robust. Models should be able to simulate the most important characteristics of the monotonic and cyclic response of concrete under triaxial states of stresses, while maintaining a certain computational simplicity to allow analyses of structural elements with reasonable computational efforts.

#### **4.2.2 Proposed Cyclic Model for Concrete**

The main features of the concrete model proposed by Balan et al (1986) are discussed in this section, with emphasis on the enhancements to the original model and on the numerical implementation issues. The proposed 3D constitutive law uses an orthotropic model with the axes of orthotropy parallel to the principal stress directions. Principal strain and principal stress directions are not coaxial. The model is based on the concept of equivalent uniaxial strains introduced by Darwin and Pecknold (1977), Bashur and Darwin (1978) and Elwi and Murray (1985). The proposed 3-D cyclic stress-strain relationship is based on hydroplastic orthotropic model with stress equivalent uniaxial strain relationship that is generalized to account for triaxial condition. The proposed model in the analysis presented herein includes the effect of the following:

- Triaxial non-linear stress-strain behavior
- Tensile cracking
- Compression crushing
- Strain softening of concrete under triaxial conditions
- Failure surface

#### 4.2.2.1 Triaxial non-linear stress-strain behavior

With respect to the orthotropic axes the constitutive equation is written as:

$$\sigma = D_L \varepsilon$$

Where  $\sigma, \varepsilon$  = stresses and strains respectively and  $D_L$  = the constitutive relations for orthotropic materials used in the analysis

$$\begin{pmatrix} \sigma_1 \\ \sigma_2 \\ \sigma_3 \\ \tau_{12} \\ \tau_{23} \\ \tau_{31} \end{pmatrix} = \begin{pmatrix} E_1 \left( \frac{1 - \nu_{23}\nu_{32}}{\Delta} \right) & E_1 \left( \frac{\nu_{21} + \nu_{31}\nu_{23}}{\Delta} \right) & E_1 \left( \frac{\nu_{31} + \nu_{21}\nu_{32}}{\Delta} \right) & 0 & 0 & 0 \\ E_2 \left( \frac{\nu_{12} + \nu_{32}\nu_{13}}{\Delta} \right) & E_2 \left( \frac{1 - \nu_{13}\nu_{31}}{\Delta} \right) & E_2 \left( \frac{\nu_{32} + \nu_{12}\nu_{31}}{\Delta} \right) & 0 & 0 & 0 \\ E_3 \left( \frac{\nu_{13} + \nu_{32}\nu_{23}}{\Delta} \right) & E_3 \left( \frac{\nu_{23} + \nu_{21}\nu_{13}}{\Delta} \right) & E_3 \left( \frac{1 + \nu_{23}\nu_{32}}{\Delta} \right) & 0 & 0 & 0 \\ 0 & 0 & 0 & G_{12} & 0 & 0 \\ 0 & 0 & 0 & 0 & G_{23} & 0 \\ 0 & 0 & 0 & 0 & 0 & G_{31} \end{pmatrix} \begin{pmatrix} \varepsilon_1 \\ \varepsilon_2 \\ \varepsilon_3 \\ \gamma_{12} \\ \gamma_{23} \\ \gamma_{31} \end{pmatrix} \dots 4.1$$

Where

$$\frac{\nu_{ij}}{E_i} = \frac{\nu_{ji}}{E_j}$$

$$\Delta = 1 - \nu_{12}\nu_{21} - \nu_{23}\nu_{32} - \nu_{31}\nu_{13} - 2\nu_{21}\nu_{32}\nu_{13}$$

$$G_{ij} = \frac{E_i E_j}{(E_i + E_j)}$$

#### 4.2.2.2 Equivalent Uniaxial Strains

The equivalent uniaxial strain is a fictitious strain with no precise material meaning. It is used to de-couple the 3D material response into three uniaxial constitutive laws. Darwin and Pecknold (1977) first introduced the concept. For a given principal stresses  $\sigma_{p_i}$ , the equivalent uniaxial strains  $\varepsilon_{ui}$  are the strains that would induce the same stresses on the equivalent uniaxial stress-strain curves. The material parameters that define the equivalent uniaxial stress-strain curves depend on the current stress ratio, as discussed later in the chapter.

Uniaxial strain increments  $d\varepsilon_{ui}$  can then be related to the true strain  $d\varepsilon_i$  increments in the current orthotropic axes as follows:

$$\begin{bmatrix} d\varepsilon_{u1} \\ d\varepsilon_{u2} \\ d\varepsilon_{u3} \end{bmatrix} = \begin{bmatrix} (1-\nu_{23}\nu_{32})/\Delta & (\nu_{21}+\nu_{23}\nu_{31})/\Delta & (\nu_{31}+\nu_{21}\nu_{32})/\Delta \\ (\nu_{12}+\nu_{13}\nu_{32})/\Delta & (1-\nu_{13}\nu_{31})/\Delta & (\nu_{32}+\nu_{12}\nu_{31})/\Delta \\ (\nu_{13}+\nu_{12}\nu_{23})/\Delta & (\nu_{23}+\nu_{13}\nu_{21})/\Delta & (1+\nu_{12}\nu_{21})/\Delta \end{bmatrix} \begin{bmatrix} d\varepsilon_1 \\ d\varepsilon_2 \\ d\varepsilon_3 \end{bmatrix} \dots\dots\dots 4.2$$

With respect to the equivalent uniaxial strain  $\varepsilon_{ui}$  the constitutive relation can be written as follows:

$$\begin{bmatrix} \partial\sigma_1 \\ \partial\sigma_2 \\ \partial\sigma_3 \\ \partial\tau_{12} \\ \partial\tau_{23} \\ \partial\tau_{31} \end{bmatrix} = \begin{bmatrix} E_1 & 0 & 0 & 0 & 0 & 0 \\ 0 & E_2 & 0 & 0 & 0 & 0 \\ 0 & 0 & E_3 & 0 & 0 & 0 \\ 0 & 0 & 0 & G_{12} & 0 & 0 \\ 0 & 0 & 0 & 0 & G_{23} & 0 \\ 0 & 0 & 0 & 0 & 0 & G_{31} \end{bmatrix} \begin{bmatrix} \partial\varepsilon_{u1} \\ \partial\varepsilon_{u2} \\ \partial\varepsilon_{u3} \\ \partial\gamma_{12} \\ \partial\gamma_{23} \\ \partial\gamma_{31} \end{bmatrix} \dots\dots\dots 4.3$$

In the present work, a different approach is followed. Two curves are used to describe the material response in uniaxial compression. The curve proposed by Popovics (1973) describes the ascending branch up to the peak point, while the curve of Saenz (1964) is used for the post peak response. The law is shown in Fig. 4.1 and is defined by a single equation as follows:

$$\sigma_i = R_{ci} \frac{K_i \left(\frac{\varepsilon_{ui}}{\varepsilon_{ci}}\right)}{1 + A_i \left(\frac{\varepsilon_{ui}}{\varepsilon_{ci}}\right) + B_i \left(\frac{\varepsilon_{ui}}{\varepsilon_{ci}}\right)^2 + C_i \left(\frac{\varepsilon_{ui}}{\varepsilon_{ci}}\right)^3}, (i = 1,2,3) \dots\dots\dots 4.4$$

Where

$$A_i = C_i + K_i - 2, B_i = 1 - 2C_i, C_i = K_i \frac{(K_{ci} - 1)}{(K_{ci} - 1)^2} - \frac{1}{K_{ci}}$$

$$K_i = E_0 \frac{\varepsilon_{ci}}{R_{ci}}, K_{ci} = \frac{\varepsilon_{fi}}{\varepsilon_{ci}}, K_{oi} = E_0 \frac{R_{ci}}{R_{fi}}$$

$R_{ci}$  are concrete strength in direction  $i$ -axis can be obtained from ultimate failure surface described in section 4.2.2.7

$$\sigma_{fi} = 0.85 R_{ci}, \varepsilon_{fi} = 1.41 \varepsilon_{ci} \quad \text{For compression loading}$$

$$\sigma_{ft} = 0.25 R_{ci}, \varepsilon_{ft} = 4.0 \varepsilon_{ci} \quad \text{For tension loading}$$

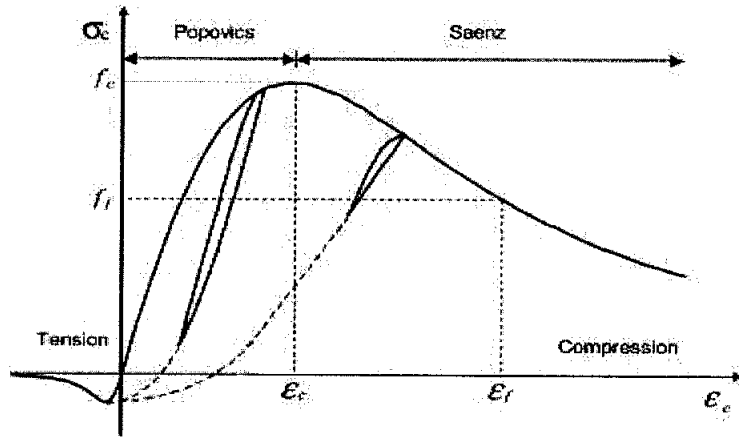


Fig. 4.1 MONOTONIC UNIAXIAL STRESS-STRAIN CURVE  
Saenz (1964)

The following rules govern the cyclic behavior of equivalent uniaxial stress-strain relation:

$$\sigma_i = R_{ci} \frac{K_i \left( \frac{\epsilon_{ui}}{\epsilon_{ci} - \epsilon_{0i}} \right)}{1 + A_i \left( \frac{\epsilon_{ui}}{\epsilon_{ci} - \epsilon_{0i}} \right) + B_i \left( \frac{\epsilon_{ui}}{\epsilon_{ci} - \epsilon_{0i}} \right)^2 + C_i \left( \frac{\epsilon_{ui}}{\epsilon_{ci} - \epsilon_{0i}} \right)^3}, (i = 1, 2, 3) \dots \dots \dots 4.5$$

where

$$\epsilon_{0i} = \epsilon_{ui} - \frac{\sigma_i}{E_0} \text{ for } \epsilon_{ui} \leq \epsilon_{ci}$$

$$\epsilon_{0i} = \epsilon_{ci} - \frac{R_{ci}}{E_0} \text{ for } \epsilon_{ui} > \epsilon_{ci}$$

Where  $\epsilon_{0i}$  = strain that corresponds to complete unloading in  $i$ -direction of orthotropy.

$A_i, B_i, C_i, K_i, R_{ci}$  = parameters as described in Equation 4.4.

For concrete cyclic law the loading/unloading criterion is based on the loading function  $f$  defined as follows:

$f > f_{max}$  for loading condition

$f \leq f_{max}$  for unloading condition

Where  $f_{max}$  is the maximum value of the loading function up to the current load step.

### 4.2.2.3 Poisson Ratio

The definition of the transverse strain ratios  $\nu_{ij}$  is an important step in the formulation of the concrete law. The following expression by Balan (1986) defines these ratios as follows:

$$\nu_{ij} = \sqrt{\frac{\nu_{ui}\nu_{uj}E_i}{E_j}}, (i, j = 1, 2, 3) \dots\dots\dots 4.6$$

Where  $\nu_{ui}$  is the uniaxial transverse strain ratio in the direction  $i$ . The following expression is used to define  $\nu_{ui}$  as cubic function of the corresponding equivalent uniaxial strain as follows:

$$\nu_{ui} = \nu_0 \left[ 1 + A_i \left( \frac{\epsilon_{ui}}{\epsilon_{ci}} \right) + B_i \left( \frac{\epsilon_{ui}}{\epsilon_{ci}} \right)^2 + C_i \left( \frac{\epsilon_{ui}}{\epsilon_{ci}} \right)^3 \right], (i = 1, 2, 3) \dots\dots\dots 4.7$$

$\nu_0$  = Initial Poisson ratio.

$\epsilon_{ci}$  = Concrete strain in direction  $i$ -axis

$\epsilon_{ui}$  = Uniaxial strain in direction  $i$ -axis

$A_i, B_i, C_i$  = Parameters as described in Equation 4.5.

### 4.2.2.4 Shear Modulus

Because the shear moduli  $G_{ij}$  ( $i, j=1, 2, 3$ ) must be invariant under an arbitrary coordinate transformation of the reference system, Lekhnitskii (1963) has shown that the shear moduli are:

$$G_{ij} = \frac{E_i E_j}{E_i(1+\nu_{ij}) + E_j(1+\nu_{ji})} \dots\dots\dots 4.8$$

Where  $E_i$  is young modulus with respect to direction  $i$ -axis defined as follows:

$$E_i = \frac{E_0}{1 + A_i \left( \frac{\epsilon_{ui}}{\epsilon_{ci}} \right) + B_i \left( \frac{\epsilon_{ui}}{\epsilon_{ci}} \right)^2 + C_i \left( \frac{\epsilon_{ui}}{\epsilon_{ci}} \right)^3}, (i = 1, 2, 3) \dots\dots\dots 4.9$$

$E_0$  = initial modulus of concrete

Other parameters can be obtained from previous equations

#### 4.2.2.5 Rotating Matrix

In finite element modelling, the incremental stress– strain relation with respect to the orthotropic axes must be rotated into the global reference system. This is done by using the rotation matrix  $T$  that contains the direction cosines of the orthotropic axes with respect to the global reference system:

$$D_G = T^T D_L T$$

Where

$D_G$  is the material matrix in the global reference system.

The rotation matrix  $T$  takes the following form according to Lekhnitskii (1963)

$$T = \begin{bmatrix} m_{11}^2 & m_{12}^2 & m_{13}^2 & 2m_{11}m_{12} & 2m_{12}m_{13} & 2m_{11}m_{13} \\ m_{21}^2 & m_{22}^2 & m_{23}^2 & 2m_{21}m_{22} & 2m_{22}m_{23} & 2m_{21}m_{23} \\ m_{31}^2 & m_{32}^2 & m_{33}^2 & 2m_{31}m_{32} & 2m_{32}m_{33} & 2m_{31}m_{33} \\ m_{11}m_{21} & m_{12}m_{22} & m_{13}m_{23} & m_{11}m_{22} + m_{12}m_{21} & m_{12}m_{23} + m_{13}m_{22} & m_{11}m_{23} + m_{13}m_{21} \\ m_{21}m_{31} & m_{22}m_{32} & m_{23}m_{33} & m_{21}m_{32} + m_{22}m_{31} & m_{22}m_{33} + m_{23}m_{32} & m_{21}m_{33} + m_{23}m_{31} \\ m_{11}m_{31} & m_{12}m_{32} & m_{13}m_{33} & m_{31}m_{12} + m_{32}m_{11} & m_{32}m_{13} + m_{33}m_{12} & m_{31}m_{13} + m_{33}m_{11} \end{bmatrix} \dots\dots\dots 4.10$$

Where  $m_{ij}$  denotes the direction cosines of the principal stress ( $i=1, 2$  and  $3$ )-axes relative to the global coordinates system  $X_j$  ( $j=1,2$  and  $3$ ) of the structure can be expressed by the following equations:

$$m_{i1}^2 = \frac{(\sigma_2 - \sigma_{ii})(\sigma_3 - \sigma_{ii}) + \tau_i^2}{(\sigma_2 - \sigma_1)(\sigma_3 - \sigma_1)}$$

$$m_{i2}^2 = \frac{(\sigma_1 - \sigma_{ii})(\sigma_3 - \sigma_{ii}) + \tau_i^2}{(\sigma_1 - \sigma_2)(\sigma_3 - \sigma_2)}, (i=1,2,3) \dots\dots\dots 4.11$$

$$m_{i3}^2 = \frac{(\sigma_1 - \sigma_{ii})(\sigma_2 - \sigma_{ii}) + \tau_i^2}{(\sigma_1 - \sigma_3)(\sigma_2 - \sigma_3)}$$

Where

$$\tau_1^2 = \sigma_{12}^2 - \sigma_{13}^2, \tau_2^2 = \sigma_{21}^2 - \sigma_{23}^2, \tau_3^2 = \sigma_{31}^2 - \sigma_{32}^2$$

$\sigma_1, \sigma_2, \sigma_3$  are principal stresses can be obtained as function of the octahedral normal and shear stress as described in section 4.2.2.

#### 4.2.2.6 Principal Stresses

The following relations express the principal stresses as function of the octahedral normal and shear stress according to Sokolovskii (1950)

$$\begin{aligned}\sigma_1 &= \sigma_0 + \frac{3 + \mu}{\sqrt{2(3 + \mu^2)}} \tau_0 \\ \sigma_2 &= \sigma_0 - \frac{\sqrt{2\mu}}{\sqrt{(3 + \mu^2)}} \tau_0 \dots\dots\dots 4.12 \\ \sigma_3 &= \sigma_0 + \frac{3 - \mu}{\sqrt{2(3 + \mu^2)}} \tau_0\end{aligned}$$

Where

$$\begin{aligned}\sigma_0 &= (\sigma_{11} + \sigma_{22} + \sigma_{33}) / 3 \\ \tau_0 &= \sqrt{[(\sigma_{11} - \sigma_{22})^2 + (\sigma_{22} - \sigma_{33})^2 + (\sigma_{33} - \sigma_{11})^2 - 6(\sigma_{12}^2 + \sigma_{23}^2 + \sigma_{31}^2)] / \sigma_{11}} \\ \mu &= \sqrt{3 \cot(\varphi + 4/3\pi)} \\ \varphi &= 1/3 \arccos\{(3\sqrt{3}/2)[I_3(D\sigma) / \sqrt{I_2^3(D\sigma)}]\} \\ I_2 &= \sigma_1\sigma_2 + \sigma_1\sigma_3 + \sigma_2\sigma_3 \\ I_3 &= \sigma_1\sigma_2\sigma_3\end{aligned}$$

Where

- $\sigma_i$  = principal stress in  $i$ -direction ( $i=1, 2, 3$ )
- $\sigma_0$  = octahedral normal stress
- $\tau_0$  = octahedral shear stress
- $D\sigma$  = deviatoric stress
- $I_2, I_3$  = second and third invariant of deviatoric stress
- $\mu$  = Lode-nadai parameter

#### 4.2.2.7 Failure surface for concrete

The strength of concrete due to multiaxial stresses is a function of the state of stress that can not be predicted by limitation of simple tensile, compressive, and shearing stresses independently of each other. Therefore, strength of concrete element is properly determined only by considering interaction of various component of state of

stresses. The surface in stress space that define the ultimate strength values  $R_{c1}$ ,  $R_{c2}$ ,  $R_{c3}$  for a given principal stress ratio  $\sigma_1/\sigma_2/\sigma_3$  is usually called failure surface. These are not failure points, but rather combinations of maximum stress values.

In this research, the proposed five-parameter failure surface depicted in Fig. 4.2 is used to describe failure criteria of concrete. Its conical shape is defined using a tensile meridian,  $\rho_t$ , where the angle of similarity  $\theta=0^\circ$ , and a compressive meridian,  $\rho_c$ , where  $\theta=60^\circ$ . These two meridians are quadratic functions, concave in the direction of the negative  $\sigma_{oct}$ - axis. An elliptical curve,  $\rho(\zeta,\theta)$ , is used to interpolate between  $\rho_t$  and  $\rho_c$  to determine the stress at failure for any state of stress with angles of similarity lying between  $0^\circ$  and  $60^\circ$ .

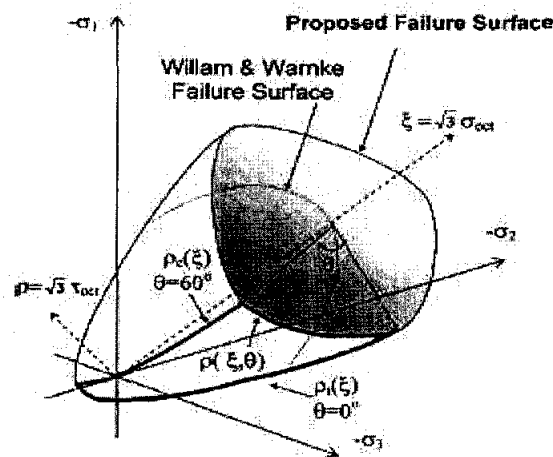


Fig. 4.2 PROPOSED UNIFIED FAILURE SURFACE

The choice of quadratic functions used in defining  $\rho_t$  and  $\rho_c$  ensures that the failure surface would not intersect the hydrostatic axis at high triaxial compressive stress, while the use of the elliptical interpolation  $\rho(\zeta,\theta)$  allows for greater flexibility in modifying a specific section of the failure surface subsequently to account for the presence of fibres in SFRC. Such a formulation also ensures that the failure surface satisfies all the requirements of being smooth, convex and having the ratio of  $\rho_t / \rho_c$  vary from 0.5 near the apex to 1 as the octahedral stress tends to infinity (Guo 1997). In this formulation, compressive stresses are taken to be negative, and the equations are expressed in terms of  $\zeta$  and  $\rho$  and where  $\zeta=\sqrt{3} \sigma_{oct}$  and  $\rho=\sqrt{3} \tau_{oct}$ . This results in a clear physical interpretation of the equations as the values of  $j$  and  $r$  correspond directly to the projections of the current state of stress in the Cartesian axes,  $\sigma_1$ ,  $\sigma_2$ ,  $\sigma_3$ , onto the hydrostatic axis and deviatoric plane, respectively. Due to the six-fold

symmetry of the surface, Eqs. 4.13 to 4.16 describing  $\rho_t$ ,  $\rho_c$ , and  $\zeta$  and  $\rho$ , are sufficient to define the entire failure surface:

$$\frac{\xi}{f_{cu}} = a_2 \left( \frac{k\rho_t}{f_{cu}} \right)^2 + a_1 \left( \frac{k\rho_t}{f_{cu}} \right) + a_0, \quad k \leq 1 \quad \dots\dots\dots 4.13$$

$$\frac{\xi}{f_{cu}} = b_2 \left( \frac{\rho_c}{f_{cu}} \right)^2 + b_1 \left( \frac{\rho_c}{f_{cu}} \right) + b_0 \quad \dots\dots\dots 4.14$$

$$\rho(\xi, \theta) = \frac{2\rho_c(\rho_c^2 - \rho_t^2)\cos\theta + \rho_c(2\rho_t - \rho_c)[4(\rho_c^2 - \rho_t^2)\cos^2\theta + 5\rho_t^2 - 4\rho_c\rho_t]^{1/2}}{4(\rho_c^2 - \rho_t^2)\cos^2\theta + (\rho_c - 2\rho_t)^2} \quad \dots\dots 4.15$$

$$\cos\theta = \left[ \frac{3(\sigma_3 - \sigma_m)}{\sqrt{6}\sqrt{\sigma_1^2 + \sigma_2^2 + \sigma_3^2 - 3\sigma_m^2}} \right] \text{ for } \sigma_3 \geq \sigma_2 \geq \sigma_1 \quad \dots\dots\dots 4.16$$

$\sigma_i$  for  $i=1$  to 3 is the principal normal stress in the  $i$ th direction;  $\sigma_m$ =mean stress;  $f_{cu}$ =uniaxial compressive strength of concrete; and  $a_2$ ,  $a_1$ ,  $a_0$ ,  $b_2$ ,  $b_1$ , and  $b_0$ =constants to be determined.

Due to the complexity of the equations describing any three dimensional failure surfaces, an iterative solution scheme is normally required that can predict the state of stress in concrete at failure, given the current state of stress. This process is time consuming and computationally inefficient in an incremental, non-linear finite-element analysis, where the state of stress at failure is required to be determined at each load increment. Thus, to facilitate the implementation of the proposed failure surface into a finite element package, a closed-form solution for predicting the state of stress in concrete under monotonically increasing, proportional multiaxial loads is developed and presented in this subsection.

The state of stress at failure is given by the point at which a line drawn through the origin and the current state of stress intersects the failure surface. This is illustrated in Fig. 4.3, whereby a cross section of the failure surface is taken along the meridian plane in which  $\rho(\zeta, \theta)$  lies. The equation of this load path is given by

$$\rho(\zeta, \theta) = \zeta \tan \theta \quad \dots\dots\dots 4.17$$

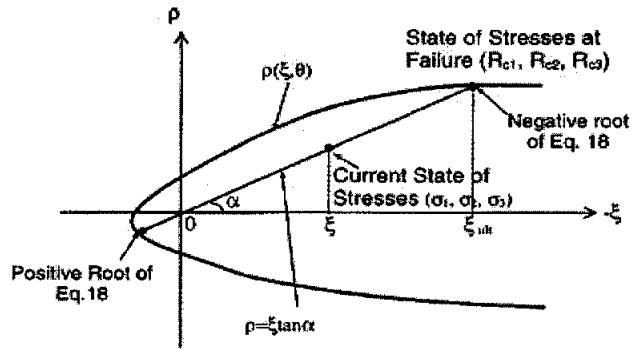


Fig. 4.3 METHOD OF DETERMINING STATE OF STRESSES AT FAILURE

Where

$$\alpha = \cos^{-1} \left( \frac{\sigma_1 + \sigma_2 + \sigma_3}{\sqrt{3} \sqrt{\sigma_1^2 + \sigma_2^2 + \sigma_3^2}} \right) \dots\dots\dots 4.18$$

Because  $\rho(\zeta, \theta)$  is interpolated from the quadratic curves,  $\rho_t$  and  $\rho_c$ , it is postulated that  $\rho(\zeta, \theta)$  at a given angle,  $\theta$ , is also a quadratic curve of the form:

$$\frac{\xi}{f_{cu}} = a \left( \frac{\rho(\xi, \theta)}{f_{cu}} \right)^2 + b \left( \frac{\rho(\xi, \theta)}{f_{cu}} \right) + c \dots\dots\dots 4.19$$

Where the coefficients,  $a$ ,  $b$ , and  $c$  may be determined through solving Eq.4.19 at three known points on the curve. To ensure a good coverage and to minimize any possible loss of accuracy due to truncation errors encountered in numerical analysis, the control points were selected to be at  $\zeta=0.1732$ ,  $\zeta=-2.0$ , and  $\zeta=-4.0$ , as they fall within the commonly encountered range of experimental values. Based on the current state of stress  $\sigma_1$ ,  $\sigma_2$ ,  $\sigma_3$ , the angle of similarity,  $\theta$ , can be evaluated from Eq. 4.16. Three sets of values of  $\rho(\zeta, \theta)$  and  $\zeta$  can then be obtained by substituting the known value of  $u$  and appropriate values of  $\zeta$  into Eqs. 4.13-4.15 Thereafter, the values of  $a$ ,  $b$ , and  $c$  may be solved for and derived to be

$$c = 0.1732$$

$$b = \frac{4.1732 \left( \frac{\rho(-2, \theta)}{f_{cu}} \right)^2 - 2.1732 \left( \frac{\rho(-4, \theta)}{f_{cu}} \right)^2}{\left( \frac{\rho(-4, \theta)}{f_{cu}} \right) \left[ \left( \frac{\rho(-2, \theta)}{f_{cu}} \right) \left( \frac{\rho(-4, \theta)}{f_{cu}} \right) - \left( \frac{\rho(-2, \theta)}{f_{cu}} \right)^2 \right]}$$

$$a = \frac{-4.1732 - b \left( \frac{\rho(-4, \theta)}{f_{cu}} \right)}{\left( \frac{\rho(-4, \theta)}{f_{cu}} \right)^2} \dots\dots\dots 4.20$$

By equating Eqs.4.17 and 4.19 and substituting the values of the coefficients  $a$ ,  $b$ , and  $c$  obtained from Eq. 4.20 the value of  $\zeta_{ult}$  corresponding to the state of stress at failure can be obtained from Eq. 4.21:

$$\frac{\xi_{ult}}{f_{cu}} = \frac{[1 - b(\tan \alpha)] \pm \sqrt{[b(\tan \alpha) - 1]^2 - 4ac(\tan \alpha)^2}}{2a(\tan \alpha)^2} \dots\dots\dots 4.21$$

From Fig. 4.3, it is observed that Eq. 4.21 will yield at a positive and a negative root. The appropriate solution to Eq. 4.21 would be the root with the same sign as  $j$  corresponding to the current state of stress. The state of stress at failure can then be determined by substituting the value of  $\zeta_{ult}$  into Eq. 4.22.

$$\begin{bmatrix} R_{c1} \\ R_{c2} \\ R_{c3} \end{bmatrix} = \frac{\xi_{ult}}{\sqrt{3}} \begin{bmatrix} 1 \\ 1 \\ 1 \end{bmatrix} + \rho(\xi_{ult}, \theta) \begin{bmatrix} \frac{-\cos \theta}{\sqrt{6}} - \frac{\sin \theta}{\sqrt{2}} \\ \frac{-\cos \theta}{\sqrt{6}} + \frac{\sin \theta}{\sqrt{2}} \\ \frac{2 \cos \theta}{\sqrt{6}} \end{bmatrix} \dots\dots\dots 4.22$$

**4.2.2.8 Post peak behavior after tensile cracking**

After the material has cracked, it start to strain-soften in the principal stress direction until the corresponding equivalent uniaxial strain  $\epsilon_{u1}$  exceeds its limited  $\epsilon_{f1}$  when this happens, stress reduces to zero and the material has no stiffness in the direction of this stress. With the assumption that poisson's ratio in the crack plane reduces to zero after cracking ( $\nu_{ij}=\nu_{ji}=0, j=1 \text{ to } 3$ ). If unloading of cracked material occurs in the strain softening region characterized by the condition ( $f \leq f_{\max}$ )  $E_I$  will be replaced by unloading modulus  $E_{ui}$  given by the following expression:

$$E_{u1} = E_0 \frac{\sigma_1}{E_0(\epsilon_{u1} - \epsilon_{c1}) + R_{c1}} \dots\dots\dots 4.23$$

**4.2.2.9 Post peak behavior after compression crushing**

After the material reaches the state of compression crushing it is assumed that it's strain-softening in all direction until minimum uniaxial strain  $\epsilon_{c3}$  reaches  $\epsilon_{\beta3}$ , all the stresses has completely released and the material has zero stiffness for subsequent loading. With the assumption that poisson's ratio reduces to zero after compression crushing ( $\nu_{ij} = 0, i=1 \text{ to } 3, j=1 \text{ to } 3$ ). The constitutive relation takes the following form for crushing material:

$$\begin{pmatrix} \partial\sigma_1 \\ \partial\sigma_2 \\ \partial\sigma_3 \\ \partial\tau_{12} \\ \partial\tau_{23} \\ \partial\tau_{31} \end{pmatrix} = \begin{pmatrix} E_1 & 0 & 0 & 0 & 0 & 0 \\ 0 & E_2 & 0 & 0 & 0 & 0 \\ 0 & 0 & E_3 & 0 & 0 & 0 \\ 0 & 0 & 0 & G_{12} & 0 & 0 \\ 0 & 0 & 0 & 0 & G_{23} & 0 \\ 0 & 0 & 0 & 0 & 0 & G_{31} \end{pmatrix} \begin{pmatrix} \partial\epsilon_1 \\ \partial\epsilon_2 \\ \partial\epsilon_3 \\ \partial\gamma_{12} \\ \partial\gamma_{23} \\ \partial\gamma_{31} \end{pmatrix} \dots\dots\dots 4.24$$

If unloading of crushing material occurs in the strain-softening region as represented by the condition  $f \leq f_{\max}$   $E_i$  will be replaced by unloading modulus  $E_{ui}$  given by the following expression:

$$E_{u1} = E_0 \frac{\sigma_1}{E_0(\epsilon_{u1} - \epsilon_{c1}) + R_{c1}} \dots\dots\dots 4.25$$

## 4.3 Steel Cyclic Model

### 4.3.1 Introduction

The evaluation of non-linear hysteretic response of reinforced concrete structures under cyclic excitations and, in particular, under severe earthquake excitation necessitates the developments of accurate and computationally efficient models of component and constituent materials. While component models might suffice to determination of global parameter of structural response of materials models become necessary in the local response evaluation and damage assessment of existing and new structures. In well designed new structures and retrofitted old structures, steel dominates the response either in the form of or in the form of steel jackets for columns and beam-column joints. The development of an accurate and computationally efficient model for ordinary and high strength steel is, therefore, an important task in the non-linear response evaluation of these structures by finite element method.

Several models of the cyclic stress-strain response of steel have been proposed in the last two decades. Following Popovics and Ortiz (1979), these can generally classified in two major categories

- macroscopic models, based on smeared stress-strain relations
- microstructures or microscopic model, based on dislocation theories

Discussion on existing models can be found in Chen et al (1983), Bate and Wilson (1986), Chang and Mander (1994), Dodd and Restrepo-Possda (1995). Microscopic models are typically derived from sound theories, but are overly complex for use in non-linear analysis of large scale structures. On other hand microscopic models are relatively simple and fail to represent important feature of hysteretic behavior. In the latter case, accuracy is increased by introduction of many parameters, with no clear significance and with significant penalty in computational efficiency

### 4.3.2 Proposed Cyclic Model for Steel

Two-node bar elements with linear displacement functions are used to model steel reinforcement. Steel tensile and compressive strains are taken as positive and negative respectively, and they can apply to the stresses as well. However, the strength values are always taken as the absolute values. The elasto-plastic stress–strain model as shown in Fig. 4.4 is used. For a given strain  $\epsilon_s$ , the stress  $\sigma_s$  on the tensile envelope is given in terms of Young’s modulus  $E_s$  and the yield stress  $f_y$  by:

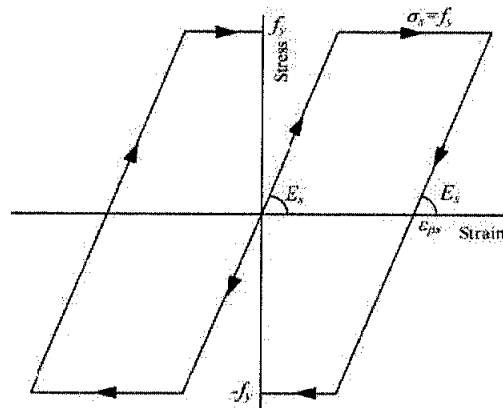


Fig. 4.4 STEEL CYCLIC MODEL

For loading condition

$$\sigma_s = E_s \epsilon_s \quad \text{for } \epsilon_s \leq \frac{f_y}{E_s} \text{ (at elastic stage)}$$

$$\sigma_s = f_y \quad \text{for } \epsilon_s > \frac{f_y}{E_s} \text{ (after yielding) .....4.26}$$

When strain reverses from a typical point on the tensile yield plateau, it follows the inclined path with slope  $E_s$  and then a horizontal line when it reaches the compressive yield stress. The stress–strain relationship along the inclined and horizontal paths is respectively given by:

$$\sigma_s = E_s (\epsilon_s - \epsilon_{ps}) \quad \text{for (inclined path)}$$

$$\sigma_s = -f_y \quad \text{for horizontal path .....4.27}$$

Where  $\epsilon_{ps}$  is the residual strain for the inclined path.

## 4.4 FRP Cyclic Model

### 4.4.1 Proposed cyclic model for FRP laminates

The behavior of FRP materials is linear elastic until failure. Failure is sudden and brittle with no load carrying capacity after failure (The stress-strain model is shown in Fig.4.5. The stress is linear up to the tensile strength and drops sharply to zero, representing the fracture of FRP plate.). Typical stress-strain relation of FRP is shown in Fig.4.5 below

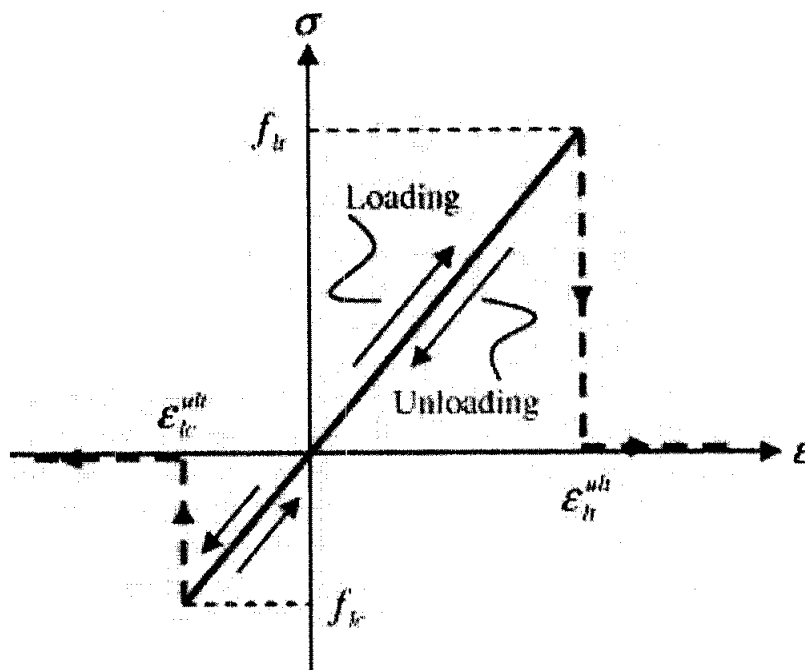


Fig. 4.5 STRESS-STRAIN RELATION OF CFRP UNDER CYCLIC LOADING

#### 4.4.1.1 Stress – strain relationship of FRP

An orthotropic material was selected to represent the behavior of CFRP laminates under triaxial condition. The constitutive relations for orthotropic FRP materials used in the analysis are the same as rule that was used to simulate the behavior of concrete (see Eq.4.1).

#### ***4.4.1.2 Failure criteria FRP***

For FRP, the failure criteria were also based on the stress-strain curve. As FRP material is brittle in nature, there is no yielding stage. It behaves elastically to failure. When the principal strain is greater than the ultimate strain, it is assumed tension failure of the elements has taken place.

## CHAPTER 5

### CHAPTER 5 MODELING OF SHEAR TRANSFER MECHANISMS AFTER CRACKING

#### 5.1 Background

Cracking in concrete beams may result in a significant reduction in their stiffness and strength. Although the flexural behaviour of cracked reinforced concrete beams can generally be well predicted, accurate prediction of the shear behaviour of reinforced concrete beams remains a formidable task due to the complexity of the shear transfer mechanism in the reinforced concrete. Shear resistance in reinforced concrete beams is provided by the shear transfer in the compression zone, aggregate interlock across the crack face, stirrups crossing the shear crack, and dowel action of longitudinal reinforcing bars crossing the crack in the concrete as well as interaction between concrete and reinforcement bars. Fig. 5.1 shows the main mechanisms affect the shear capacity of reinforced concrete beams.

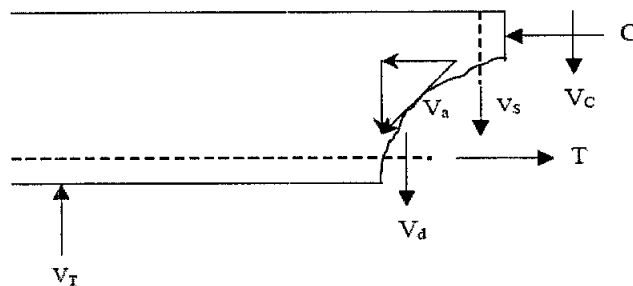


Fig. 5.1 shear resisting mechanism

Where  $V_T$  = Total shear force.

$V_c$  = Concrete in compression zone.

$V_a$  = Aggregate interlock mechanism.

$V_d$  = Dowel action mechanism.

$V_s$  = Shear transfer by web reinforcement.

This chapter presents finite element models that were used in this research to analyze the RC structures subjected to cyclic loading, for description of concrete-to-concrete

and steel-to-concrete interfaces. The attention is focused on the following mechanisms:

- Aggregate interlock
- Dowel action
- Bond-slip

## **5.2 Modelling of Aggregate interlock**

The shear transfer mechanism based on aggregate interlock has been known for long time in its behavioural aspects, owing to the many test results obtained in the 1960s, 1970s and 1980s. The different test results shed light on many parameters involved, either kinematic (crack opening and slip, crack dilatancy, initial crack width)

Walraven (1981) showed that the mechanics of aggregate interlock shear transfer is highly complex. In addition to contact between sharp edges of aggregates on joint surfaces, there may be localized crushing of the cement paste and the aggregate, as well as entry of loose materials. The amount of crushing and the bearing area of the surfaces depends on the joint opening, normal restraint developing from the rough surface of the aggregate, the strength of the concrete (both the paste and the aggregate), and the size and distribution of the aggregate particles. Walraven (1981) stated that the modelling of aggregate interlock shear transfer in rigid pavements should take all these factors into account.

During FE modelling of aggregate interlock shear transfer in rigid pavement systems, most researchers tend to use discrete linear spring elements. While this may be considered reasonable for an examination of the effect of aggregate interlock shear transfer effectiveness on the global slab response, it does not permit modelling of local response at the joint. Even when the use of linear springs is appropriate, the rational choice of spring stiffness may be difficult, if not impossible, and the appropriate spring value is valid only for one model geometry, set of material properties, and loading. The need for the more realistic FE modelling of aggregate interlock shear transfer was recognised by Davids et al. (1998). They chose the two-phase model developed by Walraven (1981) to model aggregate interlock shear transfer in the FE software Ever FE.

### 5.2.1 Proposed cyclic model for aggregate interlock

The proposed model used in this research is taken from (Vecchio and Collin 1986). Based on experimental data it was established that the shear stiffness of these mechanisms decays rapidly after cracking. In this work, shear stress due to aggregate interlocking  $v_{agg}$  was formulated explicitly as an inverse function of the principal tensile strain  $\epsilon_{cl}$ , which is an indicator of the actual crack width. Fig. 5.2 shows the proposed aggregate interlock model taken from Vecchio and Collin (1986)

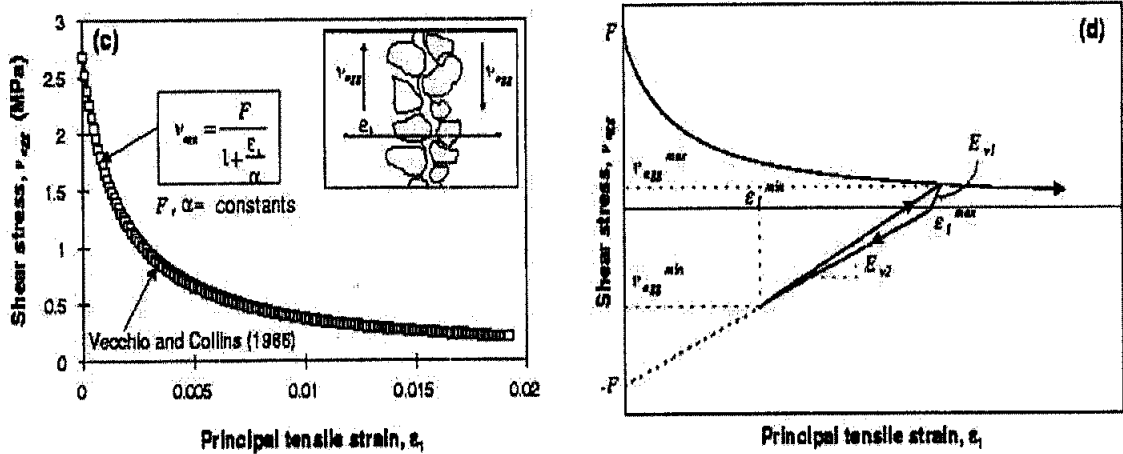


Fig. 5.2 PROPOSED MODEL FOR AGGREGATE INTERLOCK  
Vecchio and Collin (1986)

The proposed expression Eq. (5.1) was calibrated with shear panel tests to obtain the values given in the right-hand term ( $F$  represents the shear strength at cracking and  $\alpha$  is a normalizing constant, Fig. 5.2:

$$v_{agg} = \frac{F}{1 + \frac{\epsilon_{cl}}{\alpha}} = \frac{0.1342 \times 10^{-3} E_c}{1 + \frac{\epsilon_{cl}}{0.0018}} \dots\dots\dots 5.1$$

Eq. (5.1) defines the envelope of the aggregate interlock cyclic response adopted here. Unloading from the envelope was defined by two linear segments with slopes  $E_{v1}$  and  $E_{v2}$  (Fig. 5.2), where  $E_{v1}$  is the initial tangent modulus of the proposed shear stress/principal tensile strain relationship ( $E_{v1} = 0.1342 E_c$ ), and  $E_{v2}$  is given as:

$$E_{v2} = \frac{0.1342 \times 10^{-3} E_c}{E_{v1} \epsilon_{cl}^{max} - v_{agg}^{max}} E_{v1} \dots\dots\dots 5.2$$

With  $\epsilon_{cl}^{max}$  the maximum principal tensile strain that concrete has undergone in a given direction and  $v_{agg}^{max}$  the maximum in-plane shear stress developed in that direction. Reloading towards the envelope followed the slope of the straight line that passes through the points in the stress-strain curve corresponding to the maximum ( $\epsilon_{cl}^{max}$ ) and minimum ( $\epsilon_{cl}^{min}$ ) principal tensile strains that the r.c. element has undergone in the previous cycle, i.e,

$$v_{agg} = v_{agg}^{min} + E_r(\epsilon_{cl} - \epsilon_{cl}^{min}); E_r = \frac{v_{agg}^{max} - v_{agg}^{min}}{\epsilon_{cl}^{max} - \epsilon_{cl}^{min}} \dots\dots\dots 5.3$$

Where

$v_{agg}^{min}$  is the minimum in-plane shear already developed in a given direction?

### 5.3 Modelling of Dowel action mechanism

The dowel action of reinforcing bars can play an important role if other contributions to shear transfer are relatively small as in the case of a beam with a small amount of web reinforcement or the case of a post-peak stage of the loading process. It may contribute significantly to the post peak resistance and hence contribute to the shear ductility of concrete members.

From a literature survey on finite element analysis of reinforced concrete structures covering papers published from 1985 to 1991, it is noted that modelling of the dowel action has not been mentioned in any of the papers surveyed. This reflects to some extent the difficulties involved in modelling the behaviour of the dowel action. There are some major difficulties in modelling the dowel action of reinforcement bars for finite element analysis. In experimental tests, the shear force transferred by the dowel action is quite difficult to measure because it is embedded with other shear transfer components. In fact, since the dowel action involves interaction between the reinforcement bars and the concrete near the cracks and the interaction stresses are extremely difficult to measure, many details of the dowel action have never been investigated. Consequently, experimental results on the dowel action have been rather limited. Even in finite element analysis, the mechanism of the

dowel action is too complicated to describe. To analyze the details of the dowel action, the steel bars need to be individually modelled by finite elements and a very fine mesh has to be used for the concrete. As a result, the number of elements required would be very large. Furthermore, such individual modelling of the steel bars and concrete is not compatible with the common practice of modelling the concrete and the steel together in the analysis of reinforced concrete structures. To consider the dowel action in the global analysis of reinforced concrete structures, a simplified model of the dowel action that is compatible with the crack and reinforcement models is required. Thirdly, since the dowel action is usually more significant near peak load and at the post-peak stage, experimental testing or theoretical analysis extending into the post-peak range are needed to investigate the full effects of the dowel action, but such testing and analysis are generally quite difficult.

There are three major difficulties in modelling the dowel action of reinforcement bars for finite element analysis. Firstly, in experimental tests, the shear force transferred by the dowel action is often embedded with the other shear transfer components during shear force measurement and is thus quite difficult to be measured directly. Consequently, experimental results on the shear transfer by dowel action have been rather limited. Secondly, the mechanism of the dowel action is too complicated to be described in a simple manner. To analyze the details of the dowel action, the steel bars need to be individually modelled by finite elements and a very fine mesh has to be used for the concrete. As a result, the number of elements required would be very large. Furthermore, such discrete element approach of modelling each steel bar individually is not compatible with the common practice of modelling the cracks and the steel bars in smeared forms in the analysis of reinforced concrete structures. To incorporate the dowel action in the global analysis of reinforced concrete structures, a simplified model of the dowel action that is compatible with the smeared crack and smeared reinforcement models is required.

The next section gives brief description about the dowel action model that was used in this research.

### 5.3.1 Proposed cyclic model for dowel action

The analytical model used to predict the behaviour of a dowel bar embedded in concrete is based upon the work presented by Timoshenko and Lessels (1972) for the analysis of beams on an elastic foundation. A beam on an elastic foundation is made of discrete springs that connect a beam to a rigid base. The dowel action behaviour of the reinforcement bars crossing cracks in the concrete is analyzed by treating each reinforcement bar as a beam and the surrounding concrete as a bed of springs so that the reaction force of the foundation at any point may be assumed to be proportional to the deflection of the beam at that point. A physical model for dowel bars embedded in concrete after cracking is that of a beam resting on an elastic foundation (the concrete representing the flexible foundation).

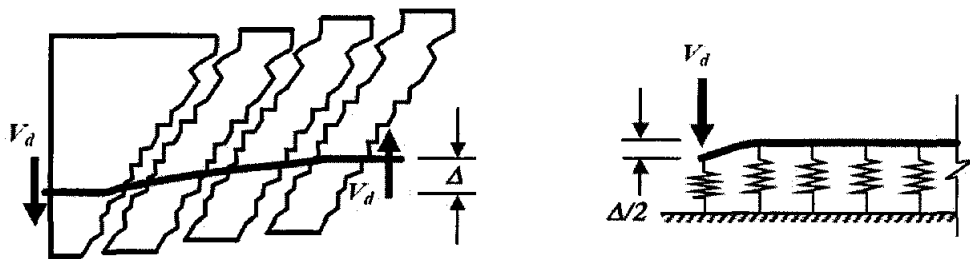
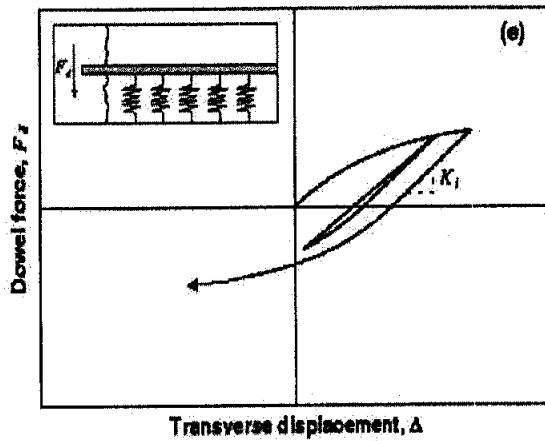


Fig. 5.3 LOAD-DISPLACEMENT RESPONSE FOR DOWEL BAR  
Timoshenko and Lessels (1972)

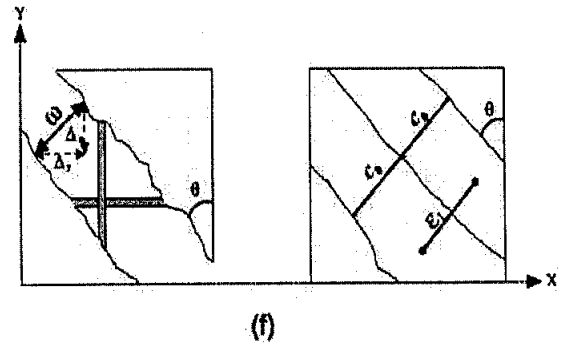
The load-deflection response for dowel bars embedded in concrete proposed by Millard and Johnson [1995] is adopted in this research (see Fig.5.4). Although it has been suggested that dowel strength across a shear plane is owing to a combination of direct shear, kinking and flexure of the reinforcing bars, Millard and Johnson have illustrated that flexure of the bars predominates, since there is a significant amount of deformation in the underlying concrete cover. They proposed the following load-deflection response for dowel bars embedded in concrete:

$$F_d = F_{du} \left[ 1 - \exp\left(\frac{-K_i \Delta}{F_{du}}\right) \right] \dots\dots\dots 5.4$$

Where  $F_d$  is the dowel force at a shear displacement across the crack equal to  $\Delta$  (Fig. 5.4),  $F_{du}$  is the ultimate dowel force, and  $K_i$  is the initial dowel stiffness.



(e) Dowel force versus transverse displacement



(f) Definition of dowel displacement

Fig. 5.4 LOAD-DISPLACEMENT RESPONSE FOR DOWEL BARS  
Millard and Johnson [1995]

When the dowel deformation is not too large and none of the materials have yielded, the dowel force–displacement relation is linearly elastic. However, when the elastic limit is exceeded, the dowel action becomes plastic. At the ultimate limit state, local crushing of the surrounding concrete and/or yielding of the dowel bar occurs. Based on experimental results, Dulacska et al (1979) has given the following equation for estimating the dowel force at ultimate limit state  $F_{du}$ ,

$$F_{du} = 1.30 D_b^2 \sqrt{f'_c f_y (1 - A^2)} \quad (N) \quad \dots\dots\dots 5.5$$

Where  $f'_c$  and  $f_y$  are concrete compressive strength and steel yield stress respectively. With  $A$  the ratio of applied axial force to the yield axial force of the bar with diameter  $D_b$ . From experimental evidence it is known that axial tension in the bars close to yielding adversely affects the dowel resistance (causing a reduction in dowel stiffness and bending capacity). This is why Eq. 5.5 results in zero dowel capacity for rebar forces equal or exceeding yield ( $A \geq 1$ ). With regards to the initial stiffness, the following expressions were adopted from the literature [Soroushian et al (1987), Millard et al (1998)]:

$$K_i = 0.166 K_f^{0.75} D_b^{1.75} E_s^{0.25} \quad (N/mm) \quad \dots\dots\dots 5.6$$

The foundation stiffness for the surrounding concrete, which governs the dowel stiffness as per Eq. (5.6), is of considerable complexity and importance. Results of past experimental research had led to somewhat scattered values for, ranging from 75 to 450 N/mm<sup>3</sup>. Before more test data are available, the following data-fitting expression proposed by Soroushian et al (1987) may be used:

$$K_f = 127\beta \sqrt{f'_c} \left(\frac{1}{D_b}\right)^{2/3} \quad (\text{N/mm}^3); E_s = 200 \text{ GPa} \dots\dots\dots 5.7$$

Where  $K_{ef}$  is the foundation stiffness of concrete and  $b$  is a coefficient ranging from 0.6 for a clear bar spacing of 25.4 mm to 1.0 for larger bar spacing and  $E_s$  is reinforcement elastic modulus. Fig.5.4 shows the dowel force-displacement relation ship and the definition of the dowel displacement.

$$\Delta_x = w \sin \theta; \Delta_y = w \cos \theta \dots\dots\dots 5.8$$

Eq. 5.4 was used as the envelope of the dowel response curve. Unloading from the envelope followed a straight line with stiffness  $K_i$  (the initial stiffness) up to zeroing of the dowel force; at that point bars were assumed to act as dowels in the opposite direction following the envelope (Eq. 5.4) in that direction. Reloading followed a straight line with slope depending on the maximum and minimum dowel shear displacements attained in the previous cycle (Fig. 5.4), i.e.,

$$F_d = F_d^{\min} = E_r(\Delta - \Delta_{\min}); E_r = \frac{F_d^{\max} - F_d^{\min}}{\Delta^{\max} - \Delta^{\min}} \dots\dots\dots 5.9$$

With  $\Delta^{\min}$  and  $\Delta^{\max}$  the minimum and maximum transverse displacements that the dowel bar has undergone,

$F_{\min}$  and  $F_{\max}$  the minimum and maximum dowel shear forces developed previously in the bar.

## 5.4 Bond-slip cyclic models

### 5.4.1 Background

Bond stress is the shear stress acting parallel to an embedded bar on the surface between the reinforcing bar and the concrete. Bond slip is the relative displacement between the bar and the concrete. Reinforced concrete depends on the combined action of the concrete and its embedded reinforcement for satisfactory operation as a construction material. This action is produced by the interaction between both of its components, plain concrete and reinforcing bars. The transfer of forces across the interface between these two materials is completed by bond action between them, so bond plays a very important role in most aspects of reinforced concrete behaviour. To better understand bond behaviour, there have been a number of studies specifically aimed at examining behaviour of bond stress-slip by way of both experiment and theory. Several laws to describe the behaviour have been developed on experimental ground. Constitutive laws between the local bond stress and the local bond slip on the interface have been formulated for theoretical analysis purposes.

The finite element method has been widely used for analyzing the response of reinforced and pre-stressed concrete structures. There are two distinct ways of representing cracks in a finite element procedure. The discrete crack model represents cracks as inter-element discontinuities. There is restriction on the crack propagation direction depending on the mesh layout. The smeared crack approach represents cracks as a change in the material property of the element over which the cracks are assumed to be smeared. In the simplified analysis of reinforced and pre-stressed concrete structures, complete compatibility between concrete and reinforcement or pre-stressed tendons is usually assumed. It means that perfect bond is presumed. For models with smeared steel, the perfect bond relationship is the easiest to adopt since it simply involves overlaying the constitutive matrix of the steel elements with concrete elements. For the models with discrete reinforcement elements, perfect bond also represents a very easy solution, since the displacements of the nodal points are the same for both concrete elements and reinforcement elements. Actually, this assumption is only valid in regions where only low transfer stresses between the two components exist. In the regions where high transfer stresses occur between the

interfaces of the two components, especially for the regions near cracks, there are different strains in concrete and reinforcement. As result of this, relative displacements, which are called bond slips, occur between concrete and reinforcement. Because bond stresses are related to bond slips between the two components, the assumption of perfect bond in a cracked region would require infinitely high reinforcement strains to explain the crack widths. It would also cause significant error in the predicted load-deflection response, stresses and strains of the reinforced structures when the bar slip is large.

There are several laws to describe the behaviour have been developed on experimental ground. Constitutive laws between the local bond stress and the local bond slip on the interface have been formulated for theoretical analysis purposes. Study of bond behaviour between steel bar and surrounding concrete began in the 1960s. Most of the studies performed in 1960s and 1970s were experimental investigations under monotonic loading. Study of bond behaviour under cyclic loading has been done since 1980s.

The bond stress between the reinforcing bar and its surrounding concrete is very complicated. It is dependent on the slip between the steel bar and the concrete, and the stress in the reinforcing bar as well as many other factors. Two alternative basic hypotheses have been used in the past; in one bond stress is considered to be a linear function of slip (Ngo and Scordelis, 1967), while in the other it is considered to be a non-linear relationship between bond stress and slip.

Early experimental studies of bond were concerned with determining bond failure strengths and the influence of surface deformations on them by push-in test. Later some researchers have found that bond failure occurs at a higher stress for a push-in test than for the normal pull-out test. The explanation for this is simple: firstly, the compressive axial stress developed in the bar during a push in test causes an increase in bar diameter because of Poisson's effect, which, in turn, causes an increase in the radial pressure between bar and concrete. Since friction is an important element in bond, this increase in pressure leads to increase bond strength; secondly, cracking is an important reason to cause degradation of bond strength. Because there is no cracking in a push-in test, this leads to the increase of bond strength.

In the ordinary pull-out test, the test specimen is typically a cylinder or prism with a bar embedded in it. Before the 1970s e bar was pulled from one side while the

concrete was held by the reaction pressure on the same end. Since the bar is in tension and concrete is in compression, differential strains force a relative slip at very low steel stresses. This is different to what occurs in an actual structure. The most serious weakness of this pull-out test is that the concrete in compression eliminates transverse tension cracking. After the 1970s, the method of pull-out test was improved. A specimen is pulled from both sides of the bar

Most researchers believe that there are different relationships for local bond stresses versus local bond slips at different points of the interface of the steel bar and the concrete. Since the properties of the interface will not be different, this change can only confirm stress effects. Some researchers (Morita, 1985; Narnmur and Naaman, 1989; Edward and Yannopoulos, 1979) thought that the relationship is a material property and, therefore, independent of location. They thought that there exists a unique bond slip relationship which depends only on material properties and steel geometry.

The strength of the bond between a rebar and the surrounding concrete is generally made up of three components:

1. Chemical adhesion;
2. Friction;
3. Mechanical interlock between reinforcement and concrete. This includes the bearing of lugs on concrete and shear strength of concrete section between lugs.

The following section gives some description about the cyclic bond-slip model used in this research.

#### **5.4.2 Proposed cyclic model for bond slip mechanism**

The bond stress–slip envelope curve normally comprises an ascending part followed by a descending part and various models comprising different number of line segments have been proposed. Fig. 5.5 shows a typical 4-segment envelope 0-1-2-3-E in accordance with the CEB-FIP Model Code 1990. The main parameters to construct the bond stress–slip envelope are the maximum bond stress  $u_p$ , the residual bond stress  $o_r$ , the slips corresponding to the maximum bond stress  $S_1$  and  $S_2$ , and the slip corresponding to the residual bond stress  $S_3$ . The CEB-FIP Model Code 1990

recommends, and for normal design purpose. It should be noted that these values are actually dependent on various conditions, including the bond failure type.

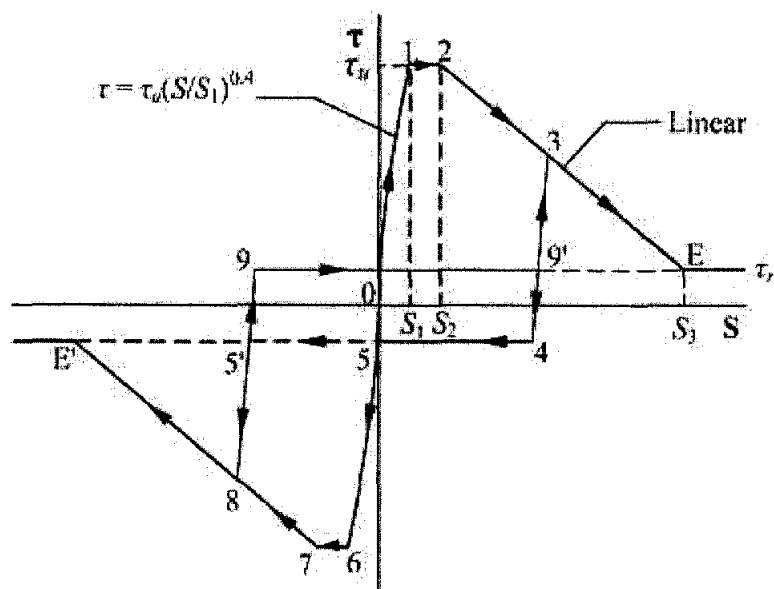


Fig. 5.5 PROPOSED CYCLIC MODEL FOR BOND-SLIP MECHANISM

According to Reynolds and Beeby (1998), the bond strength is proportional to the concrete tensile strength or the square root of the compressive strength. The bond strength increases with increasing cover but it decreases with increasing bar size.

Transverse steel also enhances the bond strength. While there is general agreement to the above statements, there is little consensus on the relative magnitudes of the bond parameters. Nilson (1999) derived a local bond stress–slip relationship based on the experimental results and gave the peak bond stress and the corresponding bond slip as 4.95 MPa. According to a study by the ACI Committee 408 (1998), the slip at bond strength shows considerable scatter and is normally below 0.25 mm. For example, Edwards and Yannopoulos (2000) observed from experiments a scatter range of 0.1–0.3 mm for  $S_1$  for 16 mm diameter hot rolled deformed bars. Also shows the relationship between bond stress  $\tau$  and slip  $S$  under monotonic and cyclic loading proposed by Tassios (2001) and it is adopted in the study. Initial monotonic loading follows the envelope curve such as path 0-1-2-3, which applies to loading in both directions. Load reversal from point 3 then follows path 3-4-5-6-7-8 if no load reversal has occurred in the negative direction before. Load reversal from point 8 then follows path 8-9- 9'-3-E. If load reversal occurs again from point 3, then it follows

path 3-4- 5'-8-E'. The loading and unloading paths such as 3-4 and 8-9 are assumed to be straight lines parallel to the tangent envelope curve at the origin. On unloading and reloading in the opposite direction, the bond stresses reach initial plateaus 9- 9' and 4- 5- 5' at residual bond strength at  $\pm \tau_r$ .

## **CHAPTER 6      INTERFACE MODEL BETWEEN CFRP SIDES PLATES AND CONCRETE**

### **6.1 Introduction**

Shear strengthening of reinforced concrete beams is required when the beam is deficient in shear, or when its shear capacity falls below its flexural capacity after flexural strengthening. An accepted technique for the shear strengthening of reinforced concrete beams is to provide an additional FRP web reinforcement in the form of externally bonded FRP sheets. The bonding interface is relatively weak in comparison with the neighbouring materials in the whole upgraded system. Premature failure by debonding of side plated CFRP reinforcement can often limit its effectiveness.

The fibre-matrix interface plays an important role in defining key properties of the composite like stiffness, strength and the fracture behaviour. The effects of damage due to interfacial decohesion on overall mechanical properties of the composite material have been studied by various authors [Benveniste et al (1984), Pagano et al (1990) and Yuan, et al (1997)]. A number of numerical models have been proposed and developed over the years to simulate the damage due to interfacial debonding in composite structures.

A comprehensive way of modelling CFRP-concrete debonding phenomena is not yet completely available, the behaviour of a specimen undergoing delamination may be highly non-linear, and a snap-back branch can be observed in applied force-total slip curve.

This chapter gives brief description about interfacial behaviour of side plated CFRP-to-concrete under cyclic loading as well as monotonic conditions.

## 6.2 Interfacial Behaviour of CFRP-to-Concrete Joints under Monotonic Loading

### 6.2.1 Shear Capacity

The results for shear capacity for push-off specimens are summarized in Table 6.1 and Table 6.2. All specimens were tested up to failure.

Table 6.1 SHEAR CAPACITY (AXIALLY LOADED CASE)

Specimen No.	Specimen type	Shear capacity, KN
$A_1$	Without CFRP	173.3
$A_2$	Without CFRP	169.4
$A_3$	Without CFRP	176.8
$A_4$	With CFRP	221.7
$A_5$	With CFRP	235.1
$A_6$	With CFRP	229.8

Inspection of Table 6.1 reveals that the results obtained from the push-off test showed that the shear capacity for strengthened specimens was much higher than unstrengthened specimens, which was about 25% to 33%. For all specimens no cracks were initiated during the entire period of testing. The failure of strengthened specimens occurred suddenly at the centre of specimens by rupture of concrete and CFRP plates at the same time. Fig.6.1 shows the mode of failure of one specimen under axially loaded condition.



Fig. 6.1 FAILURE MODE OF AXIALLY LOADED SPECIMEN

Table 6.2 SHEAR CAPACITY (ECCENTRICALLY LOADED CASE)

Specimen No.	Specimen type	Shear capacity, KN
$B_7$	Without CFRP	107.3
$B_8$	Without CFRP	103.5
$B_9$	Without CFRP	113.8
$B_{10}$	With CFRP	142.2
$B_{11}$	With CFRP	136.7
$B_{12}$	With CFRP	154.6

Inspection of table 6.1 reveals that the results obtained from the push-off test showed that the shear capacity for strengthened specimens was much higher than unstrengthened specimens, which was about 30% to 40%. For all specimens no cracks observed during the entire period of testing. The failure occurred in a brittle manner by crushing of concrete in tension zone due to high bending stress at the lower part associated with rupture of CFRP.

### 6.2.2 Monotonic Bond Stress– Slip behaviour

The average bond stress of section  $i$ ,  $\tau_{b, i}$  was calculated as dividing the difference of tensile force by the surface area of laminate, as shown in Eq. (6.1).

$$\tau_{b,i} = \frac{(\varepsilon_{f,i} - \varepsilon_{f,i-1})t_f \cdot E_f}{\Delta l_b} \dots\dots\dots 6.1$$

Where

- $\tau_{b,i}$  = bond stress
- $\varepsilon_{f,i}$  = strain of CFRP of section  $i$
- $t_f$  = thickness of CFRP
- $E_f$  = elastic modulus of CFRP
- $\Delta l_b$  = interval between strain gauges.
- $i$  = 2- $n$
- $n$  = No. of strain gauges

The slip of section  $i$ ,  $s_i$ , is the sum of the difference between the displacement of CFRP and the displacement of the concrete and epoxy layer and was obtained as follows:

$$s_i = s_{i-1} + (\delta_{f,i} - \delta_{m,i}) \dots\dots\dots 6.2$$

$$\delta_{f,i} = \frac{\epsilon_{f,i} - \epsilon_{f,i-1}}{2} \cdot \Delta I_b + \epsilon_{f,i-1} \cdot \Delta I_b \dots\dots\dots 6.3$$

$$\delta_{m,i} = \frac{\epsilon_{m,i-1} - \epsilon_{m,i}}{2} \cdot \Delta I_b + \epsilon_{m,i} \cdot \Delta I_b \dots\dots\dots 6.4$$

Where

$\delta_{m,i}$  = displacement of concrete and epoxy layer.

$\delta_{f,i}$  = displacement of CFRP.

Fig. 6.2 and Fig. 6.3 show the relationship that was determined between the bond stress and the slip for CFRP-to-concrete joints subjected to monotonic load

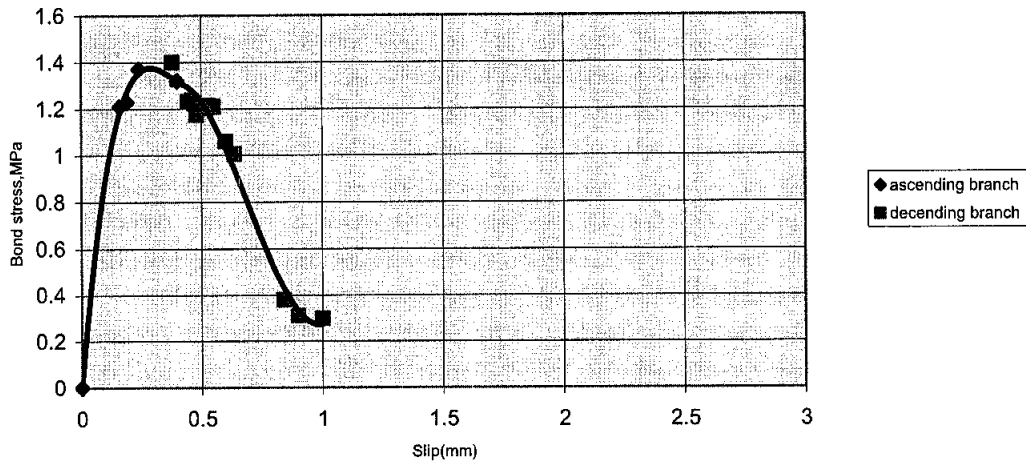


Fig. 6.2 MONOTONIC BOND-SLIP CURVE (AXIALLY LOADED CASE)

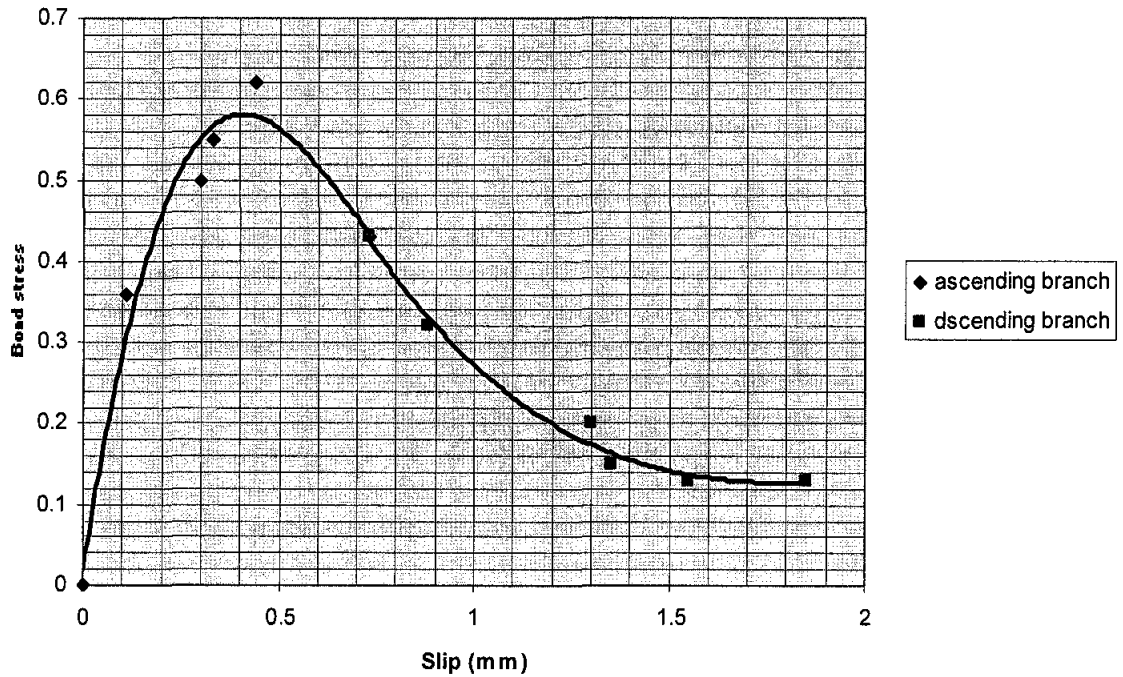


Fig. 6.3 MONOTONIC BOND-SLIP CURVE (ECCENTRICALLY LOADED CASE)

The corrected bond stress-slip curve was obtained by performing the statistical analysis to the experimental data. The ascending and descending part of the curve is described in the separate equations: for axially and eccentrically loaded specimen as below:

***Axially loaded case***

For ascending branch

$$\tau_b = 30.298s^3 - 33.995s^2 + 12.305s + .0009 \quad \text{for } 0 \leq s < s_p \dots\dots\dots 6.5$$

For descending branch

$$\tau_b = 10.394s^3 - 21.6055s^2 + 12.05s - .8205 \quad \text{for } s \geq s_p \dots\dots\dots 6.6$$

The coordinate at peak point was found to be 0.28 and 1.38 respectively for  $s_p$  and  $(\tau_b)_p$

***Eccentrically loaded case***

For ascending branch

$$\tau_b = 2.6653s^3 - 5.5401s^2 + 3.1898s + 0.021 \quad \text{for } 0 \leq s < s_p \dots\dots\dots 6.7$$

For descending branch

$$\tau_b = -0.1244 s^3 + 0.798 s^2 - 1.6633s + 1.2616 \quad \text{for } s \geq s_p \dots\dots\dots 6.8$$

The coordinate at peak point was found to be 0.4 and 0.58 respectively for  $s_p$  and  $(\tau_b)_p$

Where

$\tau_b$  = bond stress ( $N/mm^2$ )

$s$  = slip (mm)

$(\tau_b)_p$  = peak bond stress ( $N/mm^2$ )

$s_p$  = slip at peak point (mm)

### 6.2.3 Shear stiffness of interface element

In order to establish the non-linear bond stiffness of interface element Eq.6.5 and Eq.6.6 were differentiated with respect to  $s$  and the following equations were obtained:

#### 1. Axially loaded case

For ascending branch

$$\frac{\partial \tau_b}{\partial s} = E_b = 90.894s^2 - 67.98s + 12.305 \quad (N/mm^3) \dots\dots\dots 6.9$$

For descending branch

$$\frac{\partial \tau_b}{\partial s} = E_b = 31.17s^2 - 43.21s + 12.05 \quad (N/mm^3) \dots\dots\dots 6.10$$

#### 2. Eccentrically loaded case

For ascending branch

$$\frac{\partial \tau_b}{\partial s} = E_b = 7.996s^2 - 11.8s + 3.189 \text{ (N/mm}^3\text{)} \dots\dots\dots 6.11$$

For descending branch

$$\frac{\partial \tau_b}{\partial s} = E_b = 3.732s^2 - 1.596s + 1.6633 \text{ (N/mm}^3\text{)} \dots\dots\dots 6.12$$

For defining the interface stiffness in universally accepted units, equations 6.9 to 6.12 were multiplied by surface area attributed to interface element as follow:

$$K_{interface} = E_b * A_s \text{ (N/mm)} \dots\dots\dots 6.13$$

Where

$E_b$  = shear modulus.

$A_s$  = surface contact area.

#### 6.2.4 Failure criteria of interface element

Figures 6.4 and 6.5 show the relationship between the tangential bond stress  $\tau_b$  and the normal bond stress  $\sigma$  under static loading.

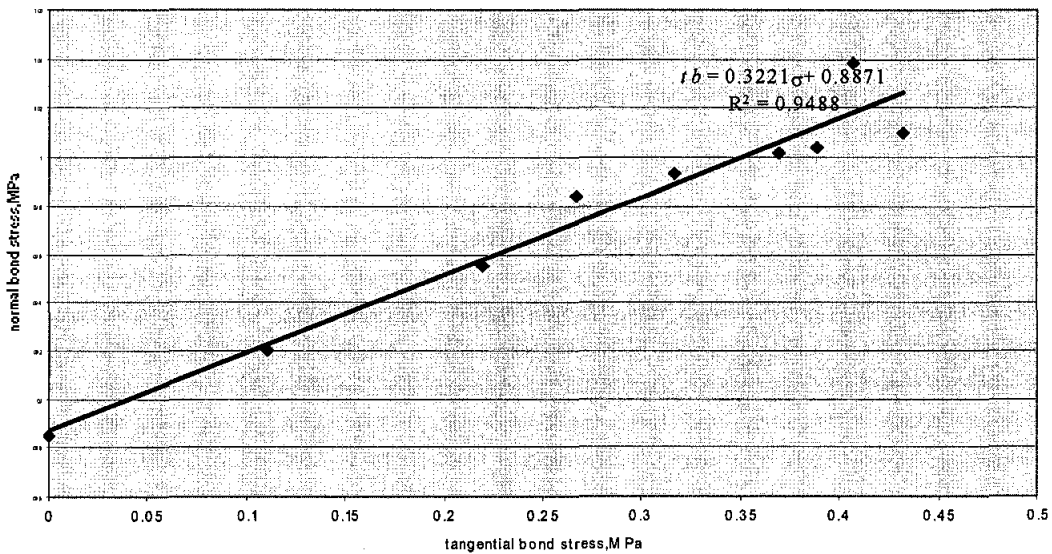


Fig. 6.4 RELATION BETWEEN  $\tau_b$  AND  $\sigma$  (AXIALLY LOADED CASE)

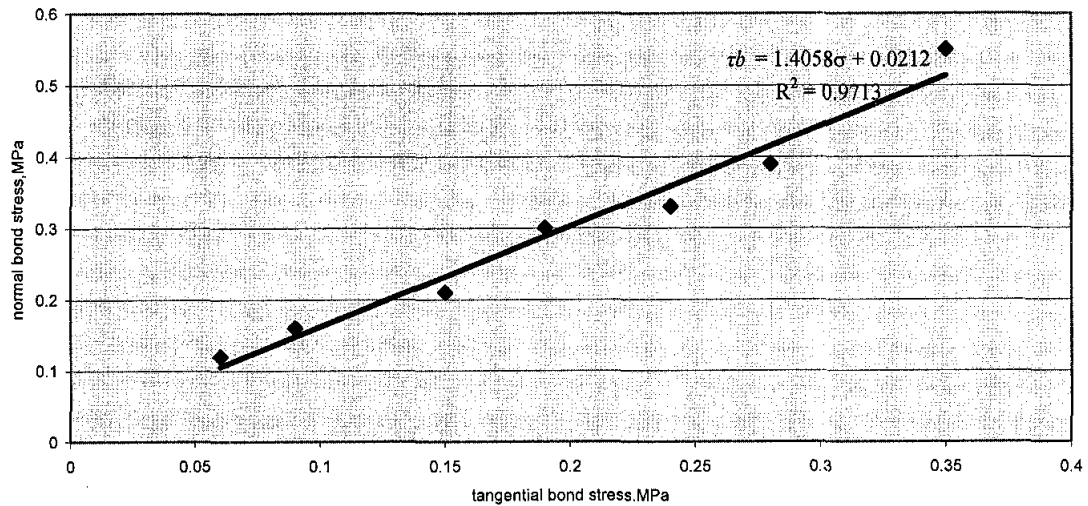


Fig. 6.5 RELATION BETWEEN  $\tau_b$  AND  $\sigma$  (AECCENTRICALLY LOADED CASE)

$$\tau_b = 0.8771 + 0.322\sigma \text{ (axially loaded case)}$$

$$\tau_b = 0.0212 + 1.4058\sigma \text{ (eccentrically)}$$

### 6.3 Interfacial Behaviour of CFRP-to-Concrete Joints under Cyclic Loading

#### 6.3.1 Fatigue Behaviour of Specimens

Results of the fatigue life of specimens tested until failure are summarized in Table 6.3 and Table 6.4.

Table 6.3 RESULTS OF FATIGUE LIFE FOR SPECIMEN IN GROUP A

Specimen No.	Type of specimen	Fatigue load, KN (10%-80%) failure load	Fatigue life, $N$
$A_2$	Without CFRP	17.3-138.4	95,763
$A_3$	Without CFRP	17.3-138.4	89,324
$A_4$	Without CFRP	17.3-138.4	97,221
$A_5$	With CFRP	17.3-138.4	551,661
$A_6$	With CFRP	17.3-138.4	533,762
$A_7$	With CFRP	17.3-138.4	591,776

The control specimen of this group " $A_1$ " was tested under static load and failed at 173.3 KN.

In the group *A* specimens, cracks were initiated and further developed when the number of cycles reached at 50%-60% of the total number of cycles until failure. After the first cracks appeared they were propagated vertically towards the shear plane. It means cracks were initiated at about half of the fatigue life after which the specimens behaved in non-linearly in plastic range. The failure occurred suddenly at the centre of specimen simultaneously due to crushing of concrete and rupture of CFRP plates.

Table 6.4 RESULTS OF FATIGUE LIFE FOR SPECIMEN IN GROUP *B*

Specimen No.	Type of specimen	Fatigue load, KN (10%-80%) from failure	Fatigue life, <i>N</i>
<i>B</i> <sub>2</sub>	Without CFRP	10.7-86	16,431
<i>B</i> <sub>3</sub>	Without CFRP	10.7-86	14,232
<i>B</i> <sub>4</sub>	Without CFRP	10.7-86	19,761
<i>B</i> <sub>5</sub>	With CFRP	10.7-86	121,342
<i>B</i> <sub>6</sub>	With CFRP	10.7-86	117,345
<i>B</i> <sub>7</sub>	With CFRP	10.7-86	132,687

The control specimen of this group "*B*<sub>1</sub>" was tested under static load and failed at 107.4 KN.

For specimens in group *B*, fatigue performance was investigated by applying the load *P* at distance of 50mm from the centre of specimens to induce both axial and flexural stresses in the specimens.

In this group of specimens, the cracks were started to appear once the number of cycles reached 45%-55% of total the number of cycles attained to failure. After the initiation of cracks, they were diagonally propagated towards the shear plane. The failure occurred in brittle manner due to the crushing of concrete in tension zone and the rupture of CFRP at lower part of the samples as shown in Fig. 6.6.

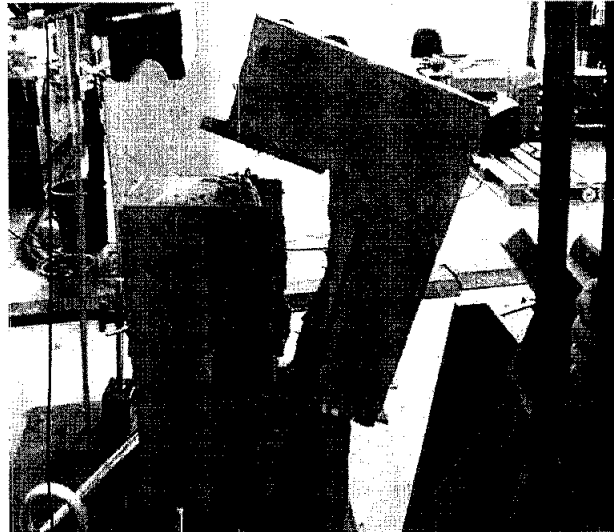
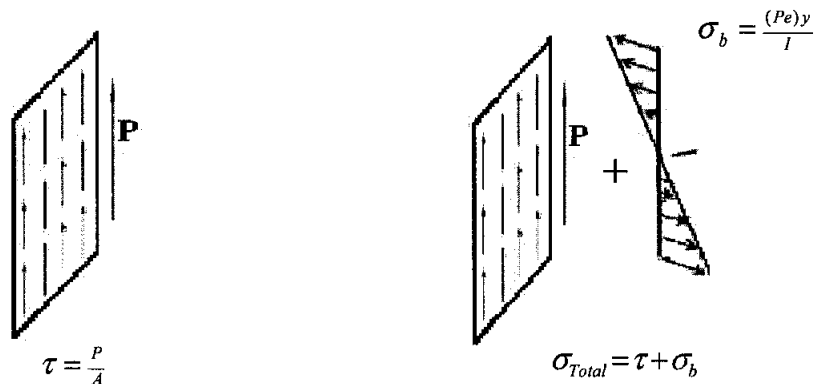


Fig. 6.6 SPECIMEN  $B_6$  AFTER TESTING

The results of the two groups of specimens showed that the bonding of CFRP laminates to concrete as external shear reinforcement has improved the performance of specimens by extending fatigue life about 6 to 7 times that of unstrengthened specimens.

The fatigue life (number of cycles at failure) for specimens in group  $A$  was 450%-500-% higher than that of the specimens in group  $B$ . This was due to the fact that the effect of bending stress developed on the shear plane that was caused by eccentricity of the load applied. Fig. 6.7 shows the stresses acting on shear plane for axially loaded case as well as eccentrically loaded case.



(a) Axially loaded case

(b) Eccentrically loaded case

Fig. 6.7 STRESS ACTING IN SHEAR PLANE

### 6.3.2 Cyclic Bond Stress– Slip Behaviour

Mathematical formulas that were used to determine the bond-slip behaviour under monotonic loading were also used to investigate the bond-slip behaviour under cyclic loading.

Fig. 6.8 and Fig. 6.9 show the relationship between the bond stress and the slip of CFRP-to-concrete joints of specimens tested under axial and eccentric cyclic loading.

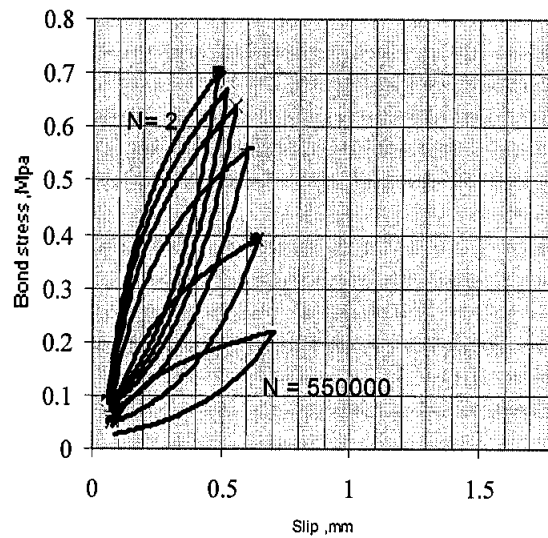


Fig. 6.8 CYCLIC BOND-SLIP CURVE (AXIALLY LOADED CASE)

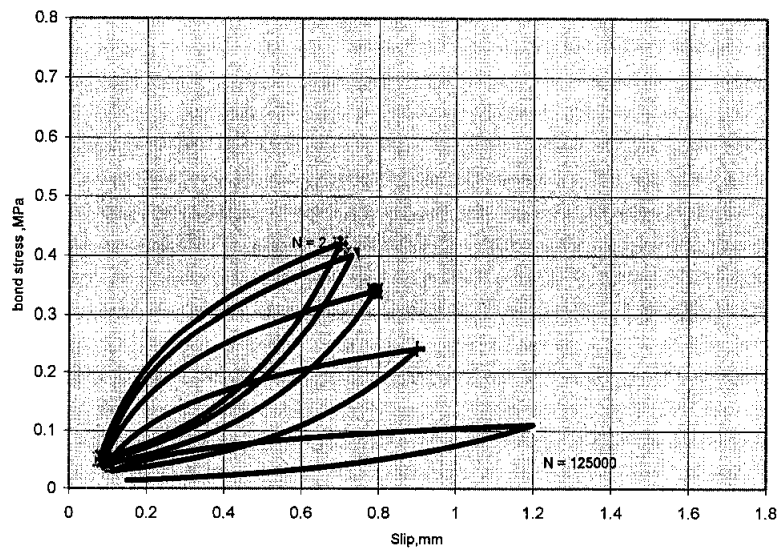


Fig. 6.9 CYCLIC BOND-SLIP CURVE (ECCENTRICALLY LOADED CASE)

The corrected cyclic bond stress-slip relationship was obtained by performing the statistical analysis to the experimental data and the following relationships were obtained for axially and eccentrically loaded specimens:

**6.3.2.1 Axially loaded specimen**

The mathematical function expresses the fitting formula of the relationship between the bond stress  $\tau_b$  and the slip  $s$  in loading branch can be take the following logarithmic rule:

$$\tau_b = C_1 \ln s + C_2 \dots\dots\dots 6.14$$

The constants  $C_1, C_2$  are dependent variables and their values change with the number of cycles of loading. Table 6.5 showed the values of these factors with respect to the number of cycles  $N$ .

Table 6.5 VALUES  $C_1$  AND  $C_2$

Number of cycles	$C_1$	$C_2$
2	0.2948	0.9137
50000	0.276	0.8505
150000	0.2653	0.7941
300000	0.2295	0.6739
550000	0.1611	0.4619

The relations between these factors and the number of cycles of loading are plotted in Fig. 6.10 and Fig. 6.11

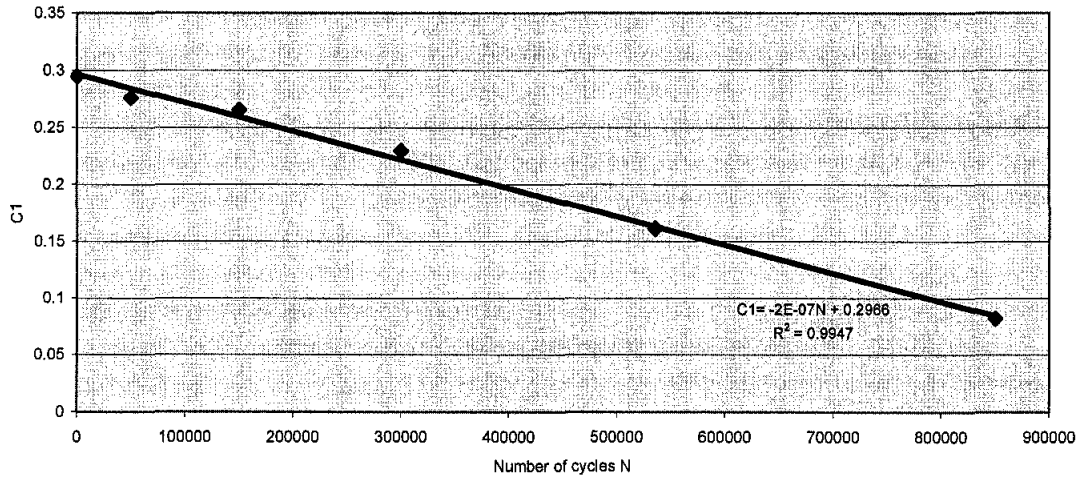


Fig. 6.10  $C_1$ - $N$  RELATIONSHIP

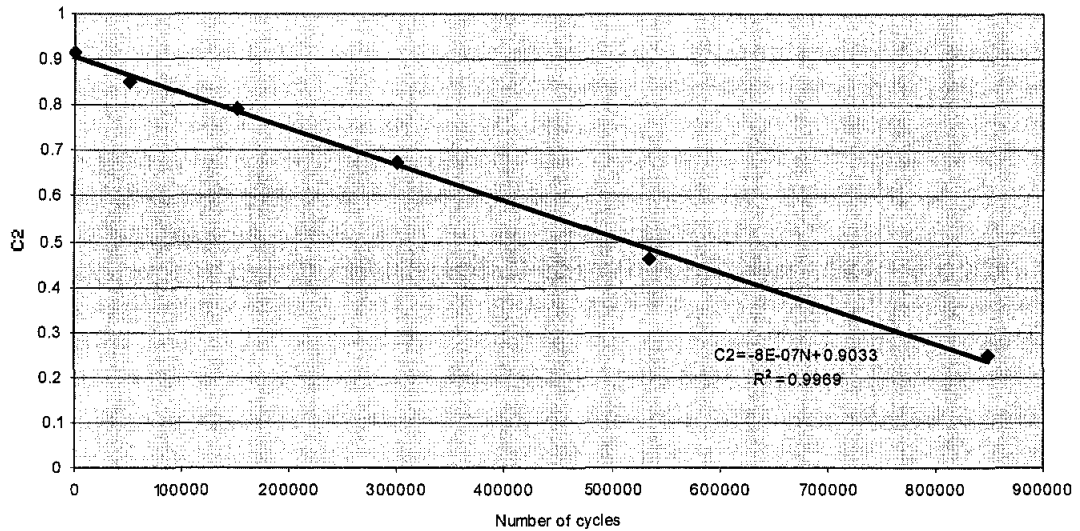


Fig. 6.11  $C_2$ - $N$  RELATIONSHIP

After performing the statistical analysis; the mathematical function expresses the fitting formulas of the relationship between constants  $C_1$  &  $C_2$  and the number of cycles of loading can be presented as follows:

$$C_1 = .29662 - 2 \cdot 10^{-7} N$$

$$C_2 = .90371 - 8 \cdot 10^{-7} N$$

By substituting these factor  $C_1$  &  $C_2$  into Eq.6.14 the following expression was obtained

For loading branch

$$\tau_b = (.29662-2*10^{-7}N) \ln s + (.90371-8*10^{-7}N) (N/mm^2) \dots\dots\dots 6.15$$

The mathematical function expresses the fitting formula of the relationship between the bond stress  $\tau_b$  and the slip  $s$  in the unloading branch can be presented in the following exponential rule:

$$\tau_b = C_3 e^{C_4 s} \dots\dots\dots 6.16$$

The constants  $C_3$  and  $C_4$  are dependent variables and their values change with the number of cycles of loading. Table 6.6 showed values of these factors with respect to the number of cycles,  $N$ .

Table 6.6 VALUES OF  $C_3$  AND  $C_4$

Number of cycles	$C_3$	$C_4$
2	0.065	4.9001
50000	0.062	4.5707
150000	0.059	4.26993
300000	0.0517	3.9549
550000	0.0362	3.7137

The relation between these factors and the number of cycles of loading are plotted in Fig.6.12 and Fig.6.13.

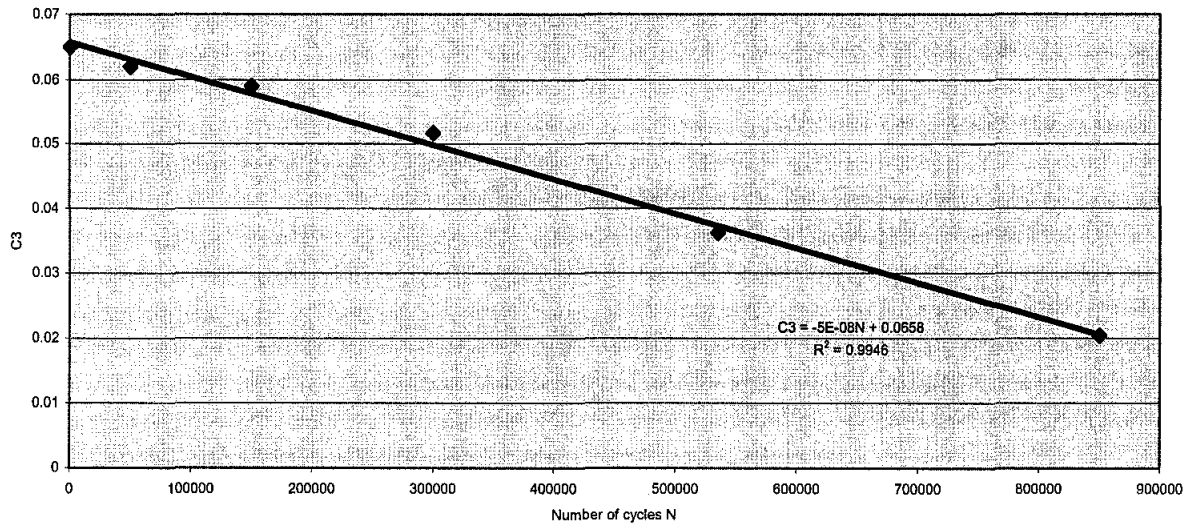


Fig. 6.12  $C_3$ - $N$  RELATIONSHIP

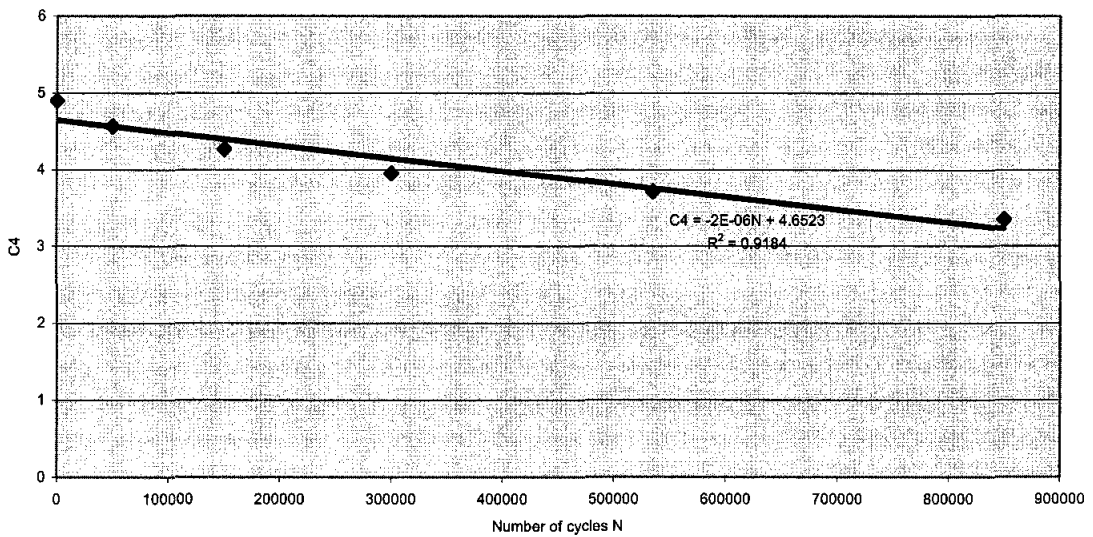


Fig. 6.13  $C_4$ - $N$  RELATIONSHIP

$$C_3 = -5 \cdot 10^{-8} N + 0.0658$$

$$C_4 = -2 \cdot 10^{-6} N + 4.6523$$

By substituting the values of  $C_3$  and  $C_4$  into Eq. (6.16) the following relationship can be obtained

For unloading branch

$$\tau_b = (.06594 - 5 \cdot 10^{-8} N) e^{(4.6559 - 2 \cdot 10^{-6} N) S} \quad (N/mm^2) \dots \dots \dots 6.17$$

### 6.3.2.2 Eccentrically loaded specimen

The mathematical function that expresses the fitting formula of the relationship between the tangential bond stress  $\tau_b$  and the slip  $s$  in the loading branch can be presented in the following logarithmic rule:

$$\tau_b = C_5 Lns + C_6 \dots \dots \dots 6.18$$

The constants  $C_5$  and  $C_6$  are dependent variables their values change with number of cycles of loading. Table 6.7 showed the values of these factors with respect to the number of cycles,  $N$ .

Table 6.7 VALUES OF  $C_5$  AND  $C_6$

Number of cycles	$C_5$	$C_6$
2	0.1706	0.4808
30000	0.1638	0.4516
70000	0.1344	0.3717
100000	0.0894	0.2494
125000	0.0338	0.1038

The relation between these factors and the number of cycles of loading are plotted in Fig.6.14 and Fig.6.15

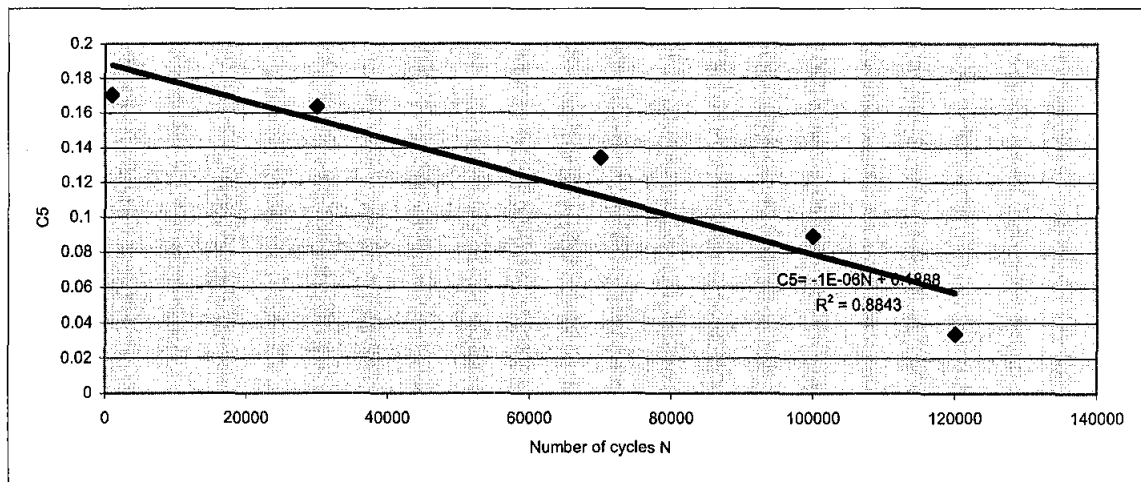


Fig. 6.14  $C_5$ - $N$  RELATIONSHIP

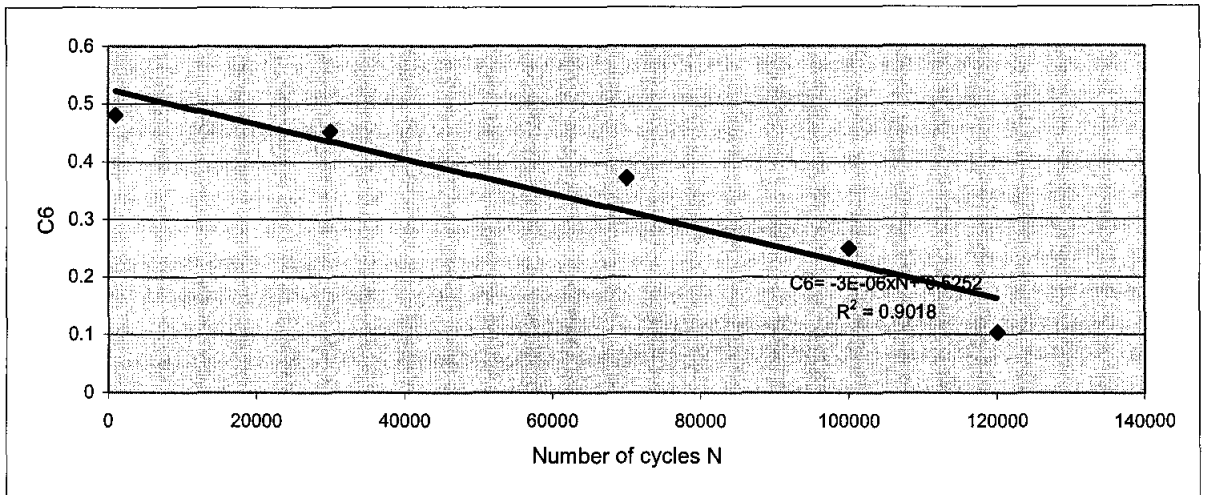


Fig. 6.15  $C_6$ - $N$  RELATIONSHIP

$$C_5 = (.1888 - 10^{-6} * N)$$

$$C_6 = .552(1 - .54348 * 10^{-6} N)$$

By substituting the values of  $C_5$  and  $C_6$  into Eq.6.18 the following logarithmic rule can be obtained:

For loading branch

$$\tau_b = (.1888 - 10^{-6} * N) \ln s + .552(1 - .54348 * 10^{-6} N) \dots \dots \dots 6.19$$

The mathematical function that expresses the fitting formula of the relationship between the bond stress  $\tau_b$  and the slip  $s$  in the loading branch can be presented in the following exponential rule:

$$\tau_b = C_7 e^{C_8 s} \dots \dots \dots 6.20$$

The constants  $C_7$ ,  $C_8$  are dependent variables and their values change with number of cycles of loading. Table 6.8 showed the values of these factors with respect to the number of cycles,  $N$ .

Table 6.8 VALUES OF  $C_7$  AND  $C_8$

Number of cycles	$C_7$	$C_8$
1000	0.039	3.396
30000	0.0371	3.255
70000	0.0316	3.008
100000	0.0223	2.64
120000	0.0102	1.96

The relationship between these factors and the number of cycles of loading are plotted in Fig. 6.16 and Fig. 6.17.

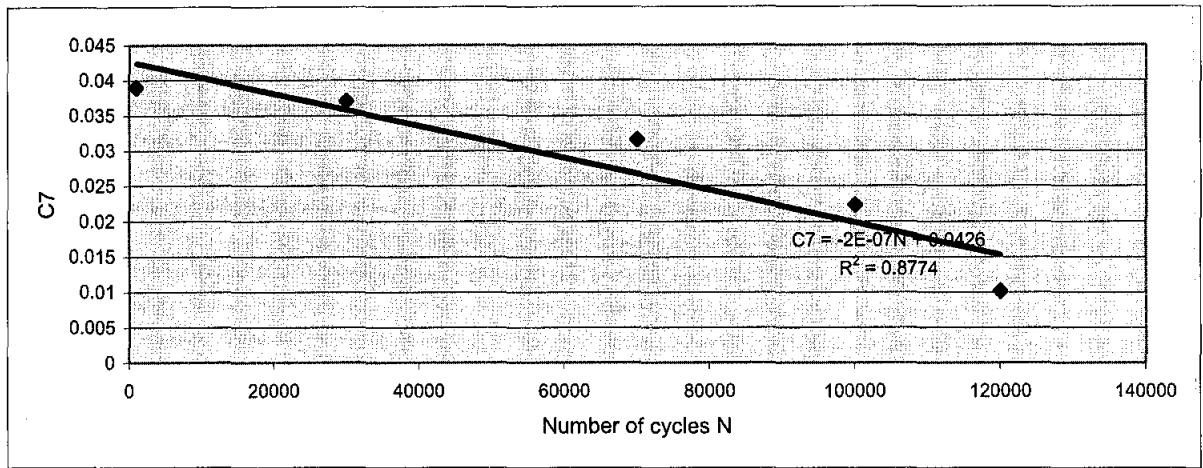


Fig. 6.16  $C_7$ - $N$  RELATIONSHIP

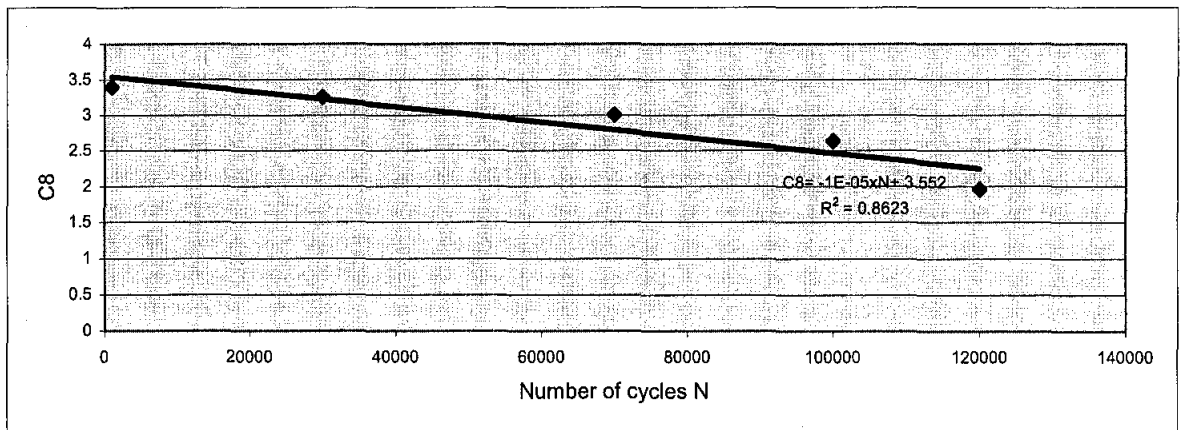


Fig. 6.17  $C_8$ - $N$  RELATIONSHIP

$$C_7 = (.0426-2*10^{-7}N)$$

$$C_8 = (3.552-10^{-5}N)$$

For Unloading branch

$$\tau_b = (.0426-2*10^{-7}N) e^{(3.552-10^{-5}N) s} \dots\dots\dots 6.21$$

Where

$$\tau_b = \text{bond stress (N/mm}^2\text{)}$$

$$s = \text{slip (mm)}$$

Cyclic bond stress-slip curve exhibited a quasi-linear hysteretic behaviour with very narrow hysteresis loops, the shape of the loop decreased with increasing the number of cycles. The narrowness of the hysteresis loops is an indication of the brittle behaviour of the joints.

### 6.3.3 Shear Stiffness of Interface Element under cyclic loading

The non-linear bond stiffness of interface element can be calculated as the slope of loading branch in the cyclic bond stress- slip curves. The mathematical formulas that represented this stiffness of interface were obtained by differentiating Eq.6.15 and Eq.6.16 with respect to  $s$  as follows:

#### 1. Axially loaded case

For loading branch

$$\frac{\partial \tau_b}{\partial s} = E_b = (0.29662-2*10^{-7}N) /s \text{ (N/mm}^3\text{)} \dots\dots\dots 6.22$$

For unloading branch

$$\frac{\partial \tau_b}{\partial s} = (E_u)_b = (.06594-5*10^{-8} N) (4.6559-2*10^{-6}N) e^{(4.6559-2*10^{-6}N) S} \text{ (N/mm}^3\text{)} \dots\dots 6.23$$

#### 2. Eccentrically loaded case

The same procedure was repeated in the eccentrically loaded case to obtain the stiffness of interface element and the mathematical formulas represented this stiffness were obtained by differentiating Eq. 6.17 and Eq. 6.18 with respect to  $s$  as follows:

For loading branch

$$\frac{\partial \tau_b}{\partial s} = E_b = (0.1888 \cdot 10^{-6})/s \text{ (N/mm}^3\text{)} \dots\dots\dots 6.24$$

For unloading branch

$$\frac{\partial \tau_b}{\partial s} = (E_u)_b = (.0426 \cdot 2 \cdot 10^{-7}) (3.552 \cdot 10^{-5} N) e^{(3.552 \cdot 10^{-5} N) s} \text{ (N/mm}^3\text{)} \dots\dots\dots 6.25$$

To obtain the interface stiffness in proper units the above equations (6.22-6.25) was multiplied by the surface area tributary to the one interface element as follows:

$$K_{interface} = E_b \cdot A_s \text{ (N/mm)} \dots\dots\dots 6.26$$

$$(K_u)_{interface} = (E_u)_b \cdot A_s \text{ (N/mm)} \dots\dots\dots 6.27$$

Where

$K_{interface}$  = shear stiffness of interface

$(K_u)_{interface}$  = unloading shear stiffness of interface

$E_s$  = shear modulus

$(E_u)_b$  = unloading shear modulus

$A_s$  = surface contact area

### 6.3.4 Degradation of the Shear Stiffness under Cyclic Loading

Besides the causes of environmentally influenced damages to RC structures; cyclic mechanical loading may also cause some damage. Therefore, the reliability of such structures depends among other influences on the degree of structural damage due to fatigue loading. In order to estimate the state of a structure it is necessary to know the development of the crucial material properties during its service lifetime. A basis for

creating a lifetime-oriented design concept it is sufficient to consider not only a general final failure, but also the information about the continuous changes in the relevant material properties of a structure such as stiffness.

In composite materials the fatigue process is thought to begin at a surface flaw (fibre/matrix interface) where the high shear stresses are concentrated, and consists initially of shear flow along slip planes. Over a number of cycles, this slip generates intrusions and extrusions that begin to cause the crack. A true crack running inward from an intrusion region may propagate initially along one of the original slip planes, but eventually turns to propagate transversely to the principal normal stress causing stiffness reduction of interface resulting in separation of laminate from adjacent neighbouring concrete into discrete manner. Changes in the characteristic properties of the interface during the deterioration process can be described as reduction in young's modulus with respect to the number of cycles of loading.

In this research the degradation of the Shear stiffness of interface element was obtained from the reduction of the slope of bond stress-slip curve. Hysteretic curves of decreasing slope were obtained as the number of cycles of loading,  $N$  is increased.

Fig. 6.18 and Fig.6.19 show the relationship between shear modulus and the number of cycles of loading in loading branch as well as unloading branch.

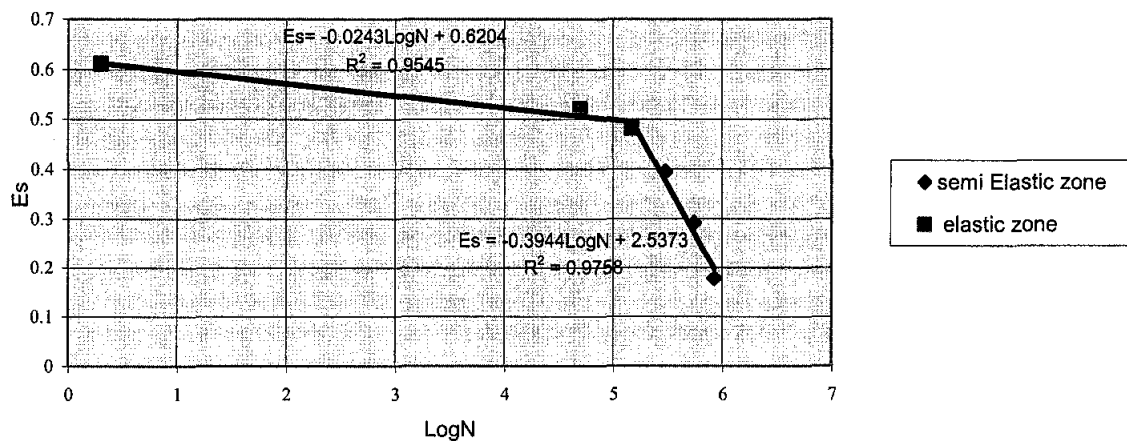


Fig. 6.18  $E_b - \text{Log}N$  (AXIALLY LOADED CASE)

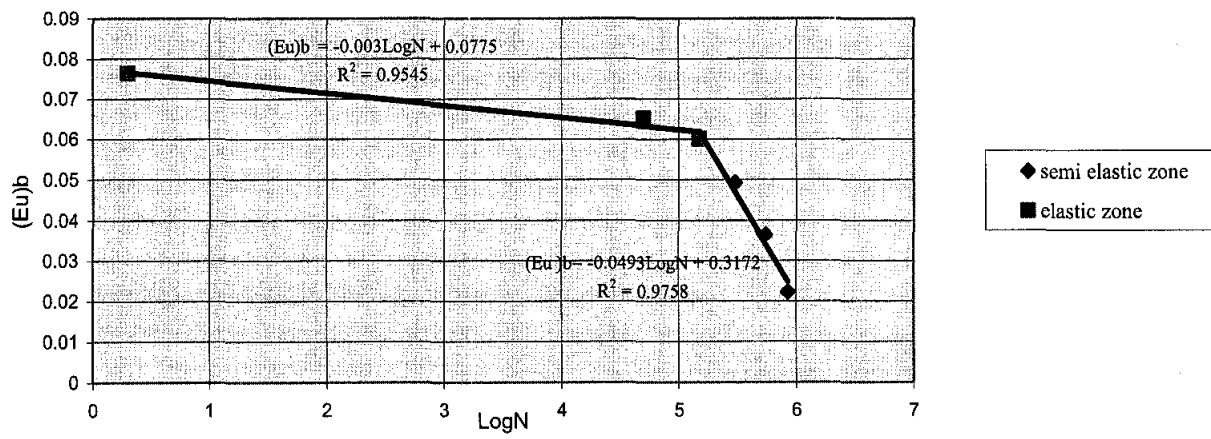


Fig. 6.19  $(E_u)_b - N$  (AXIALLY LOADED)

The corrected  $E_s - N$  curve was obtained after performing the statistical analysis to the experimental data and the following relationships were obtained:

**1. Axially Loaded Case**

*For loading branch*

For elastic zone

$$\frac{\partial \tau_b}{\partial s} = E_b = -0.0243 \text{Log}N + 0.6204 \dots \dots \dots 6.28$$

For semi elastic zone

$$\frac{\partial \tau_b}{\partial s} = E_b = -0.3944 \text{Log}N + 2.5373 \dots \dots \dots 6.29$$

*For unloading branch*

For elastic zone

$$\frac{\partial \tau_b}{\partial s} = (E_u)_b = -0.003 \text{Log}N + 0.0775 \dots \dots \dots 6.30$$

For semi elastic zone

$$\frac{\partial \tau_b}{\partial s} = (E_u)_b = -0.0493 \text{Log}N + 0.3172 \dots \dots \dots 6.31$$

**2. Eccentrically loaded case**

Fig. 6.20 and Fig. 6.21 show the response obtained between unloading shear modulus and number of cycles of loading for axially and eccentrically loading cases respectively.

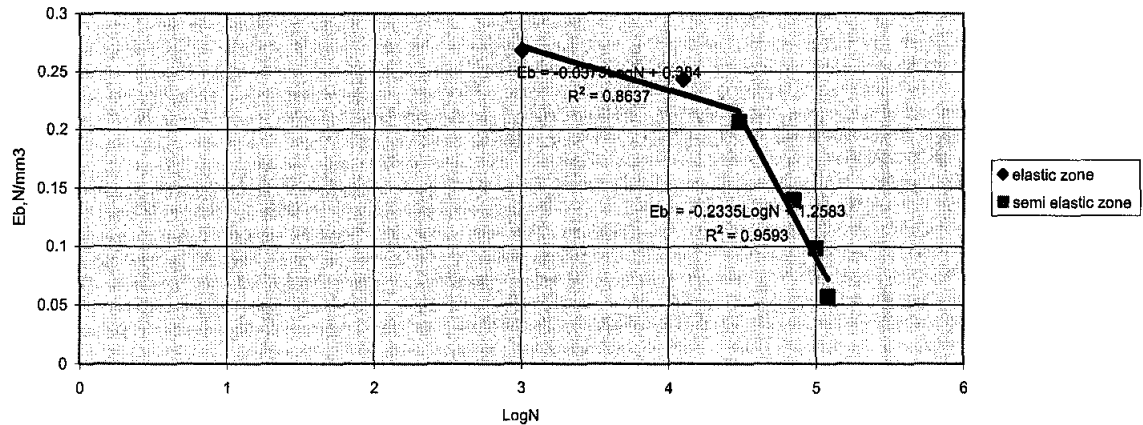


Fig. 6.20  $E_b - \text{Log } N$  (ECCENTRICALLY LOADED)

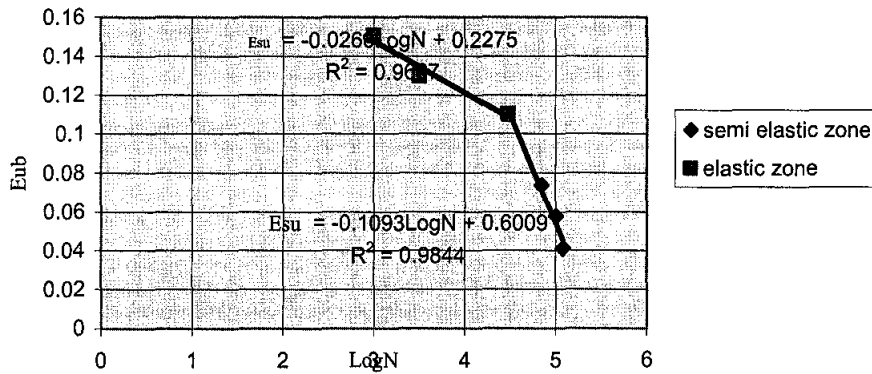


Fig. 6.21  $(E_u)_b - N$  (ECCENTRICALLY LOADED)

The same procedure that was used in axially loaded case to obtain degradation of stiffness with respect to number of cycles of loading was repeated and the following expression was obtained as follows:

**For loading branch**

For elastic zone

$$E_b = -0.02375 \text{Log} N + 0.384 \dots \dots \dots 6.32$$

For semi elastic zone

$$E_b = -0.2335 \text{Log} N + 1.2585 \dots \dots \dots 6.33$$

**For unloading branch**

For elastic zone

$$(E_w)_b = -0.0266\text{Log}N + 0.2275 \dots\dots\dots 6.34$$

For semi elastic zone

$$(E_w)_b = -0.1093\text{Log}N + 0.6009 \dots\dots\dots 6.35$$

The bend in Fig. 6.18 and Fig. 6.19 is to divide the elastic and semi elastic zones as obtained during testing for different situations. It was noted that the slope for the axially loaded case as shown in Fig. 6.20 and Fig. 6.21 is quite flat as compared with the eccentrically loaded specimens, which are quite steep. This means that the loss of stiffness of interface in eccentrically loaded members is very significant as compared with the axially loaded members.

In general for the semi elastic zone, the loss of stiffness is quite significant for all of the cases. This is because of the high cyclic deterioration in this zone compared with the elastic zone in which the specimens exhibit a small level of deformations.

**6.3.5 Stress Level– fatigue Life Relationship**

As understood by materials technologists, fatigue is a process in which damage accumulates due to the repetitive application of loads that may be well below the yield point. The process is dangerous; because a single application of the load would not produce any bad effects, and a conventional stress analysis might lead to an assumption of safety that does not exist.

Before a micro structural understanding of the fatigue processes was developed, engineers have developed empirical means of quantifying the fatigue process and designing against it. Perhaps the most important concept is the *S-N* diagram in which a constant cyclic stress amplitude *S* is applied to a specimen and the number of loading cycles *N* until the specimen fails is determined. Millions of cycles might be required to cause failure at lower loading levels, so the abscissa is usually plotted logarithmically.

The relationship between the tangential bond stress  $\tau_b$  and the number of cycles of loading,  $N$ , for the CFRP-to-concrete joints were plotted in Fig. 6.22 and Fig. 6.23 as shown below.

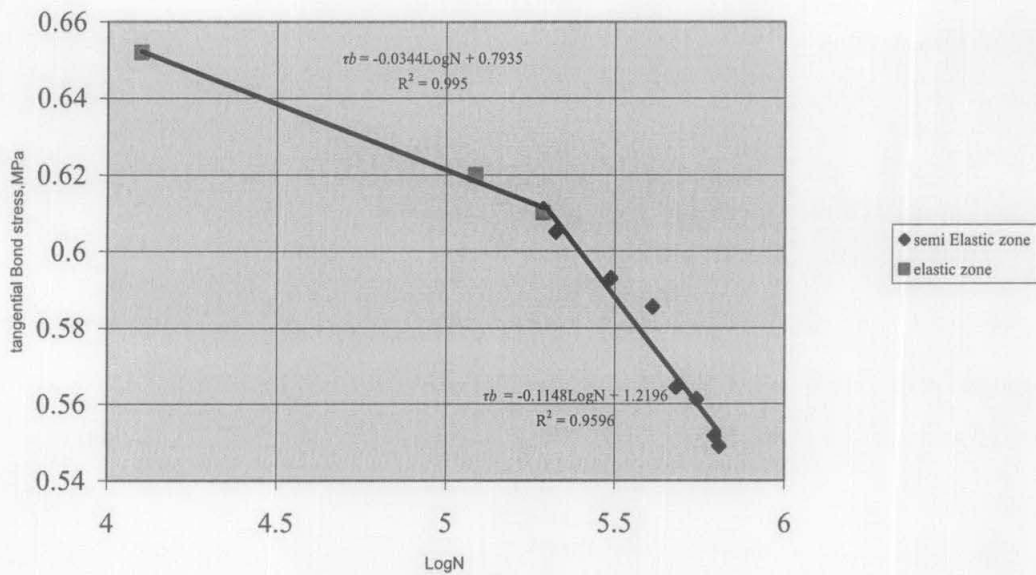


Fig. 6.22  $\tau_b$  -LogN (AXIALLY LOADED)

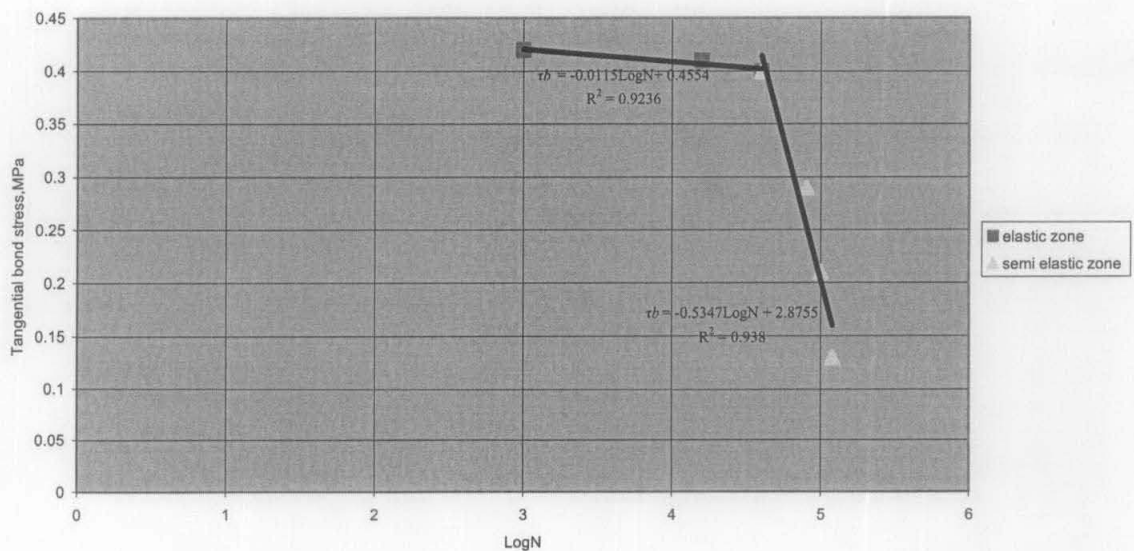


Fig. 6.23  $\tau_b$  -LogN (ECCENTRICALLY LOADED)

From the statistical analysis of data; a linear relationship between the bond stress  $\tau_b$  and the logarithm of the number of cycles at failure,  $\text{Log}N$ , was obtained and represented by the following equations:

**1. Axially loaded case**

For elastic zone

$$\tau_b = -0.0344 \text{Log}N + 0.7935 \dots\dots\dots 6.36$$

For semi elastic zone

$$\tau_b = 0.1148 \text{Log}N + 1.2196 \dots\dots\dots 6.37$$

**2. Eccentrically loaded case**

For elastic zone

$$\tau_b = -0.0115 \text{Log}N + 0.4554 \dots\dots\dots 6.38$$

For semi elastic zone

$$\tau_b = -0.5347 \text{Log}N + 2.8755 \dots\dots\dots 6.39$$

**6.3.6 Failure criteria of interface**

Fig. 6.24 and Fig. 6.25 show the relationship between the tangential bond stress and the normal bond stress for axially and eccentrically loaded case respectively.

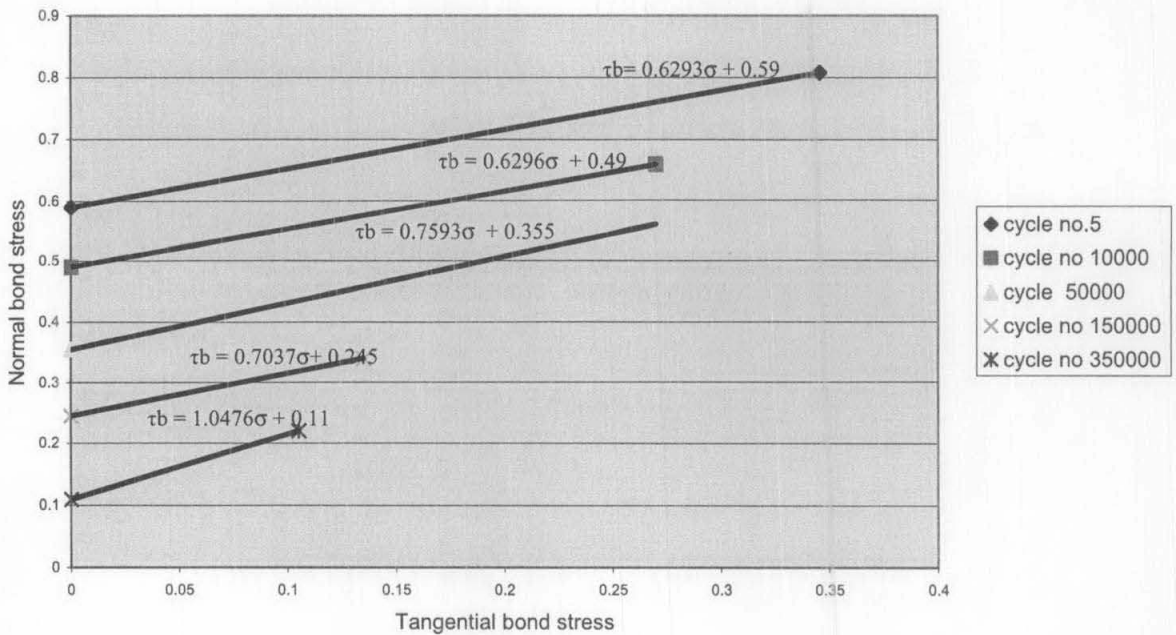


Fig. 6.24 RELATION BETWEEN  $\tau_b$  AND  $\sigma$  (AXIALLY LOADED CASE)

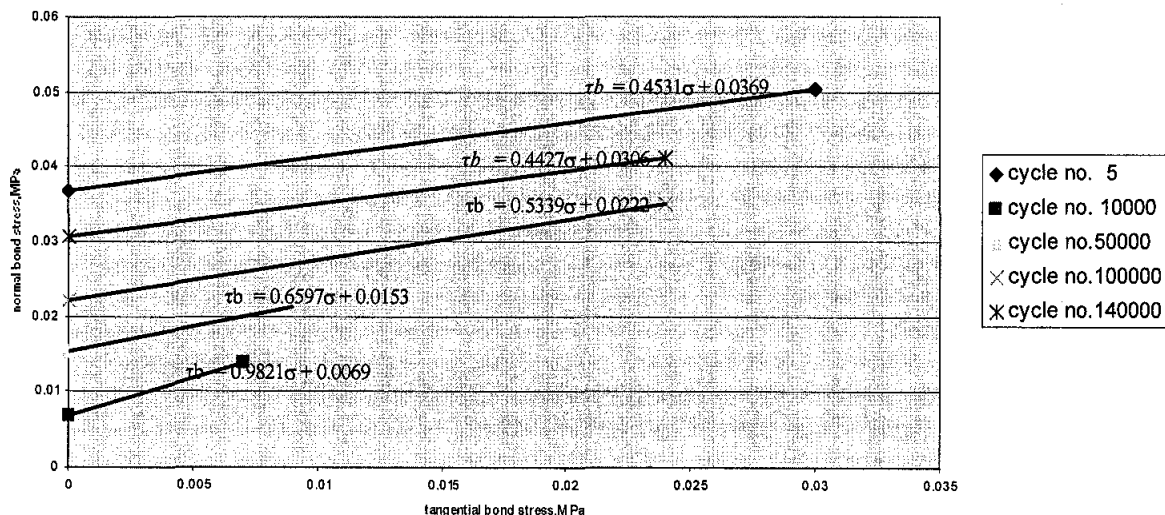


Fig. 6.25 RELATION BETWEEN  $\tau_b$  AND  $\sigma$  (ECCENTRICALLY LOADED CASE)

The corrected failure criterion was obtained by performing the statistical analysis to the experimental data and the following relationships were obtained:

**6.3.6.1 Axially loaded case**

The mathematical function expresses the fitting formula of the relationship between the tangential bond stress  $\tau_b$  and normal bond stress  $\sigma$  can be taken the following linear rule:

$$\tau_b = C + \sigma \tan\phi \dots\dots\dots 6.40$$

The constants  $C$  and  $\tan\phi$  are dependent variables and their values change with the number of cycles of loading. Table 6.7 shows the values of these factors with respect to the number of cycles  $N$ .

Table 6.9 VALUES OF  $C$  AND  $\tan\phi$  (AXIALLY LOADED CASE)

Number of cycles	$C$	$\tan\phi$
5	0.6293	0.59
10000	0.6296	0.49
50000	0.7593	0.355
150000	0.7037	0.245
350000	1.0476	0.11

The relation ship between constants  $C$  and  $\tan\phi$  are plotted in Fig. 6.26 and Fig. 6.27

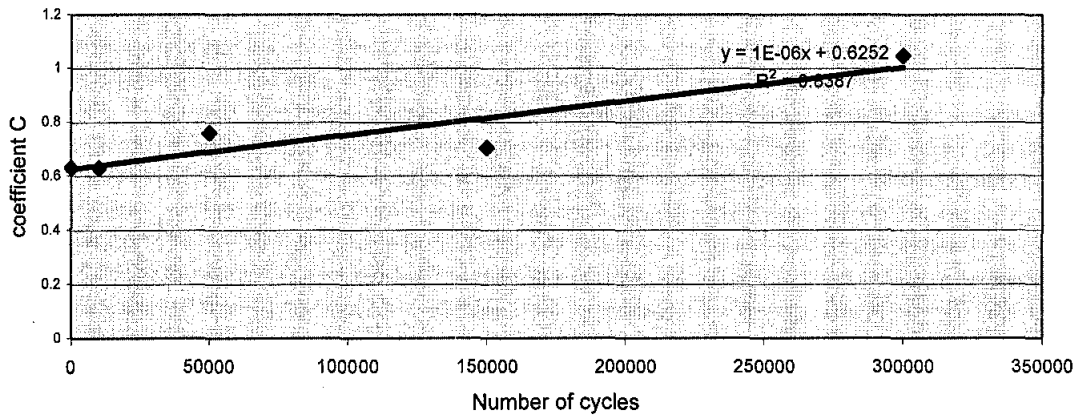


Fig. 6.26 C-N (AXIALLY LOADED CASE)

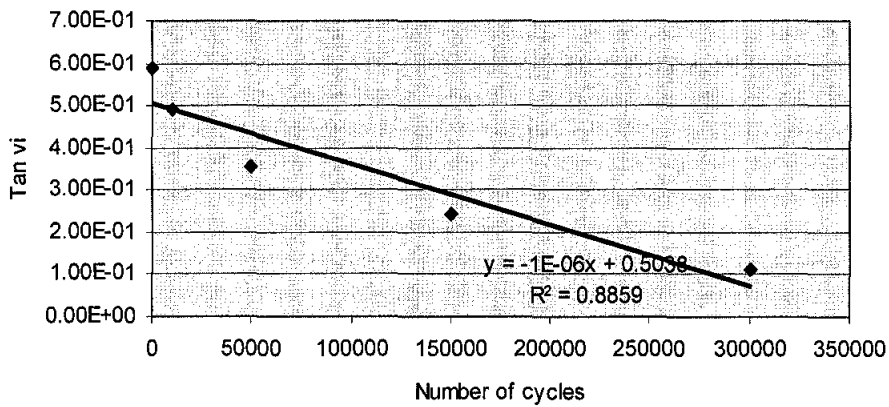


Fig. 6.27  $\tan\phi$ -N (AXIALLY LOADED CASE)

The corrected relationship was obtained by performing the statistical analysis and the following expression was obtained:

$$C = (10^{-6}N + 0.6252) \dots \dots \dots 6.41$$

$$\tan\phi = (0.5033 - 10^{-6}N) \dots \dots \dots 6.42$$

By substituting the values of these factors in Eq .6.40

$$\tau_b = (10^{-6}N + 0.6252) + (0.5033 - 10^{-6}N) \sigma \dots \dots \dots 6.43$$

### 6.3.6.2 Eccentrically loaded case

For eccentric loaded specimen similar procedure that was used for axially loaded specimen was employed. Table 7.7 shows the relationship between  $C$  and  $\tan\phi$  for this case of loading.

Table 6.10 VALUES OF  $C$  AND  $\tan\phi$  [ECCENTRICALLY LODED CASE]

Number of cycles	$C$	$\tan\phi$
5	0.4531	0.0369
10000	0.4427	0.0306
50000	0.5339	0.0222
100000	0.6597	0.0153
140000	0.9821	0.0069

The relation ship between constants  $C$  and  $\tan\phi$  are plotted in Fig. 6.28 and Fig. 6.29.

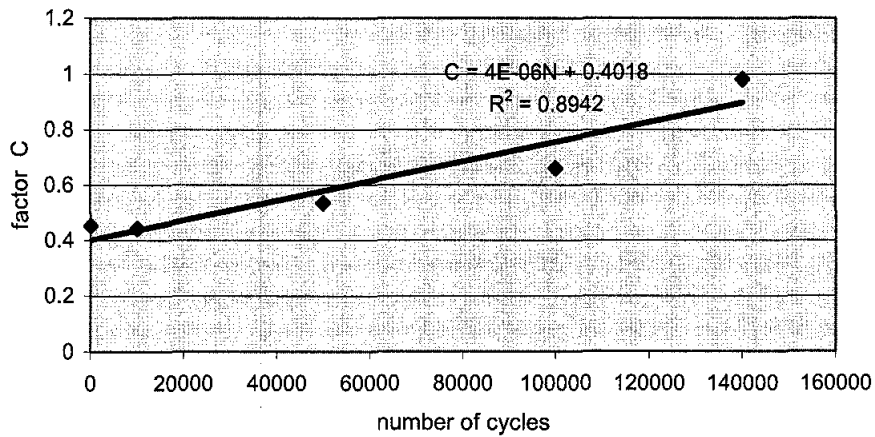


Fig. 6.28 C-N([ECCENTRICALLY LODED CASE])

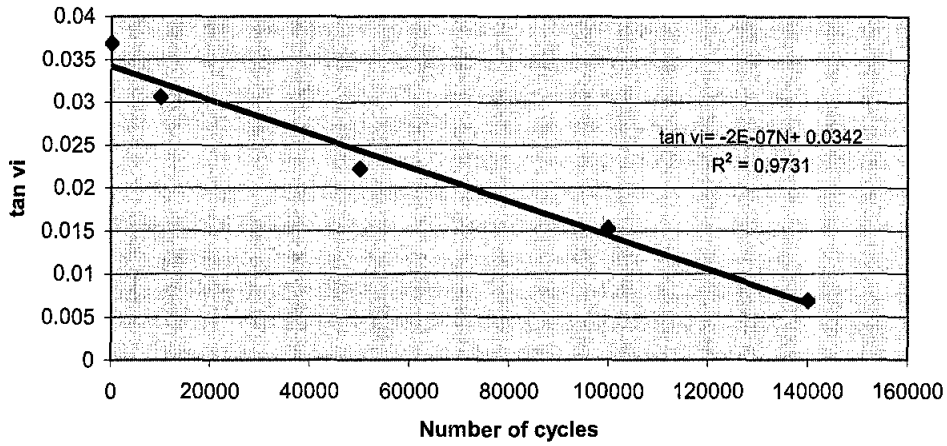


Fig. 6.29  $\tan\phi-N$ [ECCENTRICALLY LOADED CASE]

The corrected relationship was obtained by performing the statistical analysis and the following expression was obtained:

$$C = (4 \cdot 10^{-6}N + 0.4018) \dots \dots \dots 6.44$$

$$\tan\phi = (0.0342 - 2 \cdot 10^{-7}N) \dots \dots \dots 6.45$$

By substituting the values of these factors in Eq .6.40

$$\tau_b = (4 \cdot 10^{-6}N + 0.4018) + (0.0342 - 2 \cdot 10^{-7}N)\sigma \dots \dots \dots 6.46$$

The following chapter gives brief description about FE modelling used in this research to study the structural behaviour of RC beams strengthened for shear with CFRP laminates.

# CHAPTER 7

## ANALYTICAL MODELLING USING FINITE ELEMENT METHOD (FEM)

### 7.1 (FEM) Basic Concepts

The FEM has been widely used for analyzing the reinforced concrete (RC) structures since 1960s. It is an important tool in the analysis of simple structures, such as RC beam, column, slab, etc., as well as for complex structures, such as offshore wall, deep beam, shear wall, FRP strengthened RC structures and etc. The development of large memory capacity computers allows the analysis of highly complex structures that can include material and geometric non-linearity with great level of accuracy.

The FEM is a general method of structural analysis in which the solution of a problem in continuum mechanics is approximated by the analysis of an assemblage of finite elements which are interconnected at a finite number of nodal points and represent the solution domain of the problem. It is based on solving a system of equations that describe some parameter (such as displacement) over the domain of a continuous physical system, (such as a part's surface). The real power of the finite element method lies in its ability to solve problems that do not fit any standard formula. Prior to the use of the finite element method, stress analysis problems were usually matched to a handbook's formula, which was derived for a standard shaped part. If the shape of the part being analyzed did not fit any standard formula, the analyst would approximate it. This was done by envisioning some simplified shape or loading system that approximated the actual case at hand. In contrast, the finite element method is able to analyze physical parts that are of any shape or size having arbitrarily located loads and supports.

The concept of finite element method is to find the solution for complicated problem by replacing it with simpler one. This is done by modelling analytically a continuous structure (domain) and subdividing it into regions or elements (sub-

domains) which can be of many regular shapes. As the name implies, finite element analysis involves the partitioning (also called discretizing) of a structure into a finite number of elements. Elements are connected to one another at their corner points. These corner points are called nodes or nodal points. Each element is a simple geometric shape, such as a triangle or quadrilateral, which facilitates the development of the governing equations that relate the displacement and stress behaviour within the element.

In order to define a finite element model, nodal points, elements, loads, supports and element related data (such as material properties) must be defined, which is then submitted to a finite element program for the computational process. The program then formulates a set of simultaneous equations, which are the equilibrium equations corresponding to each degree of freedom (directions in which movement can occur) at each nodal point, which can have up to six degrees of freedom; translation in the  $x$ ,  $y$ , and  $z$  directions and rotation about each of these axes. As the finite element model is loaded and begins to deform, the force at each nodal point depends on the force at every other node. The finite element model, therefore, acts like a large system of springs - deflecting until all forces balance. Since there are usually hundreds or thousands of equilibrium equations generated to represent a typical finite element model, the use of a computer for the solution process is mandatory. Like any numerical method there are some margins of error inherent in the finite element method, which depends primarily on the functional representation chosen to best resemble the behaviour of actual structure and upon the size of element relative to the actual size of the regions studied. In most complicated problems approximate solutions are acceptable because the exact solutions are too elaborated or rather impossible to obtain. The non-linear problems must be satisfying the fundamental conditions of equilibrium, compatibility and constitutive relations of materials.

The solution of a typical structure subjected to cyclic load is very complicated as compare to the static analysis, which is possible only through the use of high-speed digital computer that has become the standard tool for analysis of such problems. An approach based on finite element method provides a convenient and reliable idealization of the system and is particularly effective in digital-computer analysis.

## 7.2 Advantages of using Finite Element Analysis

Use of the FEM provides several advantages over conventional stress analysis and experimental techniques. The following are the principal advantages of FEM applications:

1. Its ability to solve problems that do not fit any standard formula.
2. Allows irregularly shaped parts to easily be analyzed
3. Allows parts which are made from a combination of several different types of materials to be analyzed, since each element's equations are formulated separately.
4. Allows irregular loads to be placed on the part being analyzed.
5. Allows a large number of locations on the part to be supported.
6. Provides results of deflections and stresses throughout the entire part, rather than at just the location where strain gages are placed, as in the case of experimental evaluations.
7. Easily allows changes to be made to the model, so that alternative designs can be evaluated. This reduces the number of physical prototypes that need to be built.
8. It has proven successful in representing various types of complicated material properties that are difficult to incorporate into other numerical methods.
9. The method can be systematically programmed to accommodate such complex and difficult problems as non-homogeneous materials, non-linear stress-strain behaviour, hysteretic and complicated boundary conditions.

## 7.3 Basic Steps in Finite Element Procedure

The following steps summarize the finite element analysis procedure:

1. *Discretisation of the continuum.*

A continuum is the physical body (solid or liquid) that can be continuously subdivided into small elements with properties being those of bulk material. Discretization may be simply described as the process in which the given body is subdivided into an equivalent system of finite elements. The types of element selected to be used depend on characteristic of continuum, include one dimensional line element, two dimensional triangles, or quadrilaterals and three dimensional brick elements, etc. High order elements are sometimes employed to fit the boundary shape of the continuum. The effectiveness of continuum analysis depends on the number, size, and arrangement of the finite elements in continuum.

## **2. Displacements approximation**

The displacement field varies over the problem domain and it is assumed that the displacements within each element  $[u]_{Element}$  can be expressed as a function of its nodal displacements  $[U]_{Nodes}$  through a set of functions called the interpolation functions.

$$[u]_{Element} = [N] [U]_{Nodes}$$

Where

$[N]$  = matrix of interpolation functions

A displacement model can be expressed in various simple forms, such as polynomials and trigonometric function. Since polynomials offer ease in mathematical manipulations, they have been commonly employed in the finite element applications. The degree of the polynomial depends on the number of nodes assigned to the element. The assumed interpolation functions represent only approximately the actual or exact distribution of the displacements. Obviously, it is generally not possible to select an interpolation function that can represent exactly the actual variation of displacement in the element. Hence, the basic approximation of the finite element method is introduced at this stage.

## **3. Derivation of the element stiffness matrix using a variation principle.**

The stiffness matrix consists of the coefficients of the equilibrium equations derived from the material and geometric properties of an element that is obtained with help of principle of minimum potential energy. For stress analysis, the governing equations for a continuous rigid body are obtained by minimizing

the total potential energy of the system. The total potential energy  $\Pi$  is expressed as:

$$\Pi = U - W = 0$$

$$\Pi = \frac{1}{2} \int_{\Omega} \sigma^T \varepsilon dV - \left[ \int_{\Omega} u^T b dV + \int_{\Gamma} u^T q dS \right] = 0$$

Where  $U$  is the internal potential energy of deformation and  $W$  is the potential energy of the external loading consisted of two terms; the first term represents the potential energy contributions of the body forces and the second one represents distributed surface loads,  $\sigma$  and  $\varepsilon$  are stress and strain vectors at any point, respectively,  $u$  is the displacement vector,  $b$  is the body force vector per unit volume, and  $q$  is the vector of applied surface traction components at any surface point. The volume and surface integrals are defined over the entire region of the structure  $\Omega$  and that part of its boundary subject to load  $\Gamma$ . The total potential energy of the discretized structure will be the sum of the energy contributions of each individual element as

$$\Pi = \sum_e \Pi_e$$

Where

$$\Pi_e = \frac{1}{2} \int_{\Omega} u^T (B^T DB)^T u dV - \int_{\Omega} u^T N^T u dV - \int_{\Gamma} u^T N^T q dS = 0$$

Taking the derivative of  $\Pi_e$

$$\frac{\partial \Pi_e}{\partial u} = \partial U - \partial W = \frac{1}{2} \int_{\Omega} (B^T DB)^T u dV - \left[ \int_{\Omega} N^T u dV - \int_{\Gamma} N^T q dS \right] = 0$$

Element equilibrium equation

$$k_e u - p = 0$$

Where

$$p = \int_{\Omega} N^T u dV - \int_{\Gamma} N^T q dS, \quad k_e = \int_{\Omega} (B^T DB)^T dV$$

$[k^{(e)}]$  is known as element stiffness matrix,  $[D]$  is materials matrix and  $[B]$  is strain displacement matrix contains the global derivatives of the shape functions and  $[k^{(e)}]$  is the element stiffness matrix relates the displacements at the nodal

points (the nodal displacements) to the applied forces at the nodal points (the nodal forces). The distributed forces applied to the structure are converted into equivalent concentrated forces at the nodes. The equilibrium relation between the element stiffness matrix  $[k^{(e)}]$ , nodal force vector  $[p]$ , and nodal displacement vector  $[u]$  is expressed as a set of simultaneous linear algebraic equation  $[k^{(e)}][u] = [p]$

#### ***4. Assembly of the algebraic equations for the overall discretized continuum.***

This process includes the assembly of the overall or global stiffness matrix for the entire body from the individual element stiffness matrices, and the overall or global force or load vector from the element nodal force vectors. The most common assembly technique is known as the direct stiffness method. In general, the basis for an assembly method is that the nodal interconnections require the displacements at a node to be same for all elements adjacent to that node. The overall equilibrium equation between the total stiffness matrix  $[K]$ , the total load vector  $[P]$ , and the nodal displacement vector for the entire body  $[U]$  will again be expressed as a set of simultaneous equation.  $[K][U] = [P]$

These equations cannot be solved until the geometric boundary conditions are taken into account by appropriate modification of the equations. A geometric boundary condition arises from the fact that displacements may be prescribed at the boundaries or edges of the body or structure.

#### ***5. Solutions for the unknown displacements.***

The algebraic equations assembled in step 4 are solved for the unknown displacements. In linear equilibrium problems, this is a relatively straightforward application of matrix algebra. However for non-linear problems the desired solutions are obtained by a sequence of steps, each step involves the modification of the stiffness matrix and/or load vector.

#### ***6. Computation of the element strains and stresses.***

In certain cases the magnitudes of the primary unknowns, these are the nodal displacements, will be all that required for an engineering solution. More often, however, other quantities derived from the primary unknowns, such as strains

and/or stresses, must be computed. The strains within the element can be expressed in terms of the element nodal displacements as  $[\epsilon] = [B] [u]$ . Finally, the stresses may be related to the strains by use of material elasticity matrix (e.g., Young's modulus) as  $[\sigma] = [D] [\epsilon]$ .

#### 7.4 Non-linear Finite Element Analysis [NLFEA]

In structural mechanics, material may yield or creep; local buckling may arise; gaps may open or close. Non-linear problems pose difficulty of describing phenomena by realistic mathematical and numerical models. FEM is widely used for non-linear analysis of structures that depends on:

- The increase in computational effort which is required for a non-linear problem necessitates that considerable computing power be available at low cost to the designer. Developments in the last two decades have ensured that high-speed digital computers have gradually become available to the designers and indications are that reductions in unit computing costs will continue at an accelerating pace.
- The other factor is related to the level of complexity of non-linear analysis. Before the application of non-linear methods the accuracy and reliability of the proposed models has to be ensured. The development of improved element characteristics efficient non-linear solution algorithms and the experience gained in their application to engineering problems have ensured that non-linear finite element analysis can now be performed with some confidence. Thus, barriers to the wide use of non-linear finite element techniques are gradually removed. Nevertheless, difficulties still abound whose solution will require much effort on the part of researchers and designers.

In structural mechanics, types of non-linearity include the following:

1. **Material non-linearity**, in which material properties are functions of the state of stress or strain. Examples include non-linear elasticity, plasticity, and creep. The main sources of material non-linearity in reinforced concrete structures are:

- Cracking of concrete
  - Yielding of reinforcement
  - Non-linear stress-strain relationship of concrete
2. **Contact non-linearity**, in which a gap between adjacent parts may open or close, the contact area between parts changes as the contact force changes, or there is sliding contact with frictional forces. The main sources of contact non-linearity are:
- Concrete-to-concrete interface (aggregate interlock mechanism)
  - Steel-to-concrete interface (dowel action and bond-slip mechanisms)
  - Interaction of CFRP-to-concrete surface
3. **Geometric non-linearity**, in which deformation is large enough that equilibrium equations must be written with respect to the deformed structural geometry. This type of non-linearity is of very little importance in reinforced concrete structures because the displacements in such structures are generally very small.

In this research the geometric non-linearity is neglected and only the effects of material and contact non-linearity are considered.

#### **7.4.1 Non-linear Numerical Techniques using Finite Element Method**

The solution of non-linear problems using the finite element method is usually attempted by one of three basic techniques:

- Incremental, or stepwise method
- Iterative or Newton method
- Iterative-step or mixed procedure

#### ***7.4.1.1 Incremental Method***

The basic concept of this technique is to divide the applied load  $[F]$  into many small increments  $\Delta F$ , which are not necessarily the same. During the application of each load increment, stiffness matrix in global form  $[K]$  assumed to be fixed, linear relation between the load and displacement is assumed. The displacements resulting from each load increment  $[U_i]$  are accumulated to give the total displacement at the stage of loading. This process is repeated until the total load is reached. Using small increments improve the accuracy of this method but results in more computational effort.

This method is suitable for linear analysis where there are no residual forces produced drifting of the numerical solution from actual response of structure.

#### ***7.4.1.2 Iteration Method***

The numerical implementation of the finite element model requires the solution system of simultaneous non-linear equations, since the stiffness matrix  $[K]$ , in general, depends on the displacement vector  $[U]$ . The solution of this system of non-linear equations is typically accomplished with an iterative method. The load vector  $[F]$  is subdivided into a number of sufficiently small load increments, which are successively applied. At each load step a linear approximation of the stiffness matrix  $[K]$  is established and the resulting system of linear equilibrium equations is solved for the displacement increments which correspond to the applied load increments. Since the stiffness matrix  $[K]$  changes under these displacement increments, the resisting forces of the structure do not equilibrate the applied loads and resulted in unbalanced loads. In the subsequent correction phase the displacement increments are iteratively improved, until a specified convergence criterion is satisfied. If no correction phase is included in the non-linear analysis algorithm, the numerical error grows from one load step to the next and the numerical solution drifts away from the actual response, as shown in Fig. 7.1

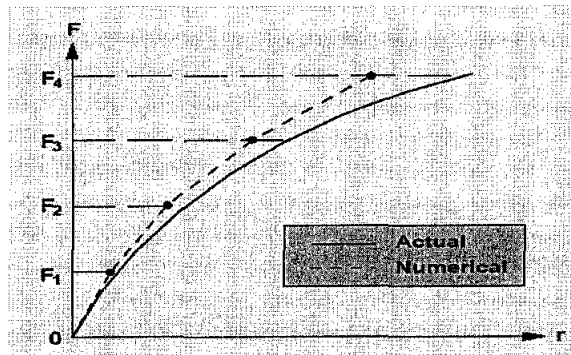


Fig. 7.1 Incremental Method

The basic concept of the iterative procedure is that the full load is applied to the structures (no divisions) and internal stresses are computed. A load system equivalent to computed stresses is evaluated and checked against the applied load system. Since approximate stiffness matrix is used, residual forces (unbalanced forces) result due to the lack of equilibrium. These residual forces are then applied to the structure to restore equilibrium and additional displacements are computed. The process is repeated until the residuals are sufficiently small.

The iterative method is suitable for non-linear analysis to avoid drifting of the numerical solutions from the actual response associated with application of incremental method which is not given any consideration to unbalanced forces result from non-linear behaviour of over all structure due to the change of stiffness during the analysis.

In the case of non-linear elastic constitutive models the elastic constitutive matrix  $[D]$  is no longer constant but varies with stress and/or strain. In elasto-plastic models this is replaced by the elasto-plastic constitutive matrix  $[D^{ep}]$ , which varies with stress and the hardening parameters. In any case the resulting global stiffness matrix  $[K]$  is not constant but changes during a finite element analysis. Depending on how the stiffness matrix  $[K]$  is updated during the correction phase, the iterative method can be classified into three broad categories even though variations of these schemes are also possible:

- The initial or constant stiffness method
- The tangent stiffness method
- Secant stiffness method

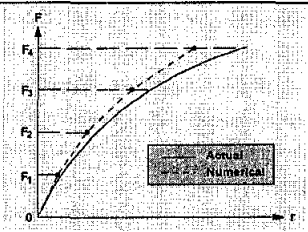
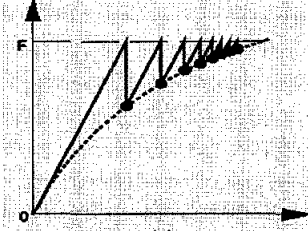
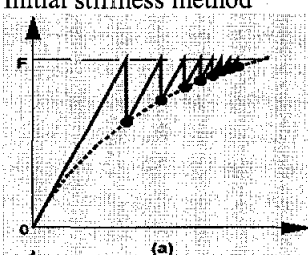
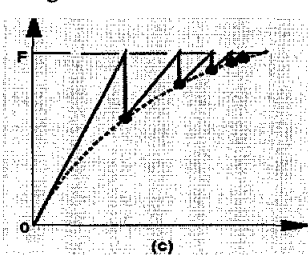
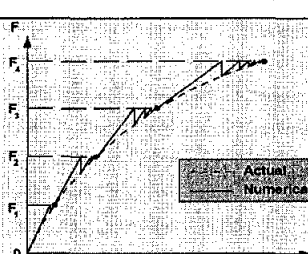
The tangent stiffness method requires the smallest number of iterations to arrive at the solution, but has the disadvantage that the stiffness matrix  $[K]$  needs to be reformed and triangularized after each iteration. The initial stiffness method, on the other extreme, requires the largest number of iterations, but the stiffness matrix  $[K]$  is only formed and triangularized once at the beginning of the load step. Generally, the tangent stiffness method is more efficient than the initial stiffness method for models with a small number of degrees of freedom, even though the selection of one method over another often depends on numerical stability considerations. The secant method, for example, is well suited for structures which exhibit softening response. Even though it is possible to use any stiffness matrix in the first iteration of a new load increment, which constitutes the advancing phase of the solution algorithm, it is quite common to use the tangent stiffness matrix for this purpose. The non-linear solution scheme selected in this study uses the tangent stiffness matrix at the beginning of the load step in combination with a constant stiffness matrix during the subsequent correction phase.

#### ***7.4.1.3 Mixed Procedure***

The mixed procedure utilizes a combination of the incremental and iterative schemes. The load applied incrementally but after each load increments successive iterations are performed until equilibrium is achieved to an acceptable level of accuracy. For every step of loading a new global stiffness matrix  $[K]$  is calculated from updated materials matrix  $[D]$ . Another approach can be used by updating the global stiffness matrix after each iteration but it needs more computational effort. The mixed procedure tends to minimize the disadvantages of previous two methods and gives higher accuracy but need more computational efforts.

Table.7.1 gives general description about each non-linear numerical technique

Table 7.1 SUMMARY OF NON-LINEAR ANALYSIS TECHNIQUES

Types	Main concept	Load-displacement feature	Remarks
Incremental Method	Division of load $K = \text{const}$ $Residual = 0$	 <p>Incremental Method</p>	Suitable for Linear analysis
Iteration Method	Total load $K = \text{varied}$ $Residual \neq 0$	 <p>Initial stiffness method</p>  <p>Tangent stiffness method</p>  <p>Secant stiffness method</p>	<p>The three methods are suitable for Non-linear analysis</p> <ul style="list-style-type: none"> <li>* Required large number of iteration</li> <li>* <math>K</math> is only formed and triangularized once at the beginning of the load step</li> <li>* Required smallest number of iteration</li> <li>* <math>K</math> needs to be reformed and triangularized at each iteration.</li> <li>* Suitable for structures which exhibit softening response.</li> </ul>
Mixed method	Division of load $K = \text{varied}$ $Residual \neq 0$	 <p>Mixed Method (Modified Newton Raphson Method)</p>	<p>suitable for Non-linear analysis</p> <ul style="list-style-type: none"> <li>* <math>K</math> is only formed and triangularized after each load increments</li> <li>* it gives higher accuracy but need more computational effort</li> </ul>

## **7.5 Selection of Element and Representation of Cracking**

To insure reliable behaviour, quick and accurate solution of the finite element system without trial and error; special consideration should be given to discretization procedure. The shapes, the sizes and configuration of elements have to be chosen carefully such that the original structure or domain is simulated as closely as possible without increasing the computational effort needed for solution.

The choice of type of element to idealize a certain structure depends on the following parameters:

- Load carrying characteristic
- Geometry of the structure
- Degree of accuracy and admissibility conditions
- Number of independent coordinates necessary to describe the system

In this research, a proper element representation to idealize the reinforced concrete beams strengthened for shear using CFRP laminates was required the employment of six types of elements:

1. Brick elements to represent concrete and CFRP laminates.
2. Space frame elements and space truss elements to represent the reinforcement bars.
3. 3-D Linkage elements to represent the reinforcement- concrete interaction and post cracking mechanism.
4. 3-D Interface element to represent CFRP-concrete interaction.

## **7.6 Representations of Elements**

For the realistic analyses of many problems; finite element (FE) analyses are performed to gain a better understanding of the behaviour and characteristics of reinforced concrete (RC) structures under a variety of loading and boundary conditions. Simplified analyses based on two-dimensional finite elements are useful for simple problems. Three-dimensional analysis is capable to fully represent all the aspects of the response of concrete structures.

The following is the brief description of the elements that are used in this research to represent the following:

- Concrete
- Reinforcement
- CFRP side plates
- Shear resisting mechanisms
- Interaction between side plated CFRP and concrete surface

### 7.6.1 Representations of Concrete and CFRP

The tetrahedron element, with four corner nodes is one of the basic elements for modelling three-dimensional problems. One of the major difficulties associated with use of three-dimensional elements (like tetrahedral and hexahedra) is that a large number of elements are required for obtaining reasonably accurate results. This will result in large number of simultaneous equations to be solved in the analysis. In spite of this difficulty, we may not have any other choice except using three dimensional elements in certain situations.

In this research; **20-noded brick** element was used to represent the concrete and CFRP elements. The element has sixty degrees of freedom in total and each of the node has three degrees of freedom,  $u_{xi}$ ,  $u_{yi}$  and  $u_{zi}$ , with local coordinate system  $r$ - $s$ - $t$ , which is non-dimensional:  $r$ ,  $s$  and  $t$  vary from 1 to -1.

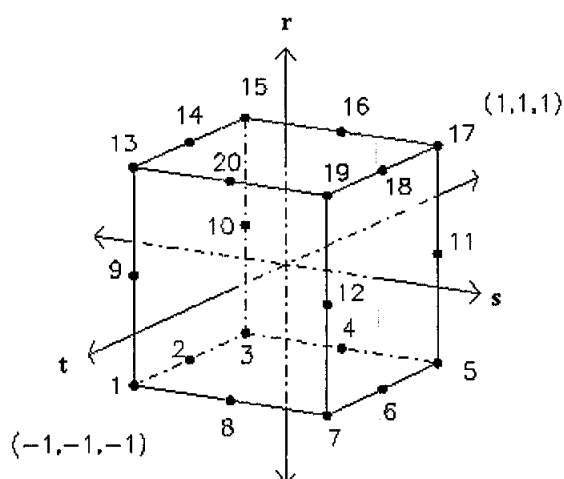


Fig. 7.2 ELEMENT LOCAL COORDINATES SYSTEM

### 7.6.1.1 Coordinates System

The global and local coordinates systems are related as follows:

$$X = \sum h_i x_i$$

$$Y = \sum h_i y_i$$

$$Z = \sum h_i z_i$$

Where

$X, Y, Z$  = global coordinates

$x_i, y_{es}, z_{ip}$  = local coordinates.

$h_i$  = shape function

$$\begin{bmatrix} X \\ Y \\ Z \end{bmatrix} = \begin{bmatrix} h_1 & 0 & 0 & h_2 & 0 & 0 & \dots & \dots & h_i & 0 & 0 \\ 0 & h_1 & 0 & 0 & h_2 & 0 & \dots & \dots & 0 & h_i & 0 \\ 0 & 0 & h_1 & 0 & 0 & h_2 & \dots & \dots & 0 & 0 & h_i \end{bmatrix} \begin{bmatrix} x_i \\ y_i \\ z_i \\ \cdot \\ \cdot \\ \cdot \\ x_i \\ y_i \\ z_i \end{bmatrix} \dots \dots \dots 7.1$$

The shape function for each node can be written in a generalized form as described in Table 7.2

Table 7.2 SHAPE FUNCTION FOR 20-NODED ISOPARAMETRIC ELEMENT

Nodes description	Shape function, $h_i$
for corner nodes	$(1+rr_0) (1+ss_0) (1+tt_0) (rr_0+ss_0+tt_0-2)$
for midside nodes along $r=0$ plane	$(1-r^2) (1+ss_0) (1+tt_0)$
for midside nodes along $s=0$ plane	$(1-s^2) (1+rr_0) (1+tt_0)$
for midside nodes along $t=0$ plane	$(1-t^2) (1+ss_0) (1+rr_0)$

### 7.6.1.2 Strain-displacement Matrix

Strain-displacement for 3-dimensional deformation can be written as follows:

$$[B_i]_{6 \times 3} = \begin{bmatrix} h_{i,x} & 0 & 0 \\ 0 & h_{i,y} & 0 \\ 0 & 0 & h_{i,z} \\ h_{i,y} & h_{i,x} & 0 \\ 0 & h_{i,z} & h_{i,y} \\ h_{i,z} & 0 & h_{i,x} \end{bmatrix} \dots\dots\dots 7.2$$

The strain-displacement matrix  $[B_i]$  used in the conventional formulations of finite elements consists of derivatives of the shape function where the comma after the subscript indicates differentiation with respect to the variable that follows.

$$h_{i,x} = \frac{\partial h_i}{\partial x}, \quad h_{i,y} = \frac{\partial h_i}{\partial y}, \quad h_{i,z} = \frac{\partial h_i}{\partial z}$$

$$[B]_{6 \times 60} = \sum_{i=1}^{20} [B_i]_{6 \times 3}$$

$$[B]_{6 \times 60} = \{ [B_1]_{6 \times 3} [B_2]_{6 \times 3} \dots\dots\dots [B_{20}]_{6 \times 3} \}$$

Where

$[B]_{6 \times 60}$  = element strain displacement matrix

The derivatives in the  $[B_i]$  can be evaluated by applying the chain rule of the differentiation as follows:

$$\begin{bmatrix} \frac{\partial h_i}{\partial r} \\ \frac{\partial h_i}{\partial x} \\ \frac{\partial h_i}{\partial s} \\ \frac{\partial h_i}{\partial t} \end{bmatrix} = \begin{bmatrix} \frac{\partial h_i}{\partial x} \frac{\partial x}{\partial r} + \frac{\partial h_i}{\partial y} \frac{\partial y}{\partial r} + \frac{\partial h_i}{\partial z} \frac{\partial z}{\partial r} \\ \frac{\partial h_i}{\partial x} \frac{\partial x}{\partial x} + \frac{\partial h_i}{\partial y} \frac{\partial y}{\partial x} + \frac{\partial h_i}{\partial z} \frac{\partial z}{\partial x} \\ \frac{\partial h_i}{\partial x} \frac{\partial x}{\partial s} + \frac{\partial h_i}{\partial y} \frac{\partial y}{\partial s} + \frac{\partial h_i}{\partial z} \frac{\partial z}{\partial s} \\ \frac{\partial h_i}{\partial x} \frac{\partial x}{\partial t} + \frac{\partial h_i}{\partial y} \frac{\partial y}{\partial t} + \frac{\partial h_i}{\partial z} \frac{\partial z}{\partial t} \end{bmatrix} = \begin{bmatrix} \frac{\partial x}{\partial r} & \frac{\partial y}{\partial r} & \frac{\partial z}{\partial r} \\ \frac{\partial x}{\partial x} & \frac{\partial y}{\partial x} & \frac{\partial z}{\partial x} \\ \frac{\partial x}{\partial s} & \frac{\partial y}{\partial s} & \frac{\partial z}{\partial s} \\ \frac{\partial x}{\partial t} & \frac{\partial y}{\partial t} & \frac{\partial z}{\partial t} \end{bmatrix} \begin{bmatrix} \frac{\partial h_i}{\partial x} \\ \frac{\partial h_i}{\partial y} \\ \frac{\partial h_i}{\partial z} \end{bmatrix} = J \begin{bmatrix} \frac{\partial h_i}{\partial x} \\ \frac{\partial h_i}{\partial y} \\ \frac{\partial h_i}{\partial z} \end{bmatrix} \dots\dots\dots 7.3$$

The partial derivatives of  $x, y, z$  in respect to  $r, s, \text{ and } t$  are found by differentiation of displacements expressed through shape functions and nodal displacement values:

$J =$

$$\begin{bmatrix} \frac{\partial x}{\partial r} & \frac{\partial y}{\partial r} & \frac{\partial z}{\partial r} \\ \frac{\partial x}{\partial x} & \frac{\partial y}{\partial x} & \frac{\partial z}{\partial x} \\ \frac{\partial x}{\partial s} & \frac{\partial y}{\partial s} & \frac{\partial z}{\partial s} \\ \frac{\partial x}{\partial t} & \frac{\partial y}{\partial t} & \frac{\partial z}{\partial t} \end{bmatrix} = \begin{bmatrix} \sum_{i=1}^{20} \frac{\partial h_i}{\partial r} x_i & \sum_{i=1}^{20} \frac{\partial h_i}{\partial r} y_i & \sum_{i=1}^{20} \frac{\partial h_i}{\partial r} z_i \\ \sum_{i=1}^{20} \frac{\partial h_i}{\partial s} x_i & \sum_{i=1}^{20} \frac{\partial h_i}{\partial s} y_i & \sum_{i=1}^{20} \frac{\partial h_i}{\partial s} z_i \\ \sum_{i=1}^{20} \frac{\partial h_i}{\partial t} x_i & \sum_{i=1}^{20} \frac{\partial h_i}{\partial t} y_i & \sum_{i=1}^{20} \frac{\partial h_i}{\partial t} z_i \end{bmatrix} \dots\dots\dots 7.4$$

Where  $J$  is Jacobian matrix to transfer variable from  $x$ - $y$ - $z$  global system to  $r$ - $s$ - $t$  element system

Cartesian derivatives can be expressed as follows:

$$\begin{bmatrix} \frac{\partial h_i}{\partial x} \\ \frac{\partial h_i}{\partial y} \\ \frac{\partial h_i}{\partial z} \end{bmatrix} = [J]^{-1} \begin{bmatrix} \frac{\partial h_i}{\partial r} \\ \frac{\partial h_i}{\partial s} \\ \frac{\partial h_i}{\partial t} \end{bmatrix} \dots\dots\dots 7.5$$

The derivatives of the interpolation functions in generalized form can be expressed in Table 7.3

Table 7.3 Derivatives of the interpolation functions for 20-noded isoparametric element

Nodes discreption.	$\frac{\partial h_i}{\partial r}$	$\frac{\partial h_i}{\partial s}$	$\frac{\partial h_i}{\partial t}$
for corner nodes	$r_0 (1+ss_0) (1+tt_0)$	$s_0 (1+rr_0) (1+tt_0)$	$t_0 (1+ss_0) (1+rr_0)$
for midside nodes along $r =0$ plane	$-2r^2 (1+ss_0) (1+tt_0)$	$s_0 (1-r^2) (1+tt_0)$	$t_0 (1-s^2) (1+rr_0)$
for midside nodes along $s=0$ plane	$r_0 (1-s^2) (1+tt_0)$	$-2s^2 (1+rr_0) (1+tt_0)$	$t_0 (1-r^2) (1+ss_0)$
for midside nodes along $t=0$ plane	$r_0 (1-t^2) (1+ss_0)$	$s_0 (1-t^2) (1+rr_0)$	$-2t^2 (1+ss_0) (1+rr_0)$

**7.6.1.3 Element Stiffness Matrix**

Element stiffness matrix in local coordinates can be written as follows:

$$[k^{(e)}] = \int_{V^{(e)}} [B]^T [D][B] dV$$

$$[k^{(e)}] = \int_{-1}^1 \int_{-1}^1 \int_{-1}^1 [B]^T [D][B] \det[J] dr ds dt \dots\dots\dots 7.6$$

Where

- $[k^{(e)}]$ = element stiffness matrix
- $[D]$ =material stiffness matrix
- $dV=dx dy dz = \det[J] . dr ds dt$

**7.6.1.4 Numerical Computation**

Since the matrix  $[B]$  is an implicit function of  $r, s$  and  $t$ , a numerical method has to be used to evaluate the multiple integral of Eq.7.6 .The Gaussian quadrature has been proved to be the most efficient method of numerical integration for this class of the

problems. By using 2x2x2 rule (or two-point Gaussian quadrature), which yields sufficiently accurate results, eq.7.6 can be evaluated numerically as follows:

$$[k^{(e)}] = \sum_{i=1}^{n-gauss} \sum_{j=1}^{n-gauss} \sum_{k=1}^{n-gauss} [B]^T [D] [B] \cdot \det[J] w_i w_j w_k \dots\dots\dots 7.7$$

Where

$w_i, w_j, w_k$  = weight functions

For the two-point rule  $r_1=s_1=t_1=-0.57735, r_2=s_2=t_2=+0.57735$  and  $w_i = w_j = w_k = 1$

**7.6.1.5 Computation of Strains and Stresses**

After solving the equilibrium equation and finding the primary unknowns  $u$ , element deformation in 3-D form can be written as follows:

$$\begin{aligned} \epsilon_x &= \frac{dU_x}{dx} = \sum h_{i,x} u_{xi} \\ \epsilon_y &= \frac{dU_y}{dy} = \sum h_{i,y} u_{yi} \\ \epsilon_z &= \frac{dU_z}{dz} = \sum h_{i,z} u_{zi} \\ \gamma_{xy} &= \frac{dU_x}{dy} + \frac{dU_y}{dx} = \sum h_{i,y} u_{xi} + \sum h_{i,x} u_{yi} \dots\dots\dots 7.8 \\ \gamma_{yz} &= \frac{dU_y}{dz} + \frac{dU_z}{dy} = \sum h_{i,z} u_{yi} + \sum h_{i,y} u_{zi} \\ \gamma_{zx} &= \frac{dU_x}{dz} + \frac{dU_z}{dx} = \sum h_{i,z} u_{xi} + \sum h_{i,x} u_{zi} \end{aligned}$$

Strain vector can be expressed as:

$$[\epsilon]_{6 \times 1} = \sum_{i=1}^{20} [B_i]_{6 \times 60} [u_i]_{60 \times 1}$$

$$\begin{bmatrix} \epsilon_x \\ \epsilon_y \\ \epsilon_z \\ \gamma_{xy} \\ \gamma_{yz} \\ \gamma_{zx} \end{bmatrix} = \sum_{i=1}^{20} \begin{bmatrix} h_{i,x} & 0 & 0 \\ 0 & h_{i,y} & 0 \\ 0 & 0 & h_{i,z} \\ h_{i,y} & h_{i,x} & 0 \\ 0 & h_{i,z} & h_{i,y} \\ h_{i,z} & 0 & h_{i,x} \end{bmatrix} \begin{bmatrix} u_{xi} \\ u_{yi} \\ u_{zi} \end{bmatrix} \dots\dots\dots 7.9$$

Stress vector can be related to the strain vector using the following constitutive rule:

$$[\sigma]_{6 \times 1} = [D]_{6 \times 6} [\varepsilon]_{6 \times 1}$$

$$\begin{bmatrix} \sigma_x \\ \sigma_y \\ \sigma_z \\ \tau_{xy} \\ \tau_{yz} \\ \tau_{zx} \end{bmatrix} = [D]_{6 \times 6} \begin{bmatrix} \varepsilon_x \\ \varepsilon_y \\ \varepsilon_z \\ \gamma_{xy} \\ \gamma_{yz} \\ \gamma_{zx} \end{bmatrix} \dots\dots\dots 7.10$$

Where

$[D]_{6 \times 6}$  = Material matrix

### 7.6.2 Representation of Reinforcement

In developing a finite element method, three different approaches are usually used for modelling of reinforcing steel in concrete:

- Distributed
- Discrete
- Embedded

**Distributed representation:** In this approach, the steel is assumed to be distributed over the concrete elements, with particular orientation angle  $\theta$  as shown in Fig.7.3. Perfect bond between steel and concrete is assumed so that a composite concrete-reinforcement constitutive relation can be derived. Distributed representation, is very unrealistic because reinforcing bar does not behaved as uniaxial member embedded inside the concrete and bonded to it.

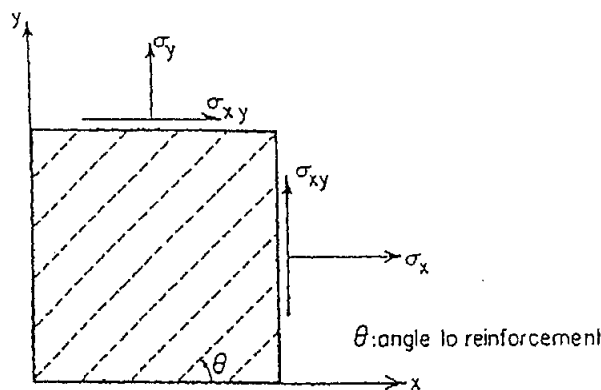
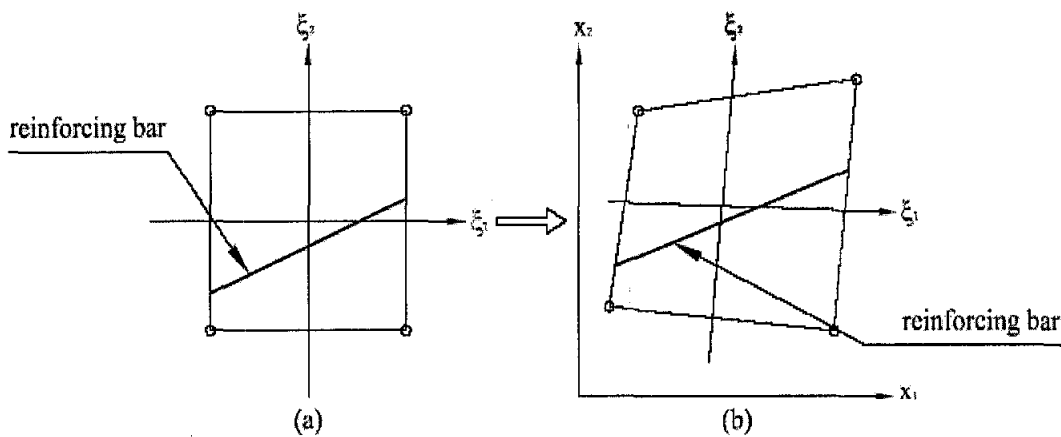


Fig. 7.3 DISTRIBUTED REPRESENTATION OF REINFORCEMENT

**Embedded Representation:** In this type of representation the reinforcing steel is considered as an axial member built into the isoparametric element such that its displacements are consistent with those of the basic element. Such a model again implies perfect bond between concrete and steel. The stiffness matrix and the internal force vector of embedded reinforcement elements only contain the contribution of reinforcement bars. They are computed by integration along the curves representing the segments of the reinforcing bars within the respective element. The embedded reinforcement elements are then superimposed on the respective concrete elements. The reinforcement bars do not follow the boundaries of the concrete elements. Hence, the embedded representation of the reinforcement allows generating a finite element mesh without giving much consideration to the reinforcement layout.

An embedded steel model is useful in connection with higher order isoparametric concrete elements. The main advantage of this technique is that the placement of steel bar is made in its exact position irrespective of the choice of the mesh. Fig. 7.4 shows element layout for embedded steel model in local and global system



Embedded steel element: (a) in the local coordinate system, (b) in the global Cartesian coordinate system.

Fig. 7.4 EMBEDDED REPRESENTATION OF REINFORCEMENT

**Discrete Representation:** The discrete modelling of steel reinforcement is the first approach that was used in finite element analysis of reinforced concrete structures. It was originally suggested by Ngo and Scordelis (1967) in their earliest published applications. In discrete modelling; reinforcement bars are generally modelled as separate element. Commonly, truss or beam element for 2-D analysis and space truss and space frame element for 3-D analysis. The location of steel element is determined

by the lay out of reinforcement. Consequently the boundaries of concrete element have to follow the reinforcement bar. In addition to its simplicity the discrete model has significant advantages of accounting for possible displacement of reinforcement with respect to surrounding concrete which make this type of representation the only way of accounting for bond-slip and dowel action mechanisms (Cervenka et al. 1990). The main disadvantage is that the finite element mesh is restricted by the location of reinforcement so it requires a very fine mesh to enable each bar to lie on boundary of concrete element (see Fig. 7.5); consequently it increases the number of concrete elements and degrees of freedom.

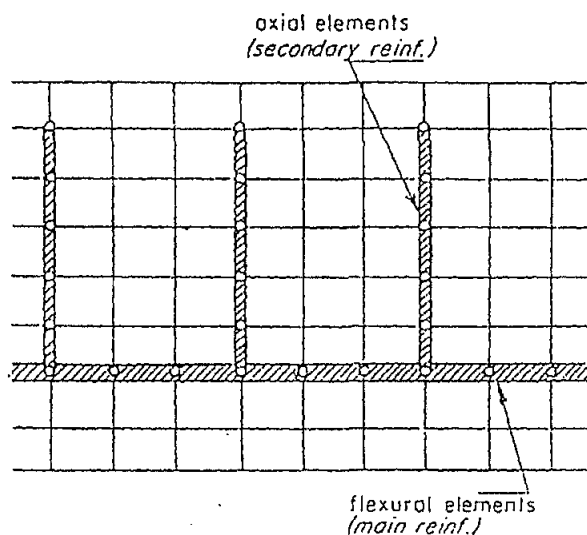


Fig. 7.5 DISCRETE REPRESENTATION OF REINFORCEMENT

In this research discretized approach was selected for representation of reinforcement for its ability to simulate bond and dowel action mechanisms by means of special elements that connected the adjacent nodes of concrete and steel elements. The system is consisted of 2-noded space frame and space truss elements. The space frame elements are used to simulate the behaviour of main reinforcement while secondary reinforcement is simulated with space truss elements.

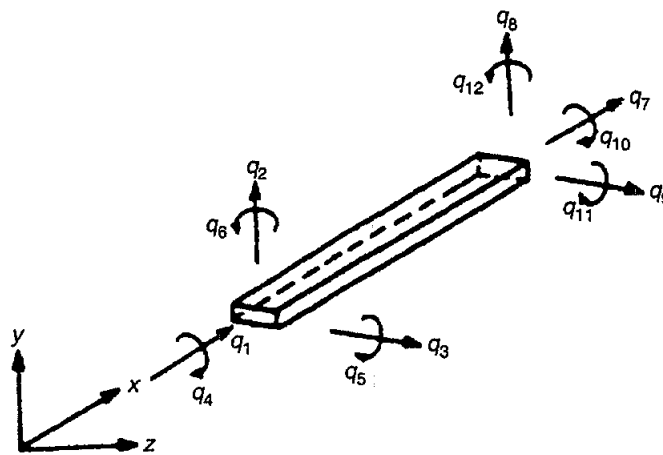
#### 7.6.2.1 Space Frame Element

In this research to represent the main reinforcement bar, 2-noded space frame elements were used. These elements are capable of resisting axial force, bending moment about the two principle axes in the plane of its  $x$ -section and twisting moment about its

centroidal axis. The member has a total of twelve degrees of freedoms as shown in Fig. 7.6, where each node has six degrees of freedom [three translations + three rotations].

Element displacement can be separated for four independent groups as follows:

1. Axial displacements ( $q_1, q_7$ )
2. Torsional displacements ( $q_4, q_{10}$ )
3. Bending displacements in the plane  $xy$  ( $q_3, q_5, q_9, q_{11}$ )
4. Bending displacements in the plane  $xz$  ( $q_2, q_6, q_8, q_{12}$ )

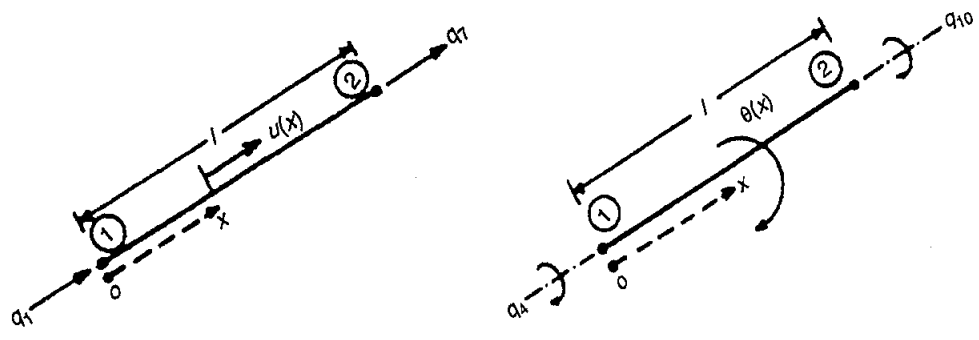


(a) Element with 12 degrees of freedom

Fig. 7.6 SPACE FRAME ELEMENT

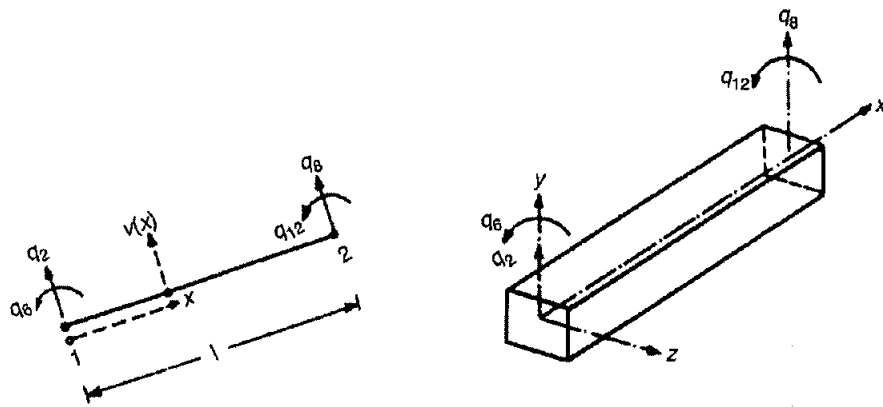
The local  $xyz$  coordinates system coincided with the principal axes of  $x$ -plane where  $x$ -axis representing the centroidal axis of frame element. Thus the displacement can be separated into four groups, each of which can be considered independently of other. First the stiffness matrix corresponding to different independent set of displacement is considered, and then the total stiffness matrix of the element is obtained by super position.

Fig.7.7 shows the degrees of freedom corresponding to each set of displacement mentioned above



(b) Axial degrees of freedom

(c) Torsional degrees of freedom



(d) Bending degrees of freedom in  $xy$  plane

(e) Bending degrees of freedom in  $xz$  plane

Fig. 7.7 DEGREES OF FREEDOM CORRESPOND TO EACH TYPE OF DEFORMATION

**7.6.2.1.1 Stiffness Matrix Correspond to Axial Displacement**

Stiffness matrix for space frame element correspond to axial displacement  $q_1, q_7$  can be obtained as follows:

$$[K_a^{(e)}] = \iiint_{v(e)} [B]^T [D] [B] dv = \frac{1}{A} \int_{x=0}^l \begin{bmatrix} -1 \\ l \\ 1 \\ l \end{bmatrix} E \begin{bmatrix} -1 & 1 \\ l & l \end{bmatrix} dx = \frac{AE}{L} \begin{bmatrix} 1 & -1 \\ -1 & 1 \end{bmatrix} \dots\dots\dots 7.11$$

Where

$E$  = modulus of elasticity

$A$  = x-sectional area

**7.6.2.1.2 Stiffness Matrix Correspond to Torsional Displacements**

Stiffness matrix for space frame element correspond to torsional displacement  $q_4, q_{10}$  can be obtained as follows:

$$[K_t^{(e)}] = \iiint_{v(e)} [B]^T [D] [B] dv = \frac{GJ}{L} \begin{bmatrix} 1 & -1 \\ -1 & 1 \end{bmatrix} \dots\dots\dots 7.12$$

Where

$G$  = shear modulus

$J$  = polar moment of inertia of the cross section which can be obtained as  $\iint_A r^2 dA$

**7.6.2.1.3 Stiffness Matrix Correspond to Bending Displacement in Plane xy**

Stiffness matrix for space frame element correspond to bending displacement  $q_3, q_5, q_9, q_{11}$  can be derived as:

$$[K_{xz}^{(e)}] = \frac{EI_{yy}}{l^3} \begin{bmatrix} 12 & 6l & -12 & 6l \\ 6l & 4l^2 & -6l & 2l^2 \\ -12 & -6l & 12 & -6l \\ 6l & 2l^2 & -6l & 4l^2 \end{bmatrix} \dots\dots\dots 7.13$$

Where  $I_{yy} = \iint_A Z^2 dA$



Where

$[K_{GL}]^e$  = Global stiffness matrix of space frame element

$[K_{Loc}]^e$  = Element stiffness matrix in local system

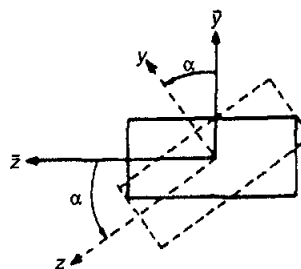
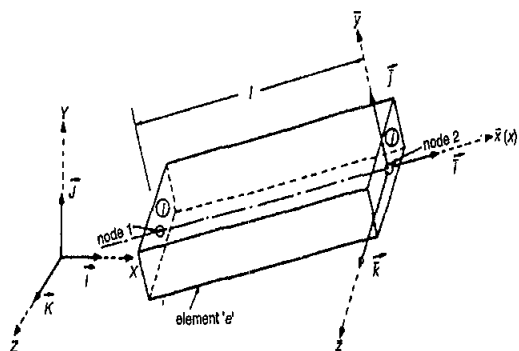
$[\lambda]$  = Transformation matrix can be identified as follows:

$$[\lambda]_{12 \times 12} = \begin{bmatrix} [\lambda] & 0 & 0 & 0 \\ 0 & [\lambda] & 0 & 0 \\ 0 & 0 & [\lambda] & 0 \\ 0 & 0 & 0 & [\lambda] \end{bmatrix} \dots\dots\dots 7.17$$

Where

$$[\lambda]_{3 \times 3} = [\lambda_1] [\lambda_2]$$

Fig. 7.8 show the local and global coordinates system for space frame element



(a) 2-axis parallel to XZ plane (principle x- sectional not

(b) General case (y and z do

axis y and z are assumed to coincide with  $\bar{y}$  and  $\bar{z}$

coincide) with  $\bar{y}$  and  $\bar{z}$ )

Fig. 7.8 LOCAL AND GLOBAL COORDINATES SYSTEM

$$[\lambda_1]_{3 \times 3} = \begin{bmatrix} l_{ox} & m_{ox} & n_{ox} \\ l_{oy} & m_{oy} & n_{oy} \\ l_{oz} & m_{oz} & n_{oz} \end{bmatrix}$$

The element of this matrix can be described as follows:

$$l_{ox} = \frac{X_j - X_i}{l}, \quad m_{ox} = \frac{Y_j - Y_i}{l}, \quad n_{ox} = \frac{Z_j - Z_i}{l}$$

$$l_{oy} = \frac{-l_{ox} m_{ox}}{d}, \quad m_{oy} = \frac{n_{ox}^2 + l_{ox}^2}{d}, \quad n_{oy} = \frac{-m_{ox} n_{ox}}{d} \dots\dots\dots 7.18$$

$$l_{oz} = \frac{-n_{ox}}{d}, \quad m_{oz} = 0, \quad n_{oz} = \frac{l_{ox}}{d}$$

Where  $l = \{[X_j - X_i]^2 + [Y_j - Y_i]^2 + [Z_j - Z_i]^2\}^{1/2}$ ,  $d = \{n_{ox}^2 + l_{ox}^2\}^{1/2}$

When the principal  $x$ -sectional axes of the frame element are arbitrary making angle  $\alpha$  with global axes the transformation matrix between the two systems can be expressed as:

$$[\lambda_2]_{3 \times 3} = \begin{bmatrix} 1 & 0 & 0 \\ 0 & c & s \\ 0 & -s & c \end{bmatrix} \dots\dots\dots 7.19$$

Where

$$c = \cos\theta, s = \sin\theta$$

Notes:

- (i) When  $\alpha=0$ , the matrix  $[\lambda_2]$  degenerates to unit matrix.
- (ii) When the element  $e$  lies vertical ( $\alpha=90$ ),  $l_{ox}=n_{ox}=0$  and hence  $d$  becomes zero this makes some of the terms in  $[\lambda_2]$ -matrix indeterminate. Thus the above procedure breaks down. In this case we can redefine the angle  $\alpha$  as angle in the horizontal ( $XZ$ ) plane between the axes  $Z$  and  $z$ , positive when turning from  $Z$  to the  $X$  as shown in Fig. 7.9. In this case the  $[\lambda]$  matrix can be derived by going through the same procedure as before, as

$$[\lambda]_{3 \times 3} = \begin{bmatrix} 0 & m_{ox} & 0 \\ -m_{ox}c & 0 & m_{oy}s \\ s & 0 & c \end{bmatrix} \dots\dots\dots 7.20$$

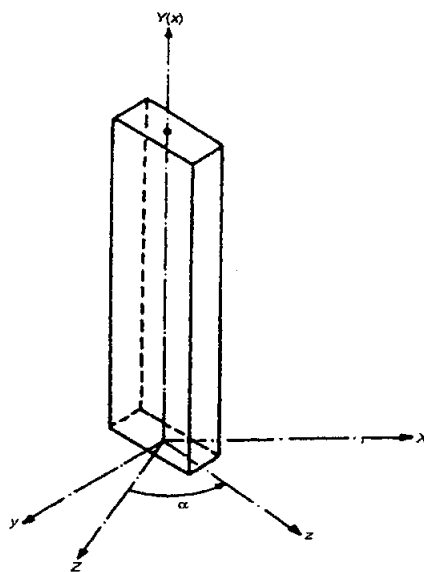


Fig. 7.9 Transformation for Vertical Element

Finally the transformation matrix  $[\lambda]_{12 \times 12}$ , relating the degrees of freedom in local and the global system is given by Eq.7.17

### 7.6.2.1.6 Computation of Strains and Stresses

After finding displacement solution of the global system  $[Q]$ , the local displacements  $[q]$  can be solved as:

$$[q]_{12 \times 1} = [\lambda]_{12 \times 12} [Q]_{12 \times 1} \dots \dots \dots 7.21$$

The axial strain  $\epsilon_{axial}$  is expressed as

$$[\epsilon_{axial}]_{1 \times 1} = [B]_{1 \times 2} [q]_{2 \times 1}$$

$$[\epsilon_{axial}] = \begin{bmatrix} -1 & 1 \\ l & l \end{bmatrix} \begin{bmatrix} q_1 \\ q_7 \end{bmatrix} = \frac{1}{l} [q_7 - q_1] \dots \dots \dots 7.22$$

The stress-strain relationship for axial deformation is given by

$$[\sigma_{axial}]_{1 \times 1} = [D]_{1 \times 1} [\epsilon_{axial}]_{1 \times 1}$$

$$[D] = [E]$$

$$[\sigma_{axial}]_{1 \times 1} = [E]_{1 \times 1} [B]_{1 \times 2} [q]_{2 \times 1}$$

Finally the axial stress induced in space frame element can be determined using the following expression:

$$[\sigma_{axial}] = [E] \frac{1}{l} [q_7 - q_1] \dots \dots \dots 7.23$$

The shear strain  $\epsilon_t$  is expressed as

$$[\epsilon_t]_{1 \times 1} = [B]_{1 \times 2} [q_t]_{2 \times 1}$$

$$[\epsilon_t] = \begin{bmatrix} -r & r \\ l & l \end{bmatrix} \begin{bmatrix} q_4 \\ q_{10} \end{bmatrix} = \frac{r}{l} [q_{10} - q_4] \dots \dots \dots 7.24$$

The stress-strain relationship for torsional deformation is given by

$$[\sigma_t]_{1 \times 1} = [D]_{1 \times 1} [\epsilon_t]_{1 \times 1}$$

$$[D] = [G]$$

$$[\sigma_t]_{1 \times 1} = [G]_{1 \times 1} [B]_{1 \times 2} [q_t]_{2 \times 1}$$

Finally the torsional stress induced in space frame element can be determined using the following expression:

$$[\sigma_i] = [G] \frac{r}{l} [q_{10} - q_4] \dots \dots \dots 7.25$$

**7.6.2.2 Space Truss Element**

The element is used to represent the secondary reinforcement is 2-noded space truss element which is capable of resisting axial force only. The member has six degrees of freedom, three degrees of freedom at each node [translations in x, y and z]

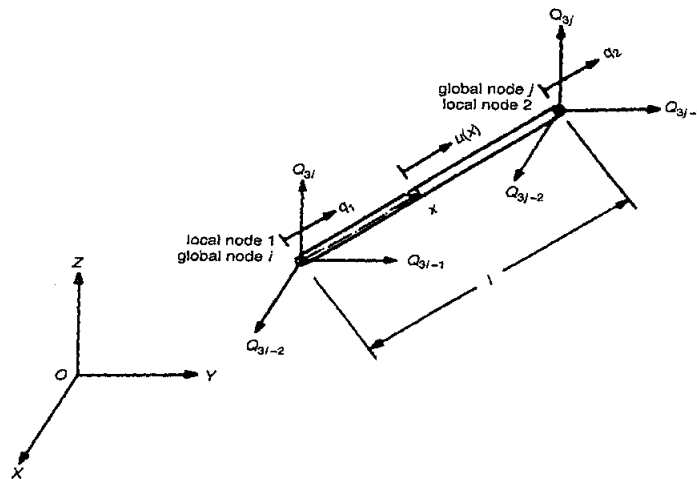


Fig. 7.10 SPACE TRUSS ELEMENT

**7.6.2.2.1 Element Stiffness Matrix**

Stiffness matrix for space truss element can be obtained using the following expression:

$$[K_{GL}]^e = [\lambda]^T [K_{Loc}]^e [\lambda]$$

Where

$[K_{GL}]^e$  = global stiffness matrix

$[K_{Loc}]^e$  = stiffness matrix in local system given by the following expression:

$$[K_{Loc}]^e = \iiint_{v(e)} [B]^T [D] [B] dv = A \int_{x=0}^l \begin{bmatrix} -1/l \\ 1/l \end{bmatrix} E \begin{bmatrix} -1 & 1 \\ l & l \end{bmatrix} dx = \frac{AE}{L} \begin{bmatrix} 1 & -1 \\ -1 & 1 \end{bmatrix} \dots \dots \dots 7.26$$

Where

$[D] = E$  = young modulus

$A$  = x-sectional area

$[B]$ = shape function can be evaluated as  $\begin{bmatrix} -1 & 1 \\ l & l \end{bmatrix}$

$l$  is length of element  $ij$  given by:  $l = \{[X_j - X_i]^2 + [Y_j - Y_i]^2 + [Z_j - Z_i]^2\}^{1/2}$

$[\lambda]$  =Transformation matrix can be defined as:

$$[\lambda] = \begin{bmatrix} l_{ij} & m_{ij} & n_{ij} & 0 & 0 & 0 \\ 0 & 0 & 0 & l_{ij} & m_{ij} & n_{ij} \end{bmatrix}$$

Where

$$l_{ij} = \frac{X_j - X_i}{l}, m_{ij} = \frac{Y_j - Y_i}{l}, n_{ij} = \frac{Z_j - Z_i}{l},$$

$(X_i, Y_i, Z_i)$  and  $(X_j, Y_j, Z_j)$  are the global coordinates of node  $i$  and  $j$  respectively

Finally element stiffness in global system can be expressed as follows:

$$[K_{GL}]^e = \frac{EA}{L} \begin{bmatrix} l_{ij}^2 & l_{ij}m_{ij} & l_{ij}n_{ij} & -l_{ij}^2 & -l_{ij}m_{ij} & -l_{ij}n_{ij} \\ l_{ij}m_{ij} & m_{ij}^2 & m_{ij}n_{ij} & -l_{ij}m_{ij} & m_{ij}^2 & -m_{ij}n_{ij} \\ l_{ij}n_{ij} & m_{ij}n_{ij} & n_{ij}^2 & -l_{ij}n_{ij} & -m_{ij}n_{ij} & -n_{ij}^2 \\ -l_{ij}^2 & -l_{ij}m_{ij} & -l_{ij}n_{ij} & l_{ij}^2 & l_{ij}m_{ij} & l_{ij}n_{ij} \\ -l_{ij}m_{ij} & -m_{ij}^2 & -m_{ij}n_{ij} & l_{ij}m_{ij} & m_{ij}^2 & m_{ij}n_{ij} \\ -l_{ij}n_{ij} & -m_{ij}n_{ij} & -n_{ij}^2 & l_{ij}n_{ij} & m_{ij}n_{ij} & n_{ij}^2 \end{bmatrix} \dots\dots\dots 7.27$$

**7.6.2.2.2 Computation of Strains and Stresses**

After finding displacement solution of the global system  $[Q]$ , the local displacements  $[q]$  can be identified as follows

$$[q]_{2 \times 1} = [\lambda]_{2 \times 6} [Q]_{6 \times 1} \dots\dots\dots 7.28$$

The axial strain can be evaluated as:

$$[\epsilon_{axial}]_{1 \times 1} = [B]_{1 \times 2} [q]_{2 \times 1}$$

$$[\epsilon_{axial}] = \begin{bmatrix} -1 & 1 \\ l & l \end{bmatrix} \begin{bmatrix} q_1 \\ q_2 \end{bmatrix} = \frac{1}{l} [q_2 - q_1] \dots\dots\dots 7.29$$

The stress-strain relationship is given by

$$[\sigma_{axial}]_{1 \times 1} = [D]_{1 \times 1} [\epsilon_{axial}]_{1 \times 1}$$

$$[D] = [E]$$

$$[\sigma_{axial}]_{1 \times 1} = [E]_{1 \times 1} [B]_{1 \times 2} [q]_{2 \times 1}$$

Finally the axial stress induced in space truss element can be determined using the following expression:

$$[\sigma_{axial}] = [E] \frac{1}{l} [q_2 - q_1] \dots\dots\dots 7.30$$

### 7.6.3 Representation of Shear Resisting Mechanism

In this research three-dimensional linkage elements were used to simulate the following mechanisms

- Concrete-to-concrete interface (aggregate interlock mechanism)
- Steel-to-concrete interface (dowel action and bond-slip mechanisms)

Three-dimensional having 3 orthogonal fictitious springs applied at each node to connect the steel bar elements and adjacent concrete elements or the two neighbouring concrete elements. The element has no physical dimensions. It connects two nodes with identical coordinates and can be conceptually thought of as consisting of three linear springs as shown in Fig.7.11. One is parallel to the steel bar axis and the other two are normal to bar axis. Both nodes occupy the same coordinate in space before loading, but they undergo to a relative displacement by the deformation of the linkage springs, resulting in different coordinates after loading. The component of linkage force in the direction of the bar axis gives the bond force, and the normal component of linkage force gives the radial splitting force.

The following section describes the formulation of stiffness matrix for 3-d link element and how the stresses correspond to each spring can be evaluated.

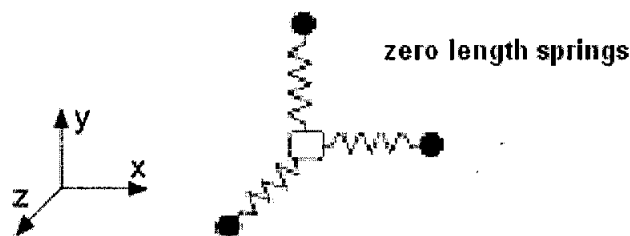


Fig. 7.11 3-D LINKAGE ELEMENT

### 7.6.3.1 Relative Displacement Field

The relative displacement vector  $[\Delta]^e$  for the joint element, at nodes  $i, j$  with respect to the global coordinates  $(X, Y, Z)$  may be expressed as

$$\Delta u_x = (a_x^e - o_x), \Delta u_y = (e_y^e - b_u^y), \Delta u_z = (U_z^i - u_s)$$

In term of matrix, relative displacement can be written as

$$[\Delta] = [N] [u]$$

Where

$[\Delta]$  = Relative displacement matrix

$[N]$  = Intermediate transfer matrix

$[u]$  = Nodal displacement matrix

$$\begin{bmatrix} \Delta u_x \\ \Delta u_y \\ \Delta u_z \end{bmatrix} = \begin{bmatrix} +1 & 0 & 0 & -1 & 0 & 0 \\ 0 & +1 & 0 & 0 & -1 & 0 \\ 0 & 0 & +1 & 0 & 0 & -1 \end{bmatrix} \begin{bmatrix} u_x^i \\ u_y^i \\ u_z^i \\ u_x^j \\ u_y^j \\ u_z^j \end{bmatrix} \dots\dots\dots 7.31$$

$$\Delta = \begin{bmatrix} \Delta u_x \\ \Delta u_y \\ \Delta u_z \end{bmatrix} = \begin{bmatrix} u_x \\ u_y \\ u_z \end{bmatrix}_i - \begin{bmatrix} u_x \\ u_y \\ u_z \end{bmatrix}_j$$

Where  $imp$  are two nodes with identical coordinates that represents concrete and steel nodes for dowel action and bond-slip mechanisms and two concrete nodes for aggregate interlock mechanism.

### 7.6.3.2 Element Stiffness Matrix

Stiffness matrix for link element in local system can be obtained as:

$$[K_{Loc}]_{6 \times 6} = [N]^T_{6 \times 3} [K]_{3 \times 3} [N]_{3 \times 6}$$

Where

$$[K]_{3 \times 3} = \begin{bmatrix} K_\xi & 0 & 0 \\ 0 & K_\eta & 0 \\ 0 & 0 & K_n \end{bmatrix}$$

$$[K_{loc}] = \begin{bmatrix} k_{\zeta} & 0 & 0 & -k_{\zeta} & 0 & 0 \\ 0 & k_{\eta} & 0 & 0 & -k_{\eta} & 0 \\ 0 & 0 & k_n & 0 & 0 & -k_n \\ -k_{\zeta} & 0 & 0 & k_{\zeta} & 0 & 0 \\ 0 & -k_{\eta} & 0 & 0 & k_{\eta} & 0 \\ 0 & 0 & -k_n & 0 & 0 & k_n \end{bmatrix} \dots\dots\dots 7.32$$

Where

$K_{\zeta}, K_{\eta}$  = tangential shear stiffness of interface.

$K_{en}$  = stiffness of interface in normal direction.

The local stiffness matrix of the bond link element should be transformed to global coordinates by a rotation matrix. This can be expressed formally as

$$[K_{GL}]_{6 \times 6} = [T]_{6 \times 6}^T [K_{Loc}]_{6 \times 6} [T]_{6 \times 6}$$

$$[K_{GL}]_{6 \times 6} = \begin{bmatrix} c^2 k_{ix} + s^2 k_{iy} & -s c (k_{ix} - k_{iy}) & 0 & -(c^2 k_{ix} + s^2 k_{iy}) & s c (k_{ix} - k_{iy}) & 0 \\ -s c (k_{ix} - k_{iy}) & s^2 k_{ix} + c^2 k_{iy} & 0 & s c (k_{ix} - k_{iy}) & -(s^2 k_{ix} + c^2 k_{iy}) & 0 \\ 0 & 0 & k_{nz} & 0 & 0 & -k_{nz} \\ -(c^2 k_{ix} + s^2 k_{iy}) & s c (k_{ix} - k_{iy}) & 0 & c^2 k_{ix} + s^2 k_{iy} & -s c (k_{ix} - k_{iy}) & 0 \\ s c (k_{ix} - k_{iy}) & -(s^2 k_{ix} + c^2 k_{iy}) & 0 & -s c (k_{ix} - k_{iy}) & s^2 k_{ix} + c^2 k_{iy} & 0 \\ 0 & 0 & -k_{nz} & 0 & 0 & k_{nz} \end{bmatrix} \dots\dots\dots 7.33$$

Where

$K_{ix} = k_{\zeta}, K_{iy} = k_{\eta}, K_{Hz} = k_{en}$

$[T]_{6 \times 6}$  = Transformation matrix can be expressed as follows:

$$[T] = \begin{bmatrix} c & s & 0 & 0 & 0 & 0 \\ -s & c & 0 & 0 & 0 & 0 \\ 0 & 0 & 1 & 0 & 0 & 0 \\ 0 & 0 & 0 & c & s & 0 \\ 0 & 0 & 0 & -s & c & 0 \\ 0 & 0 & 0 & 0 & 0 & 1 \end{bmatrix} \dots\dots\dots 7.34$$

Where

$c = \cos \theta, s = \sin \theta$

The link element stiffness matrix is general and to be applied to any of the phenomenon of shear transfer by assigning appropriate stiffness value.

### 7.6.3.3 Computation of Stresses

After solving the equilibrium equation and determining the main unknowns (displacement in global system), element displacement can be related to the global displacement as:

$$[\delta]_{3 \times 1} = [T]_{3 \times 3} [A]_{3 \times 1}$$

$$\begin{bmatrix} \delta_\zeta \\ \delta_\eta \\ \delta_n \end{bmatrix} = \begin{bmatrix} c & s & 0 \\ -s & c & 0 \\ 0 & 0 & 1 \end{bmatrix} \begin{bmatrix} \Delta u_x \\ \Delta u_y \\ \Delta u_z \end{bmatrix} \dots\dots\dots 7.35$$

Where

$[T]_{3 \times 3}$  = Transformation matrix

Stresses vector is obtained as:

$$[\sigma]_{3 \times 1} = [K_{Loc}]_{3 \times 3} [\delta]_{3 \times 1}$$

$$\begin{bmatrix} \tau_\zeta \\ \tau_\eta \\ \sigma_n \end{bmatrix} = \begin{bmatrix} K_\zeta & 0 & 0 \\ 0 & K_\eta & 0 \\ 0 & 0 & K_n \end{bmatrix} \begin{bmatrix} \delta_\zeta \\ \delta_\eta \\ \delta_n \end{bmatrix} \dots\dots\dots 7.36$$

Where

$\tau_\zeta, \tau_\eta$  = Tangential shear stresses in direction  $\zeta$  and  $\eta$

$\sigma_n$  = Bond stress in normal direction.

$E_\zeta, E_\eta$  = Shear stiffness in direction  $\zeta$  and  $\eta$ .

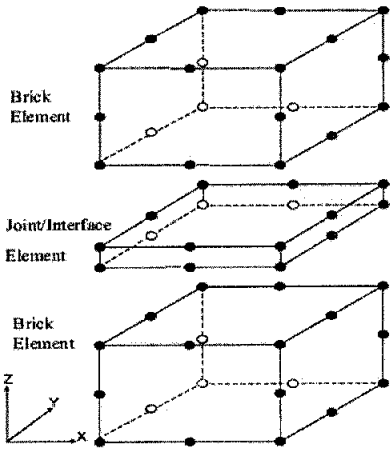
$E_n$  = Bond stiffness in normal direction

### 7.6.4 Representation of Interaction between CFRP Side Plates and Concrete Surface

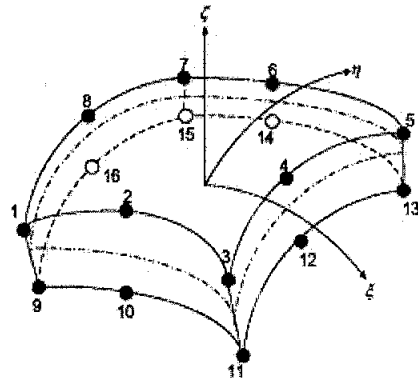
The interfacial behaviour of CFRP/concrete and the bond slip behaviour can be effectively modelled by using interface elements. This approach defines a surface of separation (a line in 2-D problems) between different materials and describe their interaction by defining a relative displacement at each contact point and the associated dual stress component. In reality, the interfacial interaction is not a phenomenon localized at the physical joint between the two materials but involves a small volume around it. The observable slip between the materials is due in reality to inelastic

deformation of a small portion of concrete (and of the adhesive for the CFRP case). Simulation of the interaction between the two materials explicitly model the local mechanism of force transfer would require a model capable of operating at the same time at the micro scale and at the mesoscale. This is not practical in a finite element analysis involving such a number of sources of non-linearity as the analysis of RC beams retrofitted with CFRP. Therefore it is convenient to represent the interfacial interaction in global terms through the introduction of an interfacial stress and a relative slip between the two materials which is a measure of the relative movement between two points in the two materials associated with the location at which the interfacial stress is evaluated. The definition of one of the points is very straightforward as it is the contact point on the CFRP or the steel, which do not generally undergo any damage. The definition of the other point is instead somewhat vague as it should be on the boundary of volume of concrete considered interface, which is not well defined. Models for the interaction between the materials based on the actual simulation of the stress, strain and damage accumulation in the vicinity of the interface, are used for the analyses of a small portion of the structure, isolated from the rest by introducing appropriate boundary conditions. In this way it is possible to operate only at the micro scale. The information derived by using this approach can be then used to characterize the global interface model to be used in the mesoscale and macro scale problems.

In this research 3-d interface element is used to simulate the interaction between CFRP side plates and concrete. The element has sixteen nodes, eight nodes connect to concrete element and the other eight nodes connected to CFRP sheet. The interface will be modelled by three linear springs connecting the joint nodes with the same coordinates. The basic purpose of the joint element is to permit relative slip at the interface of two materials blocks, made up of the same or different materials. The following section gives brief descriptions about the isoparametric formulations and constitutive equations govern the structural behaviour of such element.



(a) Element sandwiched between two parent brick elements



(b) Details of 16-node joint/interface

Fig. 7.12 16-NODE JOINT/INTERFACE ELEMENT

### 7.6.4.1 Coordinates System

The global and local coordinates systems are related as follows:

$$X = \sum N_k x_k$$

$$Y = \sum N_k y_k$$

$$Z = \sum N_k z_k$$

$$\begin{bmatrix} X \\ Y \\ Z \end{bmatrix} = \begin{bmatrix} N_1 & 0 & 0 & N_2 & 0 & 0 & \dots & N_k & 0 & 0 \\ 0 & N_1 & 0 & 0 & N_2 & 0 & \dots & 0 & N_k & 0 \\ 0 & 0 & N_1 & 0 & 0 & N_2 & \dots & 0 & 0 & N_k \end{bmatrix} \begin{bmatrix} x_1 \\ y_1 \\ z_1 \\ \dots \\ x_k \\ y_k \\ z_k \end{bmatrix} \dots 7.37$$

Where  $X, Y, Z =$  global coordinates,  $x_k, y_k$  and  $z_k$  ( $k=1,2,\dots, 8$ ) are coordinates of the double nodes and  $N_k$  are shape functions expressed in natural coordinates  $\zeta$  and  $\eta$ .

The shape functions could be written in a generalized form for corner nodes as described in Table 7.4

Table 7.3 GENERALIZED FORM FOR SHAPE FUNCTION INTERFACE ELEMENT

Nodes description.	Shape function. $N_k$
for corner nodes	$\frac{1}{4}(1 + \zeta\zeta_k)(1 + \eta\eta_k)(\zeta\zeta_k + \eta\eta_k - 1)$
for midside nodes along $\eta\zeta=0$ plane	$\frac{1}{2}(1 - \zeta^2)(1 + \eta\eta_k)$
for midside nodes along $\eta=0$ plane	$\frac{1}{2}(1 - \eta^2)(1 + \zeta\zeta_k)$

**7.6.4.2 Relative displacement field**

The relative displacement vector  $[\Delta]^e$  for the joint element, with respect to the global coordinates (X, Y, Z) may be expressed as

$$[\Delta]^e = \{[\Delta_a], [\Delta_b], [\Delta_c], \dots, [\Delta_h]\}$$

Where  $[\Delta_a]$  = Relative displacement vector at node  $a$ , which is given by

$$[\Delta_a] = [\Delta u_x^a, \Delta u_y^a, \Delta u_z^a]^T$$

Where

$$\Delta u_a = (u_{x1} - u_{x9}), \Delta v_a = (u_{y1} - u_{y9}), \Delta w_a = (u_{z1} - u_{z9})$$

In which  $a_{xe}$ ,  $e_{ye}$  and  $U_{zi}$  are defined in global X, Y and Z directions, respectively. The relative displacement  $\{[\Delta_b], [\Delta_c] \dots [\Delta_h]\}$  may be also expressed in same way. In general, for any node on midsurface, relative displacement can be written as

$$[\Delta_k] = [T] [u_k]$$

Where

$[\Delta_k]$  = Relative displacement at node  $k$

$[T]$  = Intermediate transfer matrix

$[u_k]$  = Displacement at node  $k$

$$\begin{bmatrix} \Delta u_x \\ \Delta u_y \\ \Delta u_z \end{bmatrix}_k = \begin{bmatrix} +1 & 0 & 0 & -1 & 0 & 0 \\ 0 & +1 & 0 & 0 & -1 & 0 \\ 0 & 0 & +1 & 0 & 0 & -1 \end{bmatrix} \begin{bmatrix} u_x^{CFRP} \\ u_y^{CFRP} \\ u_z^{CFRP} \\ u_x^{concrete} \\ u_y^{concrete} \\ u_z^{concrete} \end{bmatrix}_k \dots \dots \dots 7.38$$

$$[\Delta_k] = \begin{bmatrix} \Delta u_x \\ \Delta u_y \\ \Delta u_z \end{bmatrix}_k = \begin{bmatrix} u_x \\ u_y \\ u_z \end{bmatrix}_{CFRP} - \begin{bmatrix} u_x \\ u_y \\ u_z \end{bmatrix}_{concrete}$$

### 7.6.4.3 Strain-relative displacement matrix

In contrast to the strain-displacement matrix used in the conventional formulations of finite elements, the matrix  $[B]$  of the zero-thickness interface element is based on the shape functions which are not differentiated.

$$[B_k]_{3 \times 6} = \pm [R]_{3 \times 3} [N_k]_{3 \times 3} [T_k]_{3 \times 6}$$

$$[B_k]_{3 \times 6} = [R]_{3 \times 3} \begin{bmatrix} N_k & 0 & 0 & -N_k & 0 & 0 \\ 0 & N_k & 0 & 0 & -N_k & 0 \\ 0 & 0 & N_k & 0 & 0 & -N_k \end{bmatrix} \dots\dots\dots 7.39$$

A preliminary requirement in derivation of strain-relative displacement matrix for zero-thickness interface element is establishment of rotation matrix  $[R]$ .

$$[R]_{3 \times 3} = \begin{bmatrix} V_{\xi_x} & V_{\xi_y} & V_{\xi_z} \\ V_{\eta_x} & V_{\eta_y} & V_{\eta_z} \\ V_{\zeta_x} & V_{\zeta_y} & V_{\zeta_z} \end{bmatrix} \dots\dots\dots 7.40$$

Where  $V_{\xi_x}, V_{\xi_y}, V_{\xi_z}$  = direction cosines defining cosines of angles between  $V_\xi$  and  $X, Y, Z$  axes. Similarly,  $V_{\eta_x}, V_{\eta_y}, V_{\eta_z}$  and  $V_{\zeta_x}, V_{\zeta_y}, V_{\zeta_z}$  can also be interpreted.

Elements of the rotation matrix can be obtained as follows:

$$V_{\xi_x} = \frac{\sum_{k=1}^8 \frac{\partial N_k}{\partial \xi} x_k}{\sqrt{L_\xi}}, \quad V_{\xi_y} = \frac{\sum_{k=1}^8 \frac{\partial N_k}{\partial \xi} y_k}{\sqrt{L_\xi}}, \quad V_{\xi_z} = \frac{\sum_{k=1}^8 \frac{\partial N_k}{\partial \xi} z_k}{\sqrt{L_\xi}}$$

$$V_{\eta_x} = \frac{\sum_{k=1}^8 \frac{\partial N_k}{\partial \eta} x_k}{\sqrt{L_\eta}}, \quad V_{\eta_y} = \frac{\sum_{k=1}^8 \frac{\partial N_k}{\partial \eta} y_k}{\sqrt{L_\eta}}, \quad V_{\eta_z} = \frac{\sum_{k=1}^8 \frac{\partial N_k}{\partial \eta} z_k}{\sqrt{L_\eta}}$$

Where

$$L_\xi = \left[ \sum_{k=1}^8 \frac{\partial N_k}{\partial \xi} x_i \right]^2 + \left[ \sum_{k=1}^8 \frac{\partial N_k}{\partial \xi} y_i \right]^2 + \left[ \sum_{k=1}^8 \frac{\partial N_k}{\partial \xi} z_i \right]^2$$

$$L_\eta = \left[ \sum_{k=1}^8 \frac{\partial N_k}{\partial \eta} x_i \right]^2 + \left[ \sum_{k=1}^8 \frac{\partial N_k}{\partial \eta} y_i \right]^2 + \left[ \sum_{k=1}^8 \frac{\partial N_k}{\partial \eta} z_i \right]^2$$

The unit vector  $V_n$  defining normal to the surface may be now expressed as follows:

$V_n$  = cross product of unit vector  $V_{\zeta}$  and  $V_{\eta}$

$$\hat{V}_n = \begin{bmatrix} \hat{i} & \hat{j} & \hat{k} \\ V_{\zeta x} & V_{\zeta y} & V_{\zeta z} \\ V_{\eta x} & V_{\eta y} & V_{\eta z} \end{bmatrix} \quad \text{Where} \quad \begin{aligned} V_{nx} &= V_{\zeta y} V_{\eta z} - V_{\eta y} V_{\zeta z} \\ V_{ny} &= V_{\zeta z} V_{\eta x} - V_{\eta x} V_{\zeta z} \\ V_{nz} &= V_{\zeta x} V_{\eta y} - V_{\eta x} V_{\zeta y} \end{aligned}$$

By substituting the value of the rotation matrix  $[R]_{3 \times 3}$  in eq.(7.39)

$$[B_k]_{3 \times 6} = \begin{bmatrix} V_{\zeta x} & V_{\zeta y} & V_{\zeta z} \\ V_{\eta x} & V_{\eta y} & V_{\eta z} \\ V_{nx} & V_{ny} & V_{nz} \end{bmatrix} \begin{bmatrix} N_k & 0 & 0 & -N_k & 0 & 0 \\ 0 & N_k & 0 & 0 & -N_k & 0 \\ 0 & 0 & N_k & 0 & 0 & -N_k \end{bmatrix}$$

The strain- relative displacement matrix for the interface element can be expressed as follows:

$$[B]_{3 \times 48} = [R]_{3 \times 3} \sum_{K=1}^8 [N_k]_{3 \times 3} [T_k]_{3 \times 6}$$

$$[B]_{3 \times 48} = \begin{bmatrix} V_{\zeta x} & V_{\zeta y} & V_{\zeta z} \\ V_{\eta x} & V_{\eta y} & V_{\eta z} \\ V_{nx} & V_{ny} & V_{nz} \end{bmatrix} \sum_{k=1}^8 \begin{bmatrix} N_k & 0 & 0 & -N_k & 0 & 0 \\ 0 & N_k & 0 & 0 & -N_k & 0 \\ 0 & 0 & N_k & 0 & 0 & -N_k \end{bmatrix} \dots\dots\dots 7.41$$

$$[B]_{3 \times 48} = [[B_1]_{3 \times 6} [B_2]_{3 \times 6} \dots\dots\dots [B_8]_{3 \times 6}]$$

**7.6.4.4 Stiffness Matrix of Interface Element**

$$[K^e] = \int_A [B]^T [D] [B] dA$$

$$[K^e] = \int_{-1}^{+1} \int_{-1}^{+1} [N]^T [G]^T [D] [G] [N] \left| V_{\zeta} \times V_{\eta} \right| d\zeta d\eta \dots\dots\dots 7.42$$

**7.6.4.5 Numerical Integration**

The element stiffness matrix can be numerically obtained by Gaussian integration (applying 2x2 integration rule), using the following equation:

$$[K^e] = \sum_{i=1}^{n-Gauss} \sum_{j=1}^{n-Gauss} [N]^T [G]^T [D] [G] [N] \left| \vec{V}_{\zeta} \times \vec{V}_{\eta} \right| C_i \times C_j \dots\dots\dots 7.43$$

Where

$C_i, C_j$  = Weighting coefficient

$n$ -Gauss = defines the total number of Gauss points.

$|\vec{V}_\zeta \times \vec{V}_\eta|$  = area associated with a gauss points and can be obtained as determinant of

the following matrix

$$\vec{V}_\zeta \times \vec{V}_\eta = \begin{bmatrix} \hat{i} & \hat{j} & \hat{k} \\ \frac{\partial x}{\partial \zeta} & \frac{\partial y}{\partial \zeta} & \frac{\partial z}{\partial \zeta} \\ \frac{\partial x}{\partial \eta} & \frac{\partial y}{\partial \eta} & \frac{\partial z}{\partial \eta} \end{bmatrix}$$

$$|\vec{V}_\zeta \times \vec{V}_\eta| = \sqrt{\left(\frac{\partial y}{\partial \zeta} \frac{\partial z}{\partial \eta} - \frac{\partial z}{\partial \zeta} \frac{\partial y}{\partial \eta}\right)^2 + \left(\frac{\partial x}{\partial \zeta} \frac{\partial z}{\partial \eta} - \frac{\partial x}{\partial \eta} \frac{\partial z}{\partial \zeta}\right)^2 + \left(\frac{\partial x}{\partial \zeta} \frac{\partial y}{\partial \eta} - \frac{\partial y}{\partial \zeta} \frac{\partial x}{\partial \eta}\right)^2} \dots\dots\dots 7.44$$

Where

$$\frac{\partial x}{\partial \xi} = \sum_{k=1}^8 \frac{\partial N_k}{\partial \xi} x_k, \quad \frac{\partial y}{\partial \xi} = \sum_{k=1}^8 \frac{\partial N_k}{\partial \xi} y_k, \quad \frac{\partial z}{\partial \xi} = \sum_{k=1}^8 \frac{\partial N_k}{\partial \xi} z_k$$

$$\frac{\partial x}{\partial \eta} = \sum_{k=1}^8 \frac{\partial N_k}{\partial \eta} x_k, \quad \frac{\partial y}{\partial \eta} = \sum_{k=1}^8 \frac{\partial N_k}{\partial \eta} y_k, \quad \frac{\partial z}{\partial \eta} = \sum_{k=1}^8 \frac{\partial N_k}{\partial \eta} z_k$$

### 7.6.4.6 Computations of Strains and Stresses

After solving the equilibrium equation nodal displacement should be transformed to the local system (element displacements), this can be done as follows:

$$[\delta]_{3 \times 1} = \sum_{K=1}^8 [N_k]_{3 \times 3} [\Delta_k]_{3 \times 1}$$

Where

$$[\Delta_k] = \begin{bmatrix} \Delta u_x \\ \Delta u_y \\ \Delta u_z \end{bmatrix}_k = \begin{bmatrix} u_x \\ u_y \\ u_z \end{bmatrix}_{CFRP} - \begin{bmatrix} u_x \\ u_y \\ u_z \end{bmatrix}_{concrete}$$

$$\begin{bmatrix} \delta_\zeta \\ \delta_\eta \\ \delta_n \end{bmatrix} = \sum_{k=1}^8 \begin{bmatrix} N_k & 0 & 0 \\ 0 & N_k & 0 \\ 0 & 0 & N_k \end{bmatrix} \begin{bmatrix} \Delta u_x \\ \Delta u_y \\ \Delta u_z \end{bmatrix}_k \dots\dots\dots 7.45$$

**Strain vector** in the considered point along the natural coordinate axes  $\xi$ ,  $\eta$  and  $n$ : can be evaluated as

$$\begin{aligned}
 [\varepsilon]_{3 \times 1} &= [B]_{3 \times 24} \sum_{K=1}^8 [\Delta_k]_{3 \times 1} \\
 [\varepsilon]_{3 \times 1} &= [R]_{3 \times 3} \sum_{K=1}^8 [N_k]_{3 \times 3} [\Delta_k]_{3 \times 1} \\
 [\varepsilon]_{3 \times 1} &= [R]_{3 \times 3} [\delta]_{3 \times 1} \\
 \begin{bmatrix} \varepsilon_\xi \\ \varepsilon_\eta \\ \varepsilon_n \end{bmatrix} &= \begin{bmatrix} V_{\xi\xi} & V_{\xi\eta} & V_{\xi n} \\ V_{\eta\xi} & V_{\eta\eta} & V_{\eta n} \\ V_{n\xi} & V_{n\eta} & V_{nn} \end{bmatrix} \begin{bmatrix} \delta_\xi \\ \delta_\eta \\ \delta_n \end{bmatrix} \dots\dots\dots 7.46
 \end{aligned}$$

Where

$\varepsilon_\xi$ ,  $\varepsilon_\eta$  and  $\varepsilon_n$  = Tangential shear strain in direction  $\xi$ ,  $\eta$  and normal strain respectively

**Stress vector** along the same natural coordinate axes can be obtained as follows:

$$[\sigma]_{3 \times 1} = [D]_{3 \times 3} [\varepsilon]_{3 \times 1}$$

Where

$[\sigma]$  is stress vector and

$[D]$ = constitutive matrix for the interface element can be evaluated as:

$$\begin{aligned}
 [D]_{3 \times 3} &= \begin{bmatrix} E_\xi & 0 & 0 \\ 0 & E_\eta & 0 \\ 0 & 0 & E_n \end{bmatrix} \\
 \begin{bmatrix} \tau_\xi \\ \tau_\eta \\ \sigma_n \end{bmatrix} &= \begin{bmatrix} E_\xi & 0 & 0 \\ 0 & E_\eta & 0 \\ 0 & 0 & E_n \end{bmatrix} \begin{bmatrix} \varepsilon_\xi \\ \varepsilon_\eta \\ \varepsilon_n \end{bmatrix} \dots\dots\dots 7.47
 \end{aligned}$$

Where

$\tau_\xi$ ,  $\tau_\eta$  and  $\sigma_n$  = Tangential shear stresses in direction  $\xi$ ,  $\eta$  and normal stress respectively.

$E_\xi$ ,  $E_\eta$  and  $E_n$  = Shear modulus in direction  $\xi$ ,  $\eta$  and bond modulus respectively.

**7.6.5 Representation of Cracking**

One of important sources of material non-linearity in reinforced concrete member is cracking of concrete. How ever, an adequate representation of cracking in finite

element model required considerable effort. This due to difficulty, which rises from the continued propagation of cracks with increasing load. The reliable numerical simulation of the initiation and propagation of cracks plays an important role for the integrity assessment of concrete structures.

Because of its influence on the mechanism of stress transfer between the FRP and the concrete, cracking of concrete has a great influence on the behaviour of RC beams retrofitted with FRP. Within the framework of the finite element method, there exist several techniques to model crack onset and propagation. For problems in which the local distribution of stresses is not very important, methods considering the cracks like uniformly spread on a portion of material affected by cracking have become popular. Stresses and strains in such a volume (large enough to contain a few cracks) are represented by averaged values, calculated in some cases taking into account also the reinforcement and its interaction with the base material. In this approach cracking is reduced to a constitutive problem.

There are two approaches which have been traditionally used for representation of cracking.

- Discrete Cracking Approach
- Smearred or Distributed Cracking Approach

#### ***7.6.5.1 Discrete Cracking Approach***

The first reinforced concrete finite element model which includes the effect of cracking was developed by Ngo and Scordelis (1967) [83], who carried out a linear elastic analysis of beams with predefined crack patterns. The cracks were modelled by separating the nodal points of the finite element mesh and thus creating a discrete crack model. In this approach the displacement discontinuities a cross crack are accounted for by disconnecting elements at nodal points along their boundaries. The discrete crack approach requires monitoring the response and modifying the topology of the finite element mesh corresponding to the current crack configurations at each state of loading. Discrete crack models explicitly represent the crack as a separation of nodes. When the stress or strain at a node, or the average in adjacent elements, exceeds their limited value, the node is redefined as two nodes and the elements on either side are allowed to separate. While this produces a realistic representation of

the opening crack, a coarse discretization in the finite element model may result in misrepresentation of the propagating crack tip. The main problem in this approach, however, is difficulty which arises from introducing of additional nodal points required by altered topology of analytical model. These additional nodal points increase the number of degrees of freedom result in greater band width in global stiffness matrix. This leads to an unjustifiable increase in computational effort required to solve the equilibrium equation.

The discrete crack models explicitly represent each individual discontinuity. This may be integrated into the FE mesh in a very convenient way by means of joint or interface elements with the appropriate constitutive laws. Among this type of elements, we may emphasize on the zero-thickness interface elements, that were originally developed by Goodman et al. (1968) and offer a great simplicity, as well as being able to capture the basic structural behaviour of rock discontinuities and other types of interfaces. We may differentiate those schemes based on the Linear Elastic Fracture Mechanics (LEFM), where a remeshing is needed in order to model the fracture advance (Ingraffea, 1977; Saouma, 1980), and those based on the Non-Linear Fracture Mechanics - NLFM, which may be also formulated either with remeshing (Bittencourt et al., 1992) or by using a fixed FE mesh in which an interface element is introduced within each line of the mesh, or in those which are expected to be fractured (Rots, 1988; López et al., 1996; López, 1999; Carol et al., 2001).

There are two strategies by which this method of crack modelling may be implemented. In the first, the analysis is terminated when tensile cracking is detected. The topology of the structure is then redefined; the nodal points are re-numbered such that the input data is updated to the new topology. The solution process is then continuous until further cracking is detected. This strategy is lengthy and is considered in practical as an analytical tool.

The second strategy involves the definitions of two or four nodes occupying the same coordinates in space as shown in Fig.7.13. These nodes are initially rigidly joint until cracking is detected in adjacent elements. When this occurs the nodes are released by reducing stiffness of linkage to zero. In cases where the modelling of post-cracking shear resisting mechanisms is desired, these stiff linkages are replaced with ones corresponding to any of shear transfer mechanism. The difference between defining two or four nodes in probable cracking regions depends on the pattern of

cracking anticipated. If the cracking is expected to develop in two directions, situation that may arise from cyclic loading, for example then the four nodes must be used. One dimensional cracking, however, required only two nodes.

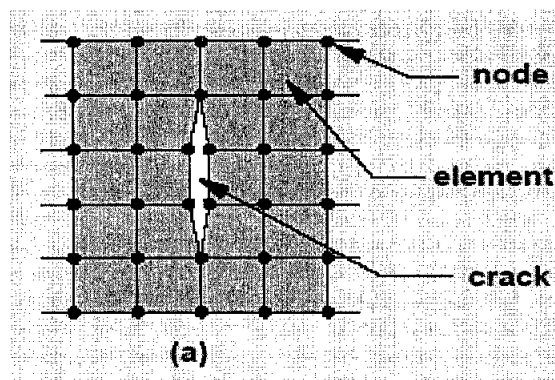


Fig. 7.13 DISCRETE CRACKING

As high stiffness values of linkages are reduced to stiffness values correspond to any of shear resisting mechanism linkage to release the rigidly connected nodes, the excess tensile forces in linkages are converted into nodal forces, which will be referred to as unbalanced forces. These unbalanced forces are applied to the system in the next iteration so as to distribute the excess tensile stresses to adjacent elements.

The main advantages of discrete cracking approach are:

1. It's more realistic representation of cracking.
2. It is better to simulate shear transfer mechanisms

The disadvantages of this approach are:

1. It requires a continuity changing definition of topology as cracking progress
2. Cracking direction is dependent on mesh geometry and the types of elements used.

#### ***7.6.5.2 Smeared Cracking Approach***

The smeared crack model first used by Rashid (1968)] represents cracked concrete as an elastic orthotropic material with reduced elastic modulus in the direction normal to the crack plane. With this continuum approach the local displacement discontinuities at cracks are distributed over some tributary area within the finite element and the behaviour of cracked concrete can be represented by average stress-strain relations. In

contrast to the discrete crack concept, the smeared crack concept fits the nature of the finite element displacement method, since the continuity of the displacement field remains intact. Smeared cracks are convenient when the crack orientations are not known beforehand, because the formation of a crack involves no remeshing or new degrees of freedom. However, they have only limited ability to model sharp discontinuities and represent the topology or material behaviour in the vicinity of the crack. The method works best when the cracks to be modelled are themselves smeared out, as in reinforced concrete applications.

The smeared crack models (Rashid (1968); Cope et al (1980); Rots et al(1985)) are based on a continuous type of modelling of the problem where the possible existence or development of discontinuities is incorporated onto the stress/strain constitutive laws of the material, so that a generalized constitutive model is used for the fractured material that will be non-linear and with softening. Although this method may be used with a fixed FE mesh during the whole analysis, it usually brings associated a large number of material parameters. However, this is not the only drawback of this method, since for instance it lacks objectivity when refining the mesh if there exists softening (Bazant, (1986)), which forces to develop a regularization procedure. Many of these procedures have been proposed although with partial validity (Coleman et al (2001); Jirásek, (2002); Jirásek Rolshoven (2003)). There exist also problems in the deformation modes of the elements that, in general, are not able to accommodate localized strains of arbitrary orientation, with the consequent bands that occupy a different number of elements (different thickness) depending on their orientation.

The method achieves stresses discontinuity state consistent with existence of crack. When principal tensile strain in an element exceeds failure criterion, the stiffness of element is reduced to zero in direction of principal strain. Elements are cracked in this manner are postulated to be incapable of carrying stresses normal to crack direction (see Fig. 7.14). These stresses are converted into nodal forces as unbalanced forces. These forces are applied to the structure in the next iteration

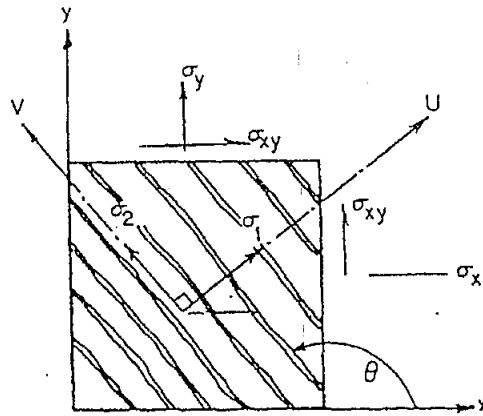


Fig. 7.14 DISTRIBUTED CRACKING

The main advantages of distributed cracking approach are:

1. No change in topology of structures as cracking progress
2. Complete generality in regard to cracking direction, independent of mesh geometry and type of elements used.

The disadvantages of this approach are:

1. It can not provide a realistic prediction of distribution of strain, and therefore the stresses in region adjacent to cracks.
2. Shear resisting mechanisms cannot be realistically modelled.

### 7.7 Solution strategy using iterative method

1. Apply the load and analyze the structure using updated stiffness matrix.
2. From the resulting displacement determined in the previous cycle calculate the strain.
3. From these strains calculate the stresses according to the cyclic model for each element.
4. Using the current strains and stresses  $(\sigma_i, \epsilon_i)$  check all the elements against their failure criterions , where  $i$  is current cycle of loading.
5. For each element, calculate the unbalanced loads resulting from the material failure or change in stiffness.
6. Assembled the global unbalanced load vector.

7. Check the current displacement and current unbalanced loads vector for convergence. If the solution is converges or pre-specified maximum number of iteration has been exceeded, go to step 1. If divergence is indicated stop the solution.
8. If the solution has not converged or pre-specified maximum number of iterations has been not exceeded reanalyze the structure for unbalanced load vector. After obtaining the displacement due to the unbalanced load go to step 2

## CHAPTER 8

### APPLICATIONS AND RESULTS

#### 8.1 Introduction

This chapter discusses the applicability of the cyclic models that were used in the finite element algorithm to study the overall structural behaviour of RC beams strengthened for shear with CFRP laminates subjected to cyclic loading and the adequacy of non-linear procedure used in computer program.

Non-linear finite-element analyses of RC beams retrofitted with fibre-reinforced-polymers (FRP) have been carried out up to failure. Unlike the previous sections, in which specific aspects have been numerically investigated in isolation, we present here models and results referring to a complete structural element.

These analyses are intended to provide a good appreciation of the importance of the different features of a model for the analysis of this type of systems and to get a better insight into their behaviour through simulations including failure modes not observed in ordinary RC beams.

The analytical results that were obtained from the finite element program are compared with their corresponding published results in order to test the efficiency of the analytical algorithm and to validate the data obtained for interface model between CFRP and concrete that was mentioned in chapter (6).

In this research, experimental tests that were carried out by Omar Chaallal et al (2009) have been chosen for a case history. This problem has been chosen because it represents a typical case of engineering interest and because the experimental setup and the results are reported with a level of detail which is sufficient to attempt reproducing them numerically. This chapter describes the following information:

- Experimental response
- Analytical response
- Comparison between analytical results and experimental results

- Parametric analysis

## 8.2 Material and Specimen Descriptions

The T-beams used in this research were 4520 mm long. Details of their cross-section are presented in Fig. 8.1. The longitudinal-steel reinforcement consisted of four M25 bars (diameter = 25.2 mm) laid in two layers. The transverse-steel reinforcements were 8 mm in diameter (area = 50 mm<sup>2</sup>) and were spaced at  $s = d/2$ , where  $d = 350$  mm represents the effective depth of the beam cross-section (see Fig. 8.1). The composite material was a unidirectional carbon-fibre fabric applied continuously over the test zone in a U shape around the web via a wet lay-up procedure. The thickness of the CFRP used was respectively 0.1 mm and 0.2 mm before saturation for one (1L) and two (2L) layers.

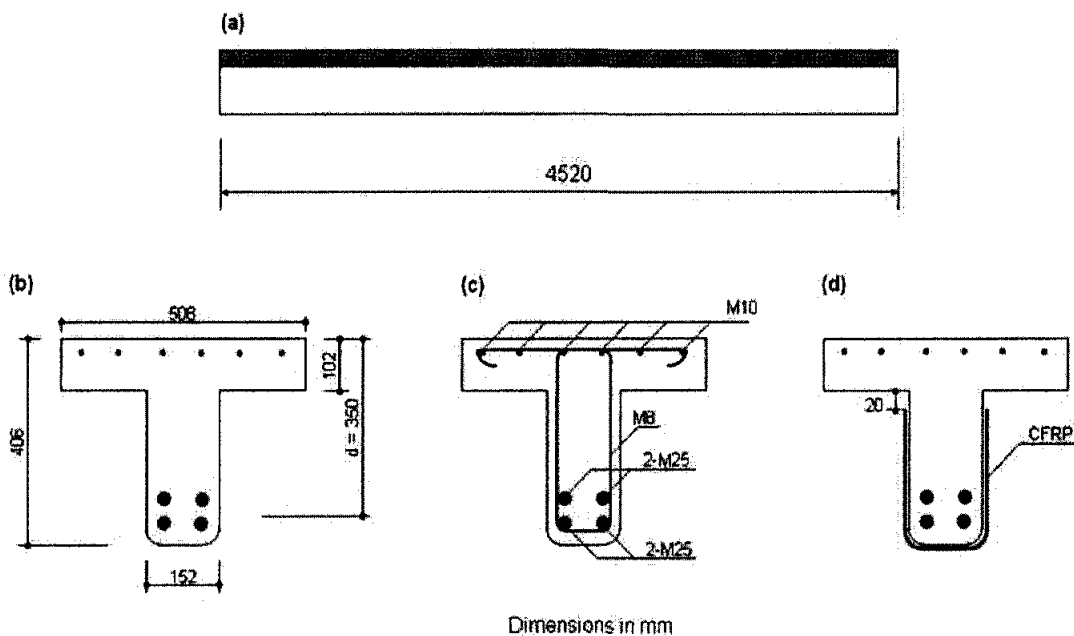


Fig. 8.1 specimen descriptions:

- (a) Elevation, (b) x-section with no transverse steel, (c) x-section with transverse steel, (d) wrapped x-section.

A commercially available concrete, delivered to the laboratory by a local supplier, was used. The concrete mix design is presented in Table 8.1. Standard compression tests on control cylinders yielded a 28-day concrete compressive strength of 29 MPa on average. The steel reinforcing bars used were also tested in tension according to

the ASTM A370 standard (ASTM 1997)(see Table 8.2), and a commercially available CFRP system, including SikaWrap Hex 230C unidirectional fabric, Sikadur 330 adhesive, and a primer, was used in this study. Table 8.3 provides a summary of the dry fabric properties provided by the manufacturer. The CFRP fabric was applied according to the manufacturer's specifications.

Table 8.1 PROPERTIES OF CONCRETE MIX

description	value
Cement (ordinary), kg/m <sup>3</sup>	255
Sand, kg/m <sup>3</sup>	1040
Aggregate (max. 14mm), kg/m <sup>3</sup>	875
Water, kg/m <sup>3</sup>	185
Volume of air entrained	2.5

Table 8.2 MECHANICAL PROPERTIES OF STEEL REINFORCEMENT BARS

Steel used	Diameter(mm)	Modulus of elasticity (GPa)	Yield strain strain	Yield stress (MPa)
M25	25.2	187	2500	500
M8	8	206	2600	540

Table 8.3 PROPERTIES OF CFRP

property	value
Tensile strength	3450
Tensile modulus	230
Ultimate elongation	1.5
Thickness (one layer)	0.1

### 8.3 Instrumentation

A comprehensive and carefully engineered measuring device was used for the study as detailed in Fig. 8.2. The vertical displacement was measured at the position under the applied load using linear displacement sensors 100 mm in length. The longitudinal steel reinforcement was instrumented with a strain gage at the location where the load was applied. Strain gages were also affixed on the stirrups located in the loading zone

along the expected plane of shear failure (Fig. 8.2). The deformations experienced by the CFRP wrap were measured using displacement sensors known as crack gages. These gages were fixed vertically on the lateral faces of the specimens at the same positions (along the longitudinal axis) as the strain gages on the stirrups (Fig. 8.5(a)). The deformations of the concrete were measured using embedded strain gages inclined at  $\theta = 35^\circ$ , installed midway between the support and the point of application of loading, at mid-height of the beam web in the support-load point direction (see Fig. 8.2). The signals from the gages and the displacement sensors were captured and monitored using an automatic data acquisition system.

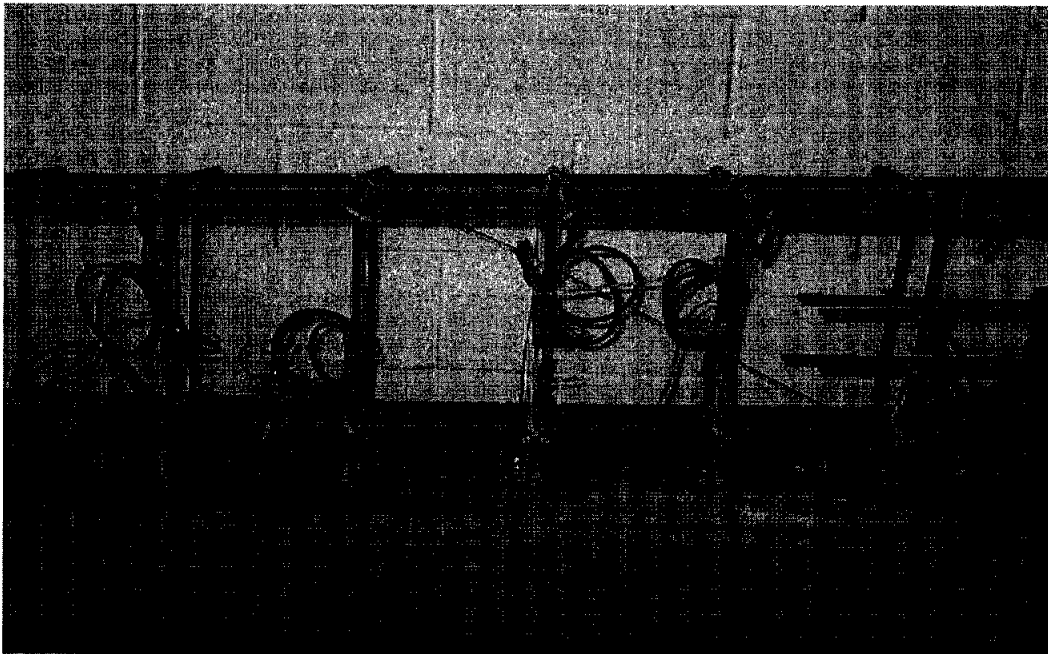
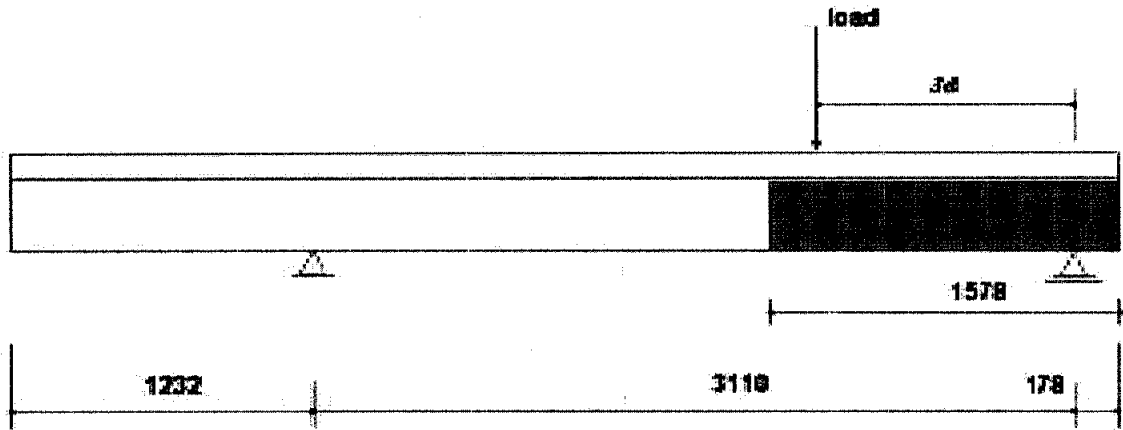


Fig. 8.2 INSTRUMENTATION

#### 8.4 Loading conditions

The specimens were subjected to fatigue loading and then tested monotonically to failure. They were first subjected to fatigue loading up to failure, with an upper limit of five million load cycles. Those specimens which did not fail under fatigue loading were then tested monotonically to failure. The loading arrangements for the fatigue tests and the subsequent static tests were identical (Fig. 8.3). Note that the test set up was designed to perform two tests on the same specimen. The second series of test which will consider static loading and  $ad=1.5$  (deep beam) on the left hand side of the beam (overhang part) is out of the scope of this paper. The specimens were tested in

three-point bending. The load was applied at a distance of  $a = 3d$  from the nearest support, which corresponds to the case of a slender beam, using a 500-kN capacity MTS hydraulic jack.



Dimensions in mm

Fig. 8.3 BEAM SET UP

In the fatigue tests, all the specimens were loaded at a rate of 2 Hz. The frequency was selected relatively low on the basis of the available equipment but also to avoid phenomena such as hysteresis effects (Barnes & Mays 1999), undesirable heating or lack of full recovery between successive cycles (Emberson 1996). The fatigue load was cycled from 35% to 65% of the load (P) corresponding to the total shear resistance of the specimen, as specified by the European recommendations (*fib* 2001). Earlier studies from the authors have shown that the *fib* model was more accurate than other codes in predicting the shear resistance. According to *fib*, the total shear resistance is equal to the sum of the contributions of concrete  $V_c$ , of steel stirrups,  $V_s$ , and of FRP,  $V_f$  as follows:

$$V_c = \left[ 0.18k(100\rho_1f_c')^{1/3} + \sigma_{cp} \right] b_w d, \quad k = 1 + \sqrt{\frac{200}{d}} \leq 2.0$$

$$V_s = \frac{A_v z f_y}{s} \cot \theta$$

$$V_f = 0.9 \epsilon_{f, \sigma} E_f \rho_f b_w d (\cot \theta + \cot \alpha) \sin \alpha$$

$\rho$  = longitudinal steel ratio; and  $\sigma_{cp}$  = normal stress due to axial force (positive for compression);  $\theta$  = diagonal crack angle;  $\alpha$  = angle of stirrup with respect to longitudinal axis; and  $s$  = stirrup spacing.

The upper and lower limits were calculated on the basis of common service load conditions that a structure like a bridge might experience during its service life. These limits evolve with respect to a mean value,  $P_{Mean}$ , estimated at 50% of ultimate, corresponding to the passage of a standard vehicle at a crawling speed. The lower and upper limits  $P_{min}$  and  $P_{max}$  are given as a function of the dynamic amplification factor ( $DAF$ ) by:  $P_{min} = P_{mean} (1-DAF)$  and  $P_{max} = P_{mean} (1+DAF)$ . Depending on the code used, the  $DAF$  values range between 0.25 and 0.40. In this paper, a value of 0.3 was considered for  $DAF$  which resulted on 35% and 65% of ultimate for the lower and the upper limit, respectively. Similar stress levels have been used elsewhere (e.g. Rosenboom & Rizkalla, 2006; Ekenel & Myers, 2009; and Czaderski & Motavalli, 2004). Thus, each beam was subjected to the same percentage of its ultimate load. It may be argued that the use of different load levels for the different test beams makes the comparison between the specimens uneasy. However, the approach used here for the loading is thought to be more realistic and representative of real-world situations since it is linked to the level of load to be supported by the retrofitted beams. It must be noted that the same approach was used elsewhere for CFRP strengthened beams (e.g. Barnes & May (1999)). As for static loading, the tests were performed under displacement control conditions at 2 mm/min.

### 8.5 Experimental response

The first part of this section describes the failure modes observed. Then the experimental results obtained from the fatigue tests and the subsequent monotonic tests on those specimens which did not fail under cyclic loading are successively presented and analyzed. The fatigue test results will be presented in terms of

- (a) The load versus deflection relationship
- (b) The strains undergone by the various components, including concrete, longitudinal and transverse-steel reinforcements, and CFRP.

The experimental results from the static tests will be discussed with regard to the load attained at rupture and the gain in capacity due to the CFRP, as well as the deflection response and the gain in stiffness due to the CFRP.

### 8.5.1 Mode of failure

All specimens failed by static shear. None of them exhibited significant signs of damage during the fatigue test which was terminated after  $5 \times 10^6$  cycles. For control beam, failure occurred by concrete crushing of the strut. In the retrofitted specimen with no transverse steel, S0-1L, failure became apparent with the sudden occurrence of a crack on the compression flange (Fig. 8.4). This crack progressed rapidly and was accompanied by fracture of the FRP prior to failure. As for the specimens with transverse steel, the primary mode of failure was yielding of the transverse steel. In un-strengthened specimen (control beam) S1-0L, this transverse steel yielding was followed by crushing of the concrete struts. However, in retrofitted specimen S1-1L (Fig. 8.5(b)), yielding of the steel stirrups was followed by both FRP debonding and crushing of the concrete strut.

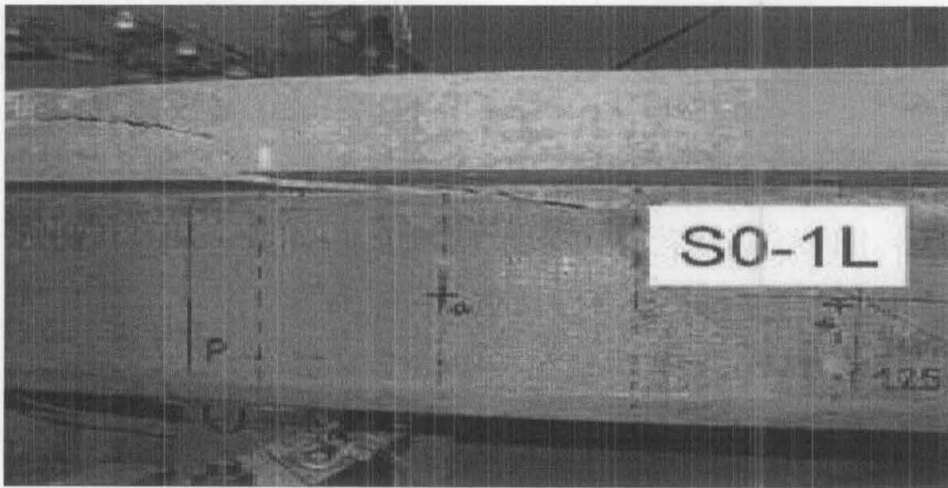
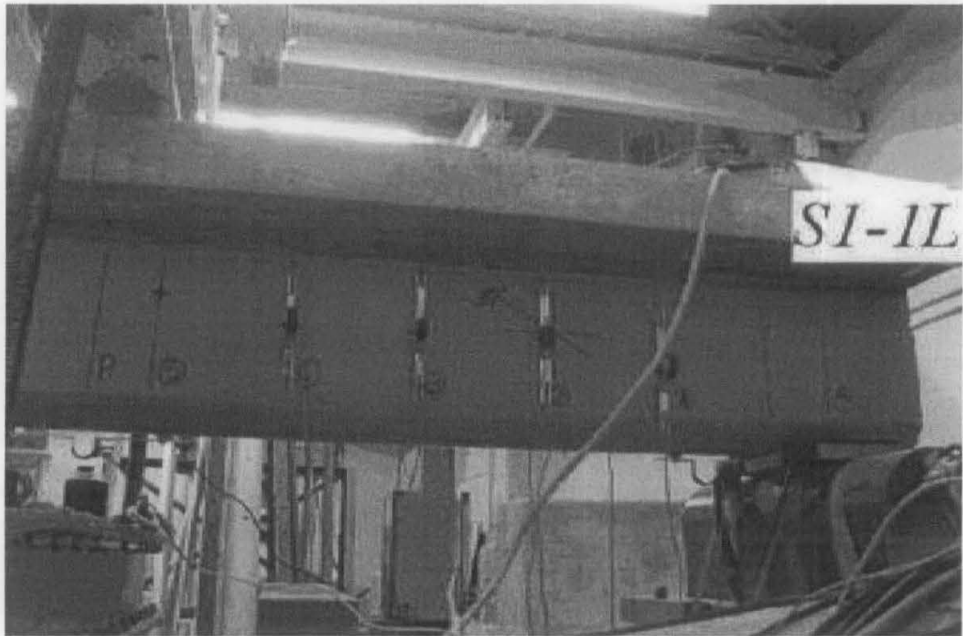
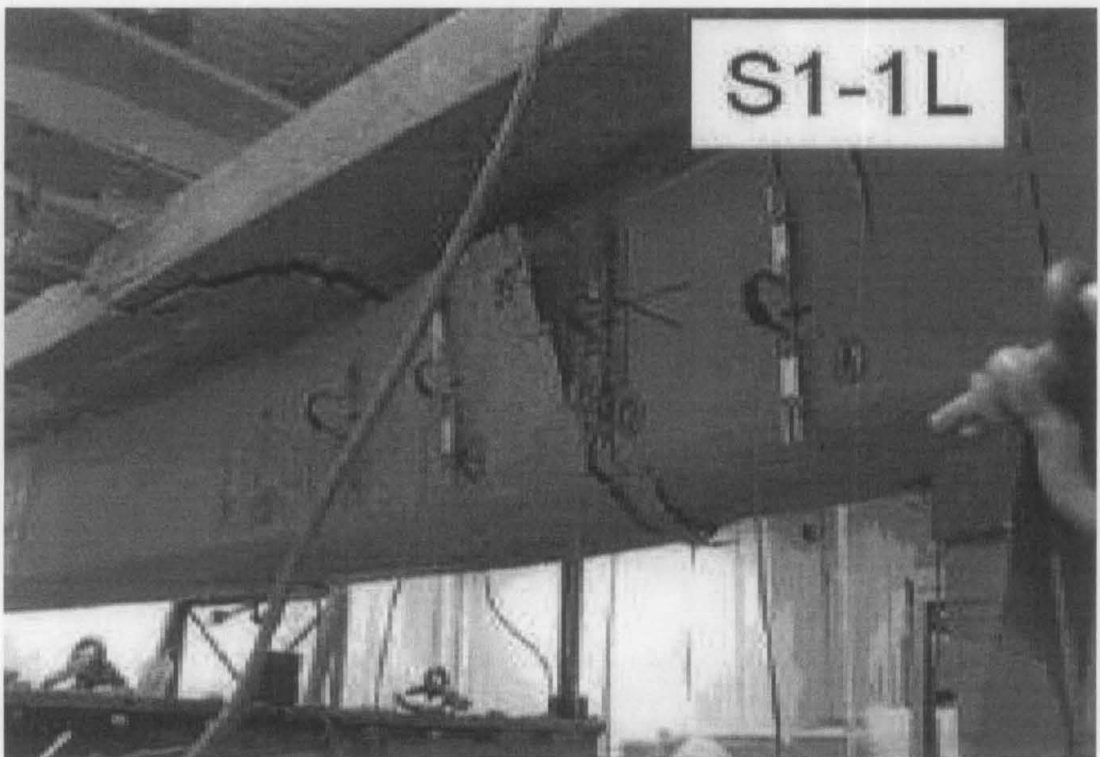


Fig. 8.4 FAILURE OF CONTROL BEAM (S0-1L)



(a) STRENGTHENED BEAM (S1-1L) BEFORE TESTING



(b) STRENGTHENED BEAM (S1-1L) AFTER TESTING

Fig. 8.5 (a) STRENGTHENED BEAM (S1-1L) BEFORE TESTING, (b) STRENGTHENED BEAM (S1-1L) AFTER TESTING

### 8.5.2 load-displacement curve

Table 8.4 provides the maximum deflection observed in the first cycle of loading as well as the maximum deflection in the last cycle under both maximum and minimum applied fatigue load ( $P_{min}$ ). The variation of the deflection as the number of cycles increases is plotted. For all the specimens, the deflection curves were measured at the load point and correspond to the maximum load applied ( $P_{max}$ ). These curves illustrate a typical pattern of damage accumulation in beams subjected to fatigue loading. All the tested specimens exhibited an initial increase in deflection during the early cycles. For control specimen, this first stage was followed by a stable region in which the deflection remained quasi-constant during cyclic loading. This was not the case for strengthened specimen S1-1L, where a more gradual deflection increase was observed. This can be attributed to a higher applied load range.

Table 8.4 DEFLECTION MEASUREMENT

specimen	Total Number of cycles (millions)	Max. Deflection under $P_{min}$ (mm) at 1 <sup>st</sup> cycle	Max. Deflection under $P_{max}$ (mm) at 1 <sup>st</sup> cycle	Max. Deflection under $P_{max}$ (mm) at last cycle	Max. Deflection under $P_{max}$ (mm) at last cycle
Control beam	5	2.41	3.35	3.67	4.73
Strengthened beam	5	3.85	5.53	5.91	7.66

### 8.5.3 Strains measurement

Table 8.5 presents for the first cycle the maximum strains corresponding to  $P_{min}$  and  $P_{max}$  attained in the concrete strut, in the longitudinal steel, in the steel stirrups and in the CFRP fabric.

Table 8.5 STRAIN MEASUREMENT

Specimen	Concrete Strut ( $\mu\epsilon$ )			Long. steel ( $\mu\epsilon$ )			Stirrups ( $\mu\epsilon$ )				CFRP ( $\mu\epsilon$ )			
	$P_{min}$	$P_{max}$	Range	$P_{min}$	$P_{max}$	Range	stirrup No.	$P_{min}$	$P_{max}$	Range	Gauge No.	$P_{min}$	$P_{max}$	Range
S1-0L	193	256	63	669	1049	380	S1	780	1137	357	CFRP1	--	--	--
							S2	810	987	177	CFRP2	--	--	--
							S3	394	483	89	CFRP3	--	--	--
							S4	659	905	246	CFRP4	--	--	--
S1-1L	411	508	97	846	1379	533	S1	720	1112	392	CFRP1	1077	1401	324
							S2	629	756	127	CFRP2	472	577	105
							S3	849	1314	465	CFRP3	918	1259	341
							S4	675	853	178	CFRP4	292	363	71

The following observations can be drawn from table 8.5

The measured strains versus the number of cycles are plotted and compared with their corresponding analytical results as describes in section 8.7.1

### 8.6 Analytical response

The finite element grid that was described in Fig.8.2 to model the beam is shown in Fig.8.6. At the support the nodes are free to move in direction x-x (parallel to the beam axis) and the displacement in y-y and z-z direction are suppressed.

Idealization of concrete required the use of twenty-nodes brick elements as shown in Fig.8.6 (a).The element has sixty degrees of freedom in total and each of these nodes has three degrees of freedom [three translations].

Lay out of reinforcement discretization is shown in Fig. 8.6 (b).The main reinforcement bars are concentrated in one layer. Space frame elements are used to idealize them. The element has a total of twelve degrees of freedoms, where each node has six degrees of freedom [three translations + three rotations]. The web

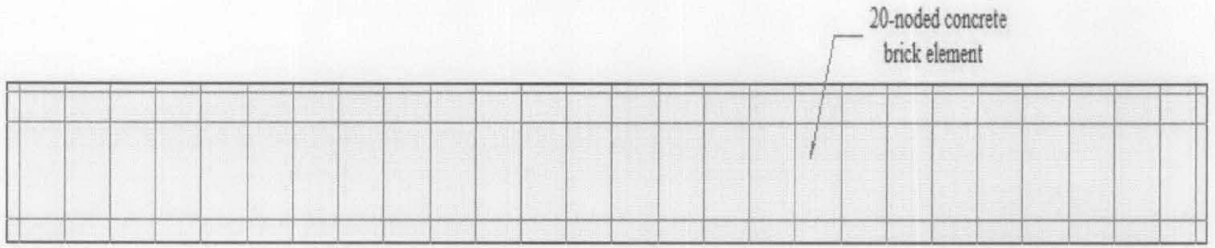
reinforcement bars were represented by space truss elements. The element has a total of six degrees of freedoms, where each node has three degrees of freedom [three translations].

Representation of CFRP laminates required the use of the same elements that were used to idealize the concrete. Fig. 8.6(c) shows the lay out of these elements.

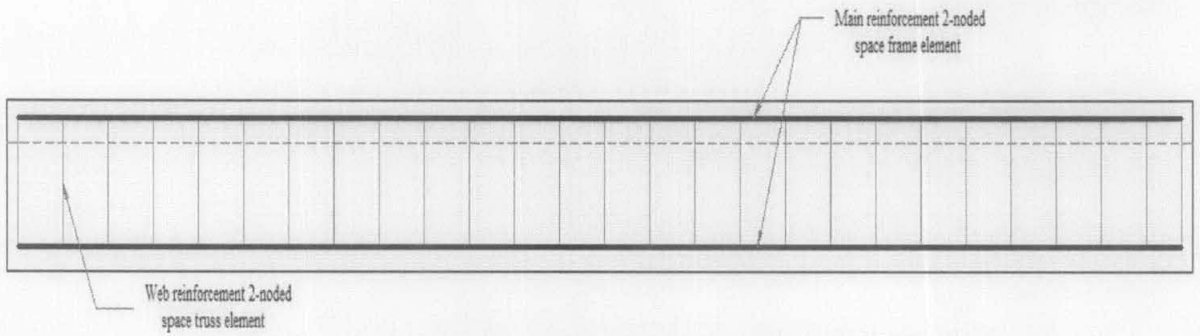
The bond slip mechanism along concrete main reinforcement interface is modelled by defining double nodes with coinciding coordinates along the interface. Fictitious springs elements (dimension less) are used to connect the concrete nodes and steel nodes. The lay out of the link elements decartelization is shown in fig. 8.6(d)

3-D interface elements are used to simulate the interaction between CFRP side plates and concrete. The element has sixteen nodes, eight nodes connect to concrete element and the other eight nodes connected to CFRP sheet. The interface was modelled by three linear springs connecting the joint nodes with the same coordinates. Fig. 8.6(e) shows the layout of these elements.

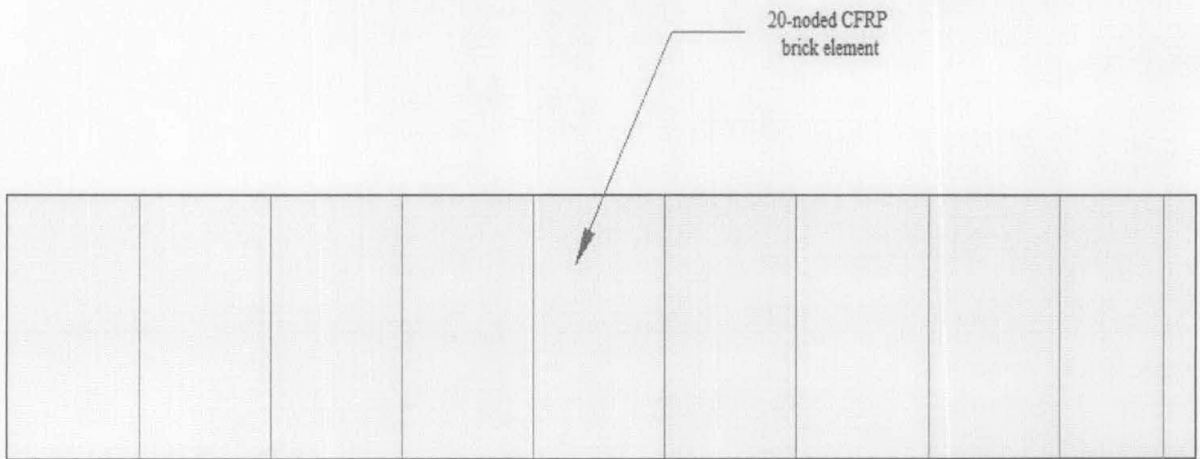
To discrete the members according to the above mention pattern led to 336 nodal points; all nodes have three translation degrees of freedom each. The nodes connecting the main reinforcement elements have, in addition to translation degrees of freedom, rotational degrees of freedom permitted in each.



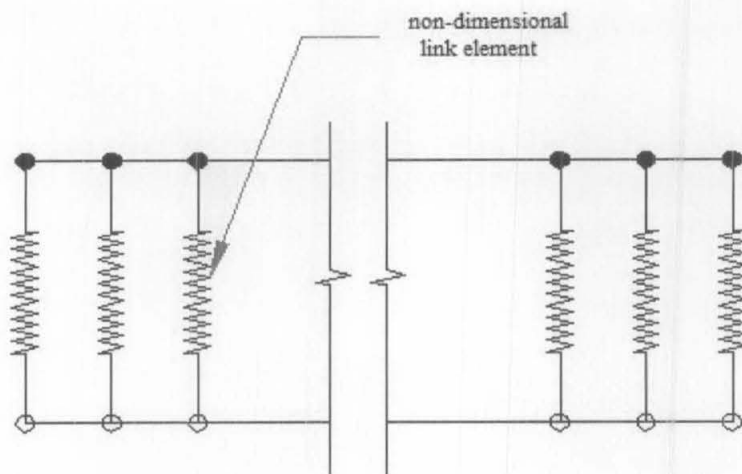
(a) CONCRETE ELEMENT LAYOUT



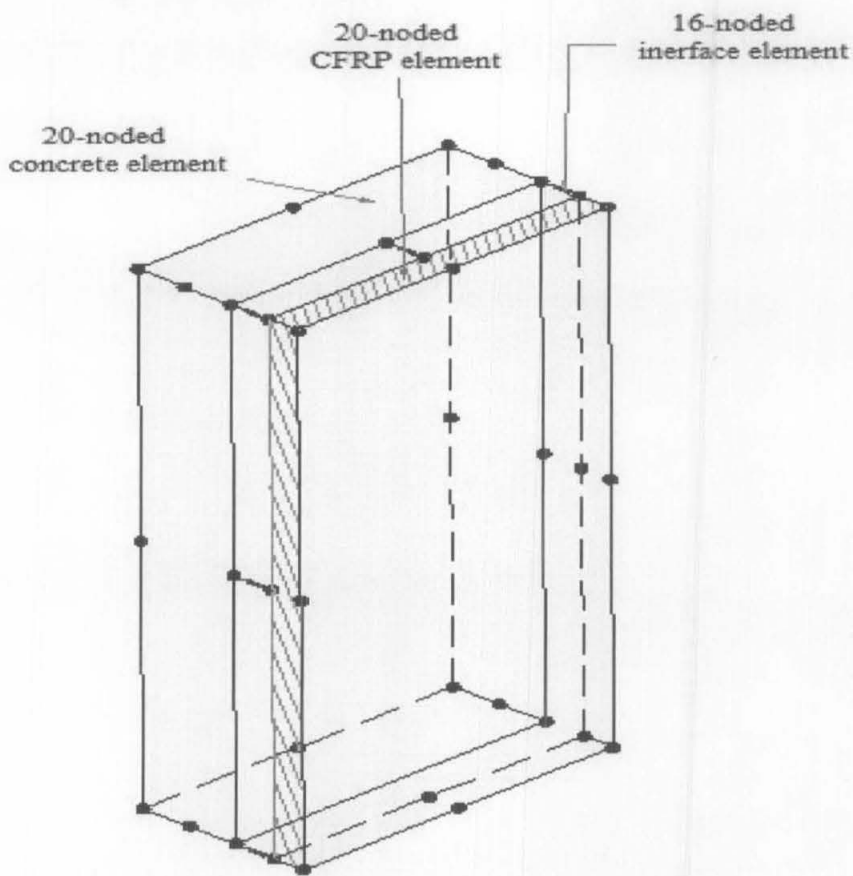
(b) STEEL ELEMENT LAYOUT



(c) CFRP LAMINATES LAYOUT



(d) LINK ELEMENT LAYOUT



(e) 16-NODE INTERFACE ELEMENT

Fig. 8.6 (a) CONCRETE ELEMENT LAYOUT, (b) STEEL ELEMENT LAYOUT, (c) CFRP LAMINATES LAYOUT, (d) LINK ELEMENT LAYOUT and (e) 16-NODE INTERFACE ELEMENT

## 8.7 Comparison between experimental and analytical results

### 8.7.1 Cyclic behaviour

Figure 8.7 shows curves representing the strains in the concrete struts versus the number of cycles for both experimental and analytical cases. The curve shows that for specimen S1-1L, the strains in the concrete strut increased continuously with respect to the number of cycles up to a maximum of approximately 1830  $\mu\epsilon$ . This relatively high level of strut strain and the resulting signs of damage observed in specimen S1-1L, clearly illustrates the beam's stiffness degradation, seem to indicate that the specimen was very close to its fatigue life, although it did not fail in shear fatigue after 5 million load cycles.

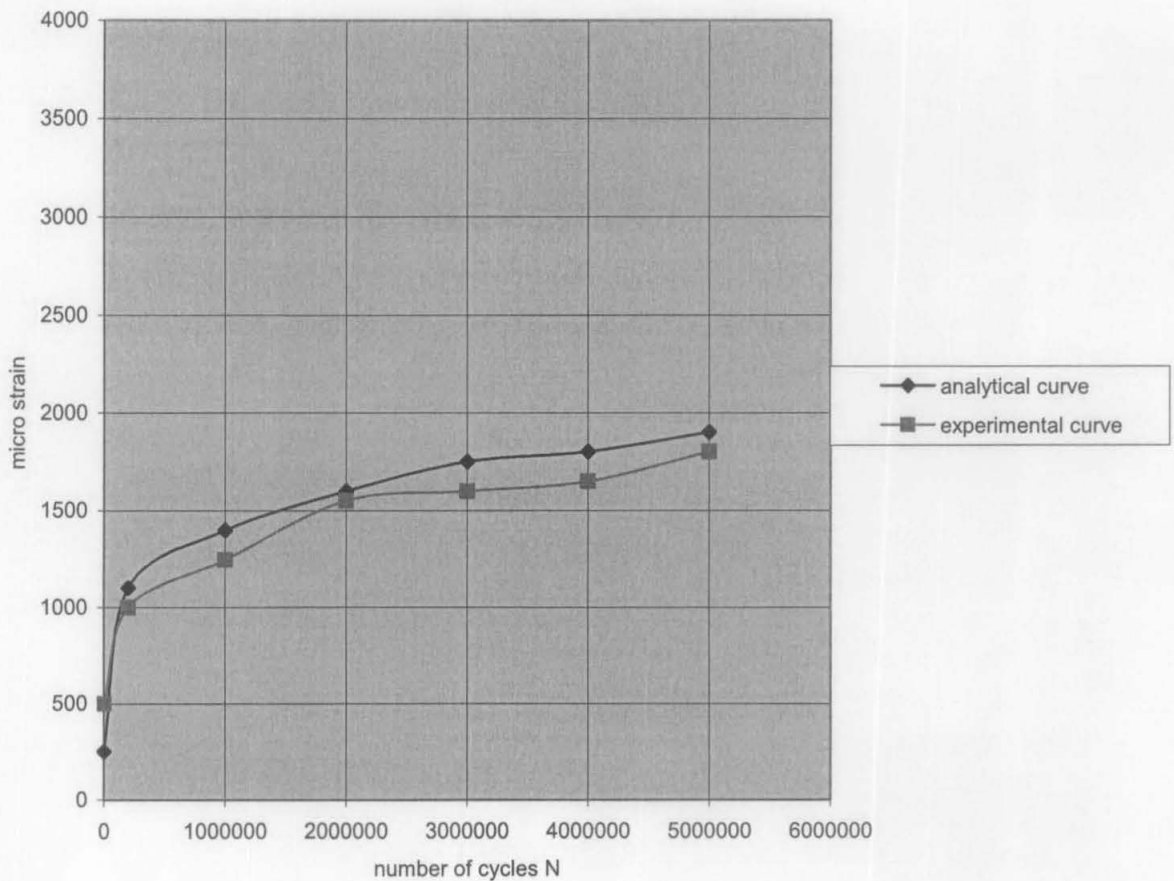


Fig. 8.7 CONCRETE STRAIN-N

As for the longitudinal steel reinforcement, the recorded strains are presented in Fig.8.8. For both cases experimental and analytical, it can be seen that there is no significant increase in strain as the number of cycle increases. This is due to the relatively high flexural capacity of the tested specimens compared with their shear capacity.

Note that yielding of the longitudinal steel never occurred in any of the test specimens.

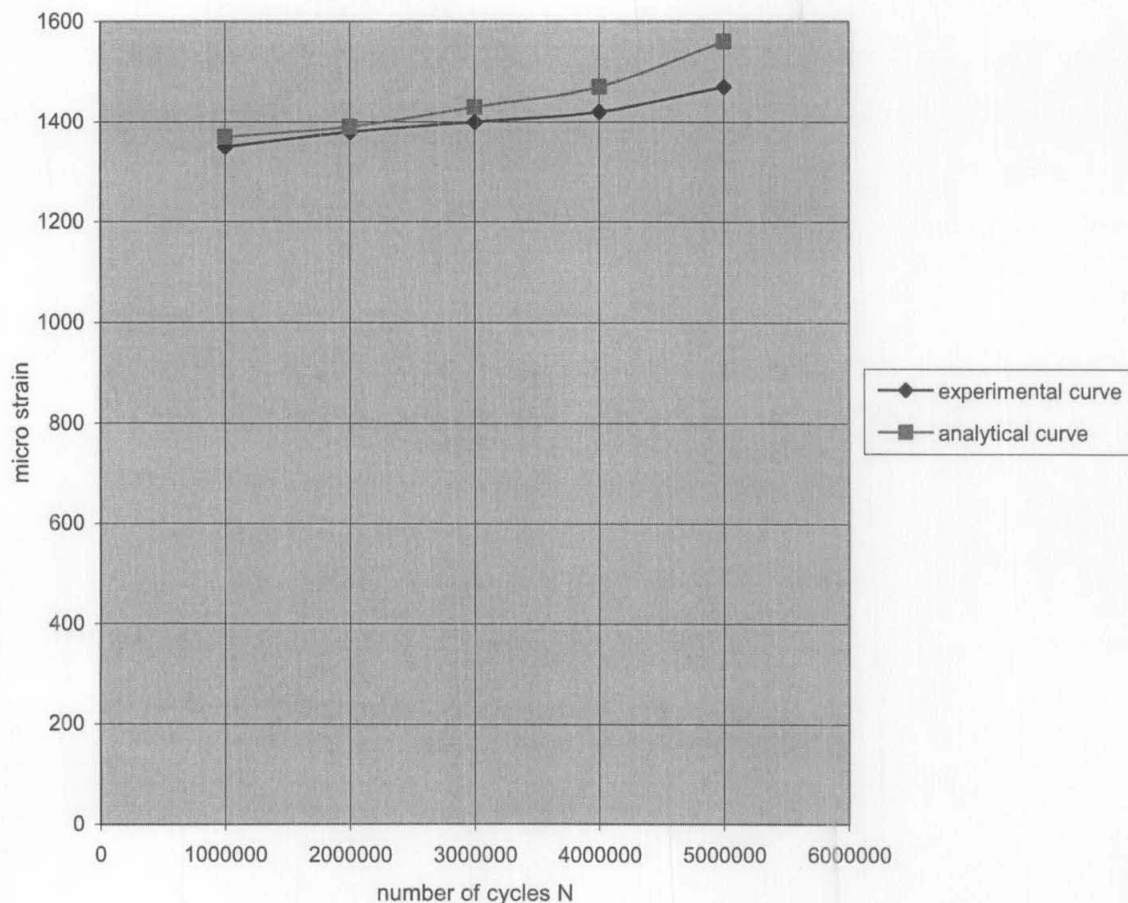


Fig. 8.8 LONGITUDINAL STEEL STRAIN-N

Figure 8.9 shows the curves representing the strains in the transverse steel versus the number of cycles. The curves presented are typical of the strains measured and correspond to the instrumented steel stirrup #S1 (see Fig. 8.2) located at 0.75d from the face of the support. In Fig. 8.9, an abrupt increase in the transverse-steel strain corresponding to specimen can be observed, similar to that observed for the concrete strut in specimen. At failure, the measured strain in stirrup #S1 was about 5200  $\mu\epsilon$ ,

whereas its yield strain is equal to  $2600 \mu\epsilon$ . The transverse steel can be seen to have been heavily strained. For instance, the maximum strain was about  $1870 \mu\text{strains}$ , which represents more than 72% of the yield stress. For comparison, the current ACI-440 guidelines (ACI 2008) state, in this context, that the stress in the longitudinal steel reinforcement under fatigue service load should be limited to 80% of the yield stress. No specific recommendations were provided for limits on stirrups; however, research seems to indicate that the fatigue service life of reinforcement is similar whether it is longitudinal tensile reinforcement or stirrups (Barnes & Mays 1999).

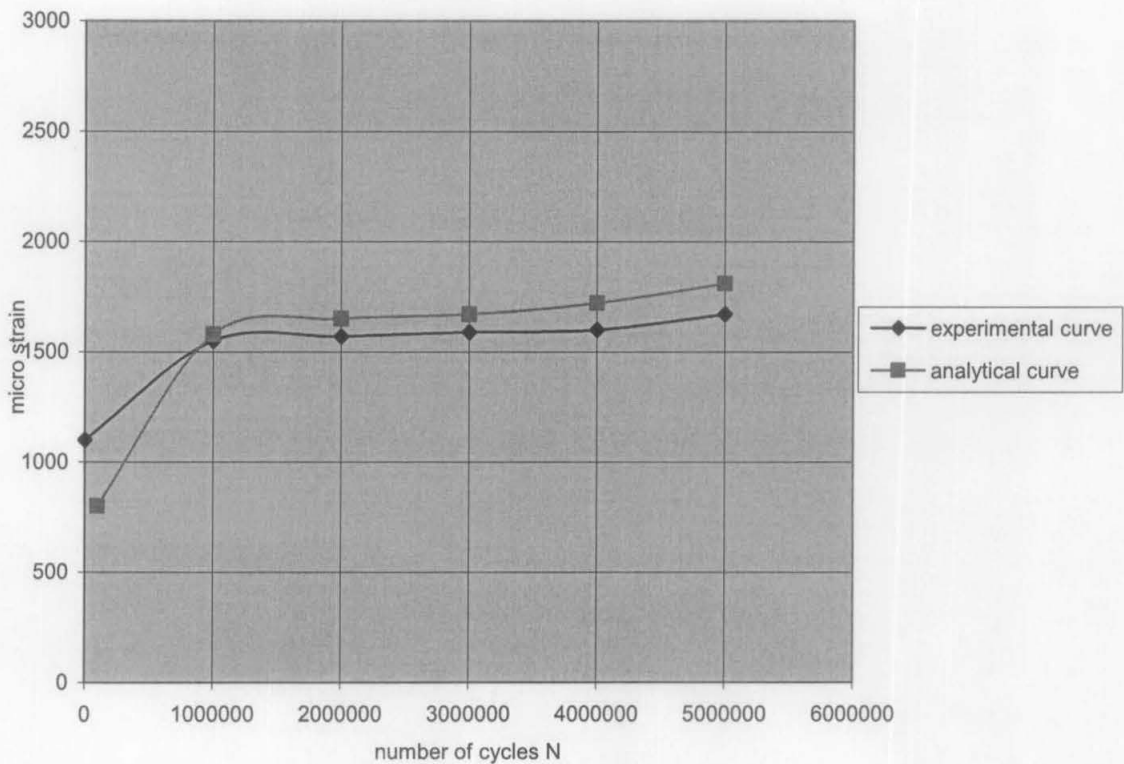


Fig. 8.9 TRANSVERSE STEEL STRAIN-N

With regard to the CFRP wrap, the measured strains versus the number of cycles for all test specimens are illustrated in Fig. 8.10. The curves shown are typical of the CFRP strains measured and correspond to the instrumented point #1 of the CFRP wrap located at  $0.75 d$  from the face of the support (see Fig. 8.3), which is the same position along the longitudinal axis as on stirrup #S1 (see Fig. 8.3). The behaviour of the CFRP wrap corresponding to specimen S0-2L illustrates a typical pattern of damage accumulation in strain due to fatigue loading. It can be seen that the strain increased suddenly to  $2500 \mu\epsilon$  before failure. At this stage of loading, the concrete

strut showed an abrupt increase in strain, reflecting the observed failure mode, that is, the crushing of the concrete strut, followed by partial debonding of the CFRP. As for specimens S0-1L and S1-1L, a rapid increase in strain was observed during the early cycles, followed by a stable region, in particular for S0-1L, where the strain remained relatively constant until 5,000,000 cycles. The fact that no sign of debonding was observed during the course of the test clearly demonstrates the effectiveness of the FRP U-wrap scheme for use in strengthening beams subjected to fatigue loading. However, it must be recognized that the effect of the stiffness of the CFRP and the applied fatigue loads may be of influence on the fatigue performance.

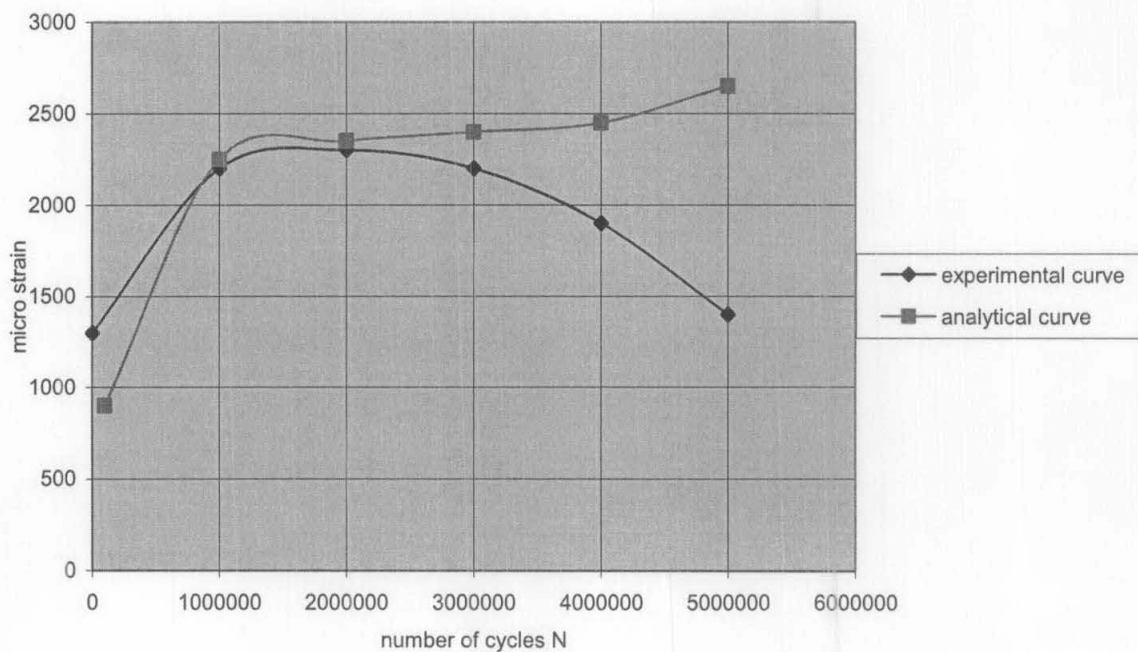


Fig. 8.10 CFRP STRAIN-*N*

Figure 8.9 shows the curves representing the deflection versus the number of cycles. The deflection curves shown were measured at the load point and correspond to the maximum load applied ( $P_{max}$ ). These curves illustrate a typical pattern of damage accumulation in beams subjected to fatigue loading. The curves show gradual increase in deflection as number of cycles of loading increased.

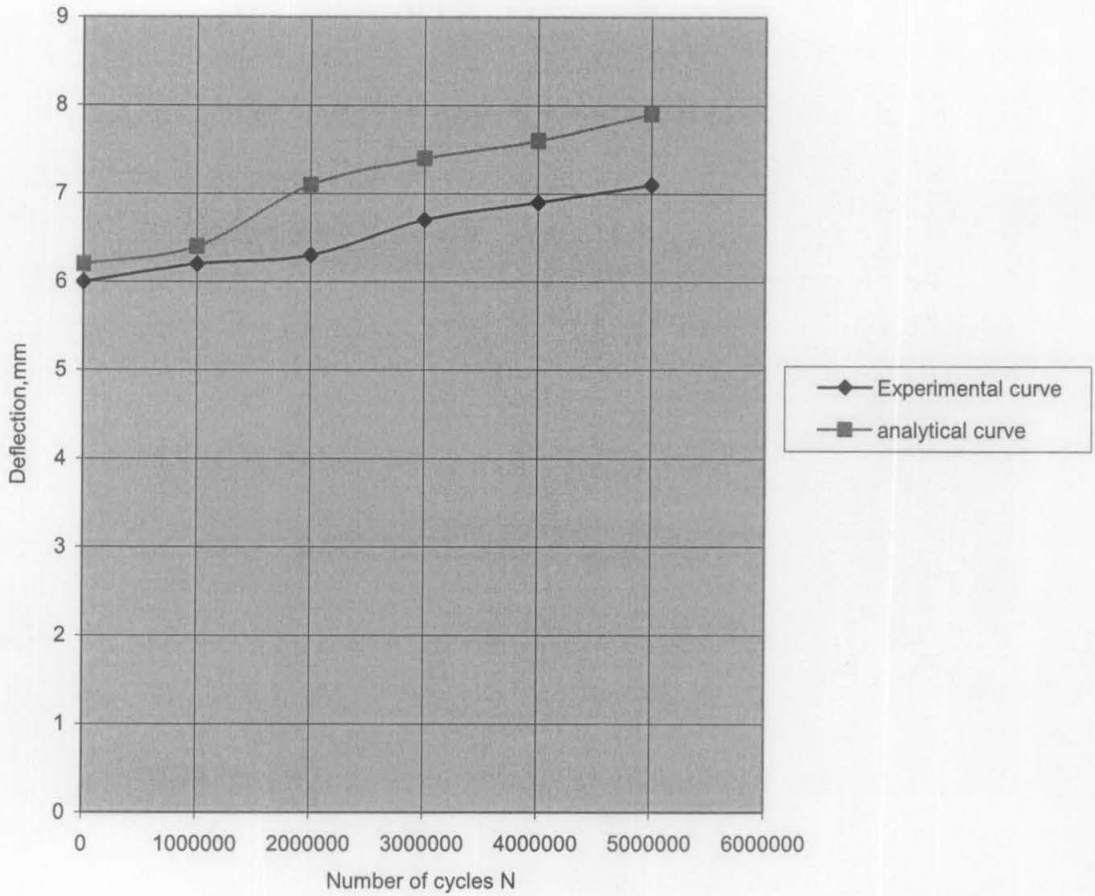


Fig. 8.11 DEFLECTION-N

### 8.7.2 Static behaviour

The deflection responses are shown in Fig. 8.12. The curves in the figure represent the shear force versus the deflection measured at the load point. The quasi-linear trend of the curves is typical of a shear failure test. No gain in stiffness due to CFRP can be observed by comparing the retrofitted specimens with the corresponding control ones. In fact, the latter featured a higher overall stiffness, as clearly indicated by the slope of the deflection curve. This can be attributed to the fact that, under previous cyclic loading, the retrofitted specimens were subjected to a relatively higher load range compared with the control ones, which resulted in a more pronounced loss of stiffness. This is particularly true for specimen S1-1L, which was more brittle at failure as shown in Fig. 8.12.

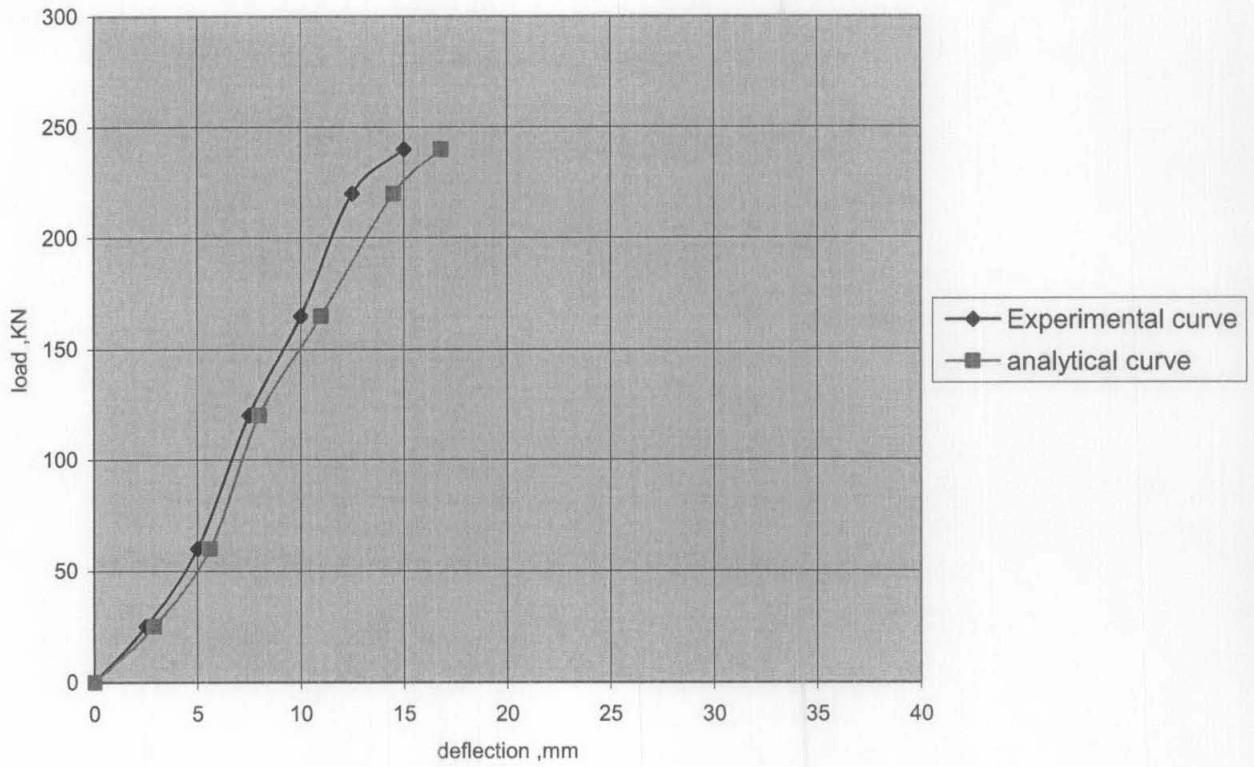


Fig. 8.12 LOAD-DEFLECTION RESPONSE

## 8.8 Parametric analysis

### 8.8.1 Introduction

The 3D FEM was conducted. This is one of the advantages of numerical modelling that parametric study can be studied easier than that in the real experiment. Beam parameter can be varied easily and freely for consideration of parameters that govern structural behaviour of RC beams strengthened for shear with CFRP laminates. In this case, the consideration is taken on some factors that govern shear capacity of such elements under cyclic loading as well as monotonic loading condition.

### 8.8.2 Effect of Shear span/depth ratio

Figure 8.13 shows the load deflection curve for different shear span-depth ratio ( $a/d$ )

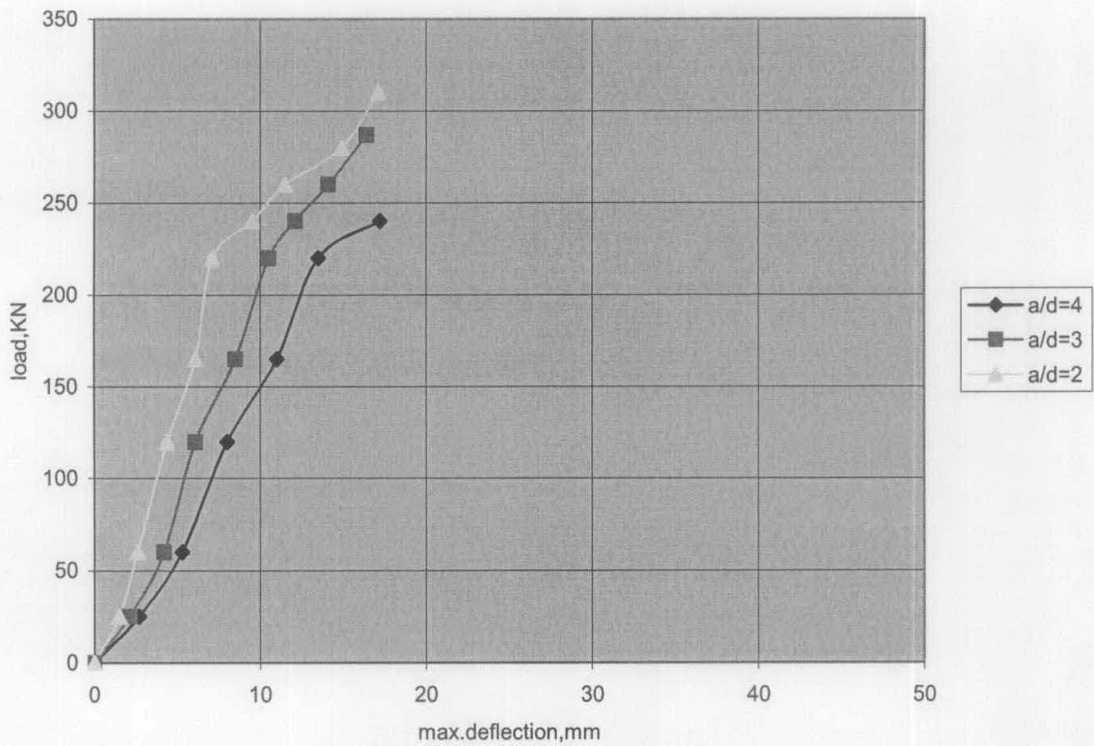


Fig. 8.13 LOAD DEFLECTION CURVES FOR DIFFERENT SHEAR SPAN-DEPTH RATIOS

Figure 8.14 shows the deflection versus number of cycles of loading for different shear span-depth ratios ( $a/d$ )

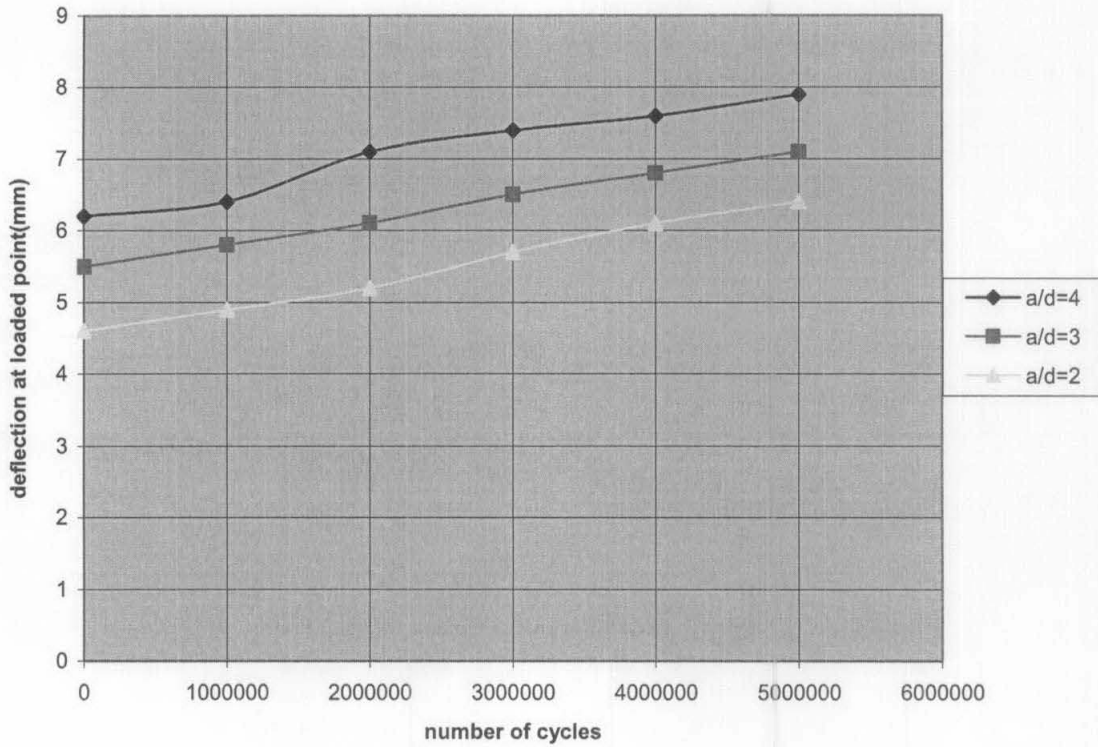


Fig. 8.14 DEFLECTION-N

### 8.8.2.1 Remarks

- It was observed that beams with small  $a/d$  carried more load after shear cracking than the beams with larger  $a/d$ . For example, at  $a/d$  of 2, the ultimate shear of the fibre-reinforced beams ranged from 250-300% of the cracking shear. In comparison, the ultimate shear ranged from 150-225% of the cracking shear for beams with  $a/d$  of 3.0 and 4.0. The difference can be attributed to the instability of arch mechanism at large  $a/d$  and to the interaction between flexural and shear modes of failure.
- The strength of fibre reinforced beams ranged from 120-180% of the strength of beams without strengthening. The strength increase was particularly 70%-80 % for the beam with low  $a/d$  ( $a/d = 2$ ) which fail in combination of shear and flexure (Table. 8.5) for larger  $a/d$  which are more typical in practice, the increase in strength ranged from 25%-

35 %. These beams failed in flexure, so the applied load at failure not equal to the shear strength; instead this load only provides a lower bound on shear strength.

- The average shear stress at failure consistently decreased with increasing  $a/d$ . also, the difference in capacity between beams with  $a/d=2$  and  $a/d=3$  was significantly larger than the difference between beams with  $a/d=3$  and  $a/d=4$ . Such behaviour is expected because arching action and dowel action mechanisms becomes less effective as  $a/d$  increase.
- Table 8.6 presents a summary for the effect of shear span-depth ratio on structural behaviour of RC strengthened for shear using CFRP laminates

Table 8.6 EFFECT OF SHEAR SPAN-DEPTH RATIO

Shear span/depth ratio $a/d$	Shear capacity	Shear stress	Max. deflection	Mechanism of loading	Mode of failure
Up to 1	Very high	Very high	Very low	Arch action	shear
2	high	high	low	Combination Beam action +arch action	Shear-flexure
3	low	low	high	Beam action	flexure
4	Very low	Very low	Very high	Beam action	flexure

### 8.8.3 Effect of CFRP thickness

Fig. 8.15 shows the deflection versus number of cycles of loading for strengthened beams with different CFRP thicknesses.

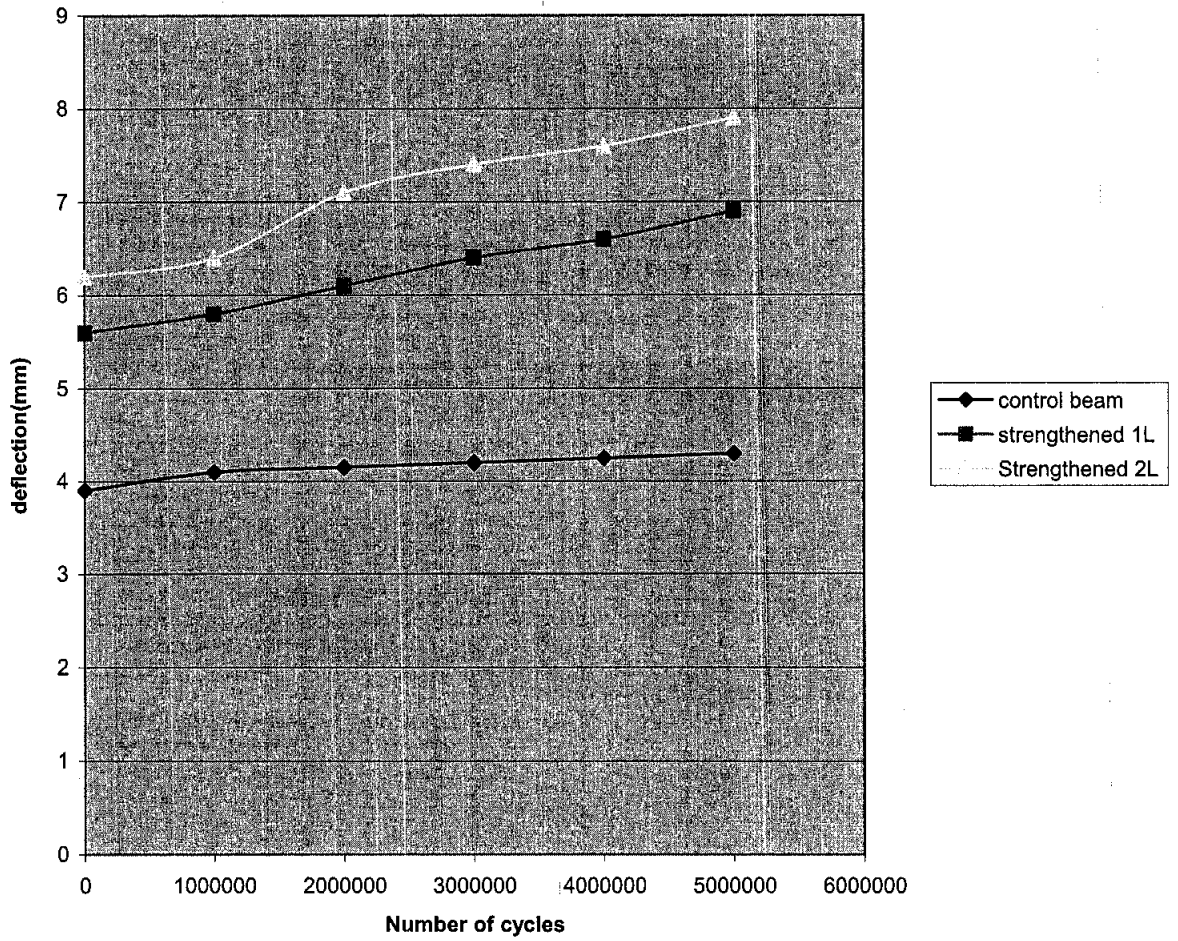


Fig. 8.15 DEFLECTION-N

Figure 8.16 shows the load-deflection curves for strengthened beams with different CFRP thicknesses.

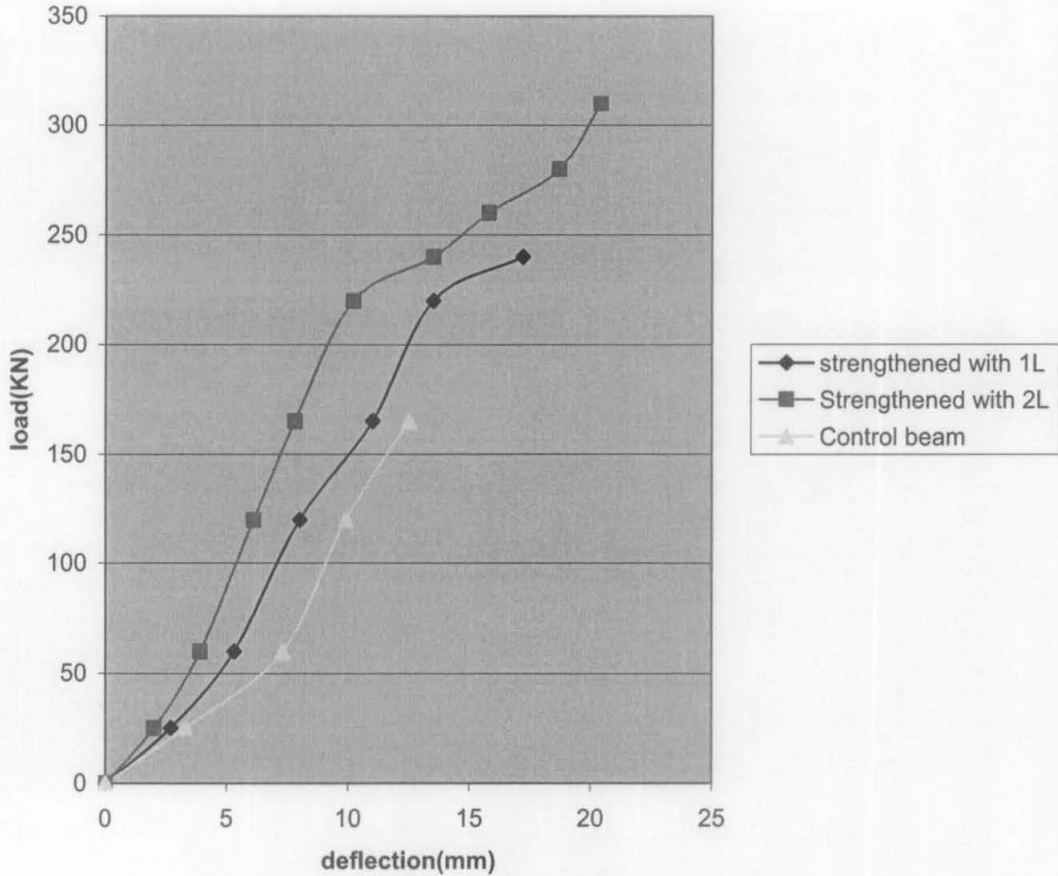


Fig. 8.16 LOAD-DEFLECTION CURVES FOR DIFFERENT CFRP THICKNESSES

### 8.8.3.1 Remarks

- For the same shear span to depth ratio ( $a/d=2$ ). The strength increase was particularly 70%-80 % for the beam strengthened with one layer of CFRP laminates which fail in combination of shear and flexure (Table. 8.6). For beam strengthened with two layer of CFRP laminates, the increase in strength ranged from 100%-120%. These beams failed in flexure, so the failure load did not represent the shear strength; instead this load only provides a lower bound on shear strength.

- It was observed that the effect of CFRP thickness on cracking shear was smaller than their effect on shear strength. Specifically, the increase in cracking shear ranged from 15%-35% of the cracking shear of similar beam without CFRP. This is due to fact that shear reinforcement does not prevent cracking but it came into the action after cracking by delaying the shear cracks propagation as well as controlling the width of these cracks.
- Specimens strengthened with one layer of CFRP survived five million cycles, some of them with no apparent signs of damage. This demonstrates the effectiveness of FRP strengthening systems on extending the fatigue life of structures.
- Specimens strengthened with two layers of CFRP failed in fatigue well below 5 million cycles as shown in Fig. 8.17. The failure mode observed for these specimens was a combination of crushing of the concrete struts, local debonding of CFRP and yielding of steel stirrups. This failure may be attributed to the higher load amplitude and also to the greater rigidity of the FRP which may have changed the stress distribution among the different components.

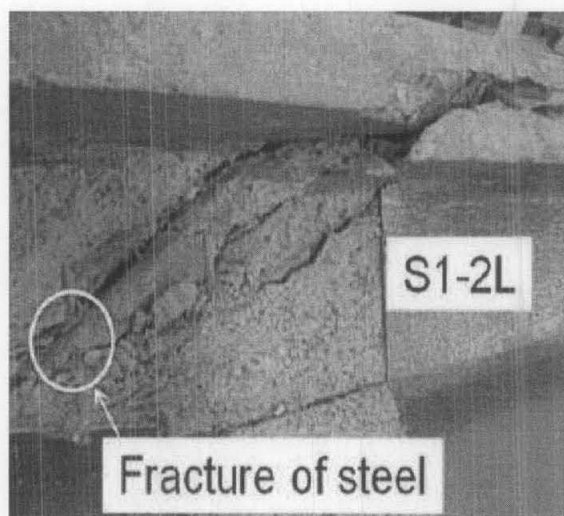


Fig. 8.17 FAILURE OF BEAM STRENGTHENED WITH TWO LAYERS OF CFRP LAMINATES

Table 8.7 represents a summary for the effect of shear span to depth ratio on the structural behaviour of RC beams strengthened for shear using CFRP laminates

Table 8.7 EFFECT OF CFRP THICKNESS

Specimen type	Shear capacity	Shear stress	Max. deflection	Mode of failure
Without CFRP	Very high	Very high	Very low	shear
Strengthened with 1L	high	high	low	Shear-flexure
Strengthened with 2L	low	low	high	crushing of the concrete struts+ debonding of CFRP and yielding of steel stirrups

## CHAPTER 9

### CONCLUSIONS AND RECOMMENDATIONS

#### 9.1 Conclusions

Based on the results and discussion of the analytical models and the experimental investigation; the following conclusions were made:

1. A new experimental methodology was introduced and studied in this investigation. It enabled the interfacial bond behaviour of CFRP-to-concrete joints under cyclic shear loading and proved to be appropriate and valid.
2. Mathematical formulation that govern the behaviour of the interface element was obtained, which are found in good agreement with the experimental results. This included the bond-slip behaviour, shear stiffness of interface and its degradation as number of cycle increased as well as the *S-N* curve.
3. A new analytical algorithm based on non-linear finite element method coded in FORTRAN language was developed to study the contribution of using CFRP as the external shear strengthening reinforcement for RC beams subjected to cyclic loads.
4. Using CFRP laminates was found to be an efficient technique to improve the shear behaviour of RC beams that can increase the shear

5. capacity of such element under monotonic loading for about 120%-180% as well as can extend the fatigue life under cyclic loading for about 6 to 7 times that of the un-strengthened beams.
6. Shear span to depth ratio  $[a/d]$  is the main controlling factor governing the behaviour of RC beams strengthened for shear using CFRP laminates. As  $a/d$  increased; the shear capacity and the average shear stress at failure consistently decreased. It also changed the mode of failure of such element from shear failure mode  $[a/d \leq 1]$  to flexure failure mode associated with  $[a/d \geq 4]$ , this was due to the change from arch action mechanism that control the behaviour of deep beams to beam action mechanism which normally govern the behaviour of shallow beams
7. Increasing the CFRP thickness did not affect the initiation of shear cracks but increased the total shear capacity. It is due to the fact that the web reinforcement did not prevent the cracking but control crack width after cracking. Increasing the thickness of CFRP laminates also changed the mode of failure from the shear mode to the flexure mode and this is in agreement with the strong shear-weak flexure philosophy.
8. If there is no proper anchorage for CFRP laminates, increasing in CFRP thickness result in high shear stress caused debonding of the fibre from concrete surface.

## **9.2 Recommendation for Future Work**

In this research the behaviour of RC beams strengthened for shear with CFRP laminates was investigated, however the study is limited to the behaviour of such element under cyclic and monotonic loading condition. Also the parametric analysis on this study is limited to the shear span depth ratio and the thickness of CFRP

laminates. The following are the main recommendations for further work of this study:

1. To study the dynamic behaviour of RC beams strengthened for shear using CFRP laminates by introducing the effect of damp and mass.
2. To increase the range of the parametric analysis by adding the effect of other controlling factor that might be a affect the behaviour of such element under dynamic loading

## REFERENCES

Arduini, M., Di Tommaso, A., and Nanni, A., 1997. "Brittle failure in FRP plated and sheet bonded beams", *ACI Structural Journal*, Vol. 94, No. 4, pp: 363-370.

Architectural Institute of Japan. AIJ structural design guidelines for reinforced concrete buildings. Tokyo: Architectural Institute of Japan, 1994.

Applied Technology Council. Seismic retrofitting guidelines for highway bridges. Technical report ATC 6-2. Redwood City, CA: Applied Technology Council, August 1983 [220 pp].

Ang BENG GHEE, Priestley MJN, Paulay T. Seismic shear strength of circular reinforced concrete columns. *ACI Struct J* 1989;86(1):45-59.

Aschheim M, Moehle JP. Shear strength and deformability of RC bridge columns subjected to inelastic cyclic displacements. Technical report UCB/EERC-92/04. Earthquake Engineering Research Center, University of California at Berkeley, March 1992 [93 pp].

American Concrete Institute. Building code requirements for structural concrete (ACI318-95) and commentary (ACZ318R-95). Detroit, MI: American Concrete Institute, 1995 [369 pp].

ASCE-ACI Committee 445 on Shear and Torsion. Recent approaches to shear design of structural concrete. *J Struct Engng*, ASCE 1998;124(12):1375-417.

Adhikary, B.H. and Mutsuyoshi, 2004. Behavior of concrete beams strengthening in shear with carbon-fiber sheets. *J. Composites Construct.*, 8: 258-264.

Al-Sulaimani, G.J., A. Sharif, I.A. Basunbul, M.H. Baluch and B.N. Ghaleb, 1994. Shear repair for reinforced concrete by fiberglass plate bonding. *ACI Structural J.*, 91: 458-464.

Anders, C. and B. Taljsten, 2005. Experimental study of strengthening for increased shear bearing capacity. *J. Composites Construct.*, 9: 488-496.

Anders, C. and T. Bjorn, 2005. Theoretical study of strengthening for increased shear bearing capacity. *J. Composites Construct.*, 9: 497-506.

Araki, N., Y. Matsuzaki, K. Nakano, T. Kataoka and H. Fukuyama, 1997. Shear capacity of retrofitted RC members with continuous fiber sheets. Non-metallic (FRP) reinforcement for concrete structures. Proceedings of the 3rd International Symposium on Non-Metallic (FRP) Reinforcement for Concrete Structures, 1997, Vol. 1.

Ashour AF. Tests of reinforced concrete continuous deep beams. *ACI Structural Journal* 1997;94(1):3-12.

Bazant ZP. Mechanics of distributed cracking. *Appl Mech Rev* 1986;39(5):675-705.

- Bazant ZP, Oh BH. Crack band theory for fracture in concrete. *Mater Struct* 1983;16(93):155-77.
- Bizindavyi, L. and Neale, K. W.: Transfer Length and Bond Strength for Composites Bonded to Concrete, *Journal of Composites for Construction, ASCE*, 3(4), 153-160, 1999.
- Brosens, K. and Gemert, D. Van.: Anchorage Stresses between Concrete and Carbon fibre Reinforced Laminates, *Non-Metallic (FRP) Reinforcement for Concrete Structures, Proceedings of Third International Symposium, Vol.1, 271-278, 1997.*
- Brosens, K. and Gemert, D. Van.: Anchorage Design for Externally Bonded Carbon Fiber Reinforced Polymer Laminates, *ACI, SP 188-56, 635-641, 1999.*
- Balan TA, Filippou FC, Popov EP. Constitutive model for 3D cyclic analysis of concrete structures. *J Engng Mech, ASCE* 1997;123(2):143-53.
- Bashur FK, Darwin D. Nonlinear biaxial law for concrete. *J Struct Div, ASCE* 1978;104(1):157-70.
- Bazant ZP. Comment on orthotropic models for concrete and geomaterials. *J Engng Mech, ASCE* 1983;109(3):849-65.
- Bouzaiene A, Massicotte B. Hypoelastic tridimensional model for Non-proportional loading of plain concrete. *J Engng Mech, ASCE* 1997;123(11):1111-20.
- Chajes, M. J., Finch, William. W., Januszka, T. F. and Thomson, T. A.: Bond and Force Transfer of Composite Material Plates Bonded to concrete, *ACI Structural Journal*, 93(2), 208-217, 1996.
- Chen WF. Plasticity in reinforced concrete. New York: McGraw- Hill, 1982.
- Darwin D, Pecknold DA. Nonlinear biaxial stress-strain law for concrete. *J Engng Mech, ASCE* 1977;103(2):229-41.
- Darwin D, editor. Finite element analysis of reinforced concrete structures II. New York: ASCE; 1993. p. 203-32.
- Červenka, J., 1994. "Discrete crack modeling in concrete structures", *PhD Thesis*, University of Colorado, Boulder.
- Limam, A. and Hamlin, P., 1998. "On the extending performance of an RC beam with a CFRP sheet: experiments and simulations", *Proceedings of the sixth International Conference on Computer Methods in Composite Materials, CADCOMP'98*, Montreal, Canada, pp: 569-578.
- Candappa, D. C., Sanjayan, J. G., and Setunge, S. ~2001!. "Complete triaxial stress-strain curves of high-strength concrete." *J. Mater. Civ. Eng.*, 13~3!, 209-215.
- Chern, J. C., Yang, H. J., and Chen, H. W. 1992 "Behavior of steel fiber reinforced concrete in multiaxial loading." *ACI Mater. J.*, (89):1 32- 40.
- CSA Standard A23.3-94. Design of concrete structures for buildings. Rexdale, Ontario: CSA, 1994 [199 pp].

- Collins MP, Mitchel D. Prestressed concrete basics. Toronto: Response Publishers, 1997.
- Collins M. Procedures for calculating the shear response of reinforced concrete elements: a discussion. *J Struct Engng, ASCE* 1998;124(12):1485-9.
- Chaallal, O., M.J. Nollet and D. Perraton, 1998. Shear strength of RC by externally bonded side CFRP strips. *J. Composite Construct. ASCE*, 2: 111-113.
- Chajes, M.J., D.R. Januszka, T.R. Thomson and W.W. Finch, 1995. Shear strengthening of reinforced concrete beams using externally applied composite fabrics. *ACI Struct J.*, 92: 295-303.
- Chen, J.F. and J.G. Teng, 2003. Shear capacity of FRP strengthened RC beams: FRP debonding. *Construct. Building Mater.*, 17: 27-41.
- Deniaud, C. and J.J.R. Cheng, 2001. Shear behavior of reinforced concrete t-beams. With externally bonded fiber reinforced polymer sheets. *ACI Struct. Eng.*, 98: 386-494.
- Deniaud, C. and J.J.R. Cheng, 2004. Simplified shear design method for concrete beams strengthened with fiber reinforced polymer sheets. *J. Composites Construct.*, 8: 425-433.
- Dai J. G., Sato Y., and Ueda, T.: Improving the Load Transfer and Effective Bond Length For FRP Composites Bonded to Concrete, *Proceedings of the Japan Concrete Institute*, Vol.24, 1423-1428, 2002.
- Dulascka H. Dowel action of reinforcement crossing cracks in concrete. *ACI Structural Journal* 1972;69(12):754-7
- El-Rafaie, S.A., Ashour, A.F. and Garrity, S.W., 2001. "Strengthening of reinforced concrete continuous beams with CFRP composites", *Proceedings of the International Conference on Structural Engineering, Mechanics and Computation*, Elsevier Science.
- Elwi AA, Murray DW. A 3D hypoelastic concrete constitutive relationship. *J Engng Mech, ASCE* 1979;105(4):623-41.
- Grace, N.F., G.A. Sayed, K.A. Soliman and R.K. Saleh, 1998. Strengthening reinforced concrete beams using fibre reinforced polymer (FRP) Laminate. *ACI Struct. J.*, 96: 186-194.
- Goodman, R.E., Taylor, R.L. and Brekke, T.L., 1968. "A model for the mechanics of jointed rock", *Journal of the Soil Mechanics and Foundation Division, ASCE*, 94(SM3), pp: 637-659.
- G.N.Wells and L.J. Sluys., A new method for modelling cohesive cracks using finite elements. *International Journal for Numerical Methods in Engineering*, 50(12):2667-2682, 2001.
- Horiguchi, T. (1997). "Effect of Test Methods and Quality of Concrete on bond strength of CFRP Sheet." *Non-Metallic (FRP) Reinforcement for Concrete Structures, Proceedings of Third International Symposium*, Vol.1, 265-270.
- Hurlbut BJ. Experimental and computational investigation of strain softening in concrete. Report AFOSR 80-0273. US Air Force Office of Scientific Research, University of Colorado, Boulder, 1985.

H. Yoshikawa, T. Tanabe, An analytical analysis for tension stiffness of R-C members, Trans. of the Japan Concrete Institute, Vol. 8, pp. 473-80, 1986.

Hobbs, D. W. ~1970!. "Strength and deformation properties of plain concrete subjected to combined stress. Part 1: Strength results obtained on one concrete." *Technical Rep. 42*, Cement and Concrete Association, London, 451, 1-12.

Hong, M., Kioussis, P. D., Ehsani, M. R., and Saadatmanesh, H. ~2001!. "Confinement effects on high-strength concrete." *ACI Struct. J.*, 98~4!, 548-553.

Hussein, A., and Marzouk, H. ~2000!. "Behavior of high-strength concrete under biaxial stresses." *ACI Mater. J.*, 97~1!, 27-36.

Hsu T, Zhang LX. Tension stiffening in reinforced concrete membrane elements. *ACI Struct J* 1996;93(1):108-15.

Hsu, C.T.T., H.T. Bian and Y.X. JIA, 1977. Reseach for bond-slip using sika's carbodur system. Report to Sika Corporation, NJIT. Newark, N.J.

Hsu T. Stresses and crack angles in concrete membrane elements. *J Struct Engng, ASCE* 1998;124(12):1476-84.

H. Yuan, J.G. Teng, R. Seracino, Z.S. Wu, J. Yao, Full-range behaviour of FRP-to-concrete bonded joints, *Engineering Structures*, Vol. 26, pp. 553-565, Elsevier, 2004.

He XG, Kwan AKJ. Modeling dowel action of reinforcement bars for finite element analysis of concrete structures. *Computer & Structures* 2001;79: 595-604

International Symposium on Latest Achievement of Technology and Research on Retrofitting Concrete Structures, *Proceedings and Technical Report on JCI Technical Committee*, July 14-15, 2003, Kyoto.

Imran, I., and Pantazopoulou, S. J. ~1996 "Experimental study of plain concrete under triaxial stress." *ACI Mater. J.*, 93~6!, 589-601.

Jiang, L. H., Huang, D. H., and Xie, N. X. ~1991 "Behavior of concrete under triaxial compressive-compressive-tensile stresses." *ACI Mater. J.*, 88~2!, 181-185.

Jansen DC, Shah SP, Rossow EC. Stress-strain results of concrete from circumferential strain feedback control testing. *ACI Journal* 1995;92(6):419-28.

J. Yang, J.G. Teng, J.F. Chen, Interfacial stresses in soffit plated reinforced concrete beams, *Proceedings of the Institution of Civil Engineers, ICE*, Vol. 157, pp. 77-89, 2004.

Kang HD, Spacone E, Willam KJ. A study of compressive failure in over-reinforced concrete beams. In: *FRAMCOS-3*, Oct 12-16; Gifu, Japan, vol. 2, 1998:1195-210.

Kolymbas D. An outline of hypoplasticity. *Arch Appl Mech* 1991;61:143-51.

Kupfer HB, Hilsdorf HK, Ru'sch H. Behavior of concrete under biaxial stresses. *ACI Journal* 1969;66(8):656-66.

Kotsovos, M. D. ~1979 "A mathematical description of the strength properties of concrete under generalized stress." *Mag. Concrete Res.*, 31~128!, 151-158.

Kupfer, H. B., and Gerstle, K. H. ~1973 "Behavior of concrete under biaxial stresses." *J. Eng. Mech. Div.*, 99~4!, 853-866.

Khalifa, A. and A. Nanni, 2000. Improving shear capacity of existing RC T-section beams using CFRP composites. *Cement Concrete Composites*, 22: 165-174.

Khalifa, A., T. Alkhrdji and S. Alnsbury, 1999. Anchorage of surface mounted FRP reinforcement. *Concrete Internationally*, 21: 49-54.

Khalifa, A., W.J. Gold, A. Nanni and A.M.I. Aziz, 1998. Contribution of externally bonded FRP to shear capacity of RC flexural members. *J. Composite Construct. ASAE*, 2: 195-202.

Lorenzis, L. De., Miller, B., and Nanni, A.: Bond of Fiber-Reinforced Polymer Laminates to Concrete, *ACI Material Journal*, 98(3), 256-264, 2001 .

Lekhnitskii SG. In: Brandstatter JJ, editor. Theory of elasticity of an anisotropic elastic body. San Francisco, CA: Holden Day, Inc., 1963. 342 *T.A. Balan et al. / Engineering Structures 23 (2001) 333-342*.

Lahlou, K., Aictin, P. C., and Chaallal, O. ~1992!. "Behavior of highstrength concrete under confined stresses." *Cem. Concr. Compos.*, 14, 185-193.

Li, Q. B., and Ansari, F. ~1999!. "Mechanics of damage and constitutive relationships for high-strength concrete in triaxial compression." *J. Eng. Mech.*, 125~1!, 1-10.

Lim, T. Y. ~1987!. "Elastic and post-cracking behavior of steel fiber concrete." PhD thesis, National Univ. of Singapore, Singapore.

Liu, J., and Foster, S. J. ~2000!. "3-dimensional finite element model for confined concrete structures." *Compos. Struct.*, 77~5!, 441-451.

Lehman DE, Lynn AC, Aschheim MA, Moehle JP. Evaluation methods for reinforced concrete columns and connections. In: 11th World Conf. on Earthquake Engineering. Elsevier Science Ltd, 1996, [paper no. 673].

Lee, K. and R. Al-Mahaidi, 2003. Strength and failure mechanism of RC T-beams strengthened with CFRP plates. Proceedings of the 6th International Symposium on Fiber Reinforced Polymers Reinforcement for Reinforced Concrete Structures, 2003, Singapore, pp: 247-256.

Loov, R. and L. Peng, 1998. The influence of concrete strength on shear friction based design of reinforced concrete beams. Proceedings of the Intentional Conference on HPHSC, 1998, IEEE Xplore, pp: 505-519.

Mattar, S. N. H. ~2003!. "Behavior of fiber reinforced concrete structures using finite element method." BEng thesis, National Univ. of Singapore, Singapore.

Mills, L. L., and Zimmerman, R. M. ~1970!. "Compressive strength of plain concrete under multiaxial loading conditions." *ACI J.*, 67~70!, 802–807.

Murugappan, K., Paramasivam, P., and Tan, K. H. ~1993!. "Failure envelope for steel-fiber concrete under biaxial compression." *J. Mater. Civ. Eng.*, 5~4!, 436–446.

Millard SG, Johnson RP. Shear transfer across cracks in reinforced concrete due to aggregate interlock and dowel action. *Magazine of Concrete Research* 1984; 36(126):9–21.

Millard SG, Johnson RP. Shear transfer in cracked reinforced concrete. *Magazine of Concrete Research* 1985;37(130):3–15.

Martí'n-Pe'rez B. A study of the mechanical response of reinforced concrete to cyclic shear reversals. M.A.Sc. thesis, Department of Civil Engineering, Univeristy of Toronto, 1995 [111 pp].

Maeda, T., Y. Asano, Y. Sato, T. Ueda and Y. Kakuta, 1997. A study on bond mechanism of carbon fiber sheet, Non-metalitic (FRP) Reinforcement for concrete structures. *Proc. Symp.*, 1: 279-286.

Menetrey P, Willam KJ. Triaxial failure criterion for concrete and its generalization. *ACI Structural Journal* 1995;92(3):311–8.

Mehlhorn, G., and Keuser, M., 1985. "Isoparametric contact elements for analysis of reinforced concrete structures", *Finite Element Analysis of Reinforced Concrete Structures*, C. Meyer, and H. Okamura, eds., ASCE, New York: 329-347.

M.S.Wendel., Significance of midspan debonding failure in FRP-plated concrete beams. *Journal of Structural Engineering - ASCE*, 127(7):792– 798, 2001

Nakaba, K., Kanakubo, T., Furuta, T., and Yoshizawa, H.: Bond Behavior between Fiber - Reinforced Polymer Laminates and Concrete, *ACI Structural Journal*, 98(3), 359-167. 2001.

Ngo, D. and Scordelis, A.C., 1967. "Finite element analysis of reinforced concrete beams", *ACI Journal*, Vol. 64, No. 3, pp: 152-163.

O'Shea, M. D., and Bridge, R. Q. ~2000!. "Design of circular thin-walled concrete filled steel tubes." *J. Struct. Eng.*, 126~11!, 1295–1303. Ottosen, N. S. ~1977!. "A failure criterion for concrete." *J. Eng. Mech. Div.*, 103~4!, 527–535.

Padmarajaiah, S. K., and Ramaswamy, A. ~2002!. "A finite element assessment of flexural strength of prestressed concrete beams with fiber reinforcement." *Cem. Concr. Compos.*, 24, 229–241.

Priestley MJN, Verma R, Xiao Y. Seismic shear strength of reinforced concrete columns. *J Struct Engng ASCE* 1994;120(8):2310–29.

Popovics S. Numerical approach to the complete stress–strain relation for concrete. *Cement Concrete Res* 1973;3(5):583–99.

Rahimi, H. and Hutchinson, A., 2001. "Concrete beams strengthened with externally bonded FRP plates", *Journal of Composites for Construction*, Vol. 5, No. 1, pp: 44-56.

Ross, C.A., Jerome, D.M., Tedesco, J.W., and Hughes, M.L., 1999. "Strengthening of

reinforced concrete beams with externally bonded composite laminates”, *ACI Structural Journal*, Vol. 96, No. 2, pp: 212-220.

Rots, J. G., 1985. “Bond-slip simulations using smeared crack and / or interface elements”, Research Report 85-01, Structural Mechanics Group, Department of Civil Engineering, Delft University of Technology.

Rots, J. G., 1988. “Computational modeling of concrete fracture”, PhD Thesis, Delft University of Technology, Delft, the Netherlands.

Sato, Y., Asano, Y., and Ueda, T. : Fundamental Study on Bond Mechanism of Carbon Fiber Sheet, *Concrete Library International, JSCE*, No.37, June 2001, 97-115, 2000 .

Sato, Y., Kimura, K., and Kobatake, Y.: Bond Behaviors between CFRP Sheet and Concrete.”, *Journal of Structural Construction Engineering, AIJ*, No.500, 75-82, 1997 (in Japanese) .

Schäfer, H., 1975. “A contribution to the solution of contact problems with the aid of bond elements”, *Computer Methods in Applied Mechanics and Engineering*, Vol. 6, pp. 335- 354.

Sang, L.K., 2003. “Effect of beam size and FRP thickness on interfacial shear concentration and failure mode in FRP-strengthened beams”, M.Eng. Thesis, National University of Singapore, Singapore, 107 pp.

Sheikh, S. A., Vecchio, F. J., De Rose, D. and Bucci, F, 1998. “Behaviour and analysis of FRP-repaired elements”, *Proceeding of International Conference on HPHSC*, Perth, Australia, pp: 669-683.

Shin, Y-S. and Lee, C., 2003. “Flexural behaviour of reinforced concrete beams strengthened with carbon fiber-reinforced polymer laminate at different levels of sustaining load”, *ACI Structural Journal*, Vol. 100, No. 2, pp: 231-239.Ltd., Oxford, UK, pp: 1591-1598.

Saenz IP. Discussion of ‘equation for the stress–strain curve of concrete, by P. Desay and S. Krishan’. *ACI Journal* 1964;61(9):1229–35.

Scavuzzo R, Stancowski T, Gerstle K, Ko H-Y. Stress–strain curves for concrete under multiaxial load histories. NSF CME 80-01508. Department of CEAE, University of Colorado, Boulder, 1983.

Smith SS, Willam KJ, Gerstle KH, Sture S. Concrete over the top, or: is there life after peak? *ACI Journal* 1989;86(5):491–7.

Setunge, S., Attard, M. M., and Darvall, P. L. ~1993!. “Ultimate strength of confined very high-strength concretes.” *ACI Struct. J.*, 90~6!, 632– 641.

Soroushian P, Obaseki K, Rojas M. Bearing strength and stiffness of concrete under reinforcing bars. *ACI Matls J* 1987;84(3):179–84.

Salles-Neto, M., G.S. Melo and Y. Nagato, 2001. T beams strengthened in shear with carbon sheet laminates (Cfrp). *Proceedings of the 5th International Conference on Fiber-Reinforced Plastics for Reinforced Concrete Structures*, 2001, Cambridge, UK., pp: 239-248.

Taliercio, A. L. F., Berra, M., and Pandolfi, A. ~1999!. “Effect of high intensity sustained triaxial stresses on the mechanical properties of plain concrete.” *Mag. Concrete Res.*, 51~6!, 437–447.

Taliercio, A. L. F., and Gobbi, E. ~1997!. "Effect of elevated triaxial cyclic and constant loads on the mechanical properties of plain concrete." *Mag. Concrete Res.*, 49~181!, 353-365.

Traina, L. A., and Mansour, S. A. ~1991!. "Biaxial strength and deformational behavior of plain and steel fiber concrete." *ACI Mater. J.*, 88~4!, 354-362.

Tho, K. K., Seow, P. E. C., and Swaddiwudhipong, S. ~2003!. "Numerical method for analysis of concrete under multi-axial loads." *Mag. Concrete Res.*, 55~6!, 537-547.

Tnantafillou, T.C. and C.P. Antonopoulos, 2000. Design of concrete flexure members strengthened in shear with FRP. *J. Composite Construct.*, 4: 198-205.

Triantafillou, T.C., 1998. Shear strengthening of reinforced concrete beams using epoxy-bonded FRP composites. *ACI Struct. J.*, 95: 107-115.

Taylor RL. FEAP user manual, v7.1. Berkeley, CA: Department of Civil and Environmental Engineering, University of California, 1999.

T.W. White, K.A. Soudki, and M. Erki., Response of RC beams with CFRP laminates and subjected to a high rate of loading. *Journal of Composites for Construction*, 5(3):153-162, 2001.

Ueda, T., Sato, Y., and Asano, Y.: Experimental Study on Bond strength of Continuous Carbon Fiber Sheet." *ACI, SP 188-37*, 407-413, 1999 .

Uji, K., 1992. Improving shear capacity of existing reinforced concrete members by applying carbon fiber sheets. *Trans. Jap. Concrete Ins.*, 14: 2453-2466.

Umezu, K., M. Fujita, H. Nakai and K. Tamaki, 1997. Shear behavior of RC beams with aramid fiber sheet non-metallic (FRP) reinforcement for concrete structures. *Proceedings of the 3rd International Symposium on Non-Metallic (FRP) Reinforcement for Concrete Structures, 1997, Tokyo, Japan*, pp: 491-498.

van Mier JGM. Strain-softening of concrete under multiaxial loading conditions. PhD thesis, Eindhoven University of Technology, Eindhoven, The Netherlands, 1984.

Van Mier, J. G. ~1984!. "Strain softening of concrete under multiaxial loading condition." PhD thesis, Eindhoven University of Technology, Eindhoven, The Netherlands.

Vecchio FJ, Collins MP. The modified compression field theory for reinforced concrete elements subjected to shear. *ACI Journal* 1986;83(2):219-31.

Vecchio F, Collins MP. The response of reinforced concrete to in-plane shear and normal stresses. Technical report 82-03. Department of Civil Engineering, University of Toronto, March 1982. p. 332.

William, K. J., and Warnke, E. P. ~1974!. "Constitutive model for the triaxial behavior of concrete." *Proc., IABSE Seminar on Concrete Structures Subject to Triaxial Stresses 19*, International Association for Bridge and Structural Engineering, Zurich, 11-30.

Watanabe F, Ichinose T. Strength and ductility design of rc members subjected to combined bending and shear. In: *Concrete shear in earthquakes*. Houston: University of Houston, 1991:429-38.

Won Y-L, Paulay T, Nigel Priestley MJ. Response of circular reinforced concrete columns to multi-directional seismic attack. *ACI Struct J* 1993;90(2):180–91.

Wood SL, Sittipunt C. Cyclic response of reinforced concrete structural walls. In: Wight JK, Kreger ME, editors. Mete A. Sozen Symposium — a tribute from his students. Farmington Hills, MI: American Concrete Institute, 1996:399–429.

Wong, R.S.Y., 2001. “Towards modeling of reinforced concrete members with externally bonded fiber-reinforced polymer (FRP) composites”, MASC thesis, University of Toronto, Toronto, Canada, 298 pp.

Wong, R.S.Y., and Vecchio, F.J., 2003. “Towards modelling of reinforced concrete members with externally bonded fiber-reinforced polymer composites”, *ACI Structural Journal*, Vol. 100, No. 1, pp: 47-55.

Willam KJ, Warnke EP. Constitutive model for the triaxial behavior of concrete. *Int Assoc Bridge Struct Engng Proc* 1975;19:1–30.

Willam KJ, Hurlbut B, Sture S. Experimental and constitutive aspects of concrete failure. In: Meyer, Okamura, editors. *Finite element analysis of reinforced concrete structures*. New York: ASCE, 1986.

Xie, J., Elwi, A. E., and MacGregor, J. G. ~1995!. “Mechanical properties of three high-strength concretes containing silica fume.” *ACI Mater. J.*, 92~2!, 135–145.

Yin, W. S., Su, E. C. M., Mansur, M. A., and Hsu, T. T. C. ~1989!. “Biaxial tests of plain and fiber concrete.” *ACI Mater. J.*, 86~3!, 236–243.

Yoshizawa, H., Wu, Z., Yuan, H., and Kanakubo, T.: Study on FRP-Concrete Interface Bond Performance, *Transactions of JSCE*, No.662/V-49, 105-119, 2000.

Zarnic, R., Gostic, S., bosiljkov, V., and Bokan-Bosiljkov, V., 1999. “Improvement of bending load-bearing capacity by externally bonded plates”, *Specialist Techniques and Materials for Concrete Construction*, Proceedings of the International Conference ‘Creating with Concrete’, Dundee, Scotland, UK, pp: 433-442.

Zienkiewicz, O.C. and Cheung, Y.K., 1967. “The finite element analysis in structural and continuum mechanics”, McGraw-Hill, London.

Z. Wu, J. Yin., *Fracturing behaviours of FRP-strengthened concrete structures*. *Engineering Fracture Mechanics*, Vol. 70, pp. 1339-1355, Elsevier, 2003.

Zheng, Z.C., T. Cheng, H. Thomas and F. Asce, 2005. Shear strengthening of reinforced concrete beams using carbon-fiber reinforced polymer laminates. *J. Composites Construct.*, 9: 158-169.

## LIST OF PUBLICATIONS

### INTERNATIONAL JOURNALS PUBLICATIONS

1. Mahmoud et al. Fatigue Behavior of CFRP-to-Concrete Joints under Shear. Proceedings of the Institution of Civil Engineers Structures and Buildings journal 162 October 2009 Issue SB5 Pages 355–364

### INTERNATIONAL CONFERENCE PUBLICATIONS

1. Louay et al. efficiency of using CFRP laminates to improve performance of R.C structures under cyclic loading. Proceedings of the International conference for construction and building technology [ICCBT] 2008, Kuala Lumpur, Malaysia, pp: 316-326.
2. Louay et al. Interaction between CFRP Side Plated to R.C Beams and Concrete under Shear Action Proceedings of the 5th International Specialty Conference on fibre reinforced materials August 2008, Singapore
3. Louay et al. Interfacial Behavior of Side Plated CFRP-to-Concrete Joints under Cyclic Shear Loading. Proceedings of ASC 23rd Annual Technical Conference 2008, Memphis, USA
4. Louay et al. Interaction between CFRP Side Plated to R.C Beams and Concrete under Shear Action Proceedings 9th International Symposium on Fiber Reinforced Polymer Reinforcement for Concrete Structures FRPCS-9 2009, Sydney, Australia